Chapter 6
Earthquake Response Evaluation of Concrete

6.1 Folsom Dam Nonoverflow Monolith

6.1-1 Background

The structure selected for this numerical example corresponds to a monolith of the concrete gravity section of the Folsom Dam and Reservoir Project, located on the American River, about 32 km (20 miles) northeast of the city of Sacramento, CA. The reservoir serves a variety of purposes. It is used to provide flood control, irrigation, and power generation. The construction of the dam, which spanned almost 8 years, was completed in 1956. The gravity dam section consists of 28 monoliths, 15.2 m (50 ft) wide each. The section selected for this numerical example corresponds to the tallest nonoverflow monolith, which was identified as the critical section in earlier studies (Hall, Woodson, and Nau 1989).

6.1-2 Purpose and Objectives

The purpose of this section is to illustrate the application of linear time-history analysis to earthquake response computation of a 2-D concrete gravity dam section. The objectives of this study are to evaluate the dynamic characteristics of the 2-D model, and to compute the seismic response of the system when subjected to horizontal ground motion using different earthquake records. Several ground acceleration records were selected to evaluate the influence of the ground excitation characteristics on the resulting dynamic performance of the structural system.

6.1-3 Scope

The scope of the study included the following:

- Definition of ground acceleration time-histories.
- Development of the 2-D finite element model of the system.
- Computation of the dynamic characteristics of the system.
- Time-history analysis of seismic performance and evaluation of results.

6.1-4 Earthquake Ground Motions

Several natural ground motions were considered for the analysis, all of them scaled up to the same value of peak acceleration. The records considered are defined in Table 6.1-1. The time-histories for these acceleration records are indicated in Figure 6.1-1, and the corresponding response spectra (3 percent damping) are shown in Figure 6.1-2.

Table 6.1-1
Ground Motion Records Used for Analysis

Event	Record	Component, deg	Peak Acceleration, g's
1966 Parkfield Earthquake	Cholame #8	320	0.30
1989 Loma Prieta Earthquake	Gavilan College	337	0.30
1987 Whittier Narrows Earthquake	Garvey Reservoir	330	0.30
1971 San Fernando Earthquake	Pacoima Dam	254	0.30

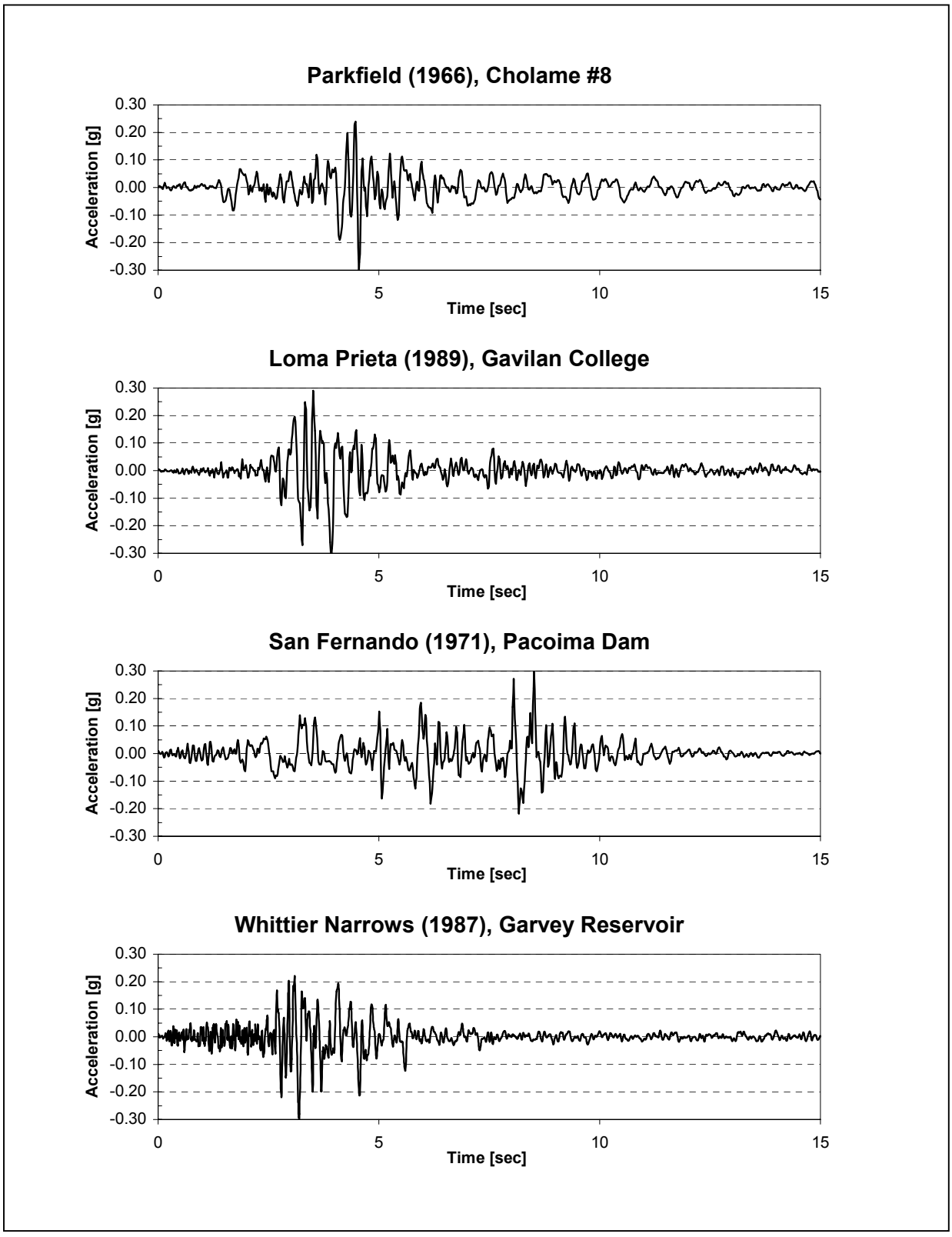

Figure 6.1-1. Ground motion acceleration time-histories used for analysis

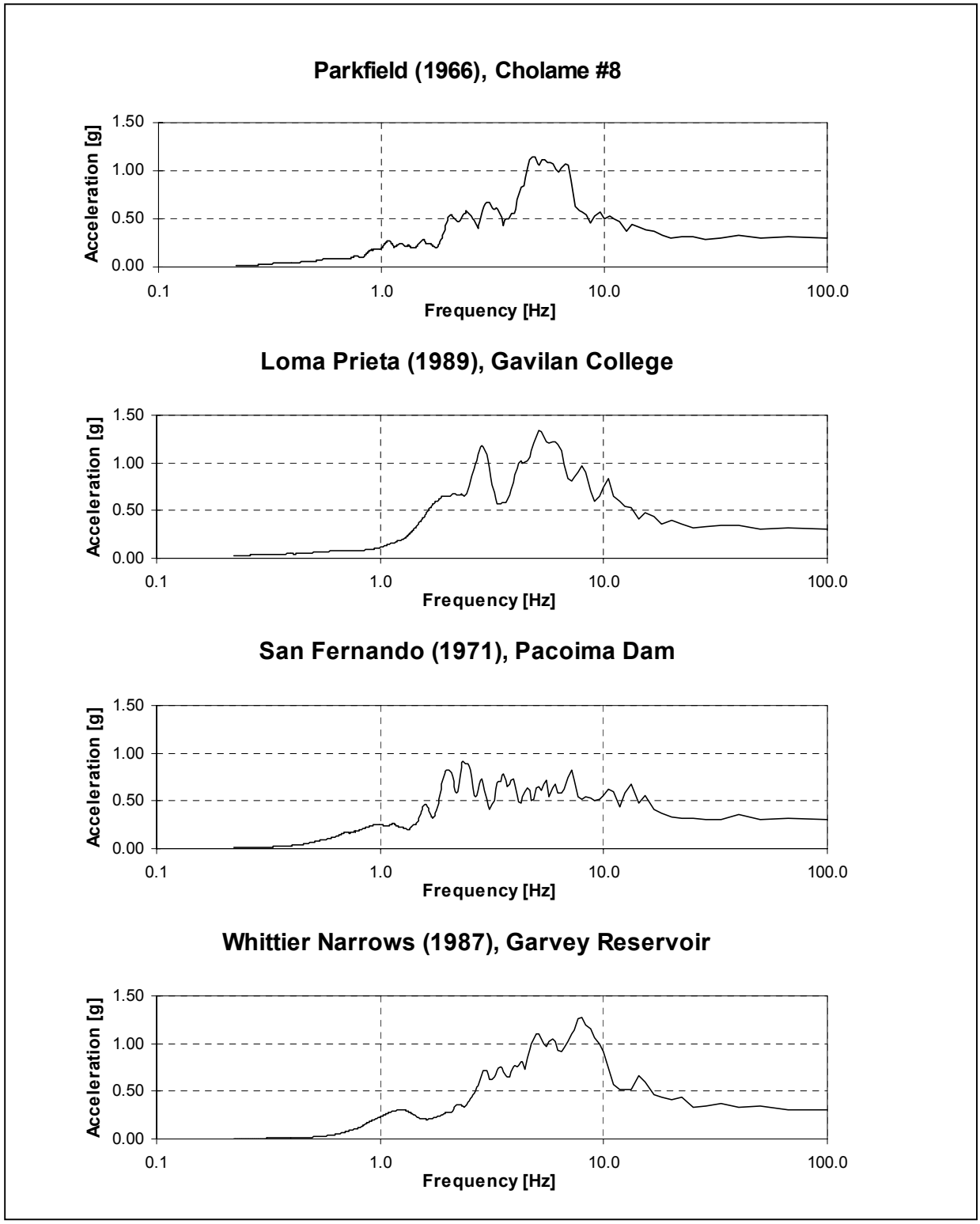

Figure 6.1-2. Response spectra for the ground motion acceleration time-histories used for analysis

6.1-5 Finite Element Analysis

The analysis in this study was restricted to the determination of the in-plane response of the critical section, which corresponds to the tallest nonoverflow monolith (monolith 11). This section was analyzed using a 2-D finite element model. The height of the monolith is 82.4 m (270.5 ft), the base is about 61 m (200 ft), and the downstream face of the section exhibits a constant-radius transition between the crest and the main body. Figure 6.1-3 shows the geometry and the finite element mesh used for the analysis. The 2-D section was modeled with 260 eight-node isoparametric elements. The foundation was assumed rigid. Assuming incompressibility of the fluid, the presence of the reservoir was incorporated into the model by a consistent added mass matrix. Linear viscous damping was represented using a proportional damping, and a 5 percent damping ratio was selected for the fundamental mode. The analyses were performed using the computer program, which computes the dynamic response of the system by implicit direct time integration of the equations of motion.

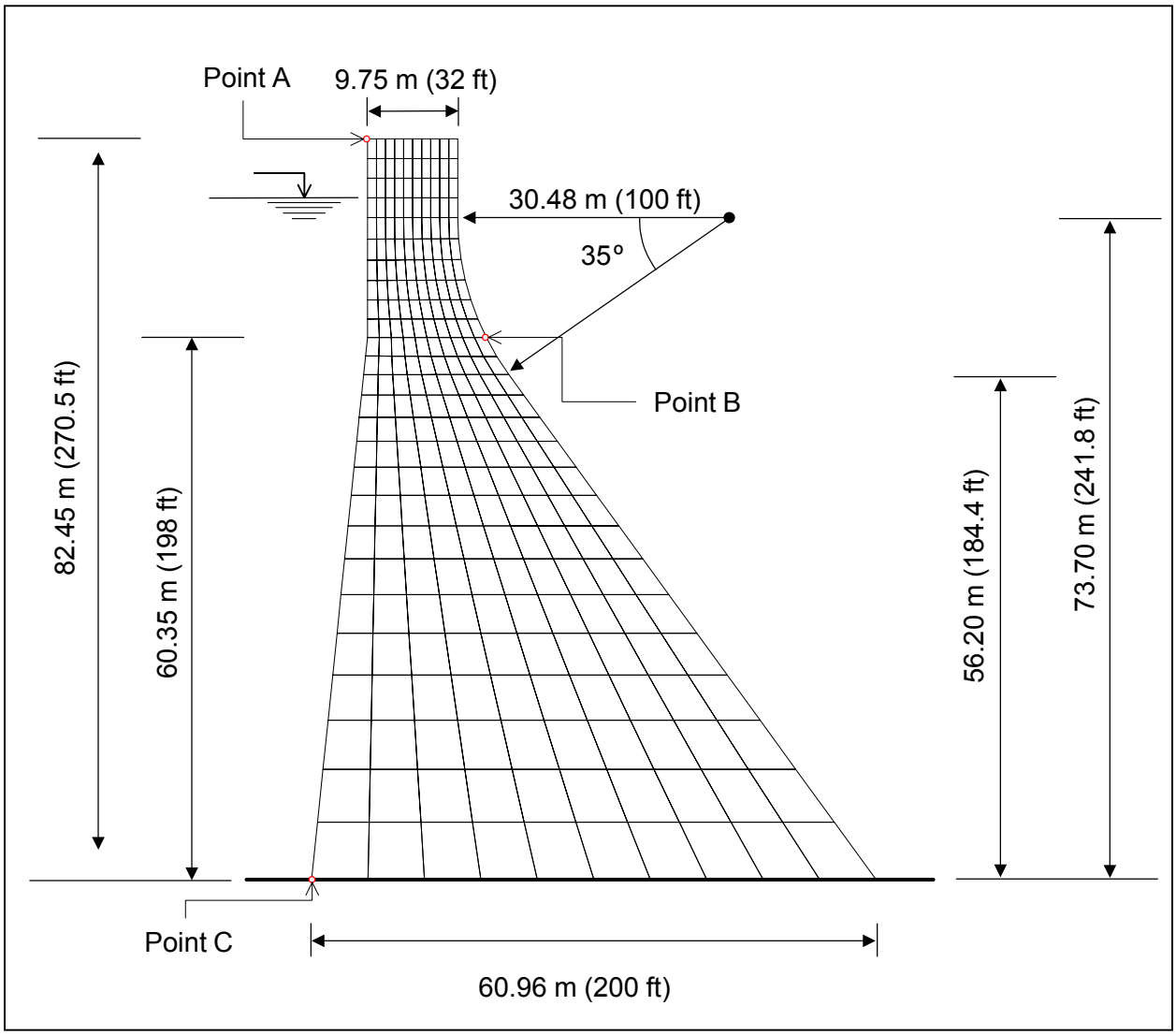

Figure 6.1-3. Section geometry and finite element model

6.1-6 Material Properties

Extensive studies have been performed to characterize the material properties of the concrete (Hall, Woodson, and Nau 1989). A summary of the results corresponding to the series of tests performed at the University of California at Berkeley is presented in Table 6.1-2.

Table 6.1-2
Summary of Test Results (Raphael 1986)

Parameter		Value
Modulus of elasticity	Static	37,576 MPa (5.45 10^6 psi)
	Dynamic	41,024 MPa (5.95 10^6 psi)
Poisson's ratio	Static	0.18
	Dynamic	0.20
Splitting tensile strength	Static	2.50 MPa (363 psi)
	Dynamic	3.72 MPa (539 psi)

The values of the material properties used in this numerical study are shown in Table 6.1-3. The values selected for the elastic modulus and the Poisson's ratio are based on the values recommended in the study by Raphael (1986).

Table 6.1-3
Material Properties Used for Analysis

Parameter	Value
Modulus of elasticity	40,679 MPa (5.90 10^6 psi)
Poisson's ratio	0.19
Unit weight (concrete)	24,820 N/m^3 (158 lb/ft^3)
Unit weight (water)	9,802 N/m^3 (62.4 lb/ft^3)

6.1-7 Dynamic Characteristics

The first ten natural frequencies are shown in Table 6.1-4, corresponding to both empty and full reservoir conditions. The mode shapes corresponding to the first four natural frequencies are shown in Figures 6.1-4 and 6.1-5. Note that the third mode is associated with mostly vertical motion. This association explains the fact that the third natural frequency appears not to be affected significantly by the presence of the reservoir. Figure 6.1-6 shows the relative change in frequency associated with the presence of the full reservoir for the first 10 natural frequencies. It can be observed that in general the frequencies are reduced about 80 percent with respect to the dry condition, with the exception of those corresponding to the third and sixth mode shapes, which are less sensitive to the presence of the reservoir.

Table 6.1-4
Natural Frequencies for Different Reservoir Conditions

	Empty		Full	
Mode	Period, sec	Frequency, Hz	Period, sec	Frequency, Hz
1	0.1802	5.5484	0.2218	4.5087
2	0.0817	12.2374	0.0996	10.0376
3	0.0580	17.2467	0.0591	16.9204
4	0.0440	22.7424	0.0549	18.2103
5	0.0290	34.5188	0.0374	26.7100
6	0.0271	36.9271	0.0296	33.7884
7	0.0208	47.9964	0.0277	36.0522
8	0.0198	50.4299	0.0252	39.7354
9	0.0189	52.9105	0.0245	40.8106
10	0.0172	58.1441	0.0220	45.3576

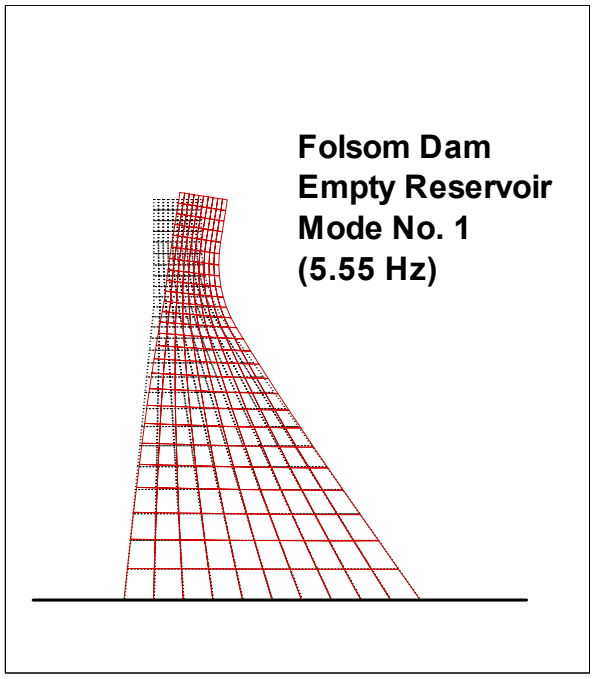

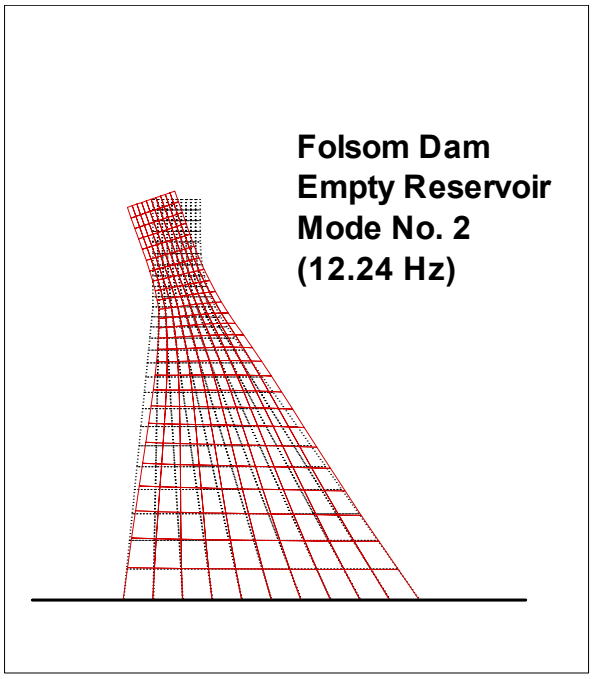

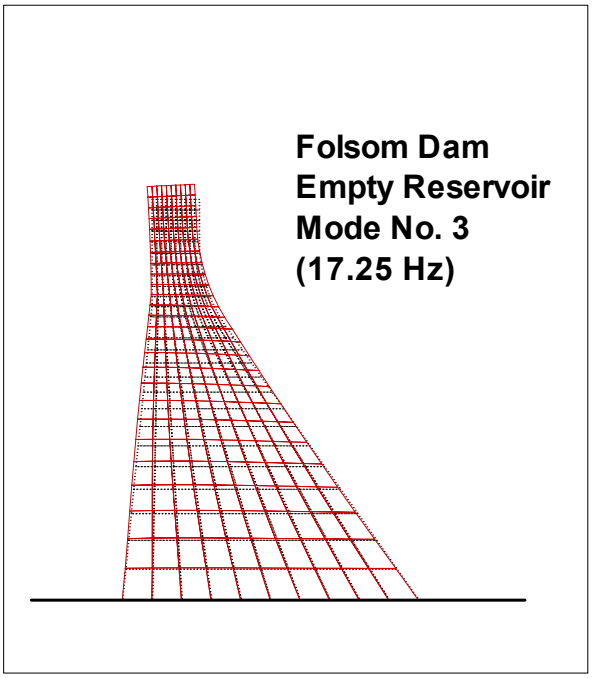

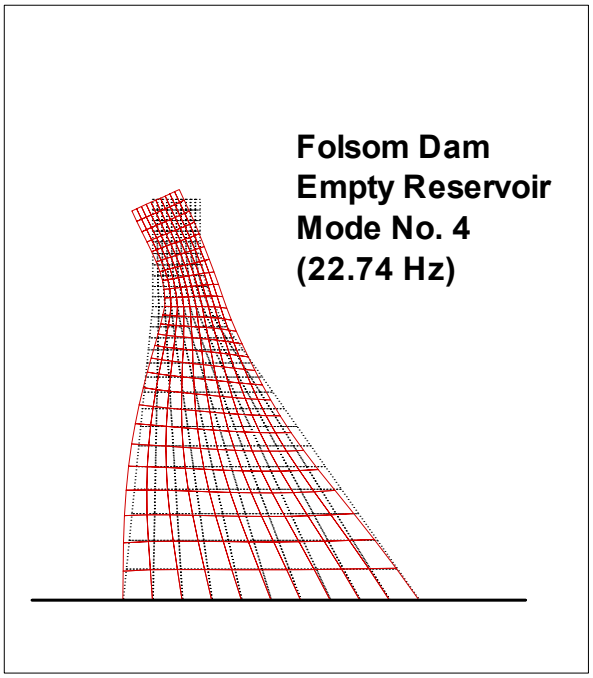

Figure 6.1-4. Mode shapes (empty reservoir)

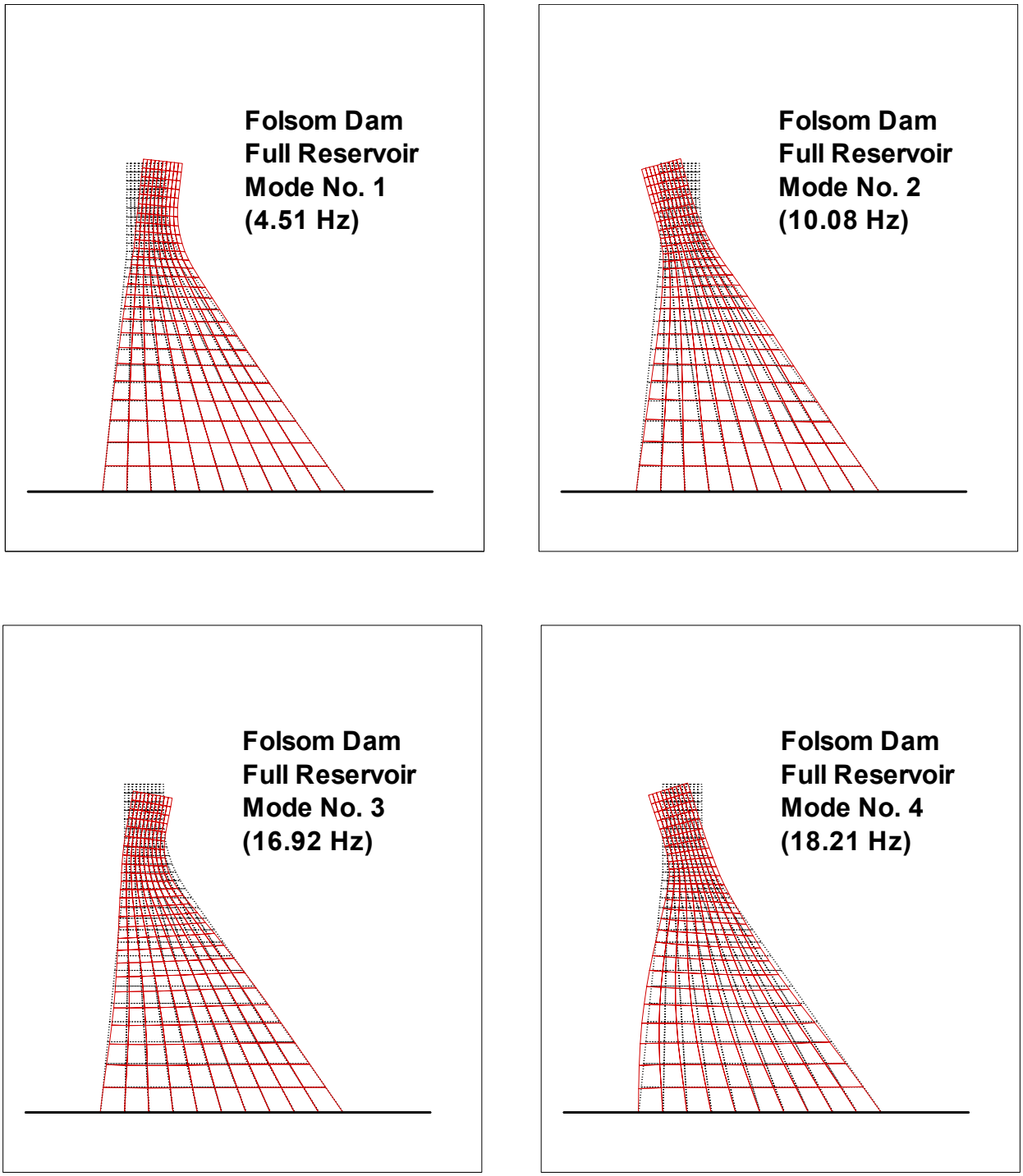

Figure 6.1-5. Mode shapes (full reservoir)

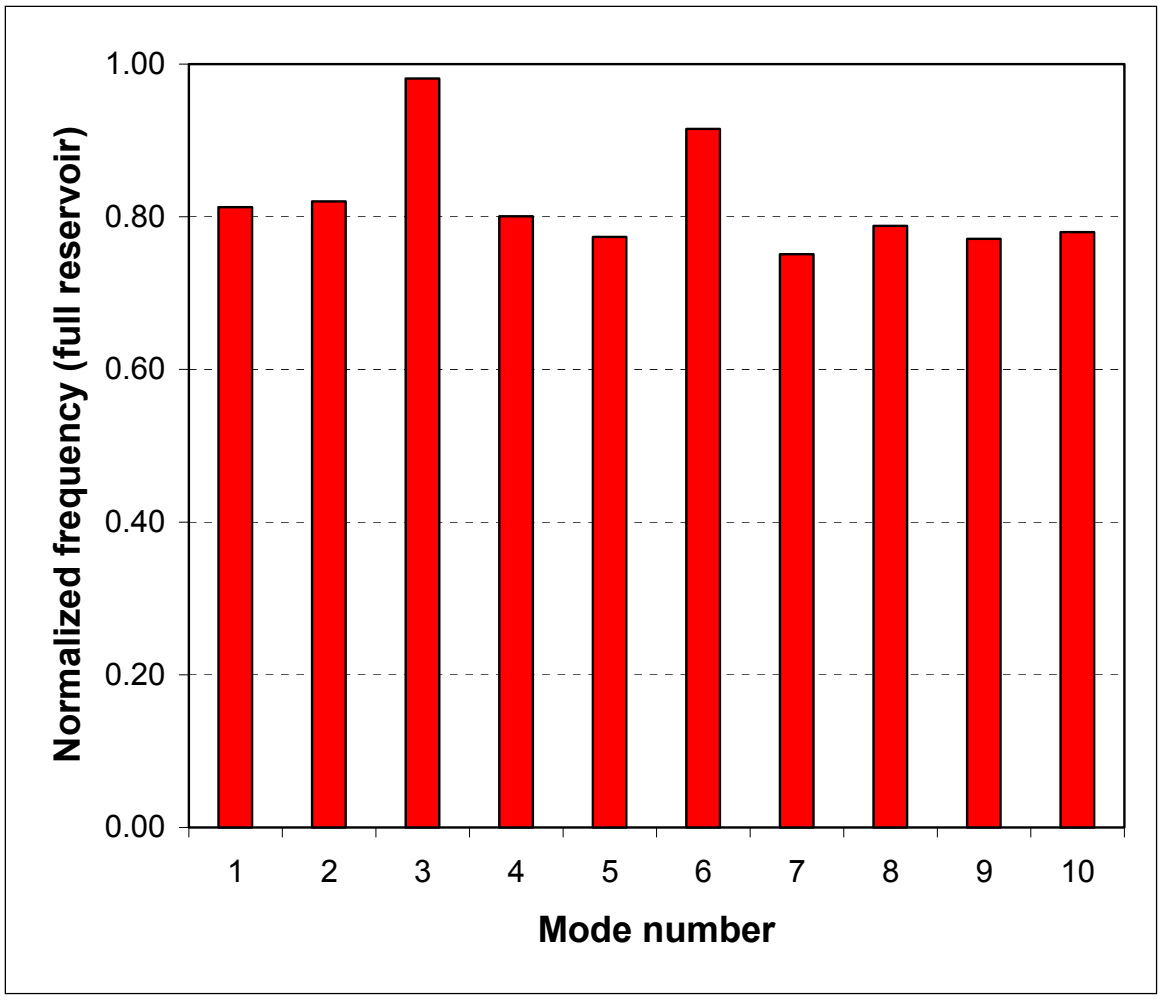

Figure 6.1-6. Effect of full reservoir condition on natural frequencies

6.1-8 Time-History Analysis

a. This section describes the results of the time-history analyses of the system subjected to different horizontal ground motions. Since the structure is not symmetric, the dynamic stresses on the upstream and downstream faces depend on the sign convention used to scale the ground acceleration record. To identify the critical loading condition, two analyses were performed for each earthquake, combining the initial static loading with the two opposite directions of horizontal excitation. Since the damage to a concrete dam is essentially associated with the development of tensile stresses, the critical loading condition for each earthquake is defined as the load combination that generates the higher tensile stress values in the section.

b. Table 6.1-5 compares the dynamic performance of the dam when subjected to the Loma Prieta earthquake for two different reservoir conditions. The presence of the reservoir not only affects the initial static loading condition through the incorporation of the corresponding hydrostatic forces, but it also modifies the dynamic characteristics of the system, as indicated previously. The table shows the peak value of horizontal dynamic displacement at the crest of the dam (Figure 6.1-3, point A), and the peak value of horizontal absolute acceleration at the same location. The table also shows the maximum value of total principal stress within the section, including the static loading contribution. The results show that the system

exhibits an overall increase in the response quantities associated with the full reservoir condition. In particular, the displacement and total

Table 6.1-5
Performance for Different Reservoir Conditions (Loma Prieta)

Reservoir Condition	Peak Crest Displacement (Dynamic)	Peak Crest Acceleration	Maximum Principal Stress (Including Static Loads)
Empty reservoir	1.85 cm (0.73 in)	2.45 g	4.62 MPa (669.84 psi)
Full reservoir	2.59 cm (1.02 in)	2.80 g	6.77 MPa (981.57 psi)

stress responses represent an increase of 134 and 146 percent, respectively, with respect to the response quantities associated with the empty reservoir condition.

c. Next, the dynamic performance of the section was investigated for different input ground motions for the full reservoir condition. The results are presented in Figures 6.1-7 to 6.1-10 for each ground motion. These figures show the time-histories for the horizontal components of displacement and absolute acceleration at the crest of the dam. The crest displacement is measured with respect to the base motion, and only the dynamic component of the displacement is considered in the figures. The figures also show the time evolution of the maximum principal stress at point B (Figure 6.1-3). The initial (static) loading state is included in the total stress computations. As indicated below, point B represents the critical location for the Loma Prieta, Parkfield, and Whittier Narrows ground motions. It is observed that for these ground motions, the principal stress time-histories show some pulses exceeding the recommended value of apparent tensile strength, 4.83 MPa (Raphael 1986). However, for this level of ground excitation (0.3 g), these tensile pulses are isolated and do not represent a continuous series of excursions beyond the tensile strength threshold.

d. Figures 6.1-11 to 6.1-14 show the contours of maximum principal stress corresponding to each earthquake, including the initial (static) loading. These stress contours represent the distribution of the peak values reached by the maximum principal stress at each point within the section. The figures show that the highest values of tensile stress occur along the downstream and upstream faces. The contour plots also show the stress concentration induced by the downstream transition between the crest and the main body of the section. The time-history results are summarized in Table 6.1-6. The four ground motions used in the analysis are indicated in the first column of the table. The second column shows the peak value of the dynamic crest displacement for each ground motion, whereas the third column shows the corresponding dynamic magnification, defined as the ratio between the peak absolute values of crest and base absolute acceleration. The fourth column shows the peak value of the maximum principal stress within the section. For the Loma Prieta, Parkfield, and Whittier Narrows ground motions, this critical value exceeded the value of apparent tensile strength and it occurred on the upper part of the transition region on the downstream face, about 22.6 m (74 ft) below the crest (Figure 6.1-3, point B). On the other hand, the critical tensile stress value corresponding to the San Fernando ground motion did not exceed the tensile strength, and it occurred at the upstream base location (Figure 6.1-3, point C).

6.1-9 Conclusions

This numerical example confirms the importance of the ground motion selection for the accurate evaluation of the seismic performance of concrete gravity dams. The different earthquake records used in this numerical study (Loma Prieta, Parkfield, Whittier Narrows, and San Fernando) were scaled up to the same peak ground acceleration level. For this example, the Loma Prieta and Parkfield ground motions represent a more severe loading condition than the other two ground motions. The results show that the dynamic performance can exhibit significant variations in selected response quantities (peak crest displacement and acceleration, and critical maximum principal stress). This highlights the importance of the frequency characteristics of the ground motion to the response of the structural system.

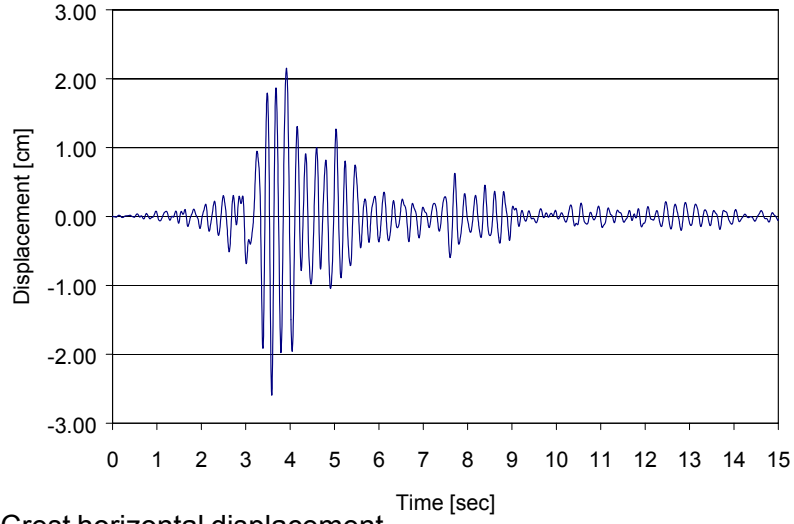

a. Crest horizontal displacement

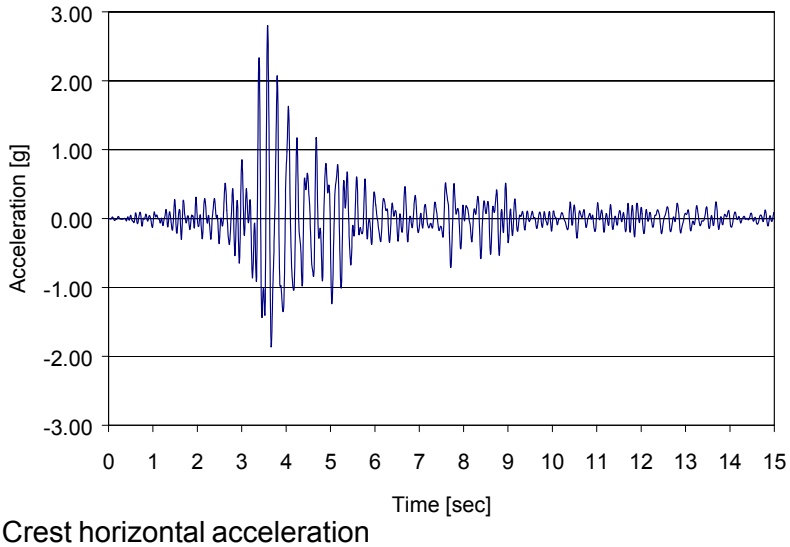

b. Crest horizontal acceleration

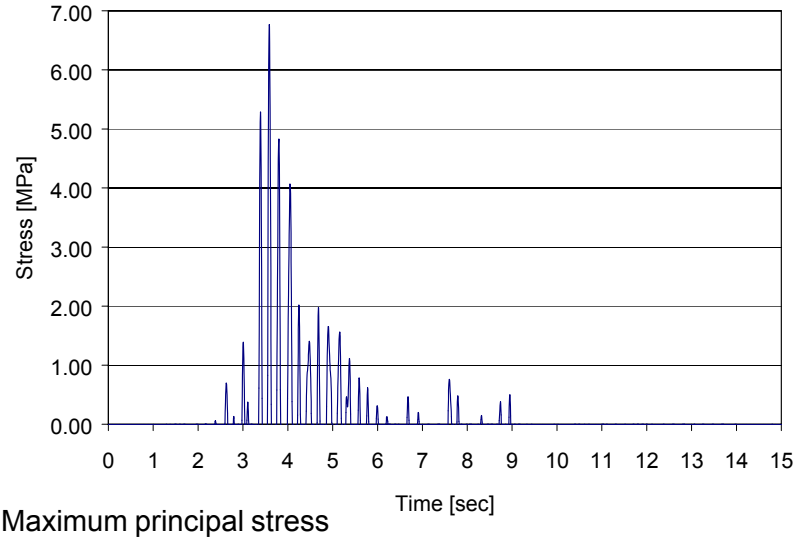

c. Maximum principal stress

Figure 6.1-7. Relative displacement and absolute acceleration time-histories at the crest, and maximum principal stress history at point B (Loma Prieta ground motion)

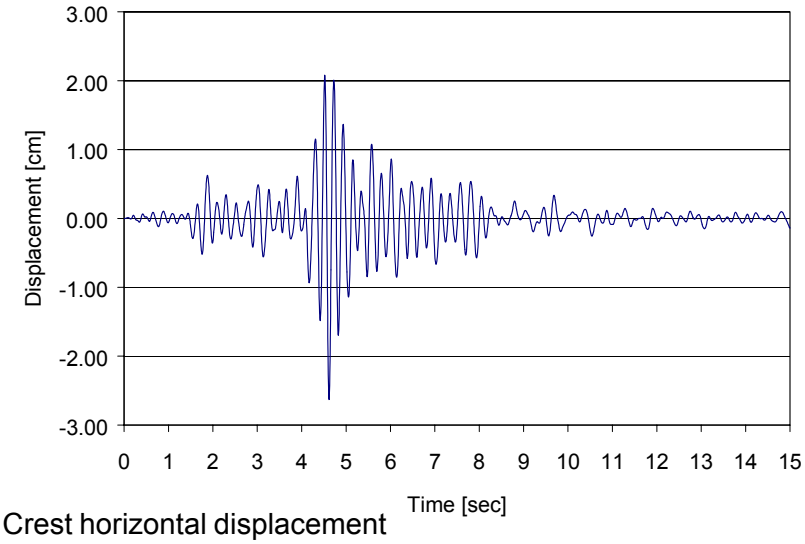

a. Crest horizontal displacement

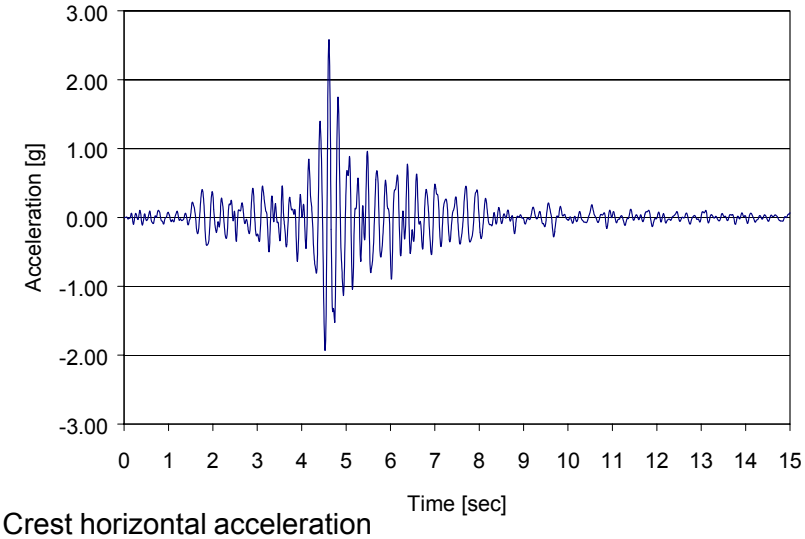

b. Crest horizontal acceleration

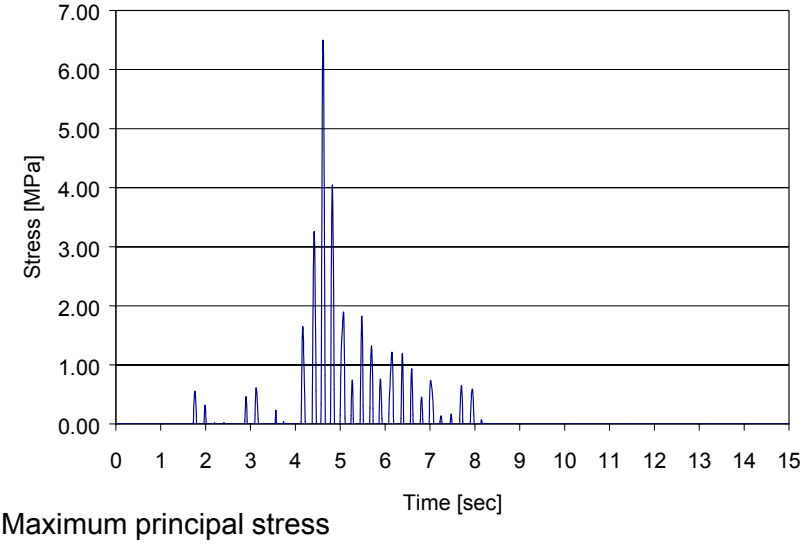

c. Maximum principal stress

Figure 6.1-8. Relative displacement and absolute acceleration time-histories at the crest and maximum principal stress history at point B (Parkfield ground motion)

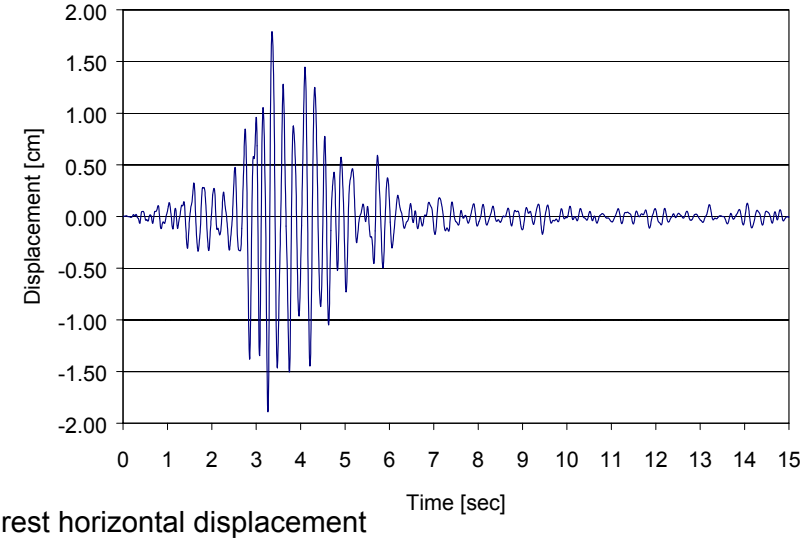

a. Crest horizontal displacement

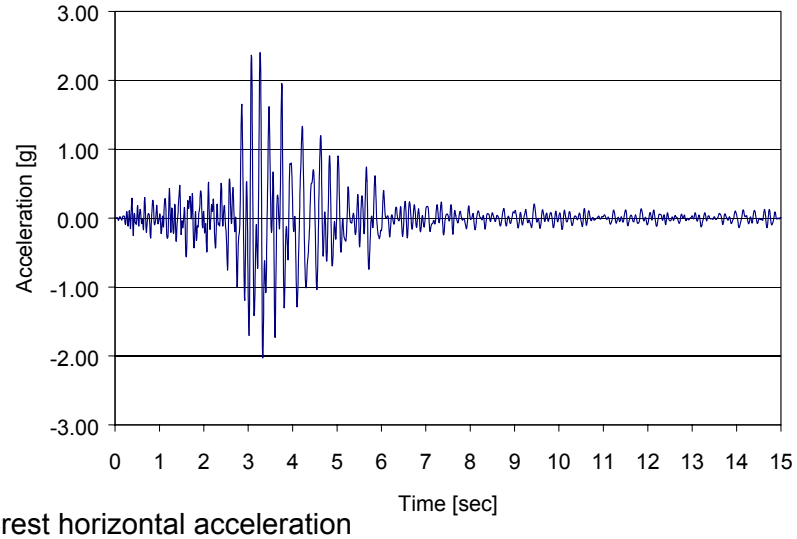

b. Crest horizontal acceleration

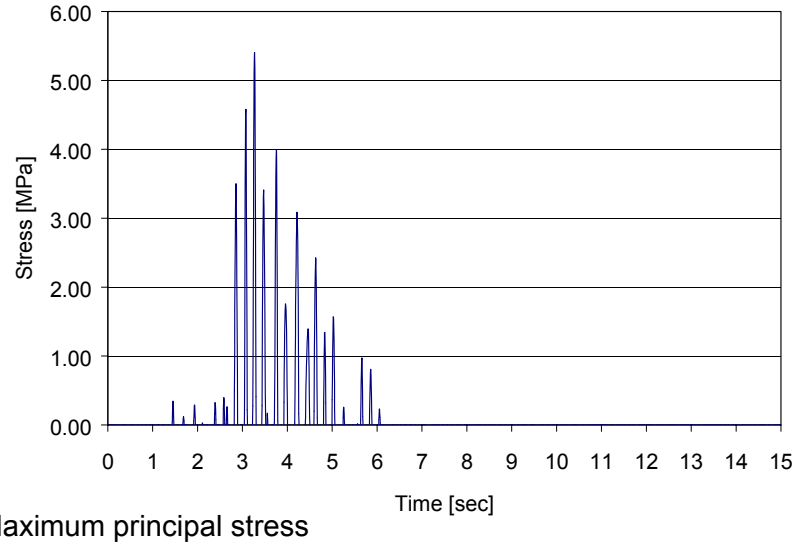

c. Maximum principal stress

Figure 6.1-9. Relative displacement and absolute acceleration time-histories at the crest and maximum principal stress history at point B (Whittier Narrows ground motion)

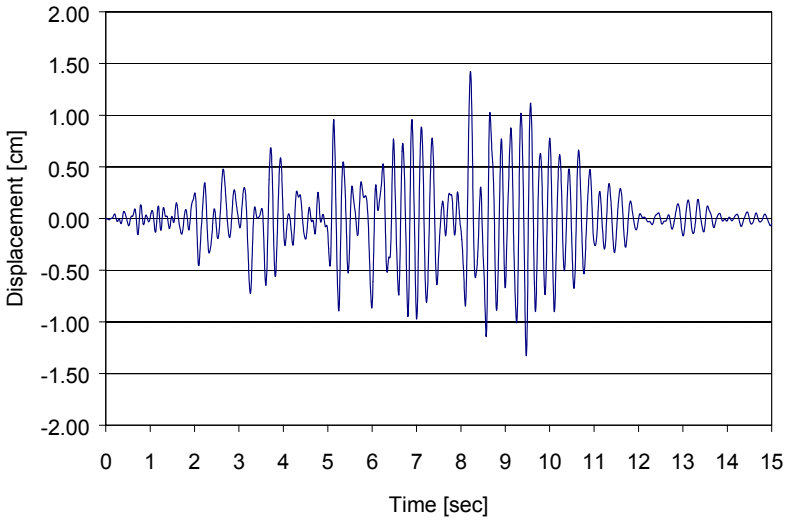

a. Crest horizontal displacement

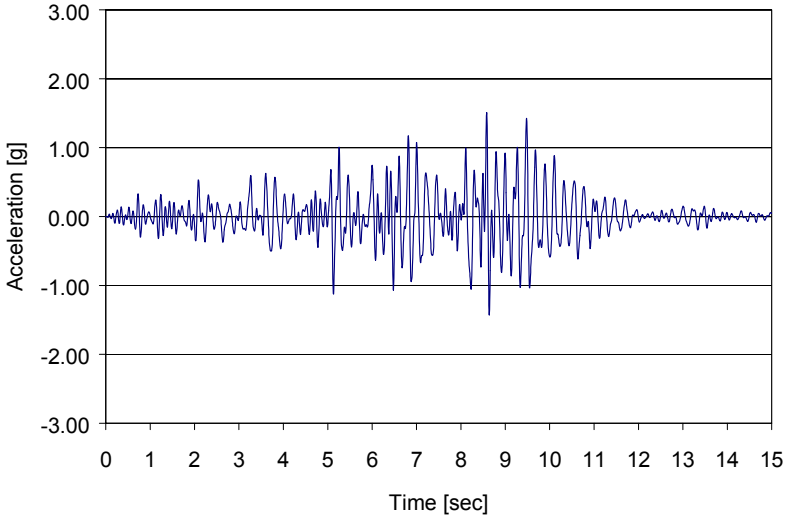

b. Crest horizontal acceleration

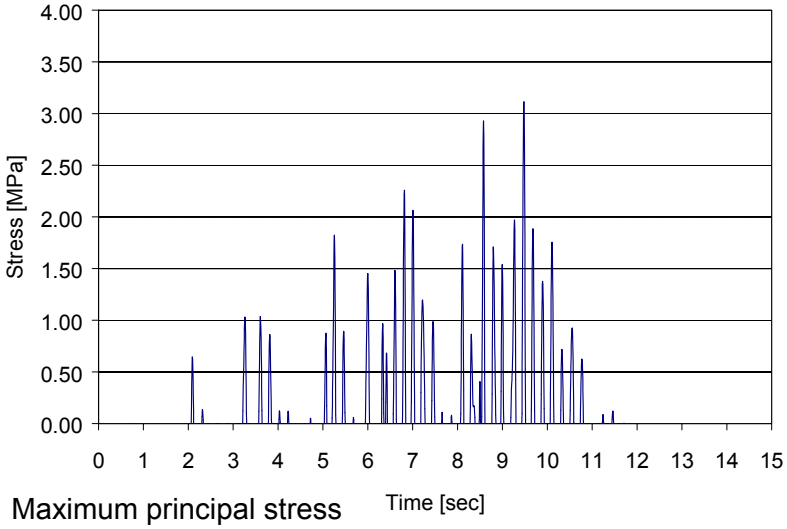

c. Maximum principal stress

Figure 6.1-10. Relative displacement and absolute acceleration time-histories at the crest and maximum principal stress history at point B (San Fernando ground motion)

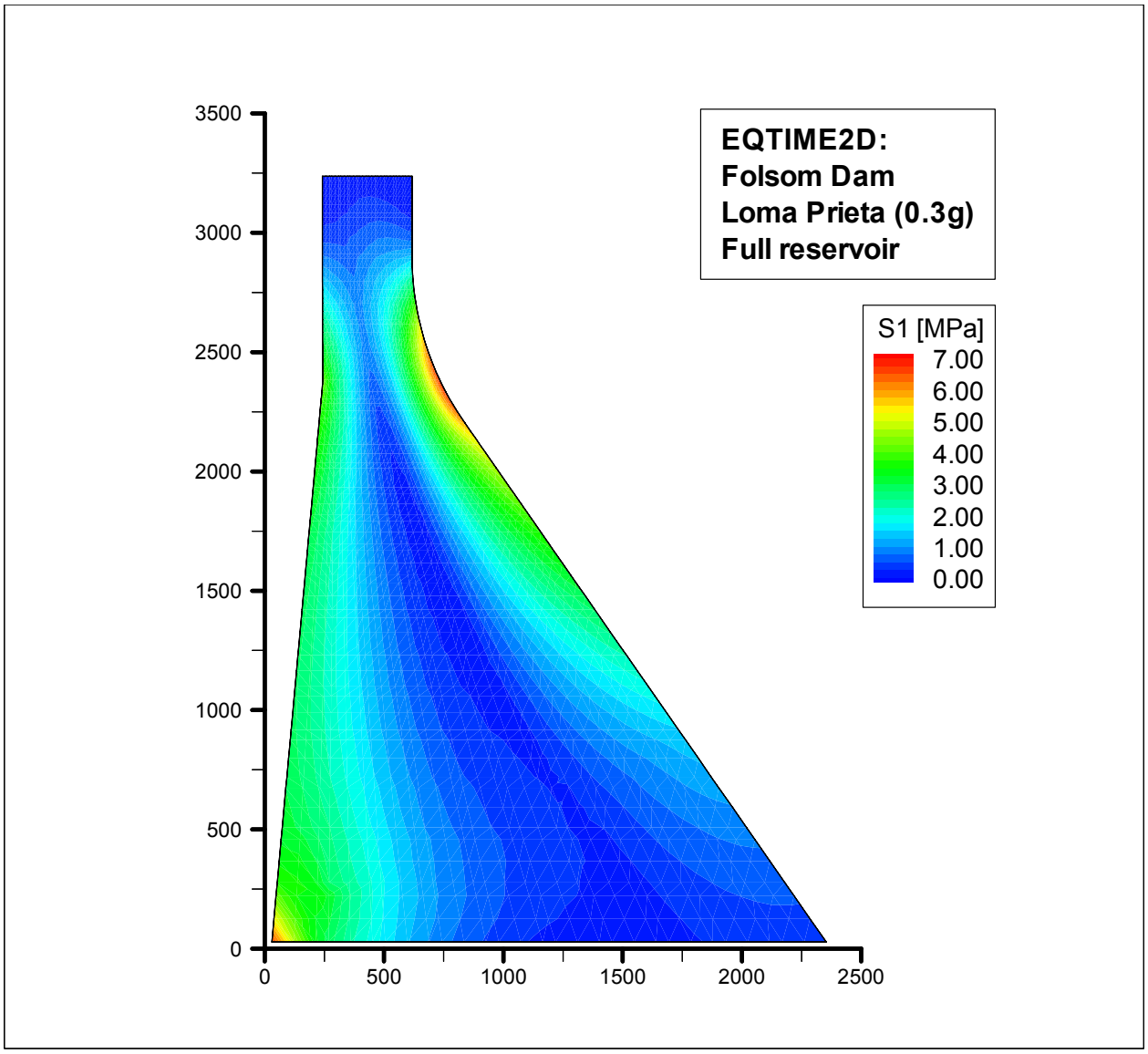

Figure 6.1-11. Maximum principal stress contour (Loma Prieta)

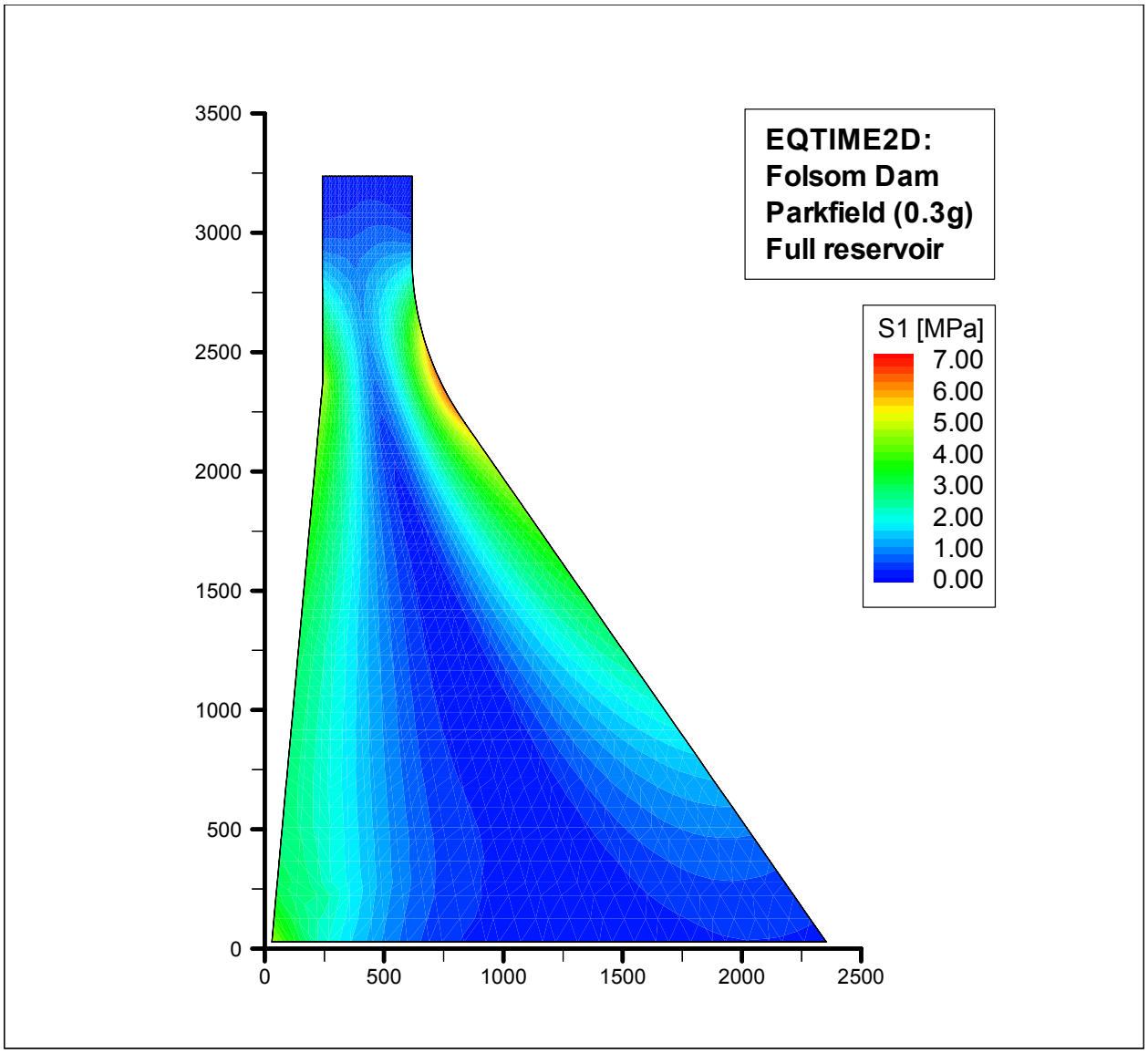

Figure 6.1-12. Maximum principal stress contour (Parkfield)

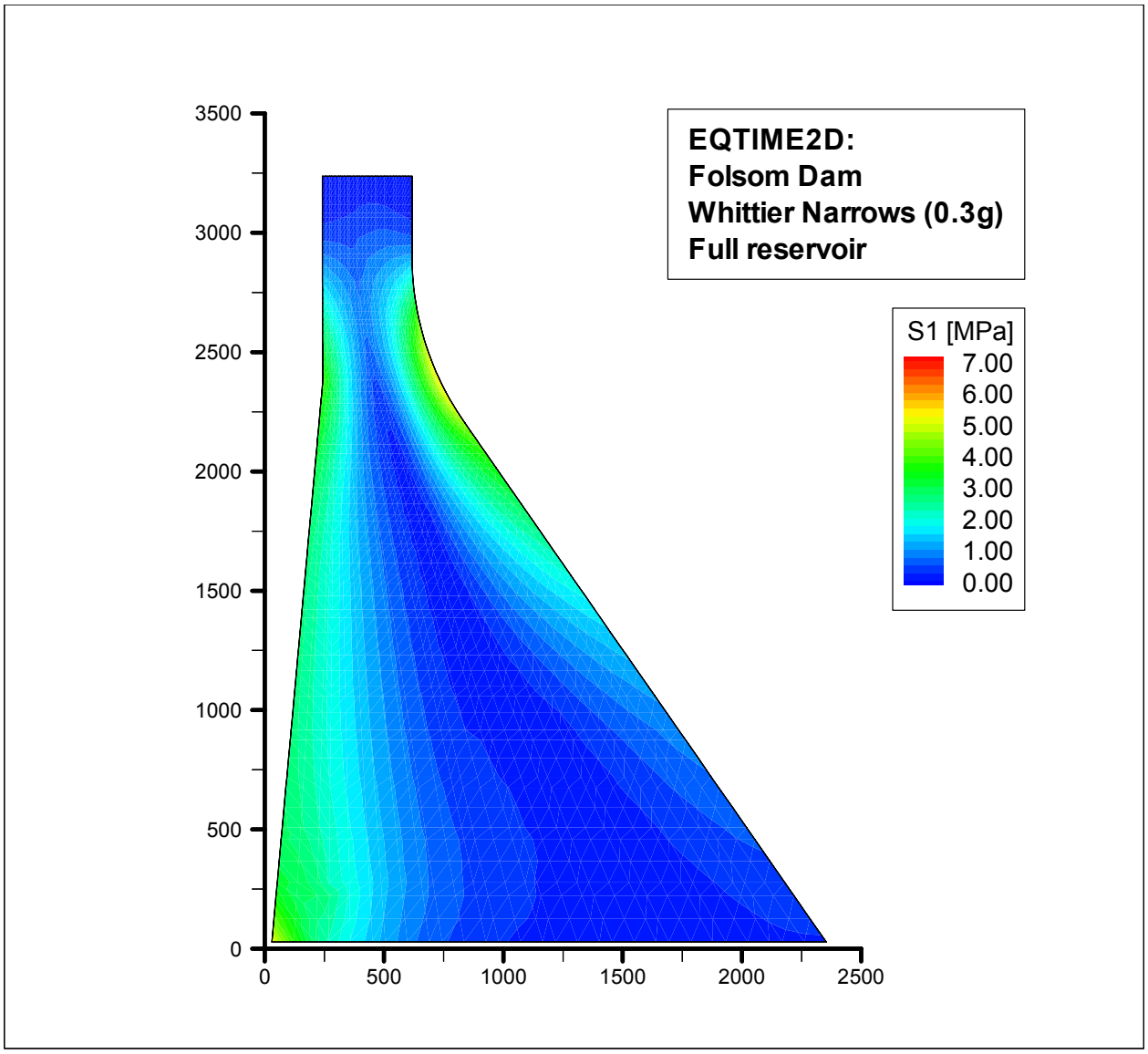

Figure 6.1-13. Maximum principal stress contour (Whittier Narrows)

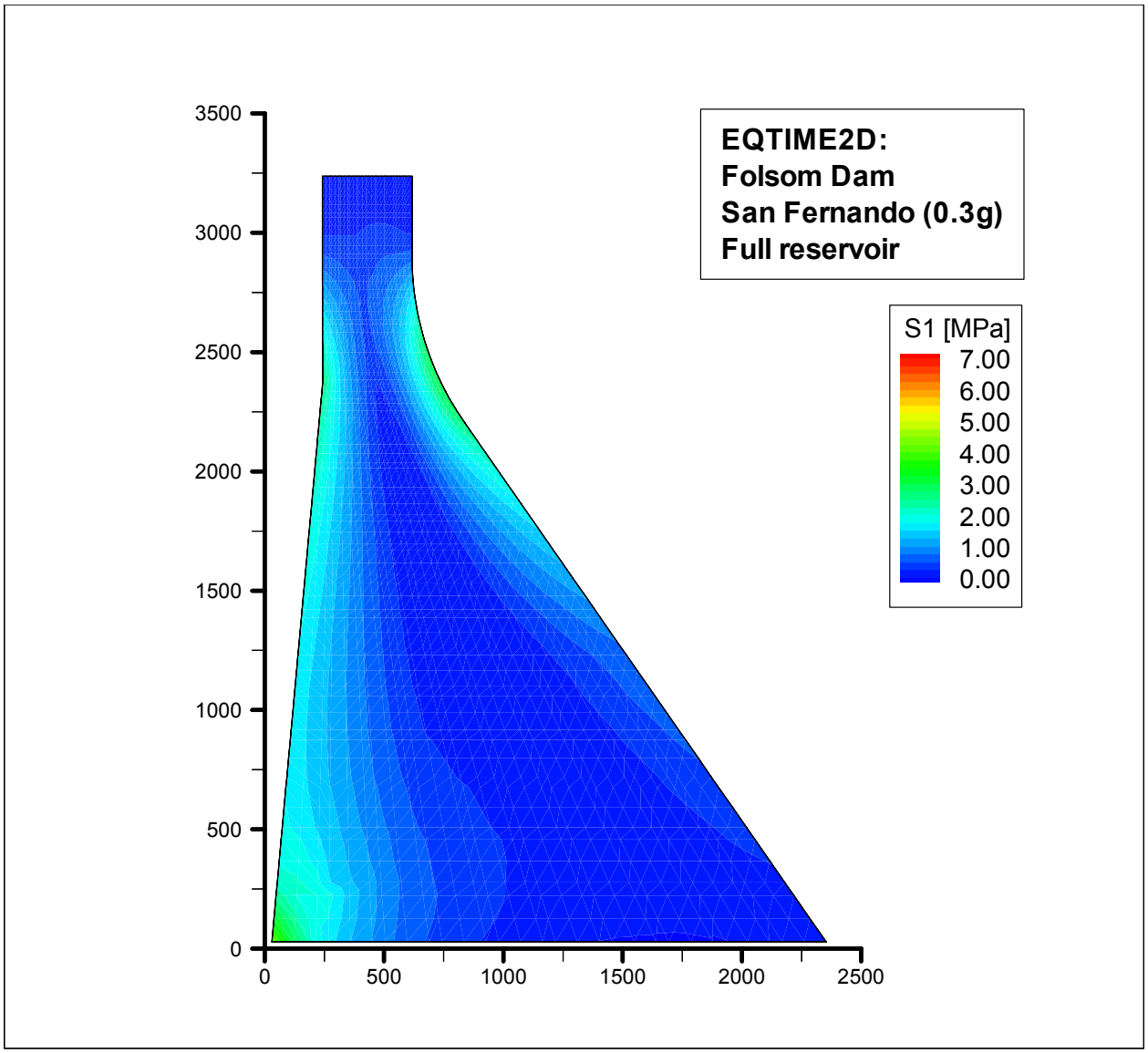

Figure 6.1-14. Maximum principal stress contour (San Fernando)

Table 6.1-6
Performance Comparison for Different Earthquakes

Ground Motion	Peak Crest Displacement (Dynamic)	Dynamic Magnification[1]	Maximum Principal Stress (Including Static Loads)
Loma Prieta	2.59 cm (1.02 in)	9.33	6.77 MPa (981.57 psi)
Parkfield	2.64 cm (1.04 in)	8.61	6.50 MPa (942.63 psi)
Whittier Narrows	1.88 cm (0.74 in)	8.01	5.41 MPa (785.05 psi)
San Fernando	1.42 cm (0.56 in)	5.03	4.24 MPa (614.27 psi)

[1] Ratio between peak absolute values of crest and base absolute acceleration.

6.2 Portugues Arch Dam

6.2-1 Background

Designed by the U.S. Army Engineer District, Jacksonville, Portugues Dam is a double-curvature three-centered arch dam to be built on the Portugues River approximately 4.5 km (2.8 miles) northwest of the city of Ponce, in south-central Puerto Rico. The 82.5-m- (270.6-ft-) high Portugues Dam is a multipurpose dam to be constructed in two phases. Initially, it will be built to a height of 67 m (219.6 ft) as a flood-control dam, and later it will be raised to its full height of 82.5 m and a crest length of 458.72 m (1,505 ft) for additional water supply and recreational benefits. The full-height Portugues Dam used in this example is 3.66 m (12 ft) thick at the crest and 12.20 m (40 ft) thick at the base. The dam includes an ungated, 45.7-m- (150-ft-) wide ogee spillway to the left of the crown section. In addition to the usual, unusual, and extreme static loading combinations, the dam was also designed to withstand the MCE and the 100-year OBE described in Section 6.2.4. The dam was initially analyzed using the response spectrum method of analysis, and later both the linear and nonlinear time-history analyses were also performed as a confirmation for the MCE.

6.2-2 Purpose and Objectives

The purpose of this section is to illustrate the application of linear time-history analysis to earthquake response computation of Portugues Arch Dam. The objectives of the time-history analysis are to compute dynamic characteristics of the dam-water-foundation system consisting of all significant vibration mode shapes and frequencies; to compute dam displacement and stress response histories under the combined vertical and two horizontal components of earthquake ground motions; and to present the results in the form of stress contour plots and stress time-histories for assessing the earthquake performance of the dam.

6.2-3 Scope

The scope of the study included the following:

- Definition of acceleration time-histories of design ground motion.
- Development of finite element models of the dam-water-foundation system.
- Computation of mode shapes and frequencies of the dam-water-foundation system.
- Analysis of static loading.
- Analysis of dynamic loading for four sets of earthquake acceleration time-histories.
- Evaluation of dam stresses under combined static and dynamic loads and their sensitivity to characteristics of acceleration time-histories. ‘

6.2-4 Earthquake Ground Motions

Based on a seismotectonic evaluation and earthquake ground motion assessment conducted for the Portugues Dam Site (Geomatrix Consultants 1988), two earthquakes were selected as the MCE and one earthquake as the OBE for design of the dam. The MCE ground motions were selected deterministically based on the maximum earthquake magnitudes on both near field and distant sources, the source-to-site distance, and attenuation effects. The OBE was selected based on these parameters and the earthquake(s) producing the

maximum ground motions at the site once in 100 years. The earthquakes selected for the design of Portugues Dam are listed in Table 6.2-1.

Table 6.2-1
Design Earthquakes for Portugues Arch Dam

MCE	M6-1/2 Earthquake on Salinas Fault at Distance = 18 km M8.0 Earthquake on Muertos Trough at Distance = 50 km
OBE	M7-3/4 Earthquake on Puerto Rico Trench at Distance = 85 km

The mean horizontal and vertical smooth response spectra for the controlling MCE ground motion associated with an M6-1/2 earthquake on Salinas Fault at a distance of 18 km from the dam are given in Figure 6.2-1. Also included in this figure are periods of vibration for Modes 1, 5, 10, and 20, so their respective spectral accelerations can be noted and compared.

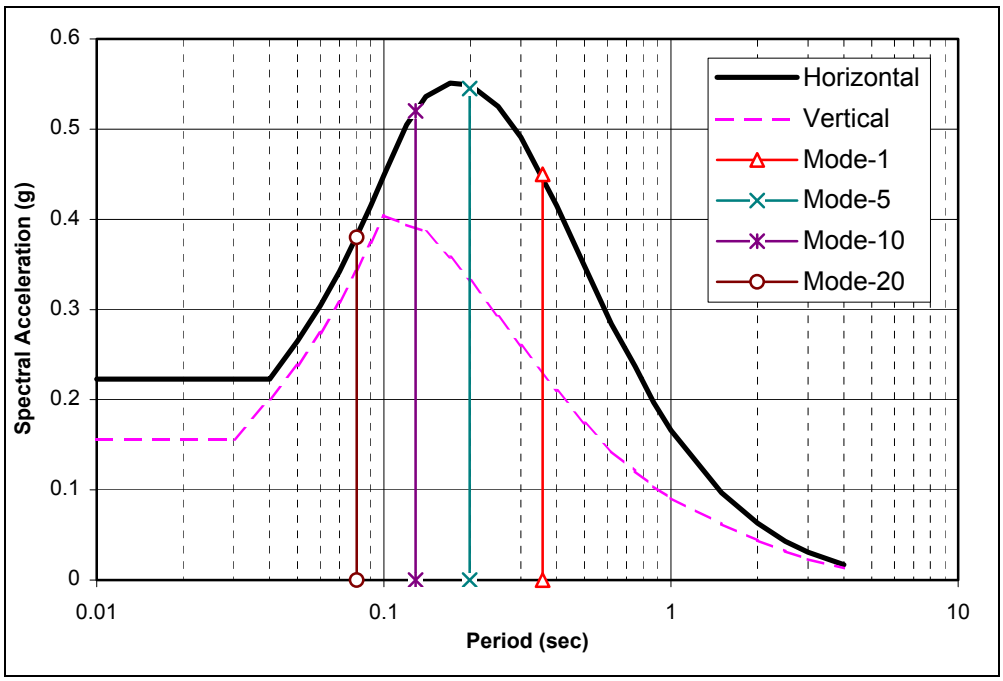

Figure 6.2-1. Horizontal and vertical smooth response spectra for MCE, M6-1/2 at distance of 18 km on the Salinas Fault (5 percent damping)

The acceleration time-histories employed in the design analysis (U.S. Army Engineer District (USAED), Jacksonville, 1990) were a set of spectrum-matched records shown in bottom graphs of Figures 6.2-2 to 6.2-4. The earthquake ground motions selected for this example consisted of the same spectrum-matched record and four additional natural records (Table 6.2-2). The natural records were scaled such that their response spectra in the range of significant periods of vibration of the dam are approximately at the level of the smooth design response spectra, in accordance with procedures outlined in Chapter 5. The natural records were selected from earthquakes with magnitudes in the range of 6.0 to 6-1/2, nearly the same as that for the controlling MCE event discussed previously. The acceleration time-histories of the scaled natural records and the spectrum-matched record are presented in Figures 6.2-2 to 6.2-4. Variation of these records in terms of frequency contents, duration of strong shaking, pulse sequencing, and the period of dominant pulses can easily be observed.

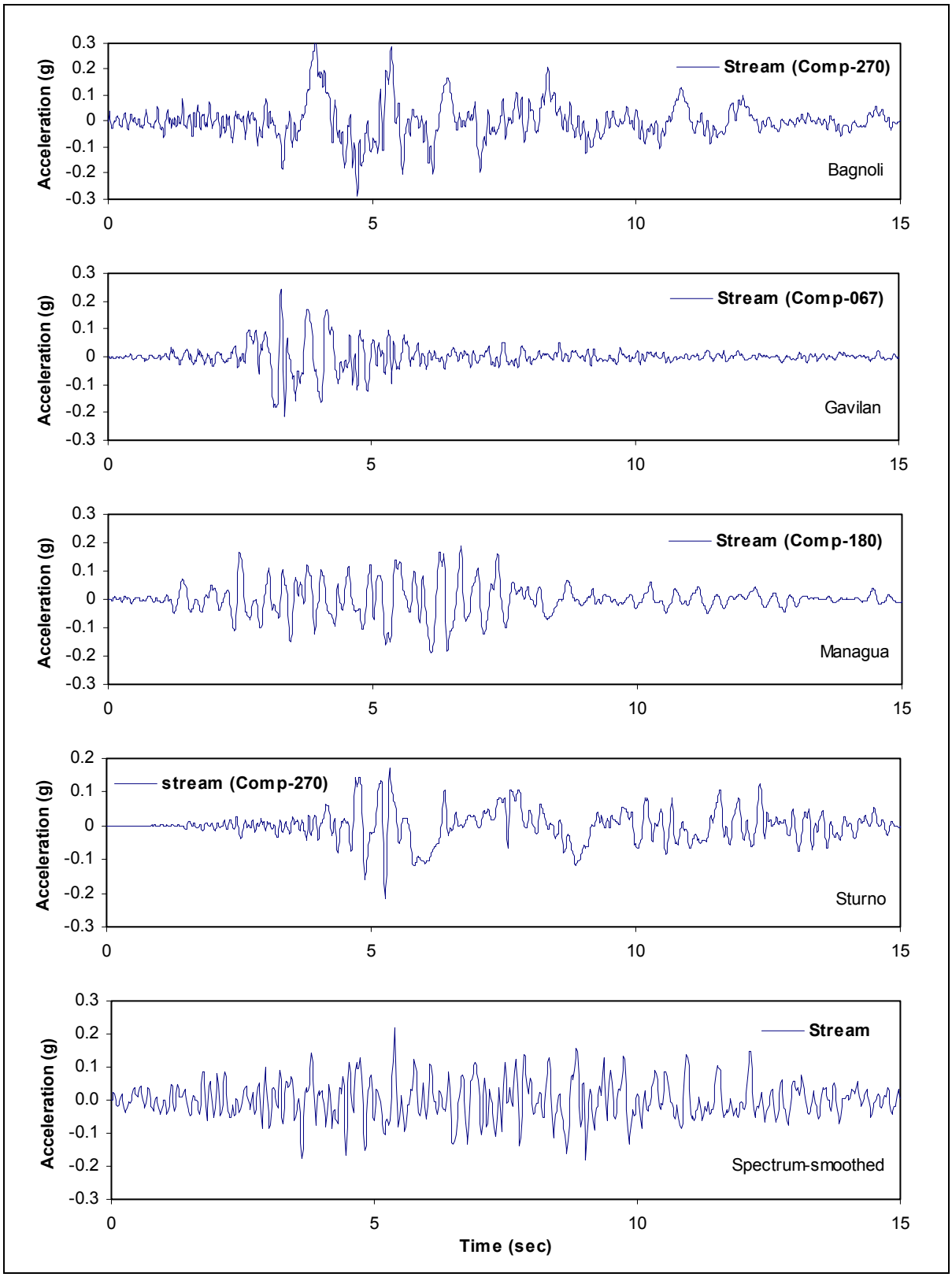

Figure 6.2-2. Acceleration time-histories of different sets of earthquake input ground motions applied in the stream direction

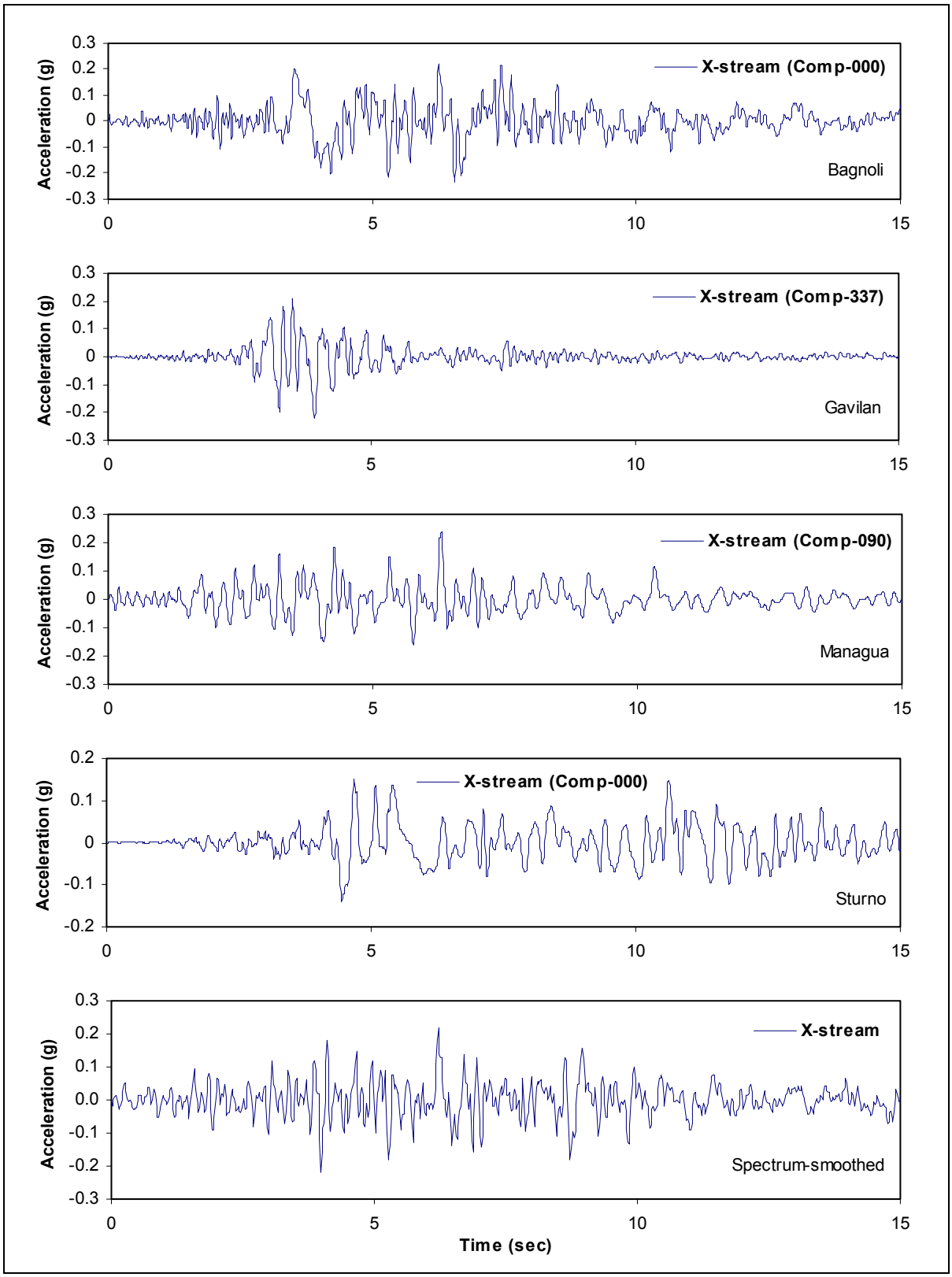

Figure 6.2-3. Acceleration time-histories of different sets of earthquake input ground motions applied in the cross-stream direction

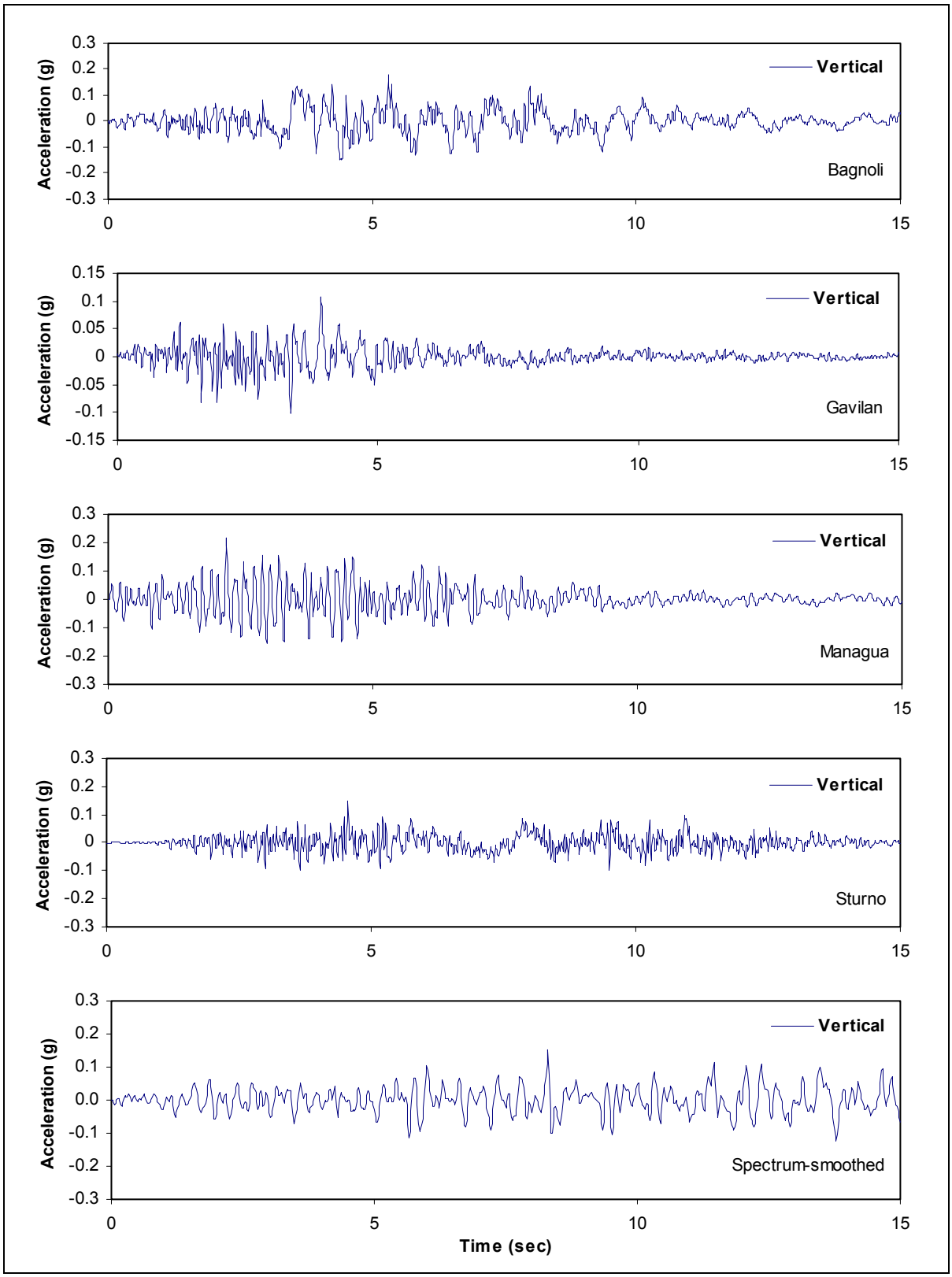

Figure 6.2-4. Acceleration time-histories of different sets of earthquake input ground motions applied in the vertical direction

Table 6.2-2
Natural Earthquake Records for Time-History Analysis

Station	Earthquake	Magnitude
Bagnoli Irpino	1980 Irpinia, Italy	6.5
Gavilan College	1989 Loma Prieta, Califorina	6.0
Managua	1972 Nicaragua	6.2
Sturno	1980 Irpinia, Italy	6.5

6.2-5 Selection of Analysis Procedures

The linear-elastic time-history analysis of arch dams is currently based on 3-D finite element procedures discussed in Chapter 2. Finite element models for the concrete arch, foundation rock, and the impounded water as well as loading combinations are developed according to criteria established in EM 1110-2-2201. Material properties are selected based on laboratory or in situ tests with the dynamic material properties reflecting the appropriate increases due to rapid rate of seismic loading. The ground motion acceleration time-history inputs for the dynamic analysis are developed or selected based on an earthquake hazard assessment of the site following the procedures discussed in Chapter 4. Interaction effects of the impounded water and foundation rock with the dam are included in the finite element stress analyses by modeling a sufficiently large portion of the foundation rock and the impounded water. Depending on the dynamic characteristics of the dam and the impounded water, a compressible or incompressible fluid mesh may be employed. When water compressibility is considered, the energy loss capability of the reservoir boundary arising from the absorption of pressure waves should be taken into account. Structural damping effects are included using a viscous damping coefficient proportional in scale to the severity of dam shaking during the earthquake. The performance of the dam is evaluated based on contours showing the extreme and instantaneous stress distribution over the entire dam at critical instants of time, as well as stress time-histories indicating magnitude and number of excursions of peak stresses beyond maximum allowable values and their relationship to surrounding stresses.

6.2-6 Finite Element Models

As described in Chapter 2, computer modeling and time-history analysis of Portugues Dam were performed using the computer program GDAP (Ghanaat 1993a). A brief description of the finite element models is given in the following section.

a. Dam model.

(1) The finite element model of Portugues Dam for this example was developed identical to that constructed by USAED, Jacksonville (1990), as shown in Figure 6.2-5. The arch structure was modeled using 56 thick-shell and 24 3-D-shell elements available in the computer program GDAP (Ghanaat 1993b). The use of a single layer of shell elements through the dam thickness was considered adequate for this thin arch dam. The thick-shell elements were employed to model the interior region of the dam where the shell behavior is dominant. The regions near the abutments were represented by 3-D-shell elements, which also facilitated the connection between the thick-shell and the solid elements of the foundation rock model.

(2) Both thick-shell and 3-D-shell elements are based on an isoparametric formulation and use quadratic geometry and displacement interpolation in the dam surface directions and linear interpolation through the thickness. The geometry of shell elements is defined by 16 nodes, 8 on each face. For thick-shell elements the 16 surface nodes are reduced to 8 midsurface nodes, each having five degrees of freedom (three translations and two rotations), while all the 16 surface nodes for the 3-D-shell elements, each having three translational degrees of freedom, are retained.

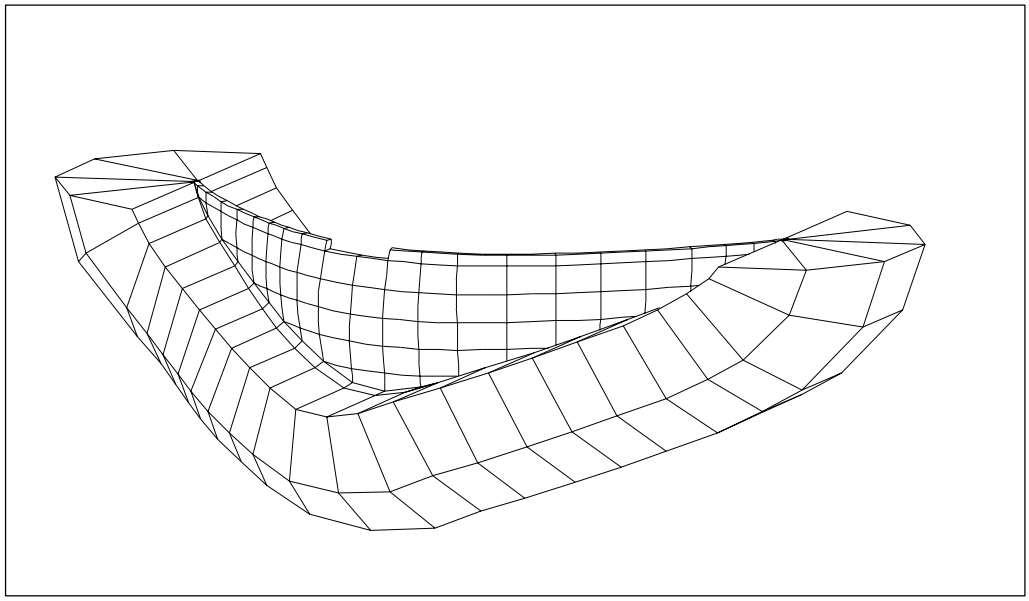

Figure 6.2-5. Finite element representation of Portugues Arch Dam and foundation rock

b. Foundation model. The finite element model of the foundation rock was constructed on the semicircular planes cut into the canyon walls perpendicular to the dam-foundation interface (Figure 6.2-5). The radius of the semicircle was selected equal to the height of the dam. The foundation mesh therefore extended one dam height in the upstream, downstream, and downward directions. Considering that the modulus ratio of rock to concrete was greater than 0.5, this foundation mesh size was judged adequate (EM 1110-2-2201). The foundation model included 176 eight-node solid elements with each node having three translational degrees of freedom. The foundation model was assumed to be massless, the assumption commonly used in practice to eliminate reflection of seismic waves at the fixed boundaries of the foundation model and to apply the earthquake records measured at the ground surface directly at the base of the foundation model.

c. Reservoir water model.

(1) The fundamental frequency for the impounded water at Portugues Dam with a maximum water depth of 56 m was estimated to be about 8.5 Hz. This frequency is more than twice the fundamental mode of the dam without water (2.97 Hz), indicating that the effects of water compressibility can be neglected (EM 1110-2-2201). Consequently the inertia forces of the impounded water were represented by the equivalent added-mass matrix coefficients applied to the upstream concrete nodes. The added mass of water was computed using a finite element mesh of incompressible water developed on the basis of site topography, as shown in Figure 6.2-6.

(2) The finite element mesh consisted of four layers of incompressible fluid elements that extended four times the water depth in the upstream direction. The fluid nodes at the dam-water interface matched the concrete nodes, and the nodes within the reservoir water were selected on one cylindrical section near the dam and on three plane sections away from the dam controlled by topography of the reservoir bottom. The dam-water interface includes forty 8-node curvilinear 2-D fluid elements, and the body of water was represented by one hundred sixty 16-node fluid elements. Both elements are based on isoparametric formulation and are described in Ghanaat (1993b).

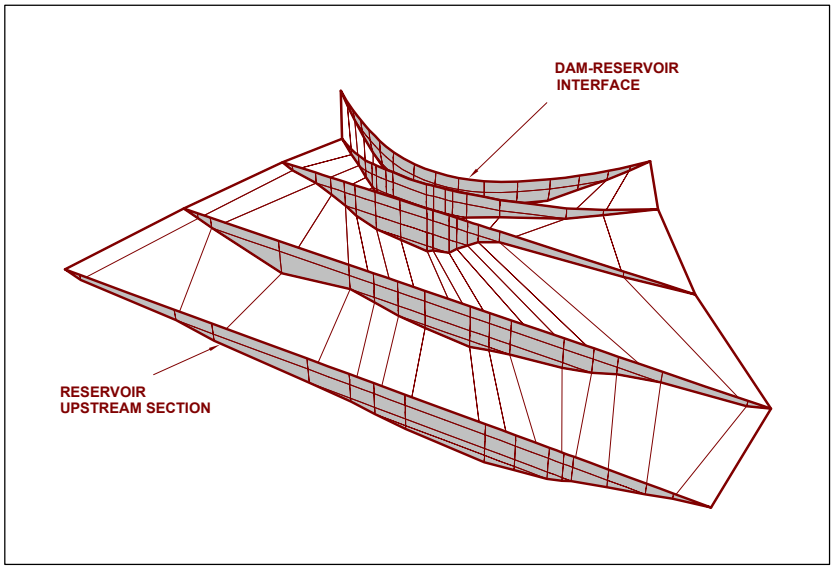

Figure 6.2-6. Finite element model of incompressible reservoir water

6.2-7 Material Properties

The material properties of the concrete dam and foundation rock for this example were based on test results published by USAED, Jacksonville (1986, 1988a, 1988b). The concrete material properties under static and dynamic loading are summarized in Table 6.2-3. These included modulus of elasticity, Poisson's ratio, and unit weight. A coefficient of thermal expansion of 5.4 H 10^{-6}/EF was used. The compressive and tensile strengths of the concrete also presented in Table 6.2-3 were employed for evaluation of the results. The foundation rock properties used in the analysis included a uniform deformation modulus of 13,793 MPa (2.0 H 10^{6} psi) and a Poisson's ratio of 0.2 for both static and dynamic analyses.

Table 6.2-3
Concrete Material Properties

Concrete	Static	Dynamic
Modulus of elasticity, MPa (psi)	13,790 (2,000,000)	33,095 (4,800,000)
Compressive strength, MPa (psi)	27.5 (4,000)	37.0 (5,400)
Tensile strength, MPa (psi)	3.1 (450[1])	5.75 (833[2])
Poisson's ratio	0.152	0.152
Weight density, kg/m^3 (pcf)	2,476 (154.6)	2,476 (154.6)

[1] USAED, Jacksonville (1988a).
[2] Apparent tensile strength obtained based on the results of modulus of rupture tests and modifications suggested by Raphael (1984).

6.2-8 Computation of Earthquake Response

The earthquake response of Portugues Arch Dam to various ground motions was obtained using the mode-superposition time-history method discussed in Chapter 1. The analysis usually consists of computation of vibration periods and mode shapes, evaluation of response of each individual mode to earthquake input using the step-by-step integration procedure (Chapter 3), and finally combination of the modal responses at each time-step in order to obtain the total response.

a. Dynamic characteristics of dam.

(1) The vibration frequencies and mode shapes required for the time-history earthquake analysis of Portugues Dam were obtained using the finite element models described in 6.2.6. The 20 lowest vibration frequencies and mode shapes were computed for both the empty and full reservoir conditions, as shown in Table 6.2-4. The results show that Portugues Dam has numerous closely spaced modes, 14 of which for the case with water are below 10 Hz and are expected to produce significant response to earthquake loading.

Table 6.2-4
Vibration Frequencies of Portugues Dam-Water-Foundation System

	Without Water		With Water	
Mode No.	**Period, sec**	**Frequency, Hz**	**Period, sec**	**Frequency, Hz**
1	0.337	2.966	0.354	2.823
2	0.280	3.568	0.291	3.440
3	0.255	3.920	0.272	3.684
4	0.230	4.356	0.234	4.282
5	0.196	5.116	0.198	5.056
6	0.169	5.923	0.171	5.862
7	0.148	6.772	0.153	6.551
8	0.130	7.679	0.147	6.822
9	0.128	7.799	0.131	7.643
10	0.117	8.540	0.129	7.741
11	0.114	8.780	0.116	8.626
12	0.103	9.673	0.112	8.930
13	0.102	9.803	0.106	9.425
14	0.099	10.076	0.103	9.724
15	0.096	10.423	0.098	10.161
16	0.093	10.794	0.095	10.488
17	0.087	11.523	0.093	10.774
18	0.083	11.984	0.084	11.862
19	0.080	12.564	0.081	12.297
20	0.077	12.993	0.080	12.444

(2) The computed mode shapes for the 10 lowest modes are displayed in the form of deflected shapes along the arch section, as shown in Figure 6.2-7. These modes represent various arch harmonic deflected shapes accompanied primarily by the first cantilever and a couple of second cantilever bending modes. The second cantilever bending means that the upper and lower parts of the dam deflect in the opposite directions (Modes 8 and 10).

b. Displacement results.

(1) Magnitudes of the maximum dam displacements are listed in Table 6.2-5, and the corresponding displacement histories for the stream direction are displayed in Figure 6.2-8. The results show that the displacements for the scaled Gavilan and Managua earthquake records are the largest with the maximum reaching a value of 38 mm at a location near the midcrest of the dam.

(2) An examination of the displacement histories indicates a predominant response frequency of about 3.5 Hz corresponding to the fundamental symmetric mode of the dam (see mode shapes in Figure 6.2-7). In particular, the displacement histories due to Gavilan and Managua excitations exhibit a much stronger and sustained harmonic response at 3.5 Hz, apparently caused by the presence of a predominant seismic pulse of about the same frequency in these earthquake records (Figure 6.2-2).

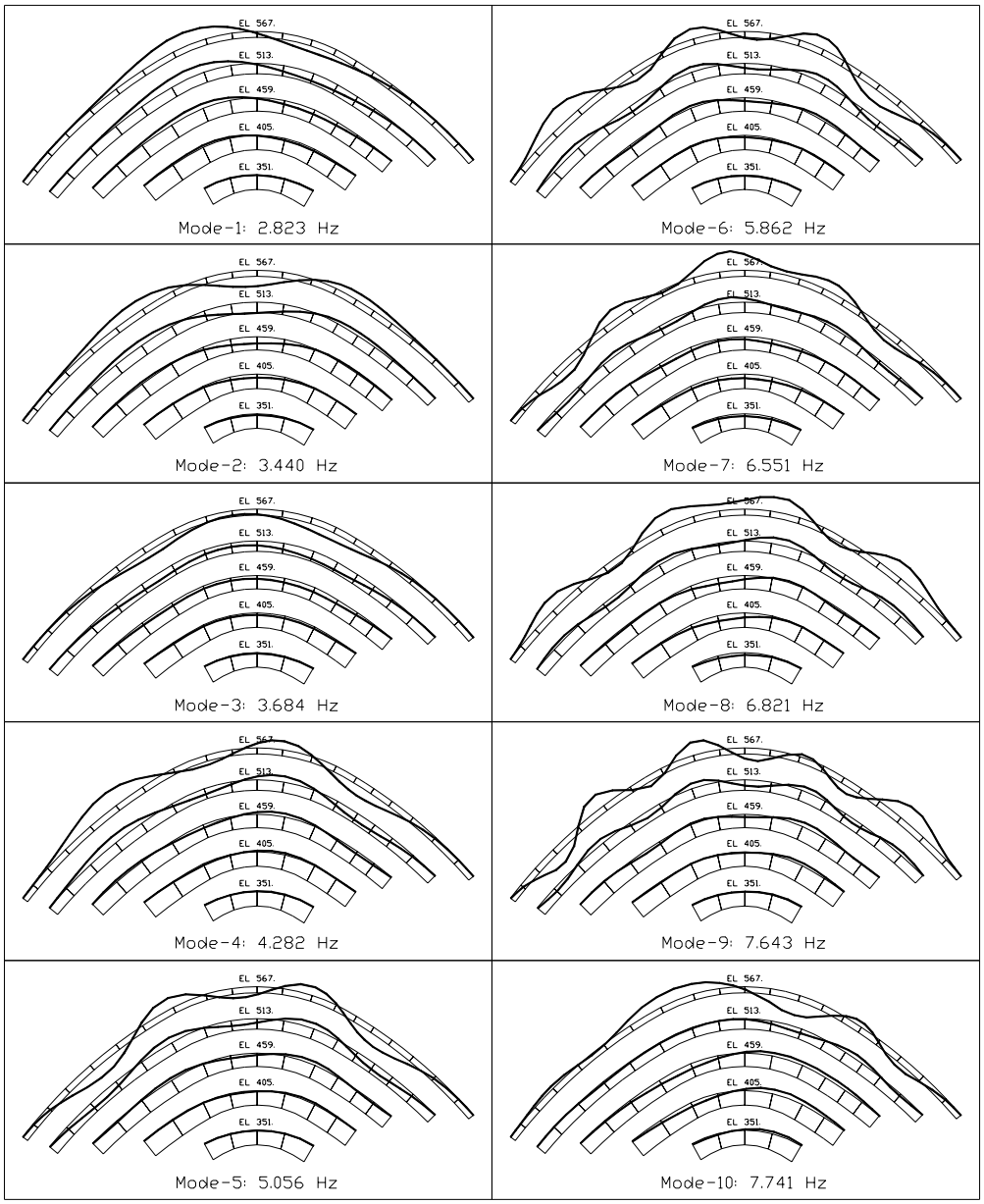

Figure 6.2-7. Ten lowest mode shapes of Portugues dam-water-foundation system

Table 6.2-5
Maximum Dynamic Displacements for Various Input Ground Motions, mm

Ground Motion	Node Number	X-stream	Stream	Vertical
Scaled Bagnoli	393[1]	8	22	2
Scaled Gavilan	637[2]	15	38	3
Scaled Sturno	637	11	29	3
Scaled Managua	637	15	38	3
Spectrum-matched	393	12	30	3

[1] At spillway crest elevation on right side of dam center.
[2] At spillway crest elevation on left side of dam center.

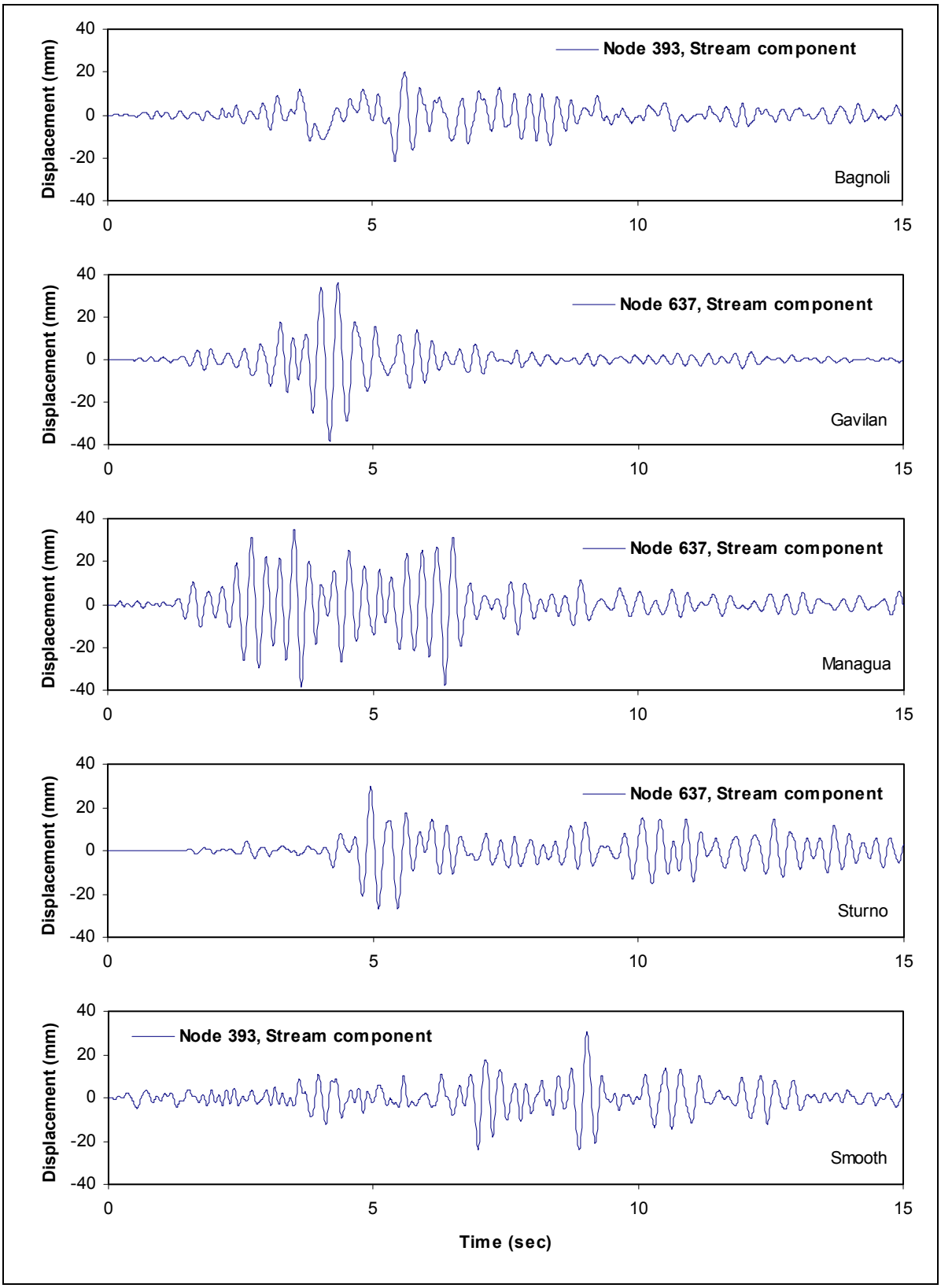

Figure 6.2-8. Maximum dynamic displacement histories due to different sets of three-component earthquake ground motions

c. Stress results.

(1) For evaluation of earthquake performance of the dam, the seismic stresses must be combined with stresses induced by the usual static load combination. The usual static load combination for Portugues Dam consisted of the gravity load due to the dead weight of the concrete, hydrostatic pressures of the impounded water, and the usual concrete temperatures. These loads were applied in a separate static analysis of the dam using the same finite element described in paragraph 6.2.6. The gravity loads were applied to individual cantilevers because they act on cantilever monoliths prior to the grouting of the vertical joints, while the hydrostatic pressures and temperature loads were applied to the monolithic structure.

(2) The maximum total stresses for the earthquake excitation plus the usual static load combination are summarized in Table 6.2-6. These represent the largest maximum arch and cantilever stresses that occur on the upstream and downstream faces of the dam during the particular earthquake excitation. Consistent with the displacement response histories discussed in *b* above, the Managua record gives the highest and Gavilan the second highest maximum tensile stresses.

Table 6.2-6
Maximum Tensile Arch and Cantilever Stresses for Various Input Ground Motions

Ground Motion	Scale Factor	Arch Stress MPa (psi)		Cantilever Stress MPa (psi)	
		Upstream	Downstream	Upstream	Downstream
Scaled Bagnoli	1.6526	3.9 (565)	4.0 (580)	2.2 (319)	3.5 (507)
Scaled Gavilan	0.6914	**5.9 (855)**	5.1 (740)	3.7 (536)	4.5 (652)
Scaled Managua	0.5682	**6.8 (986)**	**6.8 (986)**	4.4 (638)	4.6 (667)
Scaled Sturno	0.6106	4.3 (623)	3.4 (493)	3.0 (435)	2.8 (406)
Spectrum matched	1	4.9 (710)	4.7 (681)	2.7 (391)	3.3 (478)

(3) The minimum static plus seismic stresses were also evaluated to obtain the peak compressive stresses. The peak compressive stresses were well within the compressive strength of the concrete and thus are not discussed here.

(4) For each earthquake input, the stress results are also presented in the form of the envelopes of the maximum stresses, the concurrent or simultaneous stresses at critical time-steps, and the time-histories of critical tensile stresses. The envelopes of the maximum arch and cantilever stresses that usually occur at different times during the earthquake excitation are displayed in the form of stress contours, as shown in Figures 6.2-9 to 6.2-13. Each figure includes four contours showing the maximum tensile arch and cantilever stresses on the upstream (U/S) and downstream (D/S) faces of the dam. The results show that the peak tensile arch stresses occur primarily in the central region of the dam near the crest and peak tensile cantilever stresses at the dam-abutment contact regions and also at the base of the dam on the upstream side.

(5) These maximum tensile stresses are not concurrent; they rather show the maximum stresses that occur at any given locations some time during the earthquake ground shaking. For evaluation of the performance of the dam the concurrent or simultaneous stresses at the critical time-steps should also be examined. Thus for each earthquake input the concurrent stresses at the time of peak tensile arch stress were determined and are presented as stress contours in Figures 6.2-14 to 6.2-18. These so-called stress "snapshots" show that for Portugues Dam the critical tensile arch stresses occur simultaneously on both faces of the dam but are accompanied by compressive arch stresses on the lower part of the dam and compressive cantilever stresses on the upstream face.

(6) The significance of the tensile stresses in terms of producing joint opening or cracking is assessed from examination of the time-histories of the maximum tensile stresses. Stress time-histories corresponding

to the highest maximum tensile arch and cantilever stresses are displayed in Figures 6.2-19 to 6.2-23. Each figure includes two separate time-history graphs, one for arch stresses and another for cantilever stresses. The top graph shows the time-history of the maximum tensile arch stresses plotted together with arch stresses at the same location on the opposite face of the dam. Similarly, the bottom graph shows the time-history of the maximum cantilever stresses together with the cantilever stresses on the opposite face of the dam.

6.2-9 Evaluation of Results

a. Evaluation of the linear-elastic time-history analysis results for arch dams is based on the comparison of the computed stresses with the allowable values and consideration of several factors and engineering judgment. The factors commonly considered include the extent of overstressed regions, number and duration of stress cycles exceeding the allowable values, the ratio of computed to allowable limits, computed displacements, and the simultaneous stress distributions.

b. Usually two sets of allowable stress limits are specified, one for static and another for seismic, which accounts for the fast rate of seismic loading. A detailed description of allowable stress limits is given in EM 1110-2-2201. The Portugues Dam stress limits for the usual static and dynamic loads are listed in Table 6.2-7 (USAED, Jacksonville 1990). The allowable compressive stresses are obtained from the compressive strength of the concrete by applying an appropriate factor of safety, whereas the allowable tensile stresses are taken equal to the tensile strength of the concrete (EM 1110-2-2201).

Table 6.2-7
Concrete Strengths and Allowable Stresses for Usual Static and Seismic Loading

Concrete	Static **MPa (psi)**	Dynamic **MPa (psi)**
Compressive strength	27.5 (4,000)	37.0 (5,400)
Tensile strength	3.10 (450)	5.75 (833)
Allowable compressive stress	7.0 (1000)	24.8 (3,600)
Allowable tensile stress	3.10 (450)	5.75 (833)

c. A comparison of the maximum tensile stresses in Table 6.2-6 and Figures 6.2-9 to 6.2-13 with the allowable limits given in Table 6.2-7 indicates that only arch tensile stresses for the Gavilan and Managua earthquake excitations exceed the dynamic tensile strength of the concrete. However, it is important to note that the tension resistance capability of the vertical contraction joints in arch dams is limited and is expected to be much less than the tensile strength of the intact concrete. As a result the presence of net tension across the vertical contraction joints may be interpreted as the contraction joint opening. In the case of Portugues Dam, the concurrent stress contours in Figures 6.2-14 to 6.2-18 show tensile arch stresses on both faces of the dam, an indication that momentary joint opening would occur. The time-histories of arch stresses in Figures 6.2-19 to 6.2-23 demonstrate that although the joint opening may occur repeatedly during the earthquake excitation, duration of each joint opening is only a fraction of a second and should not cause any significant damage. The fact that Portugues Dam would safely withstand such joint opening was verified by a nonlinear time-history analysis of the dam that permitted contraction joints to open whenever nonzero tension forces were indicated across the joints (QUEST Structures 1990). The amount of joint opening is expected to be the highest for the Managua record and the second highest for the Gavilan record.

d. The maximum tensile cantilever stresses for all earthquake excitation cases meet the required dynamic tensile strength of 5.75 MPa for the concrete. Furthermore, the time-histories and concurrent cantilever stresses demonstrate that the significant tensile cantilever stresses are accompanied by compressive cantilever stresses on the opposite face of the dam. Therefore, should any cracks occur due to the cantilever bending, they would be minor and shallow and limited to small regions near the dam-foundation contact.

6.2-10 Conclusion and Recommendations

a. Three-dimensional finite element analysis including dam-water and dam-foundation interaction is essential for the design and evaluation of concrete arch dams. For successful analyses, realistic structural modeling, proper selection of material properties, appropriate loading combinations, and reasonable design or evaluation of earthquake ground motion(s) are among important issues that need to be carefully examined and addressed.

b. In cases similar to Portugues Dam, a finite element incompressible liquid mesh is usually adequate for modeling the dam-water interaction effects. For dams higher than 100 m and reservoirs with significant amounts of accumulated sediment, a refined dam-water interaction model including water compressibility and reservoir boundary absorption effects may be more desirable. The standard foundation model for seismic analysis of arch dams is a massless model. Such a simplified model is considered adequate for practical purposes especially where the modulus of the foundation rock is about the same as or exceeds that of the concrete. The earthquake input for time-history analysis of arch dams is defined in terms of three-component acceleration time-histories. The spectrum-matched and/or scaled natural earthquake acceleration records may be employed. As demonstrated in this example problem, the result for the spectrum-matched earthquake inputs may be considered as the average response, whereas the dam response to the scaled natural records may fall in a wide range representing both the lower and upper bound as well as the average values.

c. Following the procedures illustrated in this example, the performance of arch dams subjected to earthquake loading can be adequately analyzed and evaluated. Although only the linear-elastic response of the dam was computed, it was still possible to estimate what mode of behavior and level of damage could be expected. The results also demonstrate that even for the linear-elastic analysis the use of one set of spectrum-matched records commonly used in practice may not be sufficient. It is recommended that the spectrum-matched records be supplemented by at least three additional scaled natural records having different waveforms and frequency contents.

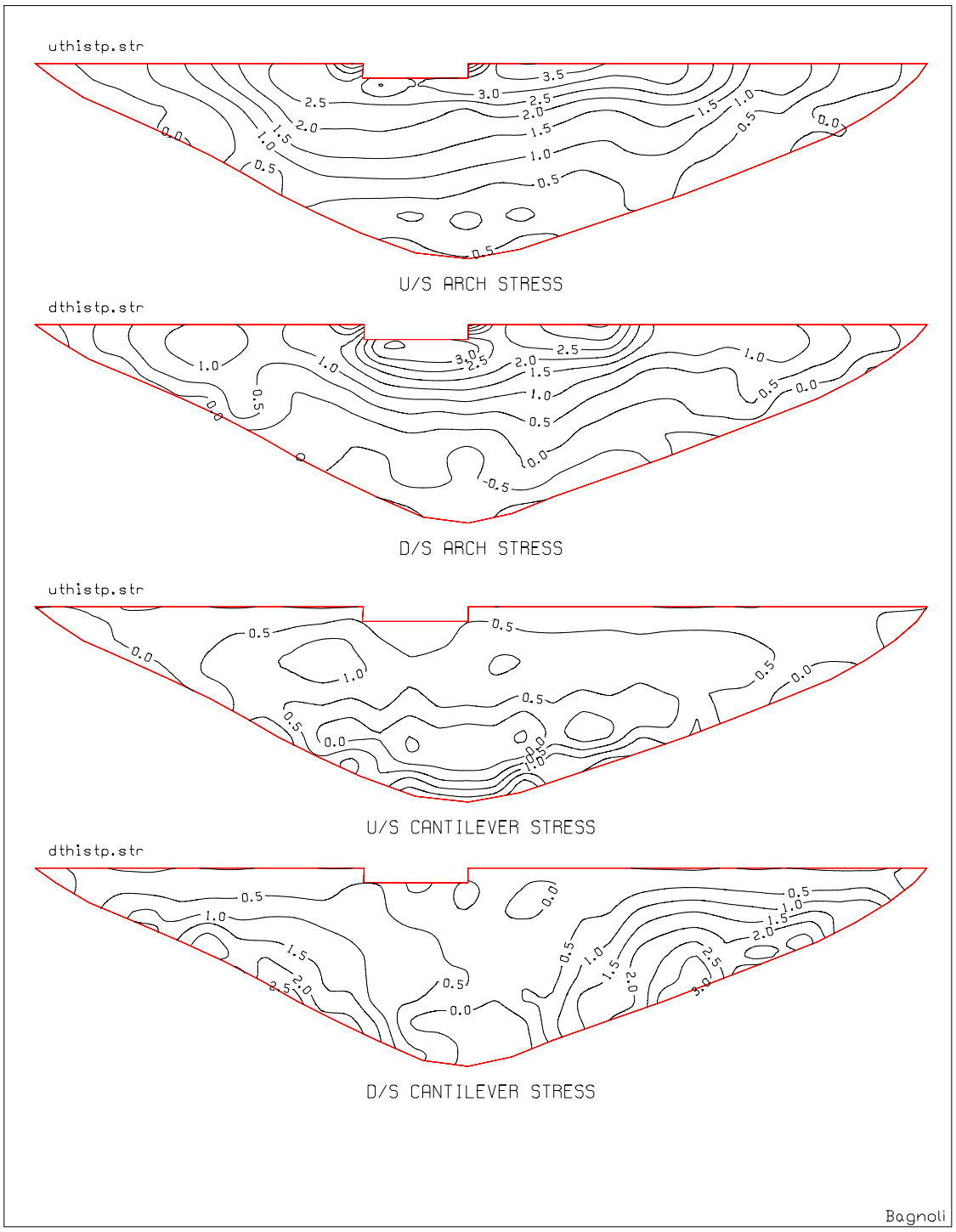

Figure 6.2-9. Envelopes of maximum stresses due to Bagnoli record plus static loads

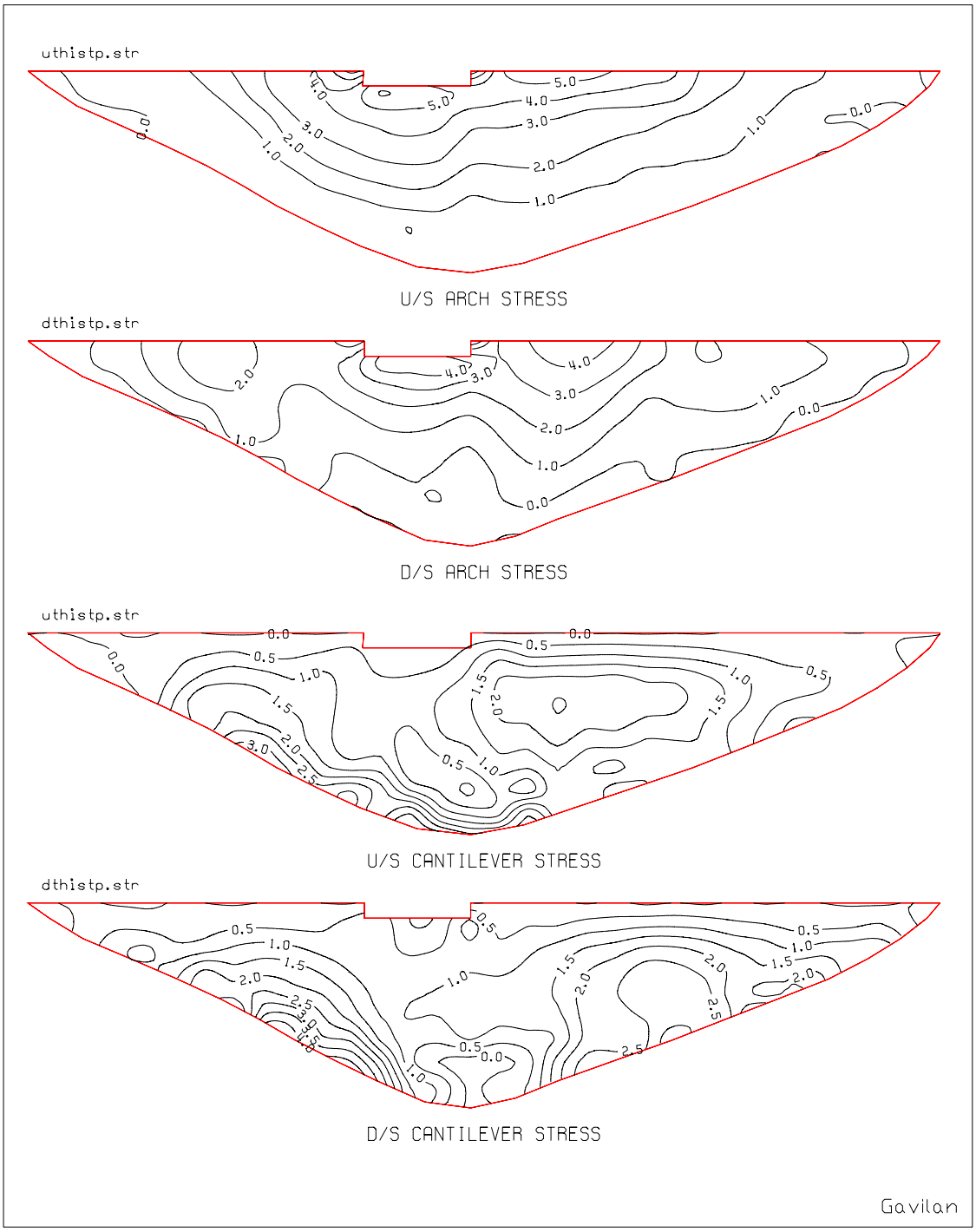

Figure 6.2-10. Envelopes of maximum stresses due to Gavilan record plus static loads

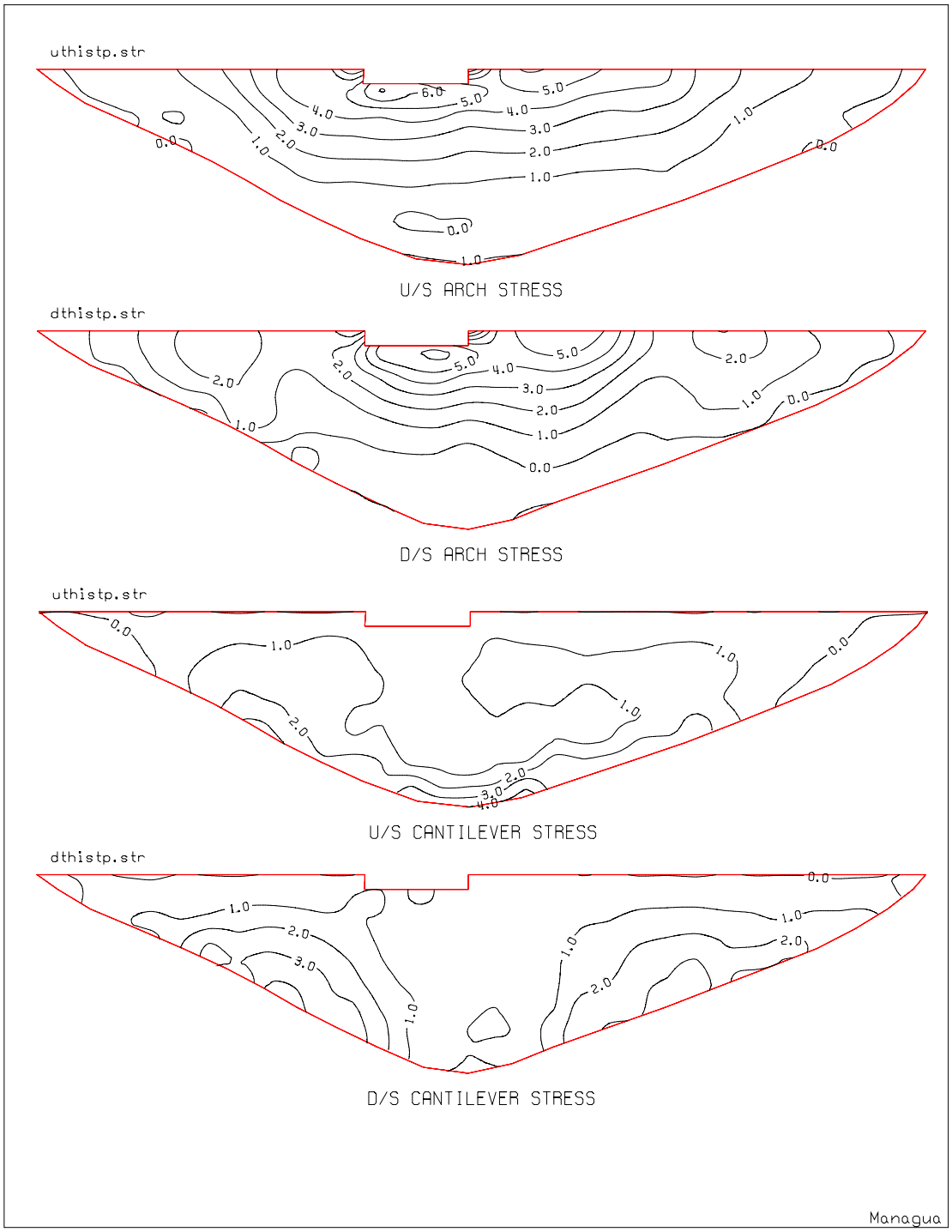

Figure 6.2-11. Envelopes of maximum stresses due to Managua record plus static loads

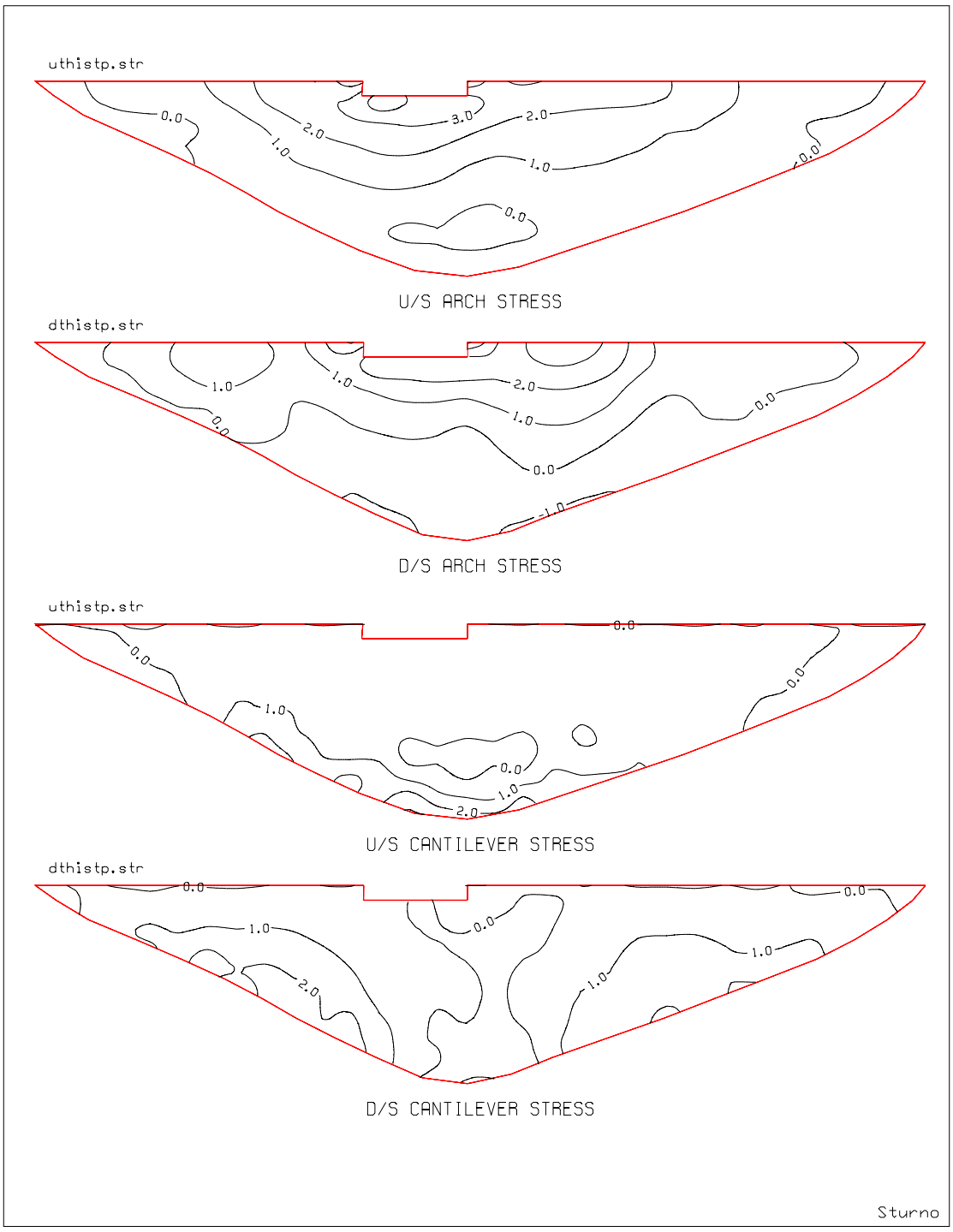

Figure 6.2-12. Envelopes of maximum stresses due to Sturno record plus static loads

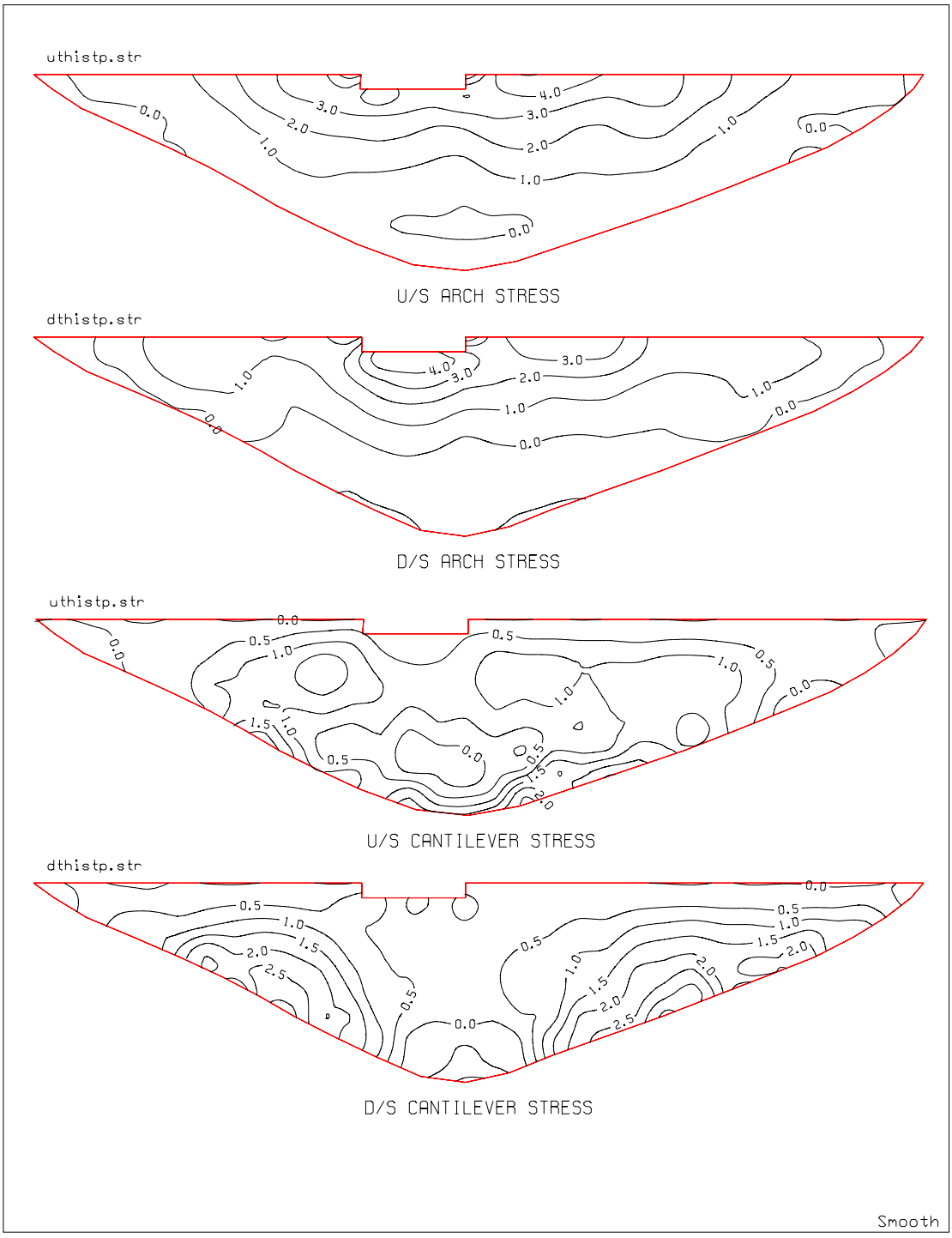

Figure 6.2-13. Envelopes of maximum stresses due to spectrum-matched record plus static loads

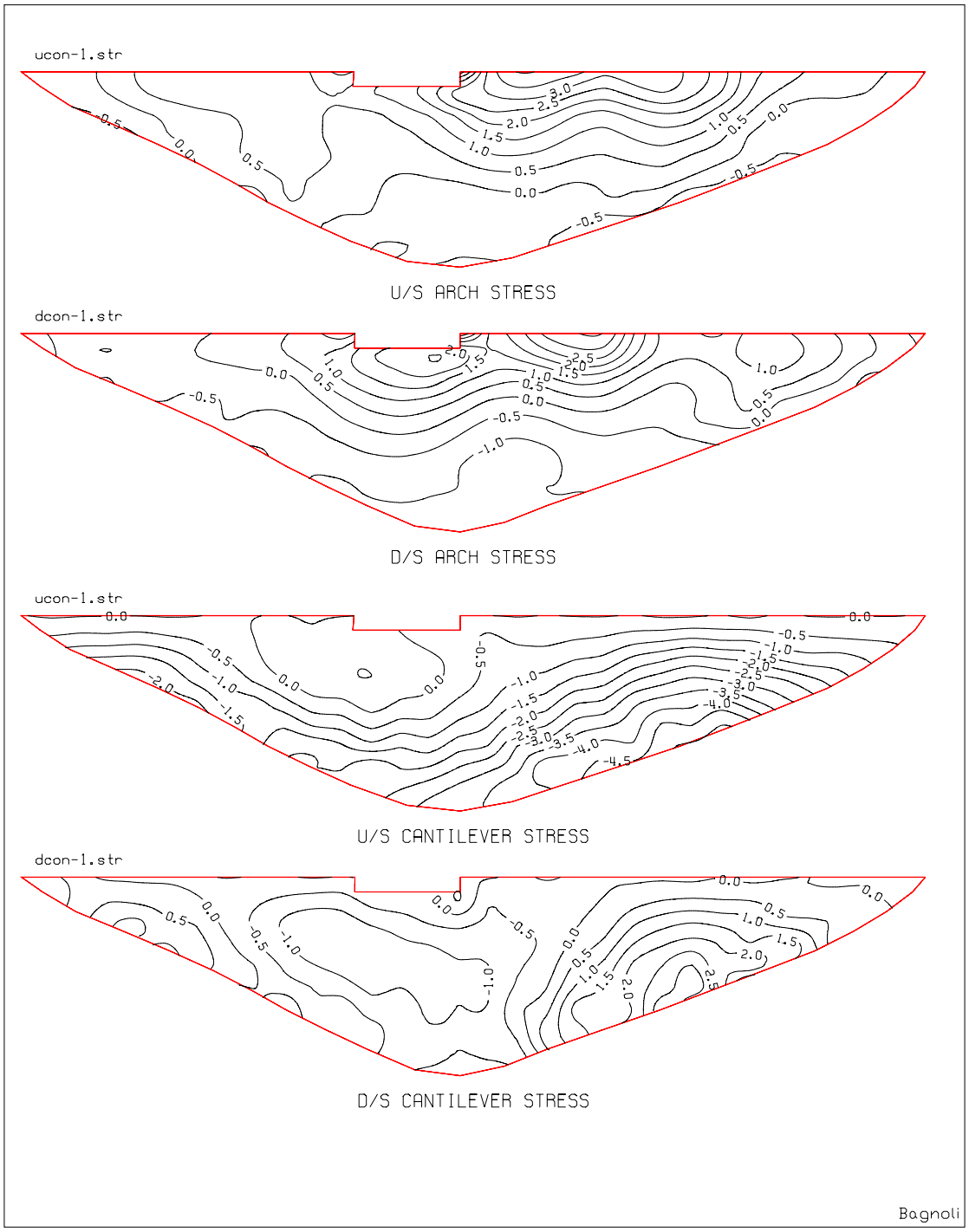

Figure 6.2-14. Concurrent stresses due to Bagnoli record plus static loads at the time of maximum arch stress

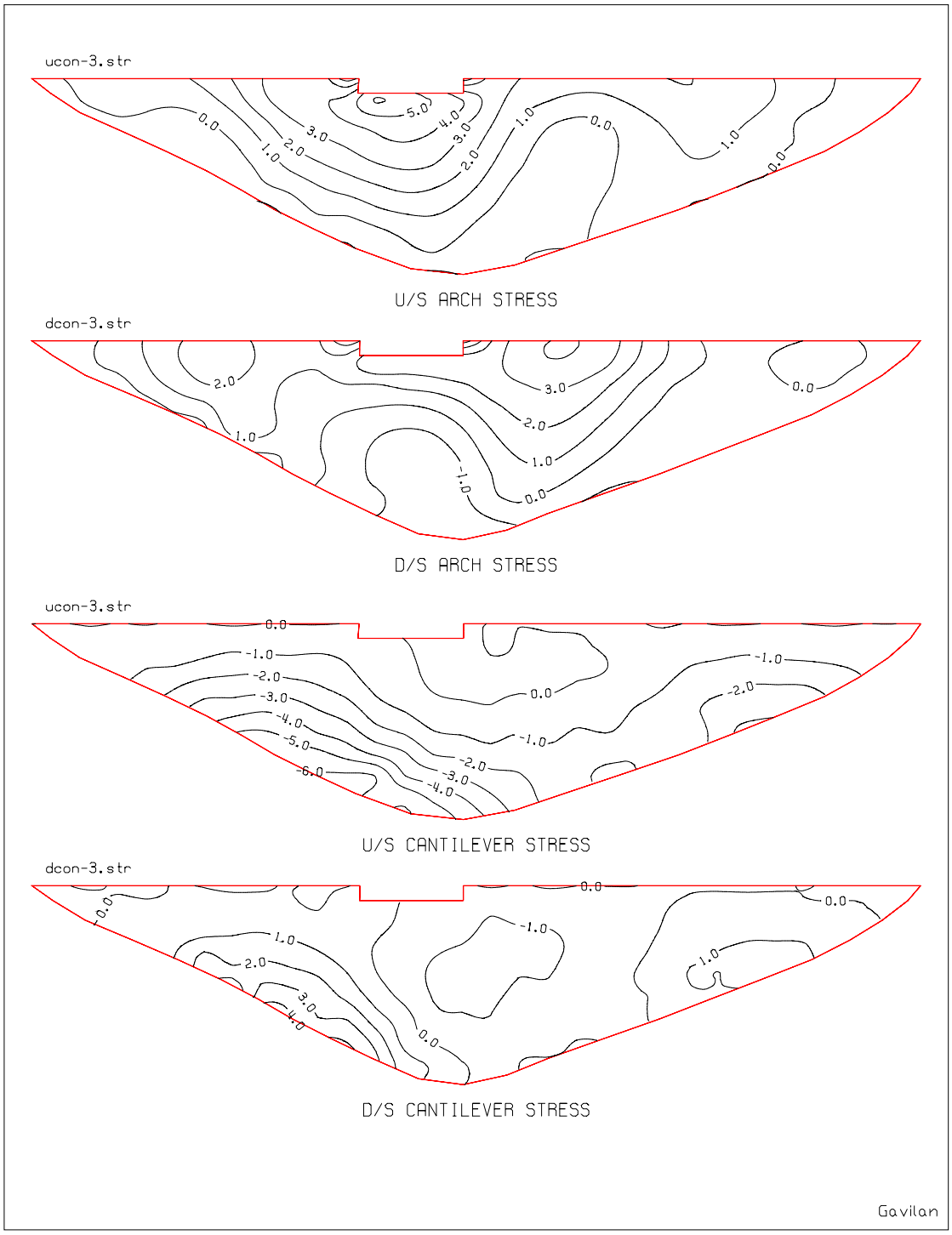

Figure 6.2-15. Concurrent stresses due to Gavilan record plus static loads at the time of maximum arch stress

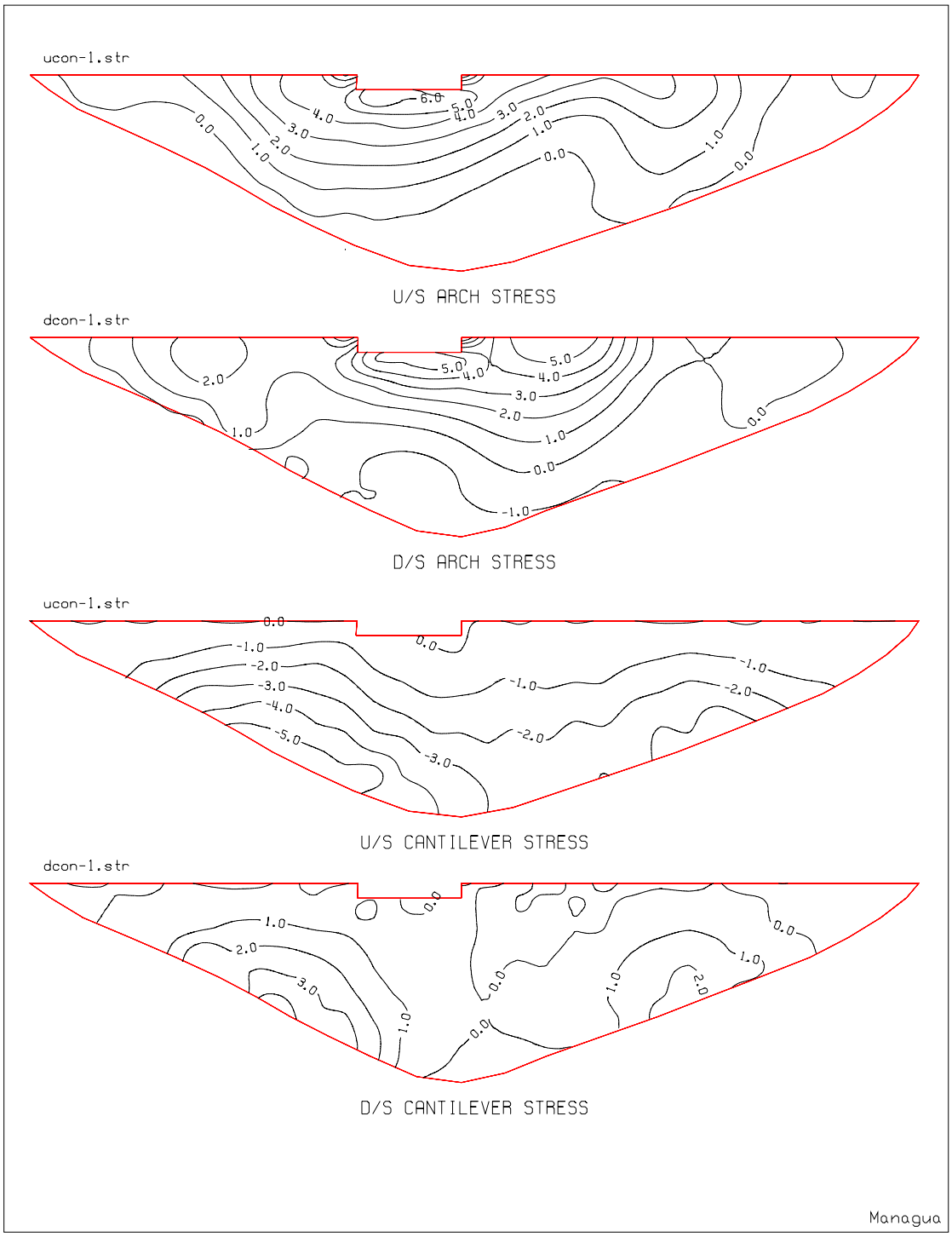

Figure 6.2-16. Concurrent stresses due to Managua record plus static loads at the time of maximum arch stress

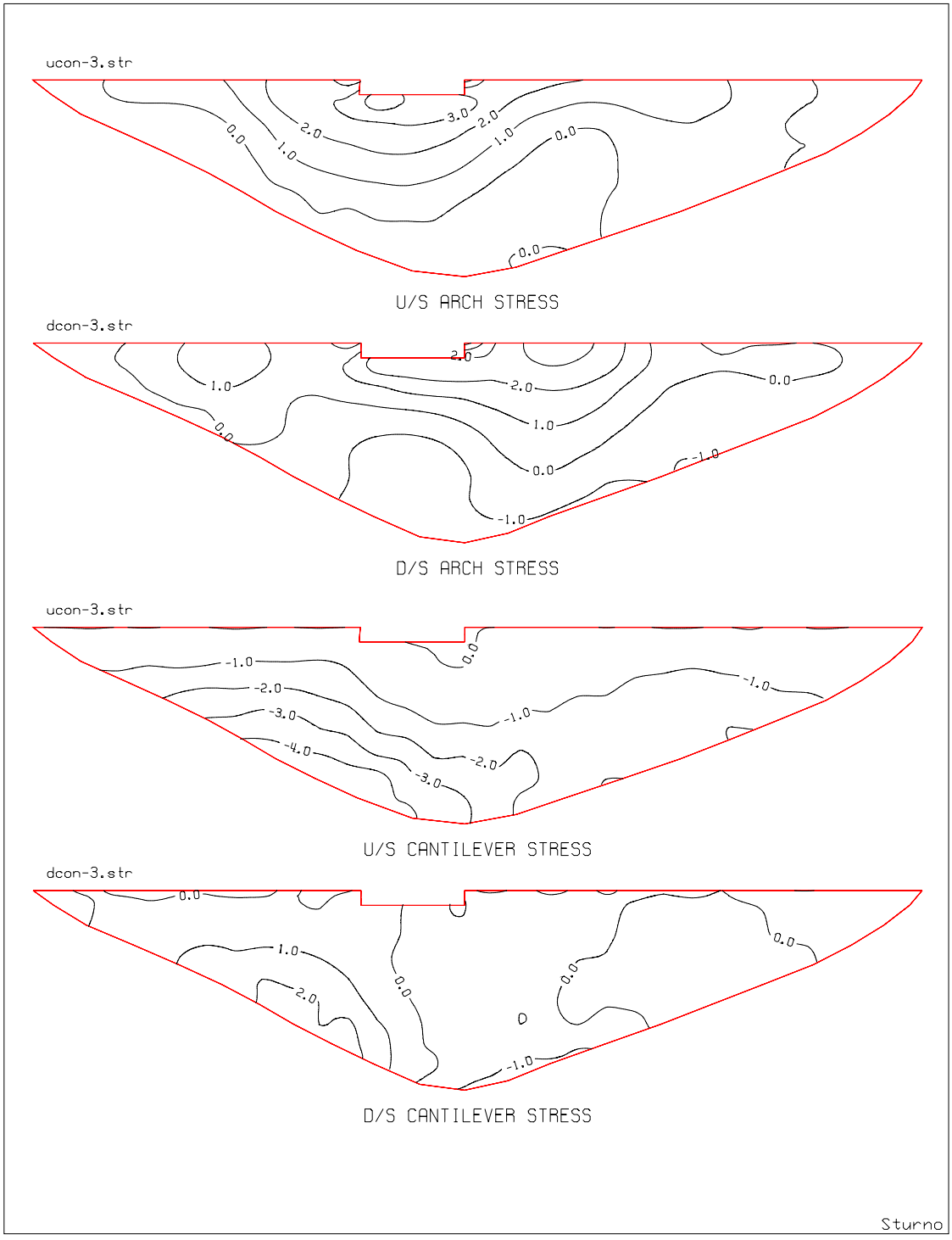

Figure 6.2-17 Concurrent stresses due to Sturno record plus static loads at the time of maximum arch stress

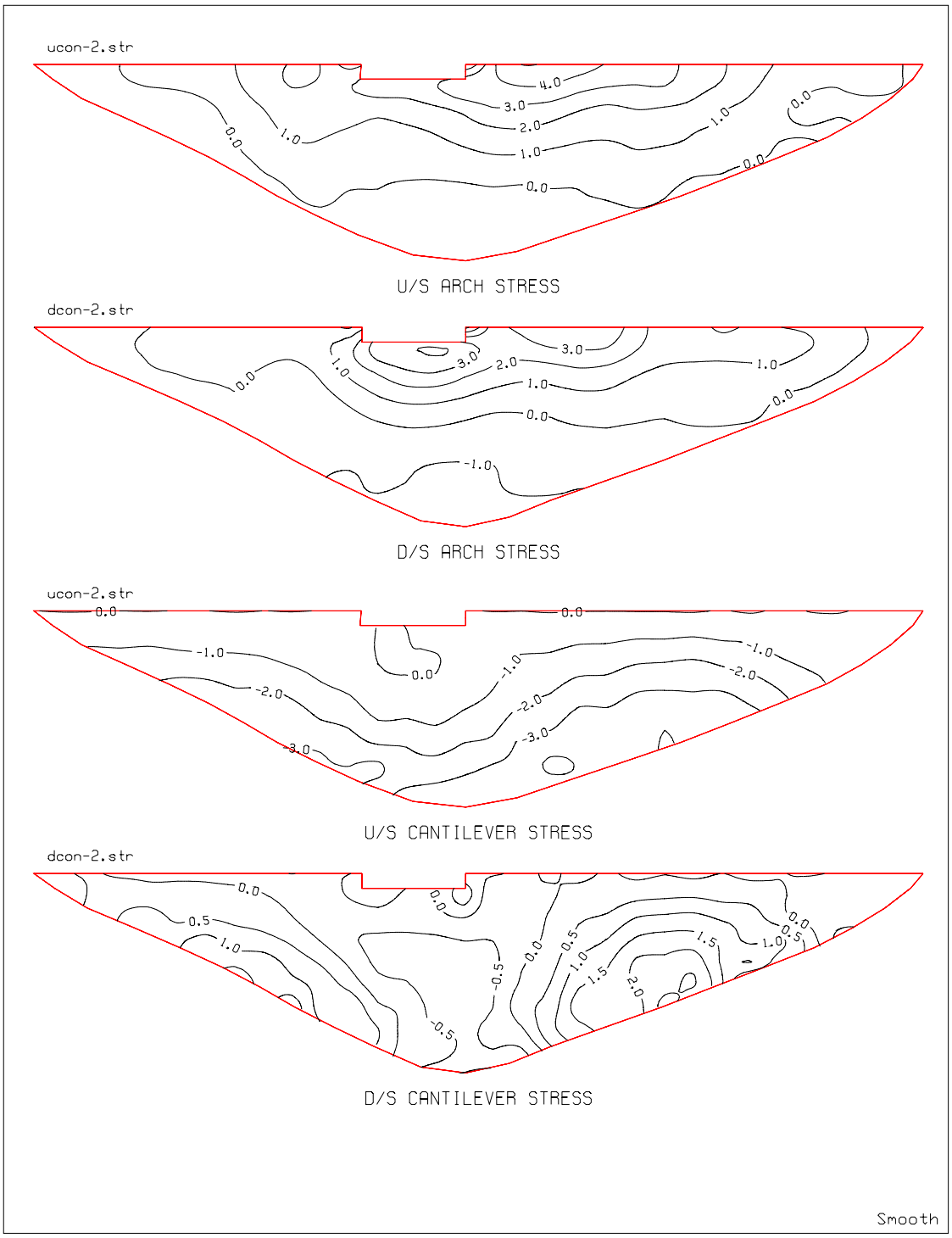

Figure 6.2-18. Concurrent stresses due to spectrum-matched record plus static loads at the time of maximum arch stress

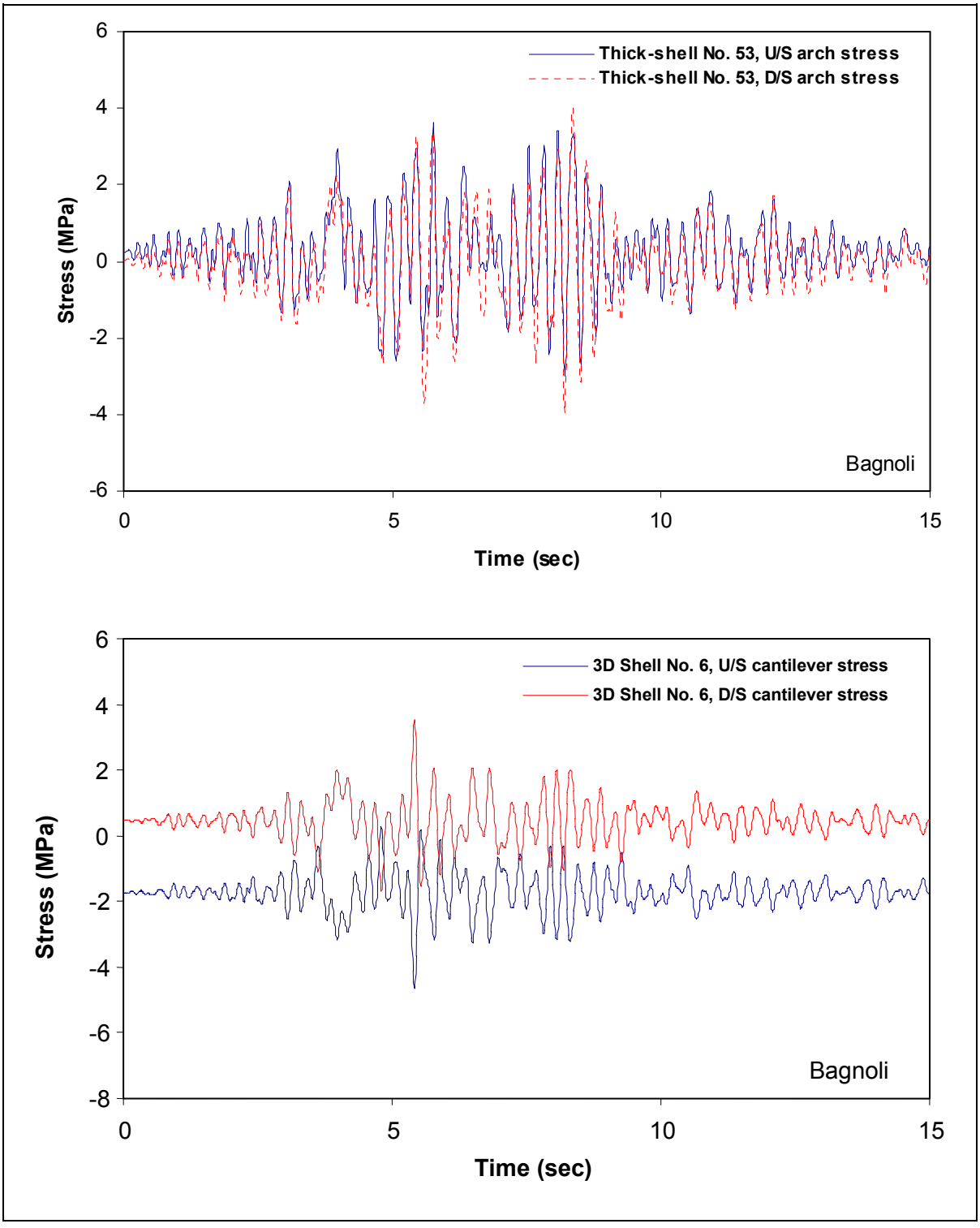

Figure 6.2-19. Time-histories of maximum arch and cantilever stresses and corresponding stresses on opposite face of the dam due to Bagnoli record plus static loads

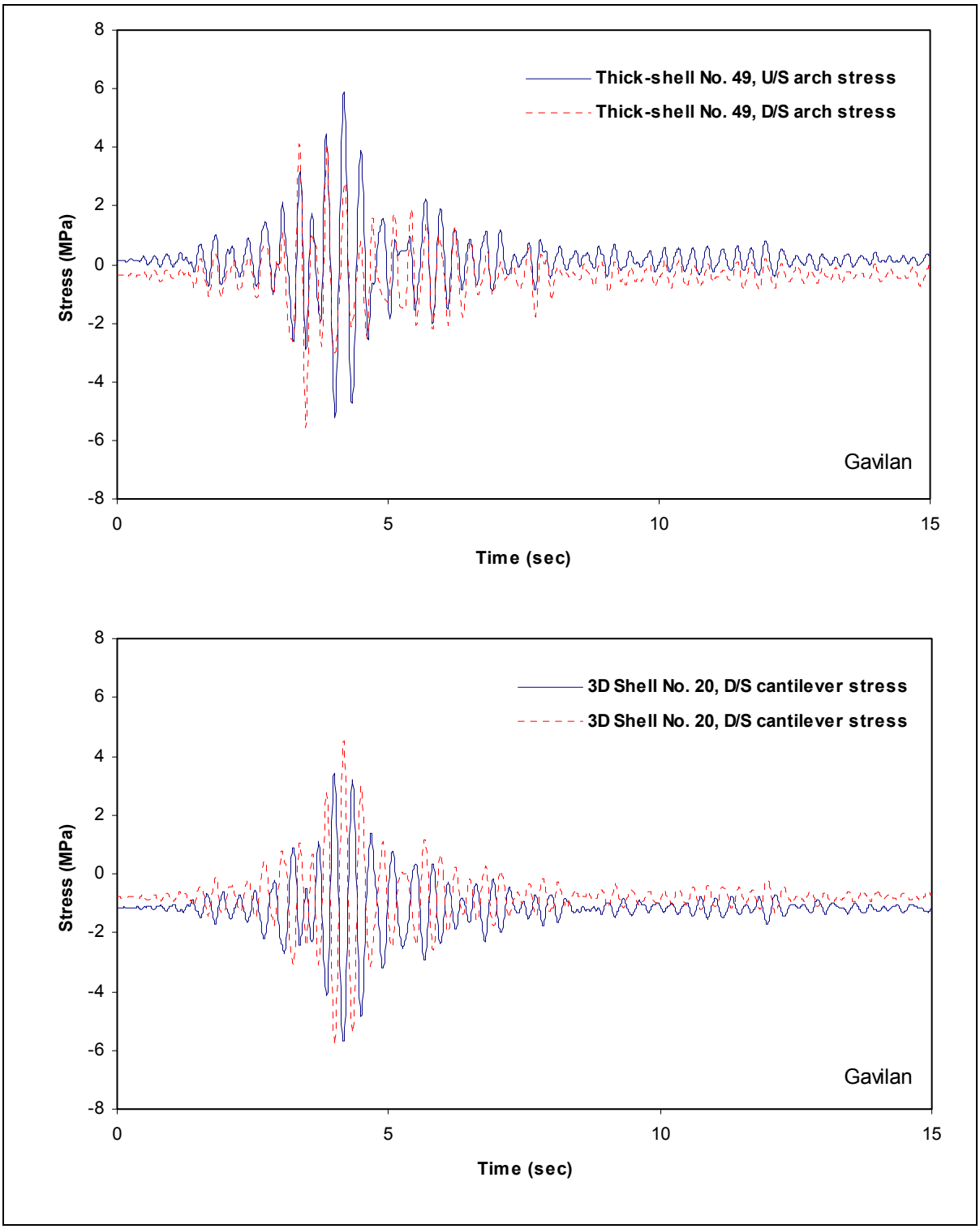

Figure 6.2-20. Time-histories of maximum arch and cantilever stresses and corresponding stresses on opposite face of the dam due to Gavilan record plus static loads

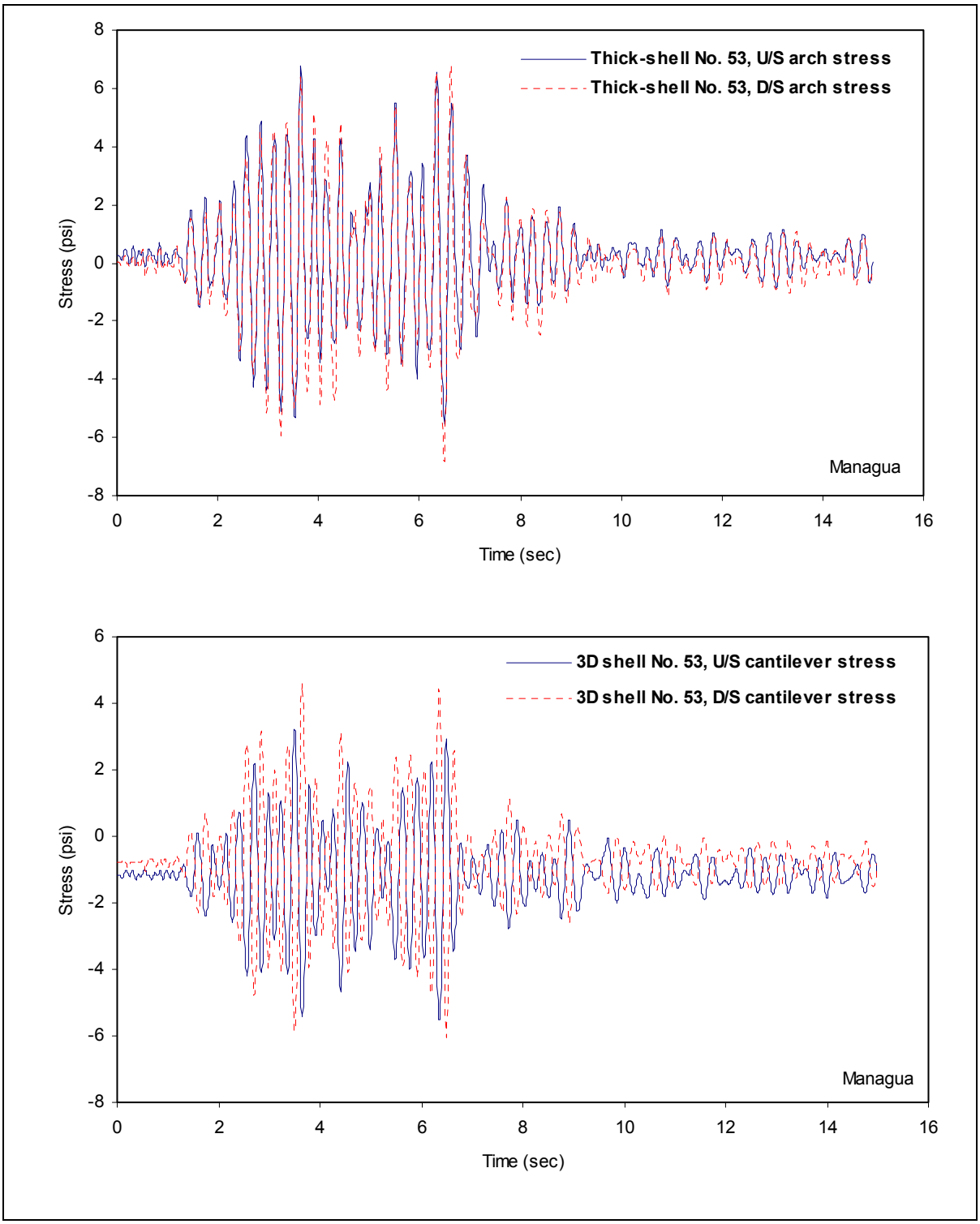

Figure 6.2-21. Time-histories of maximum arch and cantilever stresses and corresponding stresses on opposite face of the dam due to Managua record plus static loads

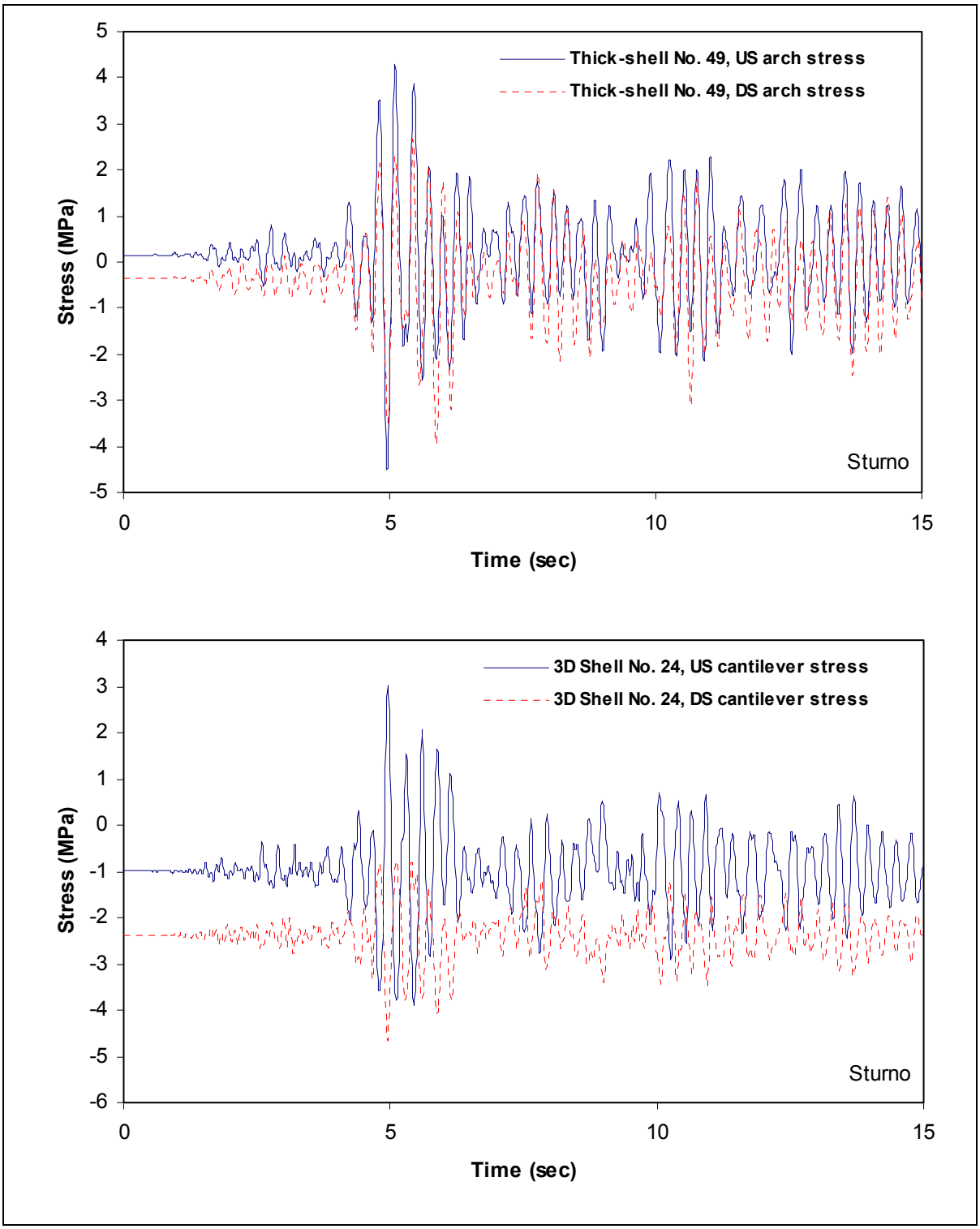

Figure 6.2-22. Time-histories of maximum arch and cantilever stresses and corresponding stresses on opposite face of the dam due to Sturno record plus static loads

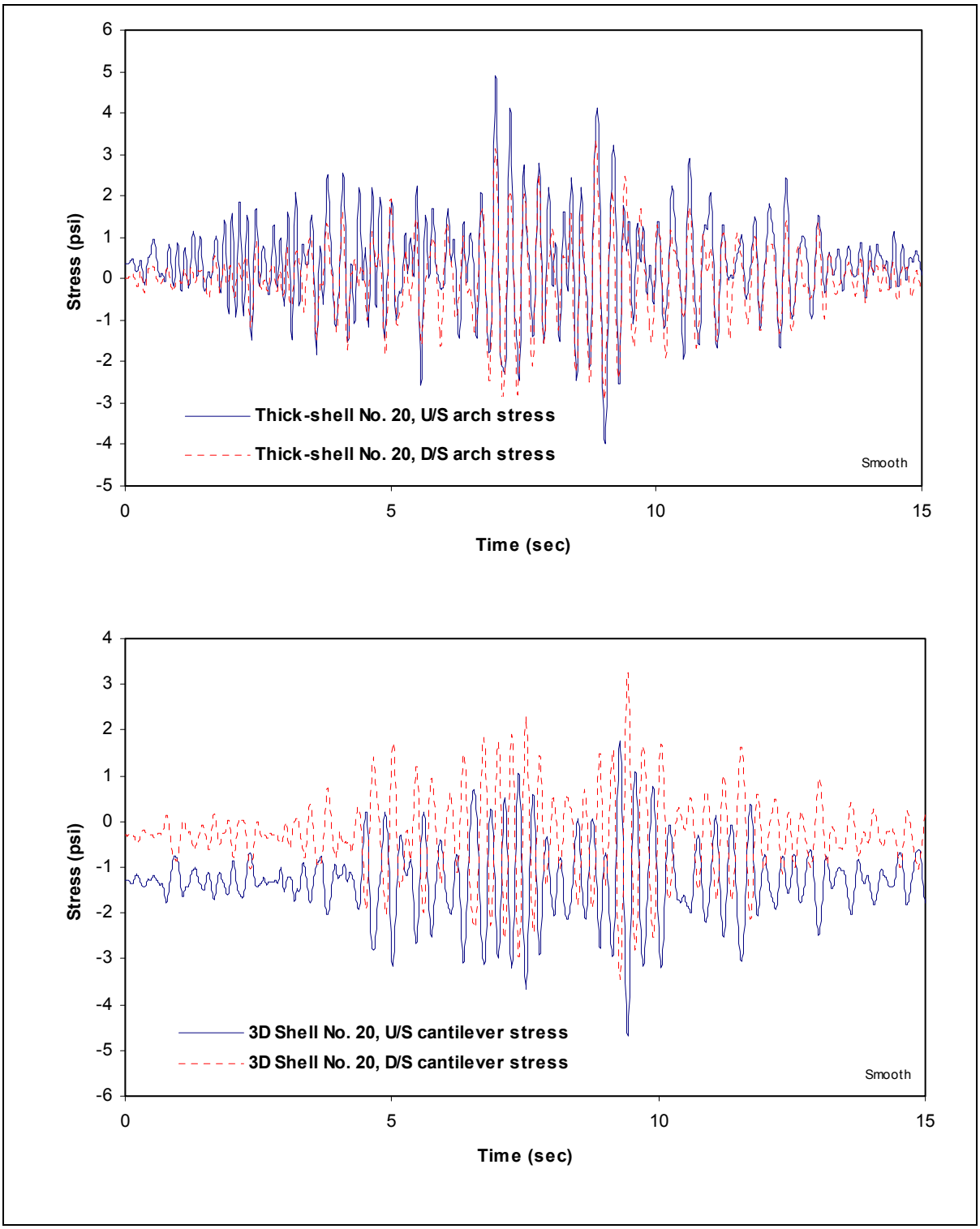

Figure 6.2-23. Time-histories of maximum arch and cantilever stresses and corresponding stresses on opposite face of the dam due to spectrum-matched record plus static loads

6.3 DYNAMIC SOIL-STRUCTURE INTERACTION ANALYSIS OF OLMSTED LOCK CHAMBER MONOLITH

6.3-1 Background

The Olmsted Locks and Dam Project replaces existing Lock and Dam 52 and 53 and is located at Ohio River Mile 964.4, approximately 2.9 km (1.8 miles) downstream of Lock and Dam 53, near Olmsted, Illinois. The lock structure consists of two 33.5-m by 365.8-m (110-ft by 1200-ft) locks adjacent to the Illinois bank (Figure 6.3-1). The locks are supported by more than 11,700 H-piles (HP 14×117) spaced 1.5 to 2.1 m (5 to 7 ft) in the upstream-downstream direction and 1.8 to 3.8 m (6 to 12.5 ft) in the cross-stream direction. The H-piles are about 12.2 to 13.7 m (40 to 45 ft) long and penetrate into the McNairy I formation, which is found to be highly over-consolidated toward the ground surface. For the chamber monoliths, the landside lock wall is backfilled to the top of the wall at El +3101. This results in about 20.1 m (66 ft) of the backfill behind the landside lock wall on the Illinois bank. The riverside lock wall is embedded to El +285 (i.e., 12.5 m (41-ft) embedment).

6.3-2 Purpose and Objectives

The purpose of this example is to illustrate an approach used to perform dynamic soil-pile-structure-interaction (SPSI) analysis for the chamber monolith of the Olmsted Locks using time-history analysis. The objectives of the SPSI analysis are:

a. To compute peak values and time histories of dynamic pile forces and moments for the combined horizontal and vertical earthquake excitations

b. To evaluate pile interaction factors for assessing demand/capacity ratio of piles

c. To compute peak values and time histories of dynamic section forces and moments at critical sections of the lock structure for reinforcement design

6.3-3 Scope

The scope of this example included consideration of one set of seismic input acceleration time histories and involved the following:

- Definition of time histories for design ground motion
- Idealization of site soil profiles and estimates of dynamic soil properties
- Development of finite element models of the soil-pile-lock structure system
- Analysis of static loading
- Analysis of dynamic loading
- Evaluation of response of pile foundation and concrete sections for static plus earthquake loads

Note that in a true seismic evaluation one needs to use more than one set of acceleration time histories to account for uncertainties in earthquake round motions.

---

1 All elevations (El) cited in this section are in feet referred to the National Geodetic Vertical Datum. To convert to meters, multiply by 0.3048.

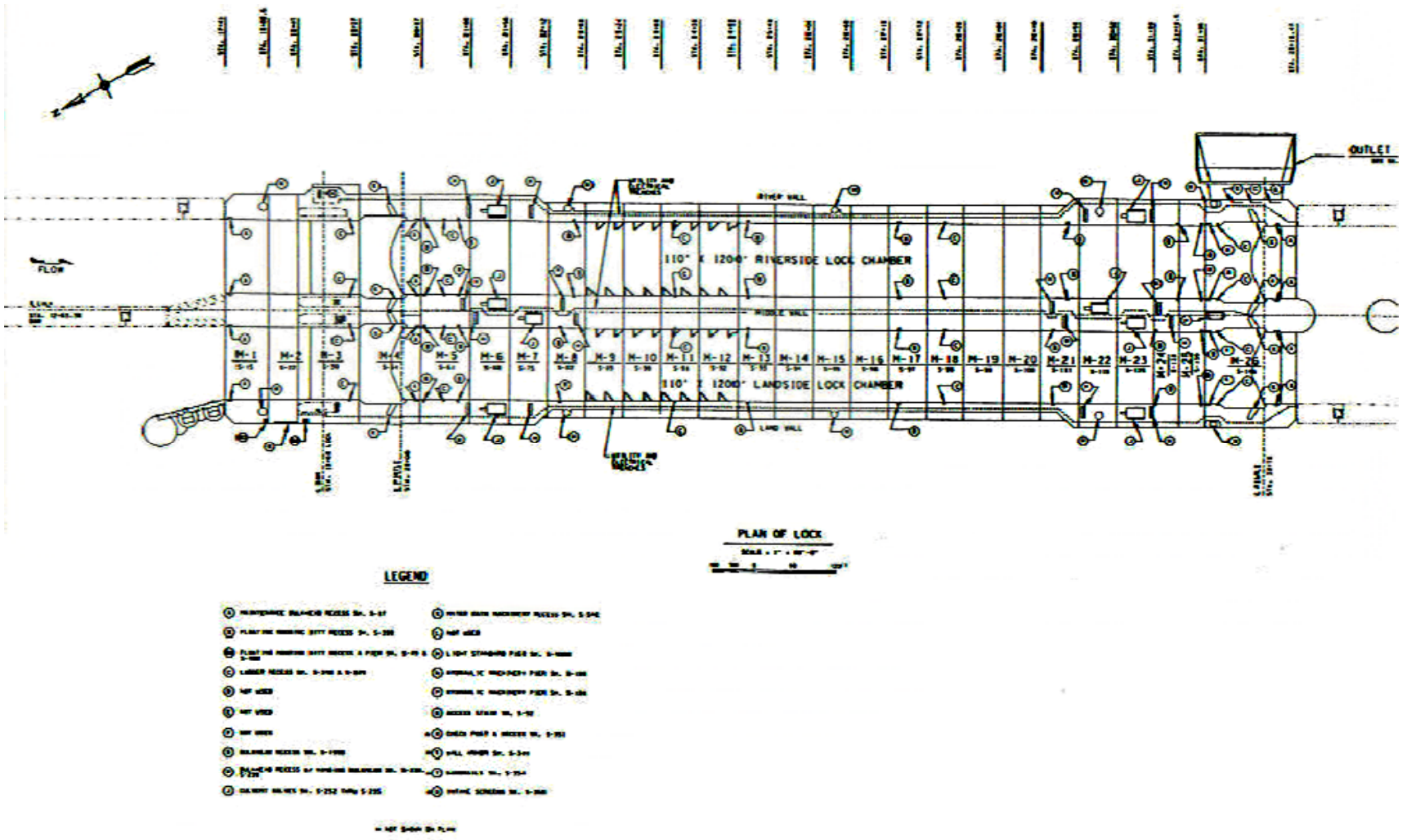

Figure 6.3-1. Plan View of Olmsted Locks

6.3-4 election of Analysis Procedures

Mainly two procedures are available for analysis of SPSI: soil spring versus soil continuum. In the soil spring procedure, the structure is supported by a series of nonlinear soil springs simulating soil-pile interaction and is loaded by lateral soil pressures acting on the embedded lock walls. In the soil continuum procedure, the structure is supported by a series of piles idealized as beam elements embedded and connected with quadrilateral soil elements beneath and surrounding the lock structure. Advantages and limitations of each analysis procedure are described in *a* and *b* below.

a. Soil spring procedure

(1) The soil spring procedure is generally based on a sub-structuring method of analysis. The lock structure is supported by a series of springs at the lock base representing the pile foundation and on the lock wall representing lateral soil pressures. The soil springs at the lock base are nonlinear and are generally approximated by nonlinear pile-head load-deflection curves. The pile-head load-deflection curves are generally developed by modeling the piles supported by a series of independent nonlinear axial (t-z) and lateral (p-y) soil springs along the length of the pile. These nonlinear axial and lateral soil springs are based on empirical relationships developed from back calculation of static axial and lateral pile load tests. For closely spaced pile foundations (e.g., pile center-to-center spacing of less than three pile diameters), pile-to-pile interaction or pile group effects are approximated by semi-empirical interaction factors. Thus, the nonlinear soil-pile interaction is approximated by nonlinear pile head stiffness through an iterative procedure.

(2) The soil spring procedure has the following limitations:

- Axial and lateral soil-pile springs are uncoupled and are generally developed for static loading conditions and used for seismic loading conditions.
- Kinematic soil-structure interaction cannot be rigorously accounted for in the analysis.
- Wave propagation phenomena and soil-pile interaction under seismic loading conditions are generally not rigorously accounted for; thus, there are uncertainties related to pile response under seismic loading conditions.
- Pile group effects on the computed response are accounted for through the use of p-multiplier based on limited empirical static pile load test data, and its modeling accuracy has not been validated.
- Soil-embedment effects especially on the landside lock wall cannot be easily accounted for.

b. Soil continuum procedure

(1) The soil continuum procedure is a direct method in which the lock structure, piles, and surrounding soil media to basement rock can be modeled and analyzed as a complete system. Using this procedure, both kinematic and inertial interaction and wave propagation phenomena are accounted for directly. Depending on the size or number of piles, the soil-pile-structure system may be approximated by a 3- or 2-D model. For a long pile-supported lock structure such as the Olmsted chamber monolith, the response of the lock in the transverse direction (cross-stream direction) can be reasonably approximated by a 2-D model. Both the lock structure and soil media are modeled by 2-D quadrilateral elements. Piles are modeled by beam elements connected to the quadrilateral soil or concrete elements. Wave propagation, pile group effects, and soil embedment effects on the lock response are rigorously accounted for in this procedure.

(2) The soil continuum procedure has the following limitations:

- For a large pile foundation, due to limitations in computing resource, the pile foundation can be approximated only by a 2-D model

- Nonlinear soil-pile interaction can only be approximated by equivalent linear techniques; thus, strong nonlinear soil-pile interaction, if present, cannot be realistically modeled.

c. Modeling procedure selected

(1) For the Olmsted locks, the soil continuum procedure implemented in the computer program FLUSH (Lysmer et al. 1975) was selected to model SPSI and the effects of deep soil embedment at the land-side on the response of the lock-pile system. In the subsequent sections, analysis steps followed and the results obtained are described.

(2) The dynamic SPSI analyses were performed using QFLUSH (QUEST Structures, www.WebDams.com), an enhanced version of FLUSH with pre- and post-processing capabilities. The analyses were performed in the frequency domain for vertically propagating shear and compression waves (horizontal and vertical excitations). Analyses for the horizontal and vertical excitations were performed separately and then combined. The nonlinear soil behavior was approximated by the equivalent linear techniques described in 5-6*b*(2) through iterative procedures for the horizontal excitation. The results for the horizontal and vertical excitations were transformed from the frequency domain back to the time domain. The time-domain results were subsequently combined to obtain the total response for simultaneous horizontal and vertical (shear- and compression- wave) excitations. For the QFLUSH analyses, the input motion at the rigid base is required. The input motion was derived as an interface motion at the boundary between the free-field soil/rock column and basement rock from the site response analysis using the program SHAKE (Schnabel et al. 1972).

6.3-5 Finite Element Modeling

a. The computer model for the SPSI analyses consisted of the lock structure, supporting soil, and the piles. The lock structure and the foundation soil were modeled by plain-strain 2-D quadrilateral solid elements. Each individual pile was modeled by a series of beam elements whose translational degrees of freedom were connected to surrounding soil or concrete elements. The finite element representation of the chamber monolith and its pile foundation is shown in Figure 6.3-2. The rigid connection between the pile head and the lock basemat was simulated by extending pile elements 1.2 m (4 ft) into the basemat. The pile foundation model included 43 piles; each modeled by 17 beam elements. The finite element model of the complete soil-pile-lock structure is shown in Figure 6.3-3. Two rock layers were incorporated in the model to minimize the effects of the rigid base on the computed response. The vertical dimensions of the soil elements depend on the maximum frequency of the motion to be retained in the analysis, and were established as suggested by Lysmer et al. (1975). It was estimated that the maximum frequency of importance to the structural response was about 10 to 12 Hz. In the analyses, the vertical dimensions of the soil elements were selected to retain a maximum frequency of 20 Hz for the horizontal excitation and at least 30 Hz for the vertical excitation. The finite element model consisted of 3,740 solid elements, 739 beam elements, and 4,716 nodal points.

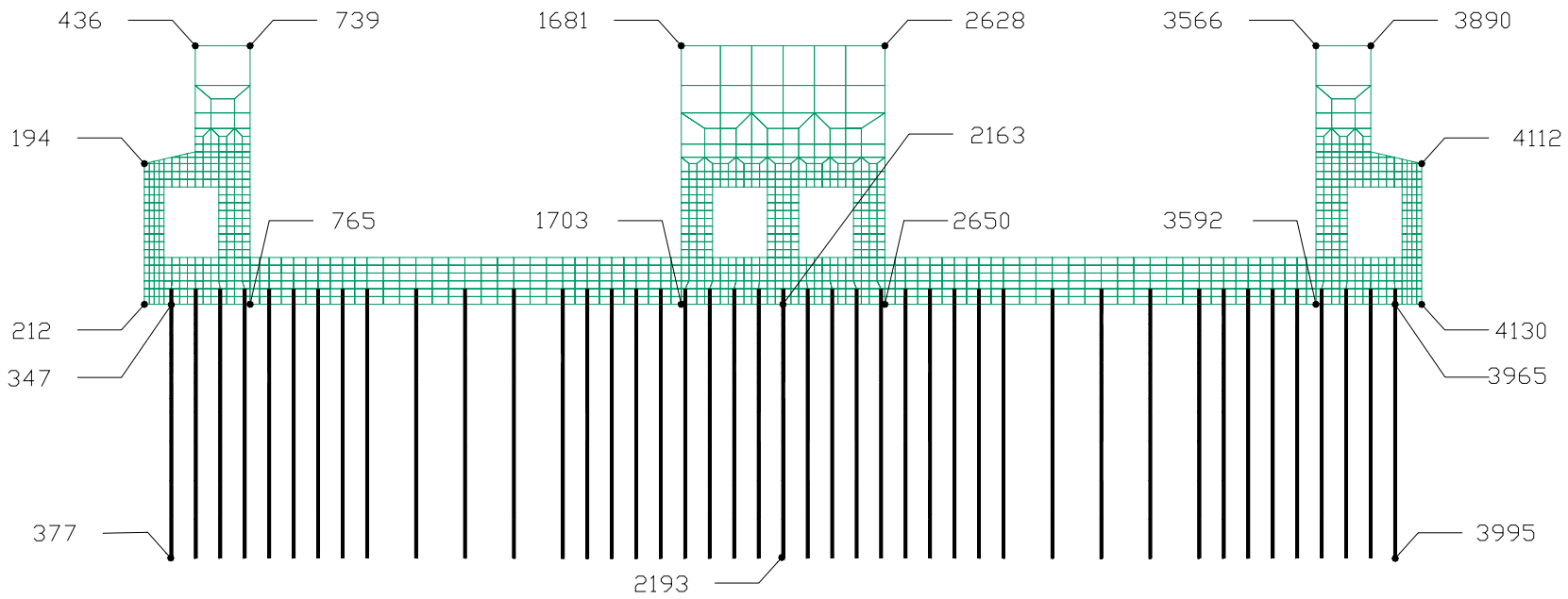

Figure 6.3-2. Finite element model of lock and piles

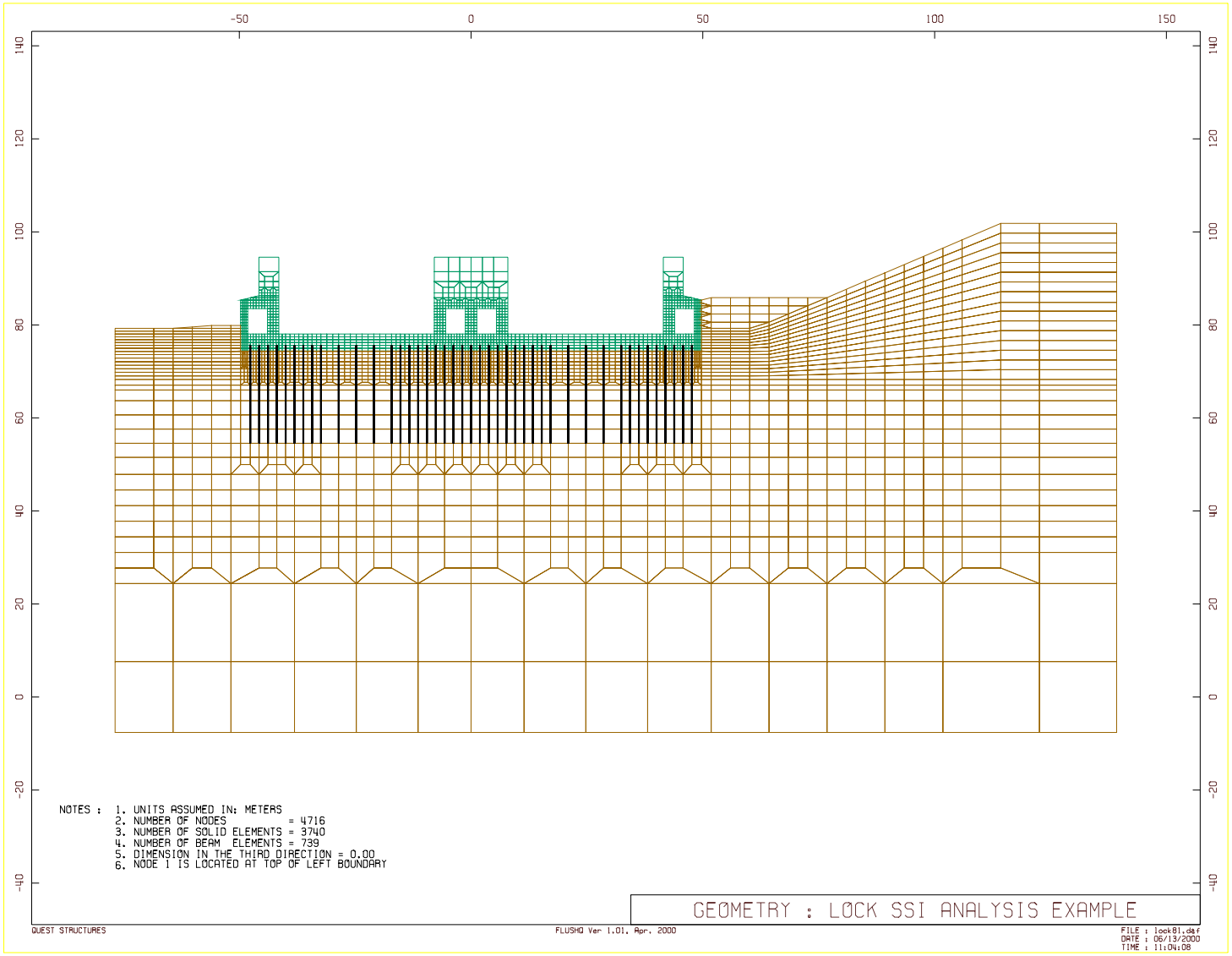

Figure 6.3-3. Finite-element mesh representation of the soil-pile-lock system

b. An energy-transmitting boundary was specified on the left side (i.e., riverside) of the model. A displacement boundary condition consisting of horizontal rollers for the horizontal excitation and vertical rollers for the vertical excitation was specified on the right side boundary (i.e., bank side).

c. The finite element model incorporated a thin soft-soil layer, 76-mm (3-in.) in thickness, beneath the lock basemat in order to compute conservative values of forces and moments at pile heads. The soft-soil layer simulates a condition where primarily piles would carry seismic loads.

6.3-6 Material Parameters

a. Stratigraphic Profile

(1) The Olmsted lock structure considered for SPSI studies is situated along the Illinois bank of the Ohio River. Subsurface soil conditions of the Illinois bank generally consist of a surficial layer of colluvium /alluvium overlying McNairy Zone I and McNairy Zone II formations. Granular backfill will be placed on both sides of the lock (river and bank sides). The McNairy Zone I formation is described in USAED, Louisville (1989 and 1990) as "a complex assemblage of interbedded partings and bands of micaceous clays, silts, and very fine to fine sands." Results of pressure meter tests performed in 1997 indicated that the McNairy I formation is highly over consolidated. The McNairy Zone II formation is described as "predominantly a clayey silt with varying amounts of organics; contains numerous gravel size fragments of black chert with some extensive layers of highly jointed indurated clayey silt to siltstone; material is rock-like in some locations and soil-like in others." Bedrock, described as a Paleozoic-age shale, was encountered at approximately Elevation 27.43 m (90 ft) immediately underlying the McNairy Zone II formation.

(2) To perform SPSI analyses, a typical stratigraphic profile through the chamber monolith was developed. Subsurface soil conditions (and associated geotechnical data) encountered in borings within reasonable proximity to the chamber monoliths were used to characterize the profile. The resulting stratigraphic profile, with the proposed lock structure superimposed, is illustrated in Figure 6.3-4.

b. Dynamic Soil Properties

(1) Geotechnical data available for the project site and experience with properties of other soils for similar conditions were used to characterize the dynamic soil properties (low-strain and strain-dependent) within the SPSI finite element model.

(2) At the Olmsted site, an empirical correlation was developed between the corrected blow counts and the normalized shear-wave velocity measured at both the Illinois and Kentucky banks (U.S. Army Engineer District, Louisville, 1994). The correlation was used to estimate low-strain shear-wave velocity or shear modulus of soils beneath the monolith using the blow counts estimated for the idealized soil profiles shown in Figure 6.3-4. The estimated low-strain shear-wave velocity profiles at the free field on the riverside are shown in Figure 6.3-5. Shear-wave velocity estimates for the McNairy Zone II materials were assumed not to be dependent on density or effective stress as are the Zone I soils. This is because of the tendency of the Zone II materials to be indurated, as described in the boring logs. Therefore, for McNairy Zone II, values of shear-wave velocities were selected based directly on interpretations of the geophysical measurements.

(3) Soil stiffness (shear modulus) and energy absorption (damping) characteristics are soil properties that have been shown by innumerable studies to be strain-level dependent. Various researchers (Seed et al. 1984; Sun et al. 1988; Vucetic and Dobry 1991) also have shown the strain dependency to be related to soil type, stress history, density state, and other factors. For SPSI analyses, a set of modulus reduction and damping curves based on data for similar soils (i.e., clayey soils with a plasticity index (PI) in a range of 10 to 30) was selected and is shown in Figure 6.3-6. In this figure, G is soil shear modulus and G_{max} is soil shear modulus at low strain (strain less than 10^{-4} percent).

(4) Comparison of shear and compression wave velocities measured at the project site indicates that Poisson's ratios for the site soils are very close to a value of 0.50. To maintain numerical stability in the finite element SPSI analyses, Poisson's ratios were limited to a value of 0.49 for the soils.

c. Dynamic properties of concrete and pile elements

Dynamic properties of the concrete elements representing the lock structure and of the beam elements representing the piles are summarized in Table 6.3-1.

Table 6.3-1
Dynamic Properties of Concrete Elements for Lock Structure and Beam Elements for Piles

Material	Shear Modulus MPa (ksf)	Poisson's Ratio	Density kN/m^3 (pcf)	Damping Ratio	Section Area cm^2 (in^2)	Moment of Inertia m^4 (in^4)		Effective Shear Area m^2 (in^2)
						X-X Axis	Y-Y Axis	
Concrete Elements for Lock Structure	9,774.07 (204,125)	0.15	23.56 (150.00)	0.05	-	-	-	-
Beam Elements for Piles (HP14x117)	76,909.31 (1,606,200)	0.30	76.82 (489.00)	0.03	222.19 (34.44)	7,925.79 (1,228.50)	2,858.70 (443.10)	66.65 (10.33)

Note: To obtain section area and moment inertia per foot along the axis of the lock, the total area and moment inertia are divided by the pile spacings

6.3-7 Loading Conditions

a. Static Loads. Analyses of static pile forces and moments and static concrete stresses of the lock structure were conducted for the normal operating condition consisting of the dead weight, normal water pressures, and the backfill earth pressures. A 2D model consisting of the foundation soil, piles, backfill soil, and the lock structure was developed and analyzed using the computer program SAP2000. The foundation and backfill soils were represented by 2D solid elements. Piles were modeled by beam elements, and lock section by solid elements with concrete properties. The SAP2000 model for static analysis was later converted to a QFLUSH model for dynamic soil-structure-interaction analysis. The static and dynamic finite-element models, therefore, were identical in terms of geometry, mesh, and element types to facilitate combination of the static with dynamic results.

b. Earthquake ground motion. The MDE ground motions were used as the seismic input. Response spectra of the MDE ground motions were derived from a probabilistic seismic hazard assessment (Geomatrix Consultants, Inc., 1996) as the equal-hazard spectra having a return period of 1,000 years. The 5-percent-damped MDE response spectra for the horizontal and vertical components of rock motion are shown in Figure 6.3-7. Time histories of the horizontal and vertical components of rock motion (i.e. H1, H2, and V)

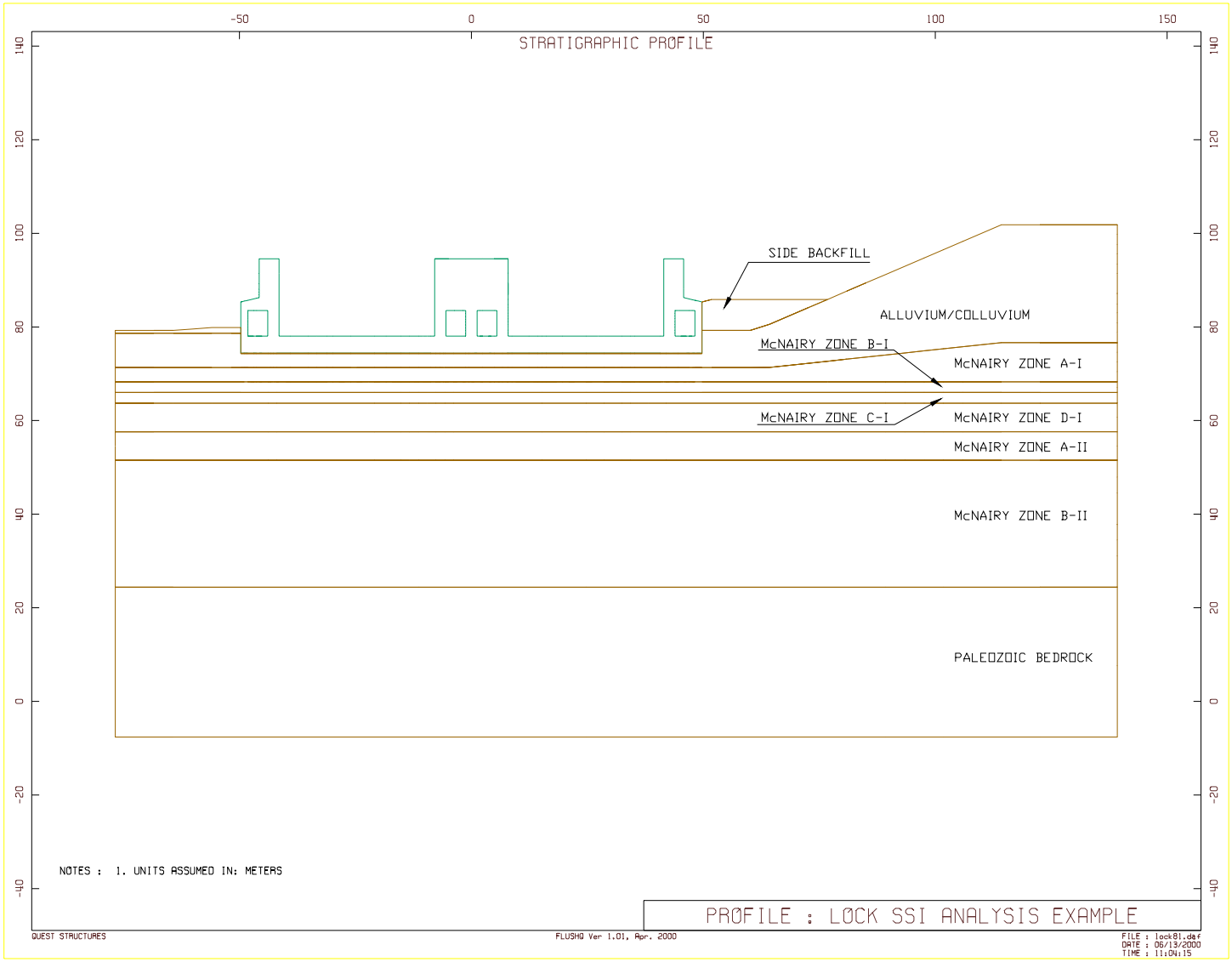

Figure 6.3-4. Idealized stratigraphic profile at Olmsted Locks and Dam site

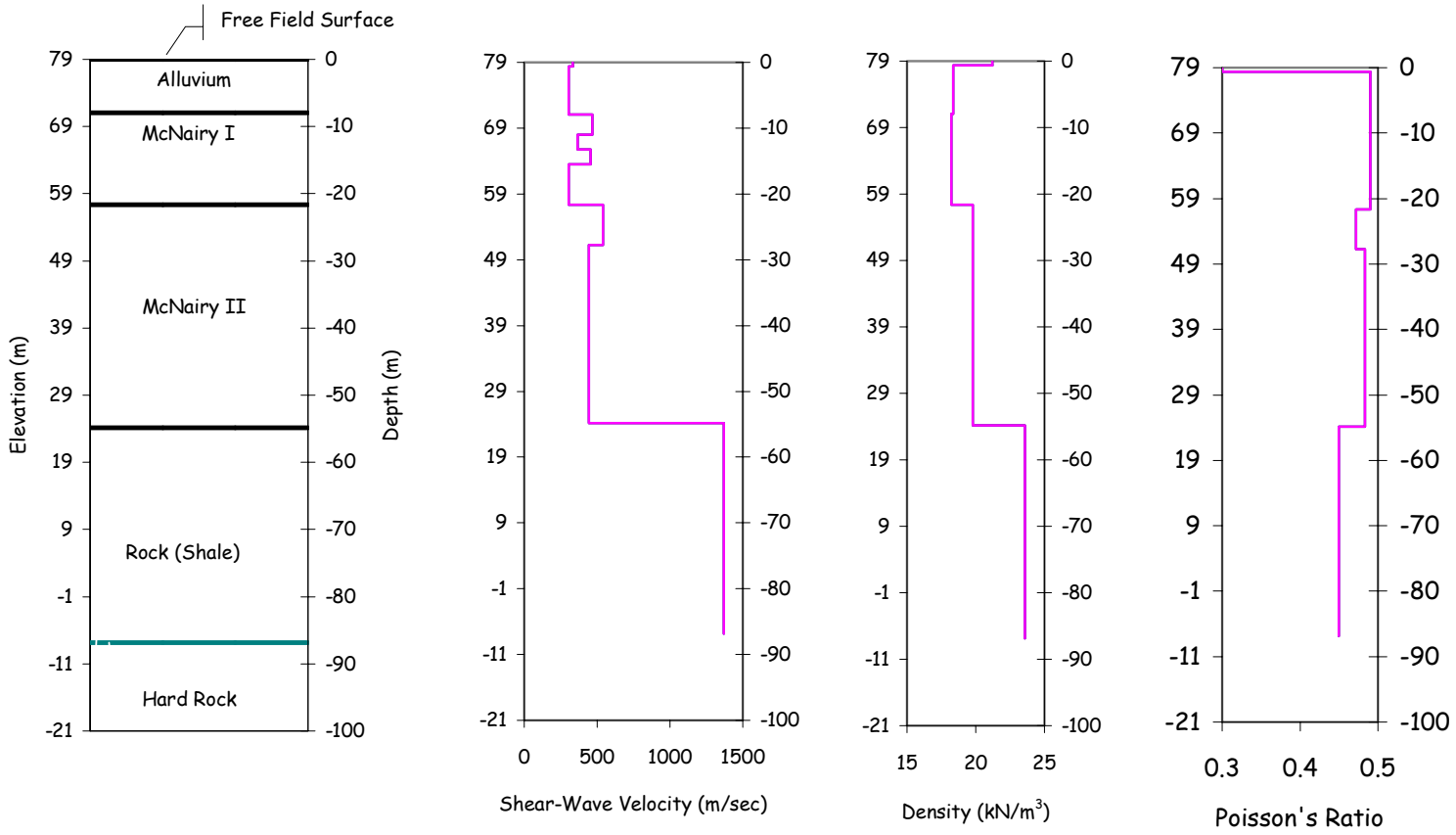

Figure 6.3-5. Estimated low-strain shear-wave velocity profile in the free field on the river side

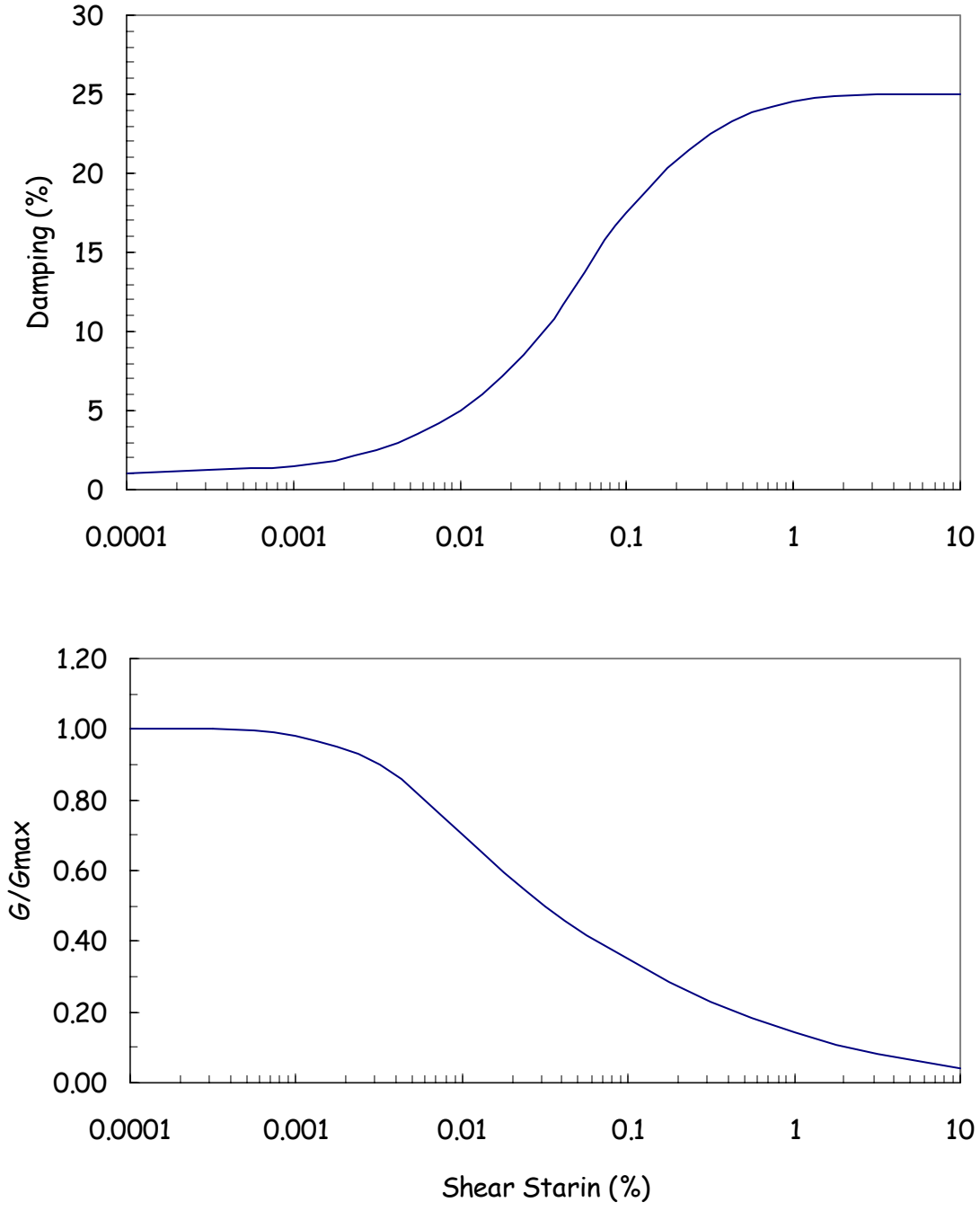

Figure 6.3-6. Damping curves and shear modulus reduction for soils

were developed to envelop the 1000-year design response spectra. Figure 6.3-7 shows that the resulting rock motion time histories have a return period in the range of 1000 to 1500 years. These time histories and their corresponding Fast Fourier Transform (FFT) are shown in Figures 6.3-8 through 6.3-10. The FFT results indicate that the rock motion energy is mainly in the frequency range of less than 15 Hz.

Time histories of the horizontal and vertical components of rock motion (i.e. H1 and V) were used as the outcrop motion at the basement rock of a free-field soil/rock column. As described previously, the seismic input for QFLUSH analyses, referred to as interface motion, was obtained at an elevation higher than the basement rock (i.e. at the fixed base of the finite-element model). The interface motion was computed from a separate free-field site response analysis. Because of large velocity contrast at the top of the basement rock, the interface motions are similar when computed from the free-field site response analyses at the river and bank sides.

c. Hydrodynamic forces

(1) Earthquake ground motions generate two types of dynamic fluid pressures in a lock structure – impulsive and convective. The impulsive pressure represents the effects of that portion of the fluid that moves in unison with the lock; the convective pressure represents the effects of the sloshing action of the fluid.

(2) The calculated fundamental period of water sloshing for the Olmsted Lock chamber is 7.07 sec (0.411 Hz). At this long period, the sloshing hydrodynamic pressures induced during earthquake excitation are two orders of magnitude smaller than the impulsive hydrodynamic pressures. Therefore, the sloshing effects were considered negligible and were not considered in this study.

(3) The impulsive pressures exerted on the lock walls during earthquake ground shaking were computed and compared using three different procedures: the velocity potential method, the Westergaard method, and the Housner method. The velocity potential method computes hydrodynamic pressure distributions on the lock walls by solving the Laplace equation for the velocity potential with appropriate boundary conditions. As with the Westergaard and Housner methods, the lock walls were assumed rigid.

(4) The hydrodynamic pressures obtained from the velocity potential method were used in the SPSI analyses. First, the hydrodynamic pressures were converted into nodal lumped masses according to the tributary area associated with each node. Then they were added to the lock wall nodal points as additional masses to account for the water inertia forces during earthquake excitation. The computed nodal added masses for the center, bank, and river walls of the example monolith are shown in Table 6.3-2. For the river wall, the added masses were computed for the inside and outside faces of the wall.

(5) Impulsive pressures are also exerted on the lock floor, but the added masses associated with the floor pressures must be considered active only in the vertical direction. The original version of FLUSH applies the added mass assigned to a nodal point to both the horizontal and vertical translational degrees of freedom associated with that node. To apply added masses to appropriate degrees of freedom, the original FLUSH was modified. The revised and enhanced version of the program (QFLUSH) allows added masses to be either applied to the horizontal or vertical, or both horizontal and vertical degrees of freedom.

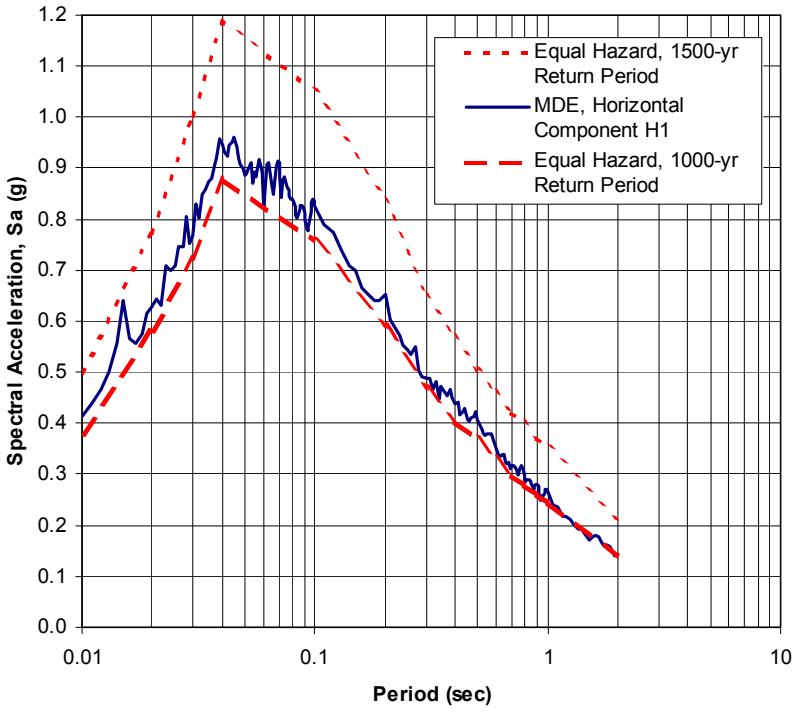

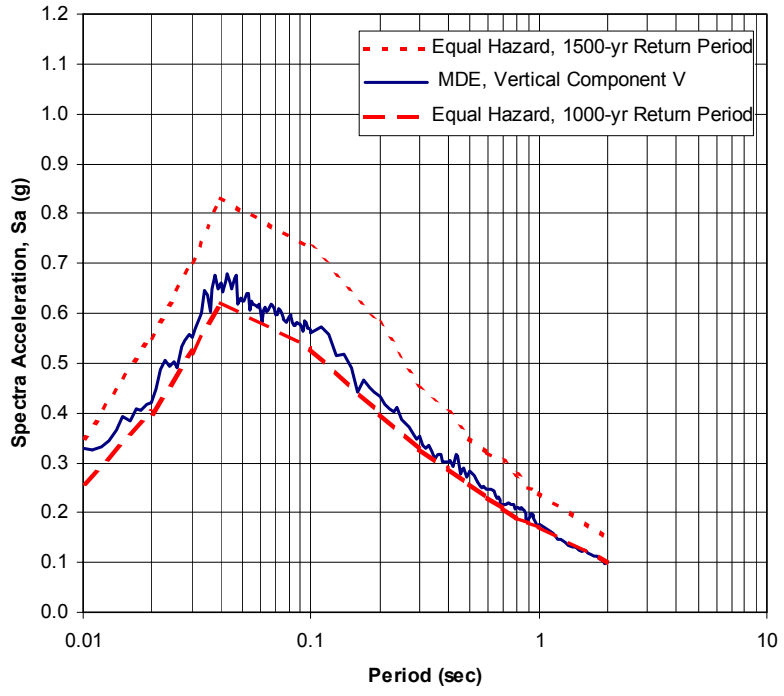

Figure 6.3-7. Comparison of 5%-damped rock motion response spectra with equal-hazard spectra

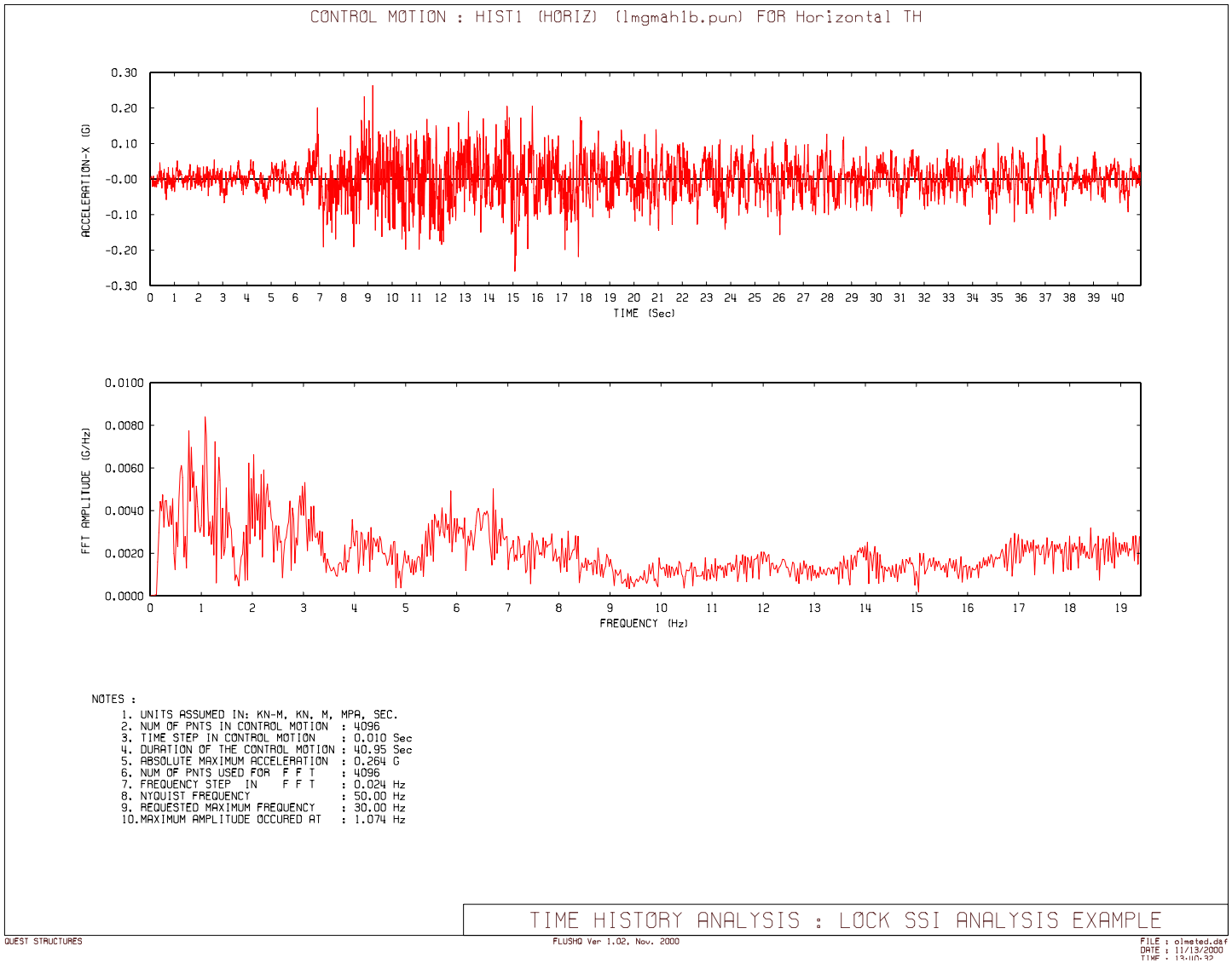

Figure 6.3-8. Time history and FFT of rock outcrop motion at Olmsted Locks and Dam (Horizontal component H1)

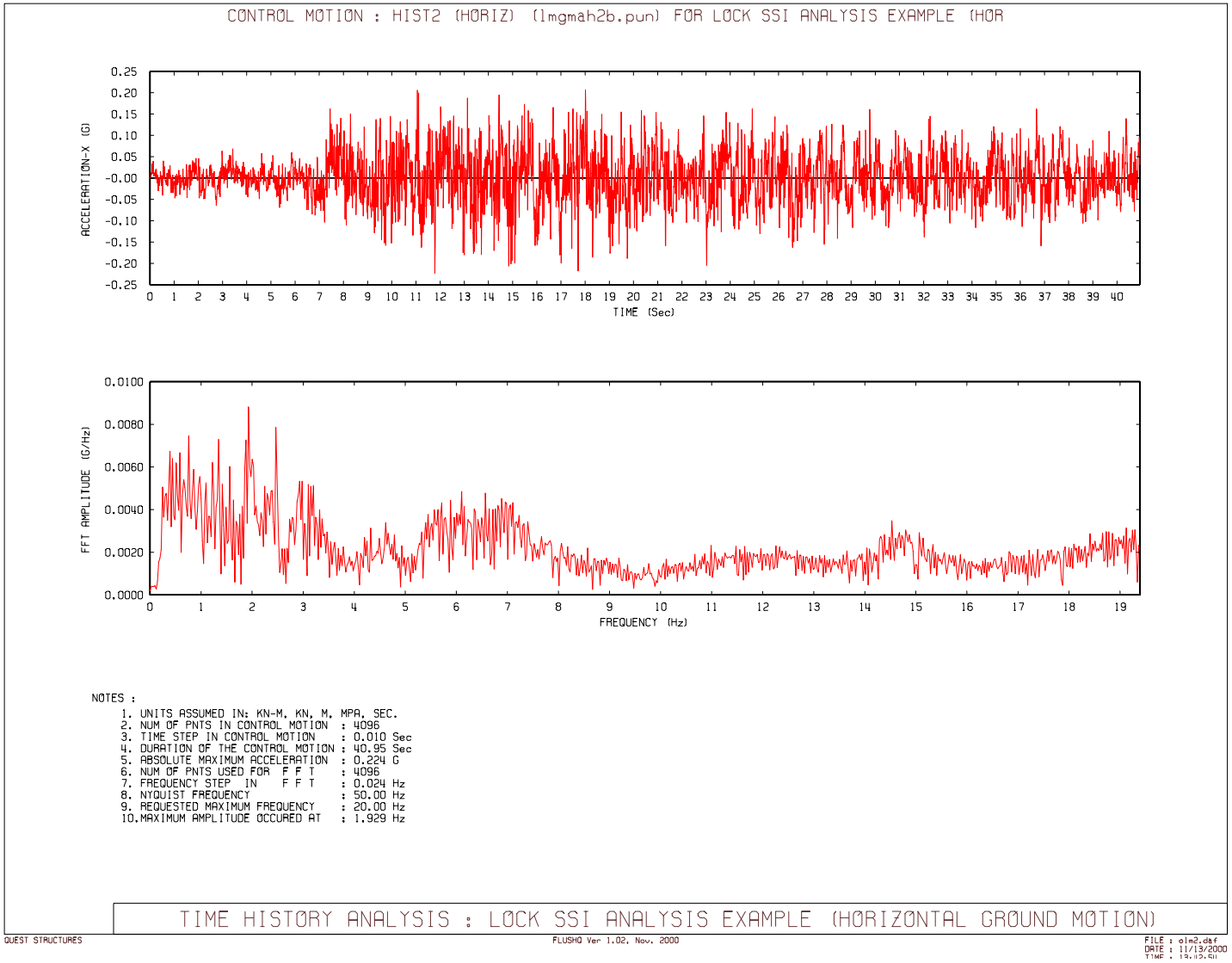

Figure 6.3-9. Time history and FFT of rock outcrop motion at Olmsted Locks and Dam (Horizontal component H2)

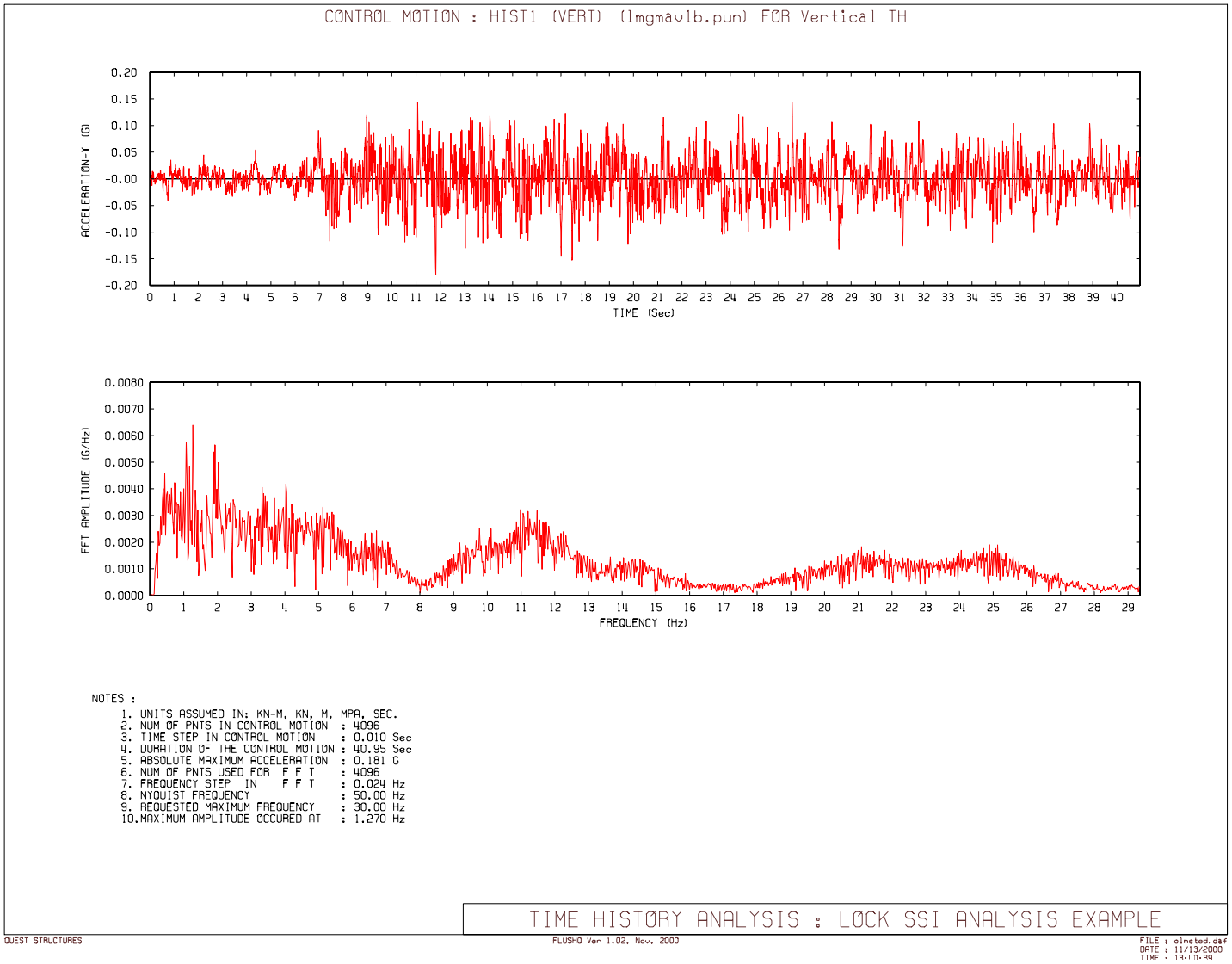

Figure 6.3-10. Time history and FFT of rock outcrop motion at Olmsted Locks and Dam (Vertical component V)

Table 6.3-2
Calcualted Added Mass Values for 1-ft-thick Lock Chamber Monolith

Node Elevation m (ft)	Bank and River Walls (Inside Face) Horizontal Mass kN-sec²/m (lb-sec²/ft)	Bank and River Walls (Inside Face) Vertical Mass kN-sec²/m (lb-sec²/ft)	Center Walls Horizontal Mass kN-sec²/m (lb-sec²/ft)	Center Walls Vertical Mass kN-sec²/m (lb-sec²/ft)	River Wall (Outside Face) Horizontal Mass kN-sec²/m (lb-sec²/ft)	River Wall (Outside Face) Vertical Mass kN-sec²/m (lb-sec²/ft)	Bank Wall (Outside Face) Horizontal Mass kN-sec²/m (lb-sec²/ft)	Bank Wall (Outside Face) Vertical Mass kN-sec²/m (lb-sec²/ft)
91.44 (300.00)	2.31 (158.60)		2.31 (158.60)					
89.31 (293.00)	4.91 (336.64)		6.70 (459.05)					
88.09 (289.00)	2.95 (202.47)							
87.48 (287.00)	2.06 (141.04)							
86.87 (285.00)	2.14 (146.79)		6.10 (417.80)					
86.26 (283.00)	1.87 (128.41)				0.21 (14.15)	0.06 (3.88)	0.10 (6.60)	0.06 (3.88)
86.12 (282.54)					0.09 (5.89)	0.14 (9.54)	0.04 (2.75)	0.14 (9.54)
85.98 (282.08)					0.09 (6.42)	0.17 (11.33)	0.04 (2.99)	0.17 (11.33)
85.84 (281.62)	1.69 (116.00)		3.95 (270.67)		0.10 (6.90)	0.19 (13.12)	0.05 (3.22)	0.19 (13.12)
85.70 (281.15)					0.09 (5.98)	0.18 (12.11)	0.04 (2.79)	0.18 (12.11)
85.61 (280.87)					0.07 (4.77)	0.15 (10.02)	0.03 (2.22)	0.15 (10.02)
85.52 (280.58)					0.07 (4.93)	0.16 (10.71)	0.03 (2.30)	0.16 (10.71)
85.43 (280.29)					0.07 (5.09)	0.17 (11.41)	0.03 (2.37)	0.17 (11.41)
85.34 (280.00)	2.08 (142.52)				0.30 (20.81)	0.09 (6.06)	0.02 (1.22)	0.09 (6.06)
84.73 (278.00)	2.35 (161.23)		3.30 (226.35)		0.63 (43.03)			
84.12 (276.00)	2.40 (164.78)		2.40 (164.78)		0.71 (48.79)			
83.52 (274.00)	2.45 (168.12)		2.45 (168.12)		0.79 (53.94)			
82.91 (272.00)	2.49 (170.86)		2.49 (170.86)		0.86 (58.64)			
82.30 (270.00)	2.52 (172.93)		2.52 (172.93)		0.92 (62.99)			
81.69 (268.00)	2.55 (174.62)		2.55 (174.62)		0.98 (67.06)			
81.08 (266.00)	2.57 (176.27)		2.57 (176.27)		1.03 (70.89)			
80.47 (264.00)	2.60 (177.88)		2.60 (177.88)		1.09 (74.53)			
79.86 (262.00)	2.61 (179.15)		2.61 (179.15)		0.57 (39.00)			
79.25 (260.00)	2.62 (179.81)		2.62 (179.81)					
78.64 (258.00)	2.63 (179.96)		2.63 (179.96)					
78.03 (256.00)	1.31 (89.97)	1.50 (103.03)	1.31 (89.97)	1.63 (111.91)				

6.3-8 Presentation and Evaluation of the Results

Dynamic SPSI analyses were performed for the primary horizontal component (H1) and for the vertical component (V) of the MDE rock motion described previously. Responses due to the horizontal and vertical excitations were combined in the time domain taking into account differences in phasing between the horizontal and vertical ground motion. Figures 6.3-11 and 6.3-12 show the strain-compatible shear-wave velocity profile and damping ratio profile, respectively, for a free-field soil column at the riverside. Results show that shear wave velocity drops as much as 50% and damping ratio reaches as high as 11% during the MDE excitation. Variation of free-field peak accelerations with depth at the riverside is shown in Figure 6.3-13. An amplification of about 2 is observed between the peak ground surface and interface accelerations.

a. Dynamic response of the soil-pile-lock structure system. Dynamic response of the soil-pile-lock structure was examined in terms of transfer functions between the top and bottom of the lock walls and between the top of lock walls and the free field ground surface at the riverside. These transfer functions are shown on Figure 6.3-14. As shown on this figure the river wall appears to have a fundamental frequency of about 4 Hz and the middle wall a fundamental frequency of about 6.2 Hz. The land wall appears to have a higher fundamental frequency of about 9 Hz because of the resistance of the backfill. The fundamental frequency of the foundation soil appears to be about 1 Hz and that of the soil-pile-lock system about 2.5 Hz.

b. Design criteria. The design criteria for the pile foundation and the lock structure are described in USAED, Louisville (1992). Allowable stresses and loads for HP 14×117 piles and allowable stresses for the reinforced concrete used in this study are summarized below.

c. Allowable stresses and loads for HP 14x117 (A-36 grade). For the extreme loading conditions (MDE), the allowable loads and allowable deflections are summarized in Table 6.3-3.

Table 6.3-3
Allowable Loads and Deflections for Steel H-Piles (HP 14 x 117) Under Extreme Loading Conditions (MDE)

Allowable Loads					Allowable Deflection	
Axial Compression at Pile Tips F_a kN (kips)	**Axial Tension[1] F_t, kN (kips)**	**Bending kN-m (k-ft)**	**Combined Axial and Bending[2] kN (kips) kN-m (k-ft)**	**Shear F_v kN (kips)**	**Vertical cm (in)**	**Horizontal cm (in)**
3,212 (722)	1,548 (348)	M_x = 680 (502) M_y = 236 (174)	$(F_a)_l$ = 4,824 (1,084) M_x = 680 (502) M_y = 236 (174)	1,068 (240)	<1.12 (<0.44)	<2.29 (<0.9)

[1] Soil is limiting factor.
[2] $(F_a)_l$ = allowable axial force for combination with allowable moment.

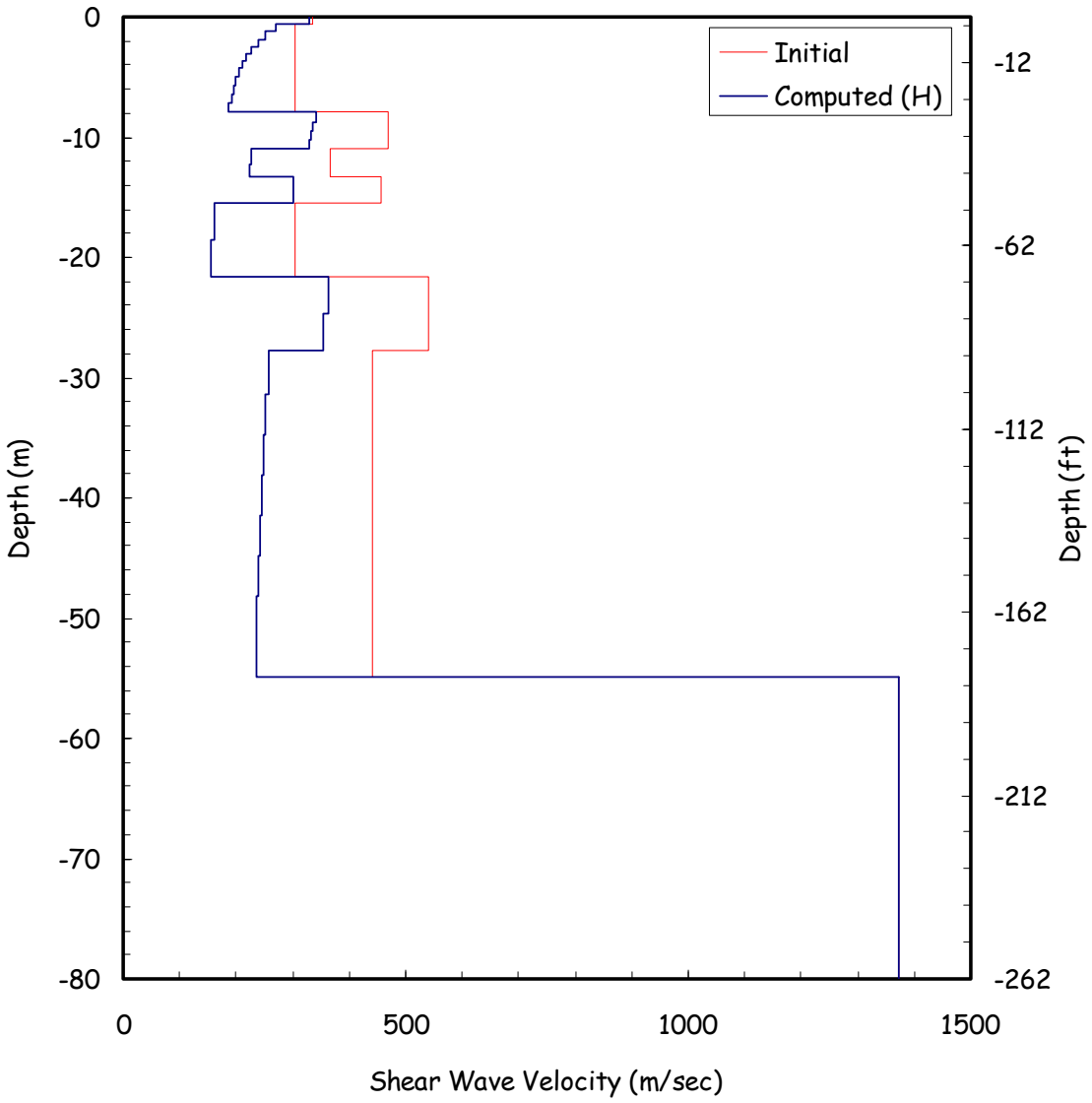

Figure 6.3-11. Comparison of initial shear-wave velocity with strain-compatible shear-wave velocity obtained from MDE excitation.

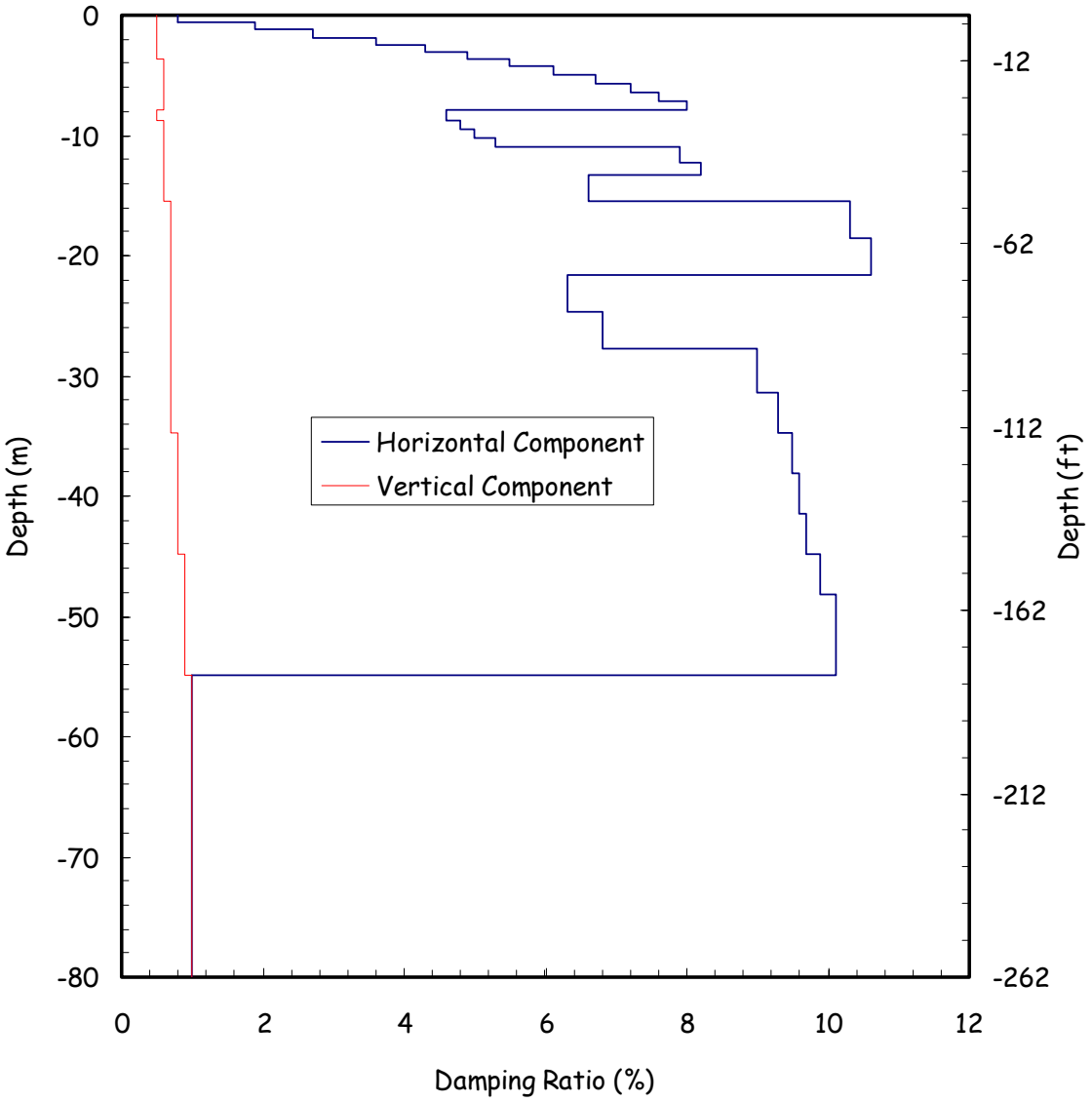

Figure 6.3-12. Strain-compatible damping ratio profile obtained from MDE excitation.

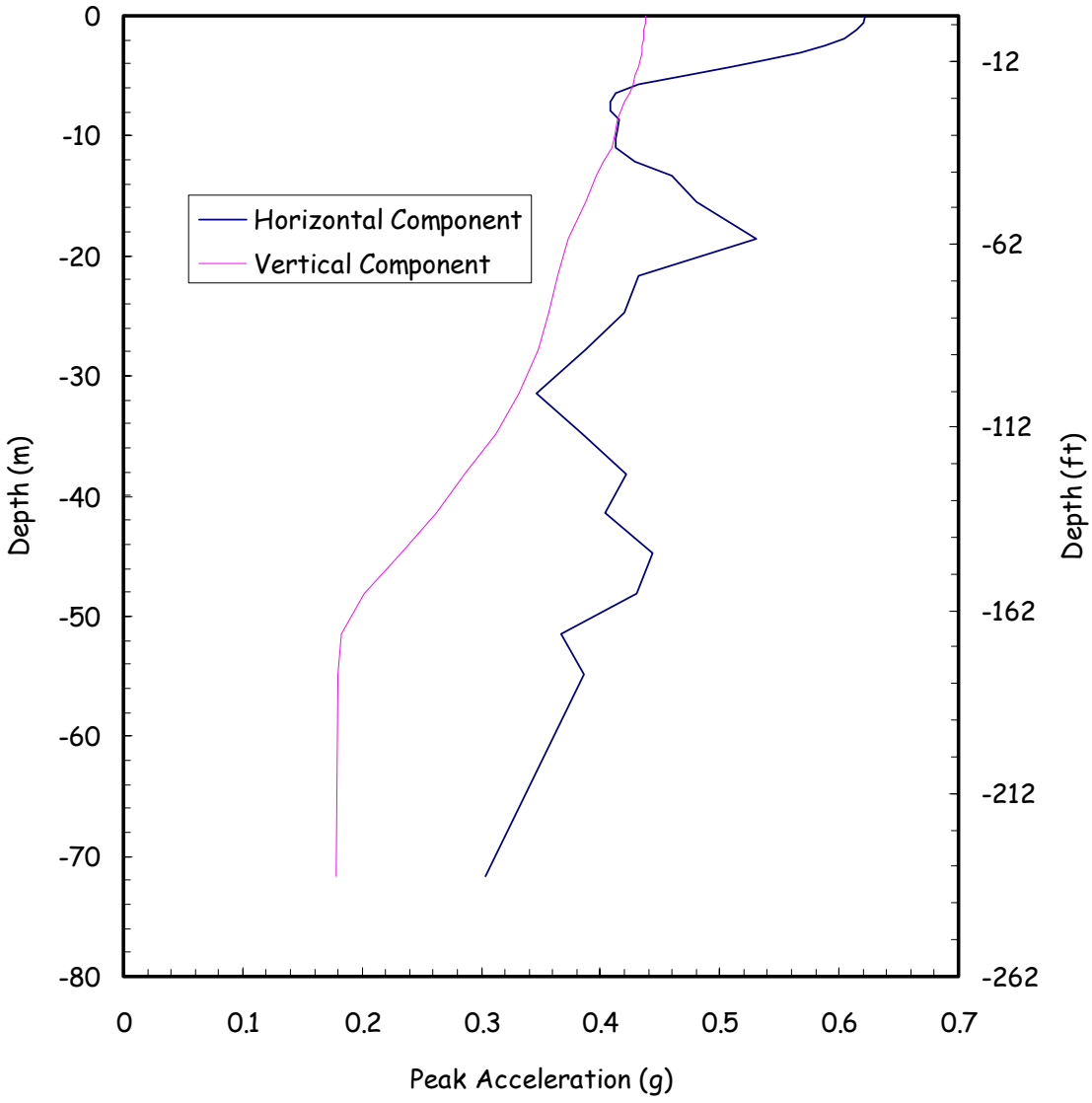

Figure 6.3-13. Variation of peak acceleration with depth for MDE excitation

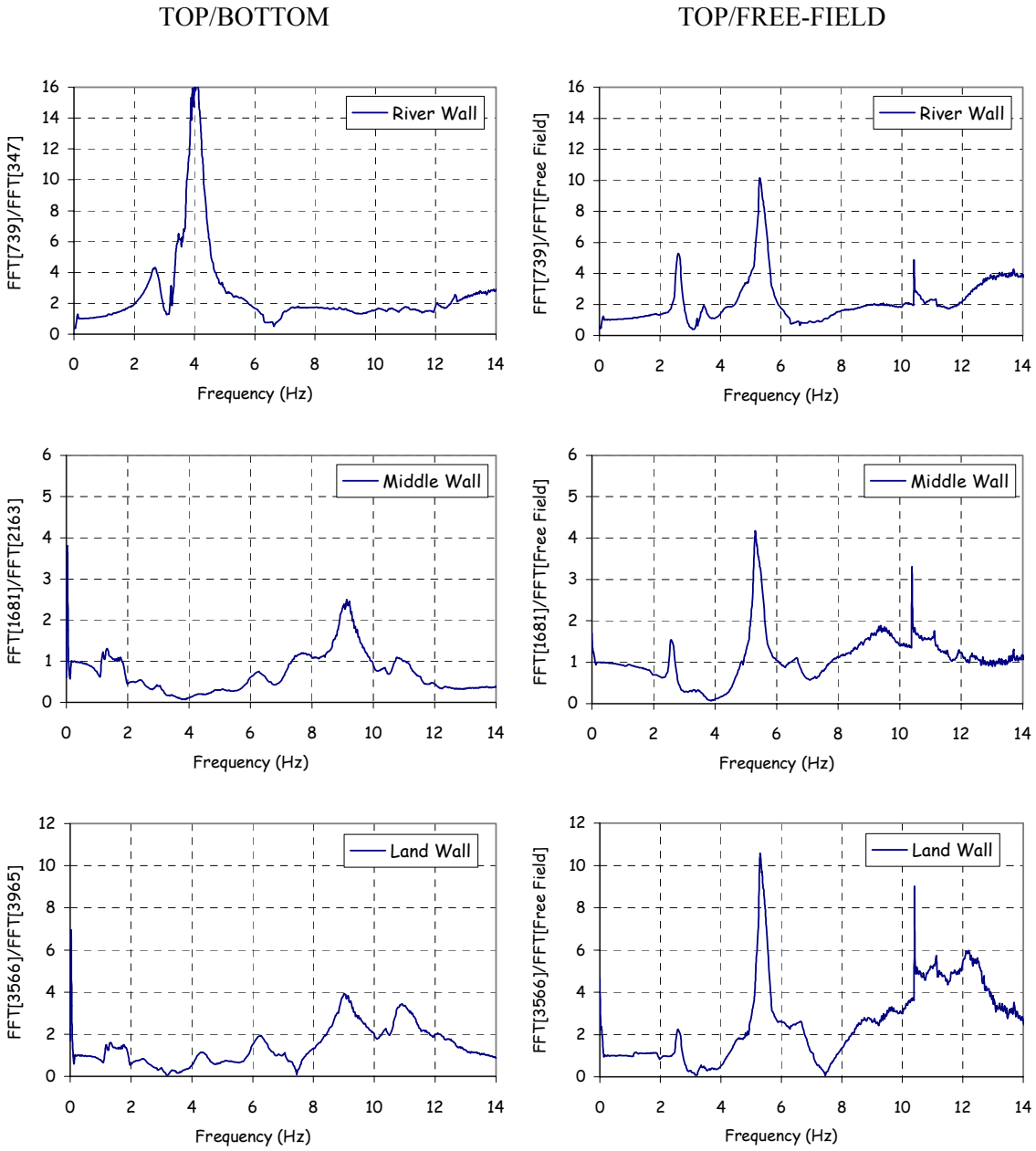

Figure 6.3-14. Transfer functions between top and bottom of lock walls, and top of lock walls and free field ground surface

d. Allowable stresses for reinforced concrete. The design of the lock concrete structure is in accordance with the strength design requirements for reinforced concrete hydraulic structures contained in EC 1110-2-267. The design of the concrete components of the lock is based on a minimum concrete compressive strength of 3,000 psi. Reinforced concrete design is based on billet steel bars conforming to the yield strength of 60,000 psi. Main reinforcement that is required by analysis is at a minimum as limited by ACI 318. Maximum tension reinforcement is as required by EC 1110-2-267.

e. Pile forces and moments.

(1) To consider possible phasing of the horizontal and vertical motions when the response from the horizontal and vertical excitations are combined with static loads, four loading combinations summarized in Table 6.3-4 are used.

Tabel 6.3-4

Various Static and Seismic Loads Combinaitons Evaluated

Case	Seismic Loads		Static Loads	
	Horizontal Excitation	Vertical Excitation	Bending Moment	Axial Force
1	+	+	+	+
2	+	-	+	+
3	-	+	+	+
4	-	-	+	+

(2) Table 6.3-5 shows peak values of static plus dynamic pile forces and moments for all piles for the load combination Case 3. Also shown in Table 6.3-5 are values of axial and shear forces at times of peak moments, values of moments and shear forces at times of peak axial forces, and values of moments and axial forces at times of peak shear forces. It is noted that peak moments and peak shear forces occur at the same time. However, peak moments and peak axial forces do not occur at the same time. The peak axial and shear forces shown in Table 6.3-5 indicate that they are substantially lower than the allowable values.

(3) To evaluate demand/capacity ratios for the H-piles, interaction factors of each pile I_p beneath the chamber monolith are computed in accordance with Equation (4-1). The interaction factors for the maximum pile moments and axial forces for the four load combination cases were computed and plotted, as shown in Figure 6.3-15. The interaction factors for load combination Case 3 are listed in the last column of Table 6.3-5. Figure 6.3-15 shows that the interaction factors depend on the phasing of the ground motion. To obtain maximum interaction factors for all possible ground motion phasing, Figure 6.3-16 was generated by selecting the maximum interaction factor for each individual piles from the four cases shown in Figure 6.3-15. The interaction factors were also computed in time domain for all the four combination cases. The resulting interaction factors at each time step for three typical piles located at the two extreme edges (i.e., river and bank sides) and at the center of the lock are shown in Figures 6.3-17 through 6.3-19. The results in Figures 6.3-16 through 6.3-19 show that values of the interaction factor are less than 0.82 with an average value of about 0.6, indicating the piles have adequate factors of safety.

f. Pile deflection. Relative displacements between selected locations of the lock structure (i.e., top and bottom of the lock walls, middle level of lock and lock base), and between pile head and pile tip computed from the combined horizontal and vertical excitations are summarized in Table 6.3.6. Relative displacements between the pile head and pile tip are slightly higher than the allowable values shown in Table 6.3-3.

g. Concrete section forces and moments

(1) Section forces and moments for critical sections shown on Figure 6.3-20 were computed from time histories of the concrete element stresses. Table 6.3-7 shows peak static plus dynamic forces and moments for the critical sections. Also shown in Table 6.3-7 are values of forces when the peak moments occur or values of moments when the peak forces occur. These data indicate that due to differences in phasing, the peak values of force and moment generally do not occur at the same time. However, peak values of shear force and moment tend to occur about the same time. Table 6.3-8 summarizes static section forces and moments used in combination with the dynamic section forces and moments.

(2) Time histories of the dynamic section forces and moments (combined horizontal and vertical excitations) for the selected sections are combined with the static forces and moments. The reinforced concrete strengths (the nominal strength and design strength) were computed in accordance with ACI-318 for each section using the post processing capabilities of QFLUSH. Examples of the interaction diagrams for concrete vertical sections 1, 3, 4, and 6 are shown on Figures 6.3-21 to 6.3-24 and for horizontal sections 4, 5, 15, and 16 are shown in Figures 6.3-25 to 6.3-28. Also shown on these figures for comparison are the nominal strength (dashed line) and design strength (solid line) envelopes of the reinforced concrete of the respective sections. The data shown on Figures 6.3-21 and 6.3-28 were used for the reinforcement design and evaluation. The results show that axial force-moment demand pairs for all sections fall within the interaction capacity diagrams, except for vertical Sections 1 and 6. At these sections less than 10% of axial force-moment pairs fall outside the interaction diagrams. This response behavior, however, is acceptable because the high axial-force demand pairs are associated with transient moments with little damage potential, as illustrated by the time histories of the axial force-bending moment interaction factors in Figure 6.3.29. Thus the reinforced concrete design, represented by the interaction diagrams, is considered adequate for the computed seismic demands.

6.3-9 Conclusions

In this section, an example of seismic time-history analysis of a pile-supported lock structure was illustrated. The procedure was used to analyze the seismic response of the Olmsted Locks under the MDE loading conditions and to provide data for the design of the pile foundation and the reinforcement steel of the concrete sections.

Table 6.3-5
Combined Static and Dynamic Pile Forces, Moments, and Interaction Factors for MDE Loading

LOAD COMBINATION: -1.0(Horizontal) + 1.0(Vertical) + 1.0(Static)

Pile	X-Coordinate m (ft)	Time History Peak values			At Peak Moment		At Peak Axial		At Peak Shear		Peak Interaction Factor
		Moment kN-m (k-ft)	Axial Force kN (kips)	Shear Force kN (kips)	Axial Force kN (kips)	Shear Force kN (kips)	Moment kN-m (k-ft)	Shear Force kN (kips)	Moment kN-m (k-ft)	Axial Force kN (kips)	
1	-47.63 (-156.27)	-283.25 (-208.90)	-1,581.87 (-355.60)	606.77 (136.40)	-1,403.04 (-315.40)	606.77 (136.40)	47.28 (34.87)	-148.44 (-33.37)	-283.25 (-208.90)	-1,403.04 (-315.40)	0.74
2	-45.72 (-150.00)	-246.37 (-181.70)	-1,088.98 (-244.80)	467.09 (105.00)	-979.55 (-220.20)	467.09 (105.00)	30.95 (22.83)	-78.92 (-17.74)	-246.37 (-181.70)	-979.55 (-220.20)	0.59
3	-43.82 (-143.77)	-232.40 (-171.40)	-854.10 (-192.00)	446.62 (100.40)	-742.89 (-167.00)	446.62 (100.40)	34.86 (25.71)	-104.41 (-23.47)	-232.40 (-171.40)	-742.89 (-167.00)	0.52
4	-41.91 (-137.50)	-223.72 (-165.00)	-758.02 (-170.40)	446.18 (100.30)	-544.49 (-122.40)	433.77 (97.51)	-65.14 (-48.04)	173.31 (38.96)	-202.30 (-149.20)	-663.26 (-149.10)	0.49
5	-40.01 (-131.27)	-212.87 (-157.00)	-739.33 (-166.20)	475.10 (106.80)	-436.30 (-98.08)	412.46 (92.72)	-67.04 (-49.44)	191.19 (42.98)	-210.98 (-155.60)	-692.18 (-155.60)	0.47
6	-38.10 (-125.00)	-218.43 (-161.10)	-734.88 (-165.20)	480.88 (108.10)	-655.26 (-147.30)	480.88 (108.10)	-60.49 (-44.61)	166.68 (37.47)	-218.43 (-161.10)	-655.26 (-147.30)	0.47
7	-36.19 (-118.73)	223.72 (165.00)	-129.81 (-29.18)	-316.20 (-71.08)	-127.67 (-28.70)	-316.20 (-71.08)	222.77 (164.30)	-314.73 (-70.75)	223.72 (165.00)	-127.67 (-28.70)	0.36
8	-34.29 (-112.50)	234.03 (172.60)	-129.32 (-29.07)	-327.41 (-73.60)	-125.31 (-28.17)	-327.41 (-73.60)	231.31 (170.60)	-323.40 (-72.70)	234.03 (172.60)	-125.31 (-28.17)	0.37
9	-32.39 (-106.27)	250.30 (184.60)	-134.97 (-30.34)	-346.89 (-77.98)	-127.18 (-28.59)	-346.89 (-77.98)	238.09 (175.60)	-329.19 (-74.00)	250.30 (184.60)	-127.18 (-28.59)	0.40
10	-28.58 (-93.77)	275.25 (203.00)	-141.95 (-31.91)	-381.59 (-85.78)	-126.02 (-28.33)	-381.59 (-85.78)	124.44 (91.78)	-167.66 (-37.69)	275.25 (203.00)	-126.02 (-28.33)	0.43
11	-24.76 (-81.23)	272.67 (201.10)	-150.80 (-33.90)	-377.72 (-84.91)	-120.60 (-27.11)	-377.72 (-84.91)	130.49 (96.24)	-177.05 (-39.80)	272.67 (201.10)	-120.60 (-27.11)	0.43
12	-20.95 (-68.73)	269.14 (198.50)	-126.74 (-28.49)	-372.87 (-83.82)	-98.36 (-22.11)	-372.87 (-83.82)	181.15 (133.60)	-249.38 (-56.06)	269.14 (198.50)	-98.36 (-22.11)	0.42
13	-17.15 (-56.27)	248.13 (183.00)	-133.77 (-30.07)	-344.04 (-77.34)	-93.11 (-20.93)	-344.04 (-77.34)	-138.30 (-102.00)	200.85 (45.15)	248.13 (183.00)	-93.11 (-20.93)	0.39
14	-15.24 (-50.00)	234.98 (173.30)	-141.42 (-31.79)	-323.00 (-72.61)	-92.93 (-20.89)	-323.00 (-72.61)	-125.41 (-92.49)	186.61 (41.95)	234.98 (173.30)	-92.93 (-20.89)	0.37
15	-13.34 (-43.77)	228.60 (168.60)	-163.53 (-36.76)	-312.28 (-70.20)	-77.85 (-17.50)	-312.28 (-70.20)	-115.98 (-85.54)	175.63 (39.48)	228.60 (168.60)	-77.85 (-17.50)	0.37
16	-11.43 (-37.50)	221.96 (163.70)	-179.94 (-40.45)	-302.09 (-67.91)	-74.51 (-16.75)	-302.09 (-67.91)	-105.27 (-77.64)	162.01 (36.42)	221.96 (163.70)	-74.51 (-16.75)	0.36
17	-9.53 (-31.25)	210.84 (155.50)	-216.42 (-48.65)	-285.77 (-64.24)	-74.47 (-16.74)	-285.77 (-64.24)	-87.17 (-64.29)	136.17 (30.61)	210.84 (155.50)	-74.47 (-16.74)	0.35
18	-7.62 (-25.00)	192.81 (142.20)	-251.65 (-56.57)	-259.48 (-58.33)	-109.12 (-24.53)	-259.48 (-58.33)	-73.58 (-54.27)	108.81 (24.46)	192.81 (142.20)	-109.12 (-24.53)	0.34
19	-5.72 (-18.75)	183.32 (135.20)	-210.95 (-47.42)	-249.65 (-56.12)	-142.84 (-32.11)	-249.65 (-56.12)	-63.65 (-46.94)	90.53 (20.35)	183.32 (135.20)	-142.84 (-32.11)	0.31
20	-3.81 (-12.50)	180.47 (133.10)	-189.01 (-42.49)	-250.14 (-56.23)	-135.59 (-30.48)	-250.14 (-56.23)	99.83 (73.63)	-137.68 (-30.95)	180.47 (133.10)	-135.59 (-30.48)	0.30
21	-1.91 (-6.25)	175.45 (129.40)	-187.37 (-42.12)	-243.02 (-54.63)	-136.70 (-30.73)	-243.02 (-54.63)	98.11 (72.36)	-135.63 (-30.49)	175.45 (129.40)	-136.70 (-30.73)	0.30
22	0.00 (0.00)	170.84 (126.00)	-195.29 (-43.90)	-235.81 (-53.01)	-163.17 (-36.68)	-235.81 (-53.01)	96.89 (71.46)	-134.92 (-30.33)	170.84 (126.00)	-163.17 (-36.68)	0.29
23	1.91 (6.25)	-173.55 (-128.00)	-1,179.29 (-265.10)	401.70 (90.30)	-1,022.26 (-229.80)	401.70 (90.30)	-76.21 (-56.21)	166.64 (37.46)	-173.55 (-128.00)	-1,022.26 (-229.80)	0.50
24	3.81 (12.50)	-176.81 (-130.40)	-1,265.59 (-284.50)	410.10 (92.19)	-1,098.77 (-247.00)	410.10 (92.19)	-79.59 (-58.70)	173.09 (38.91)	-176.81 (-130.40)	-1,098.77 (-247.00)	0.52
25	5.72 (18.75)	-182.64 (-134.70)	-1,383.91 (-311.10)	413.97 (93.06)	-1,209.98 (-272.00)	413.97 (93.06)	-86.37 (-63.70)	182.61 (41.05)	-182.64 (-134.70)	-1,209.98 (-272.00)	0.56
26	7.62 (25.00)	-201.62 (-148.70)	-1,482.67 (-333.30)	462.64 (104.00)	-1,304.73 (-293.30)	462.64 (104.00)	-106.60 (-78.62)	235.59 (52.96)	-201.62 (-148.70)	-1,304.73 (-293.30)	0.60
27	9.53 (31.25)	-228.20 (-168.30)	-1,464.88 (-329.30)	556.95 (125.20)	-1,295.39 (-291.20)	556.95 (125.20)	-135.47 (-99.91)	338.84 (76.17)	-228.20 (-168.30)	-1,295.39 (-291.20)	0.64
28	11.43 (37.50)	-236.87 (-174.70)	-1,331.42 (-299.30)	561.40 (126.20)	-1,157.04 (-260.10)	561.40 (126.20)	-144.54 (-106.60)	349.34 (78.53)	-236.87 (-174.70)	-1,157.04 (-260.10)	0.62
29	13.34 (43.77)	-237.96 (-175.50)	-1,246.01 (-280.10)	551.61 (124.00)	-969.76 (-218.00)	550.27 (123.70)	-143.86 (-106.10)	336.13 (75.56)	-237.15 (-174.90)	-1,053.39 (-236.80)	0.61
30	15.24 (50.00)	-237.15 (-174.90)	-1,211.31 (-272.30)	541.38 (121.70)	-905.26 (-203.50)	541.38 (121.70)	-137.89 (-101.70)	321.18 (72.20)	-237.15 (-174.90)	-905.26 (-203.50)	0.60
31	17.15 (56.27)	-241.48 (-178.10)	-1,380.36 (-310.30)	697.96 (156.90)	-990.67 (-222.70)	697.96 (156.90)	-130.99 (-96.61)	390.00 (87.67)	-241.48 (-178.10)	-990.67 (-222.70)	0.64
32	20.95 (68.73)	-255.31 (-188.30)	-1,517.81 (-341.20)	859.00 (193.10)	-1,012.02 (-227.50)	859.00 (193.10)	-141.15 (-104.10)	482.66 (108.50)	-255.31 (-188.30)	-1,012.02 (-227.50)	0.69
33	24.76 (81.23)	-248.26 (-183.10)	-1,429.73 (-321.40)	836.75 (188.10)	-907.48 (-204.00)	836.75 (188.10)	-135.03 (-99.59)	465.75 (104.70)	-248.26 (-183.10)	-907.48 (-204.00)	0.66
34	28.58 (93.77)	-233.21 (-172.00)	-1,333.20 (-299.70)	794.49 (178.60)	-716.65 (-161.10)	794.49 (178.60)	97.08 (71.60)	-349.29 (-78.52)	-233.21 (-172.00)	-716.65 (-161.10)	0.62
35	32.39 (106.27)	-206.23 (-152.10)	-1,076.08 (-241.90)	576.96 (129.70)	-278.38 (-62.58)	569.40 (128.00)	85.57 (63.11)	-275.27 (-61.88)	-199.45 (-147.10)	-402.10 (-90.39)	0.53
36	34.29 (112.50)	-194.30 (-143.30)	-884.35 (-198.80)	443.16 (99.62)	-195.82 (-44.02)	443.16 (99.62)	84.17 (62.08)	-196.89 (-44.26)	-194.30 (-143.30)	-195.82 (-44.02)	0.47
37	36.19 (118.73)	-187.66 (-138.40)	-875.01 (-196.70)	469.31 (105.50)	-159.08 (-35.76)	464.42 (104.40)	80.28 (59.21)	-252.85 (-56.84)	-185.89 (-137.10)	-145.55 (-32.72)	0.46
38	38.10 (125.00)	183.86 (135.60)	-143.95 (-32.36)	-258.28 (-58.06)	-6.14 (-1.38)	-258.28 (-58.06)	-131.37 (-96.89)	189.50 (42.60)	183.86 (135.60)	-6.14 (-1.38)	0.30
39	40.01 (131.27)	178.30 (131.50)	-178.56 (-40.14)	-247.38 (-55.61)	2.16 (0.49)	-247.38 (-55.61)	-71.58 (-52.79)	108.05 (24.29)	178.30 (131.50)	2.16 (0.49)	0.30
40	41.91 (137.50)	170.03 (125.40)	-177.67 (-39.94)	-231.28 (-51.99)	-19.28 (-4.34)	-231.28 (-51.99)	-12.16 (-8.97)	16.60 (3.73)	170.03 (125.40)	-19.28 (-4.34)	0.29
41	43.82 (143.77)	167.05 (123.20)	-152.94 (-34.38)	-226.96 (-51.02)	-60.54 (-13.61)	-226.96 (-51.02)	-82.80 (-61.07)	121.98 (27.42)	167.05 (123.20)	-60.54 (-13.61)	0.28
42	45.72 (150.00)	183.32 (135.20)	-1,548.51 (-348.10)	-395.47 (-88.90)	-725.10 (-163.00)	-395.38 (-88.88)	120.54 (88.90)	-229.99 (-51.70)	181.01 (133.50)	-747.79 (-168.10)	0.59
43	47.63 (156.27)	230.23 (169.80)	-2,308.75 (-519.00)	-589.87 (-132.60)	-1,098.77 (-247.00)	-589.87 (-132.60)	179.25 (132.20)	-463.53 (-104.20)	230.23 (169.80)	-1,098.77 (-247.00)	0.82

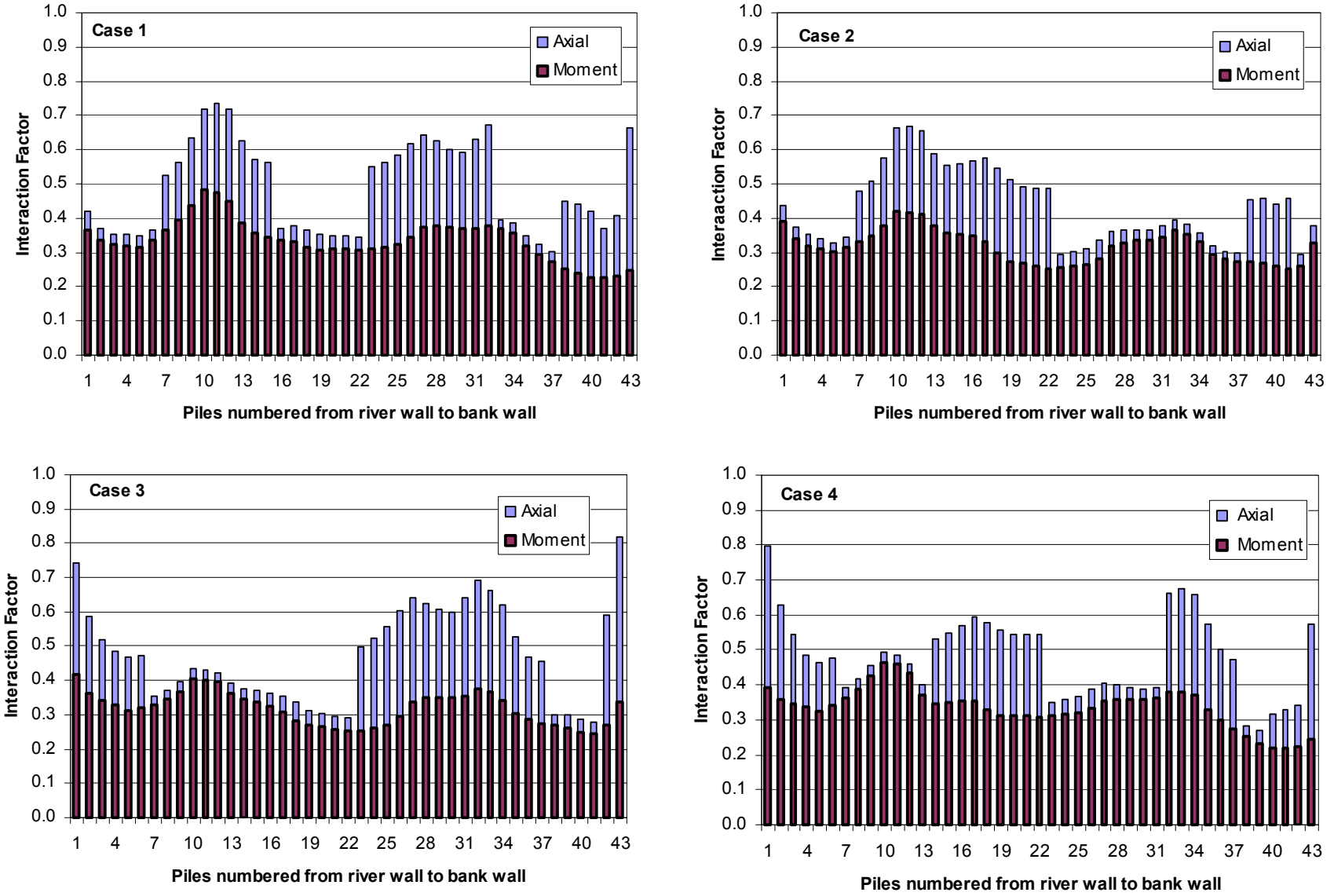

Figure 6.3-15. Maximum piles interaction factors for each load combination case listed in Table 6.3-4.

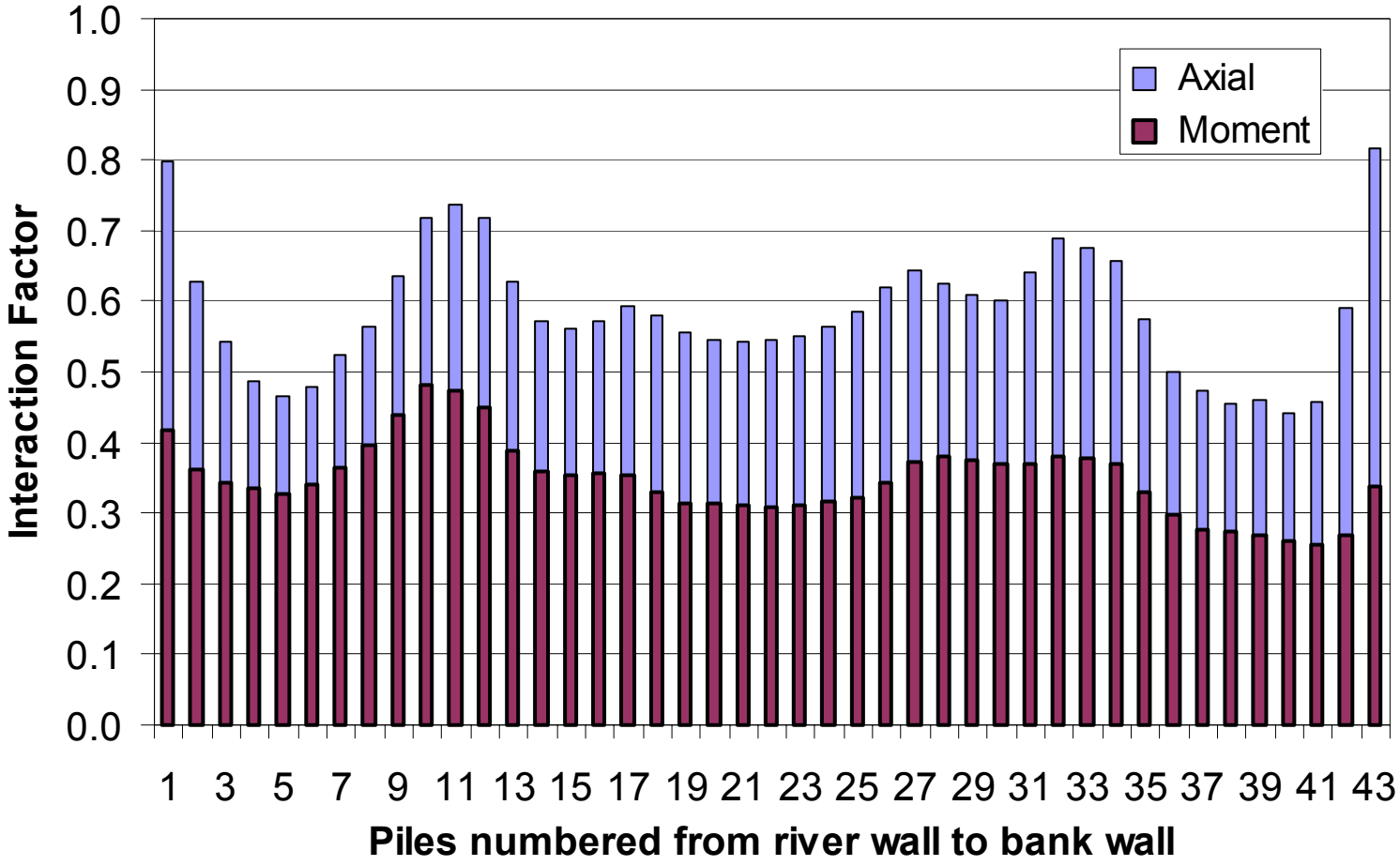

Figure 6.3-16. Envelopes of Maximum piles interaction factors for all load combination cases

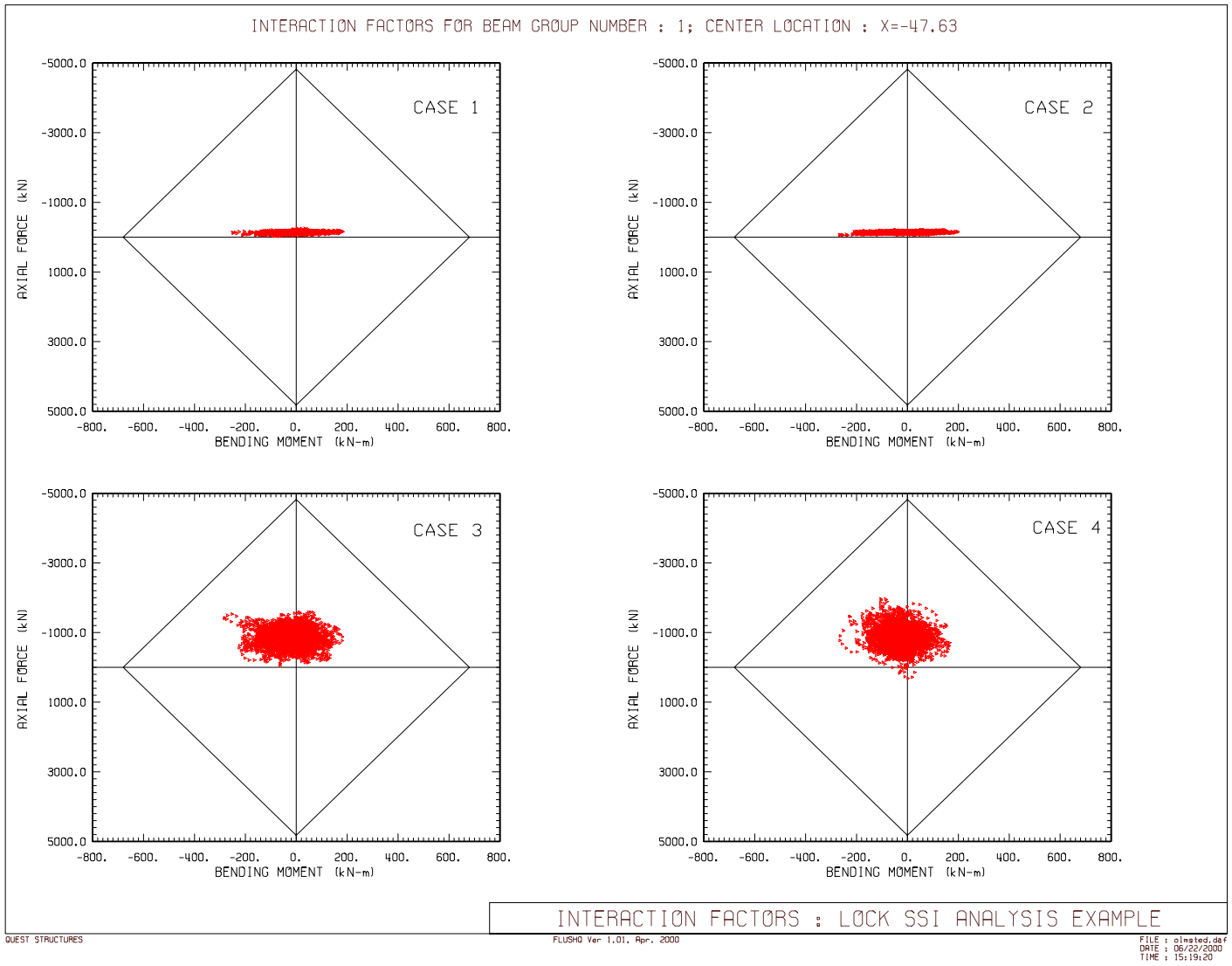

Figure 6.3-17. Comparison of Pile 1 (river side) bending moment-axial force demands with bending-moment-axial force capacities for load combination cases shown in Table 6.3-4.

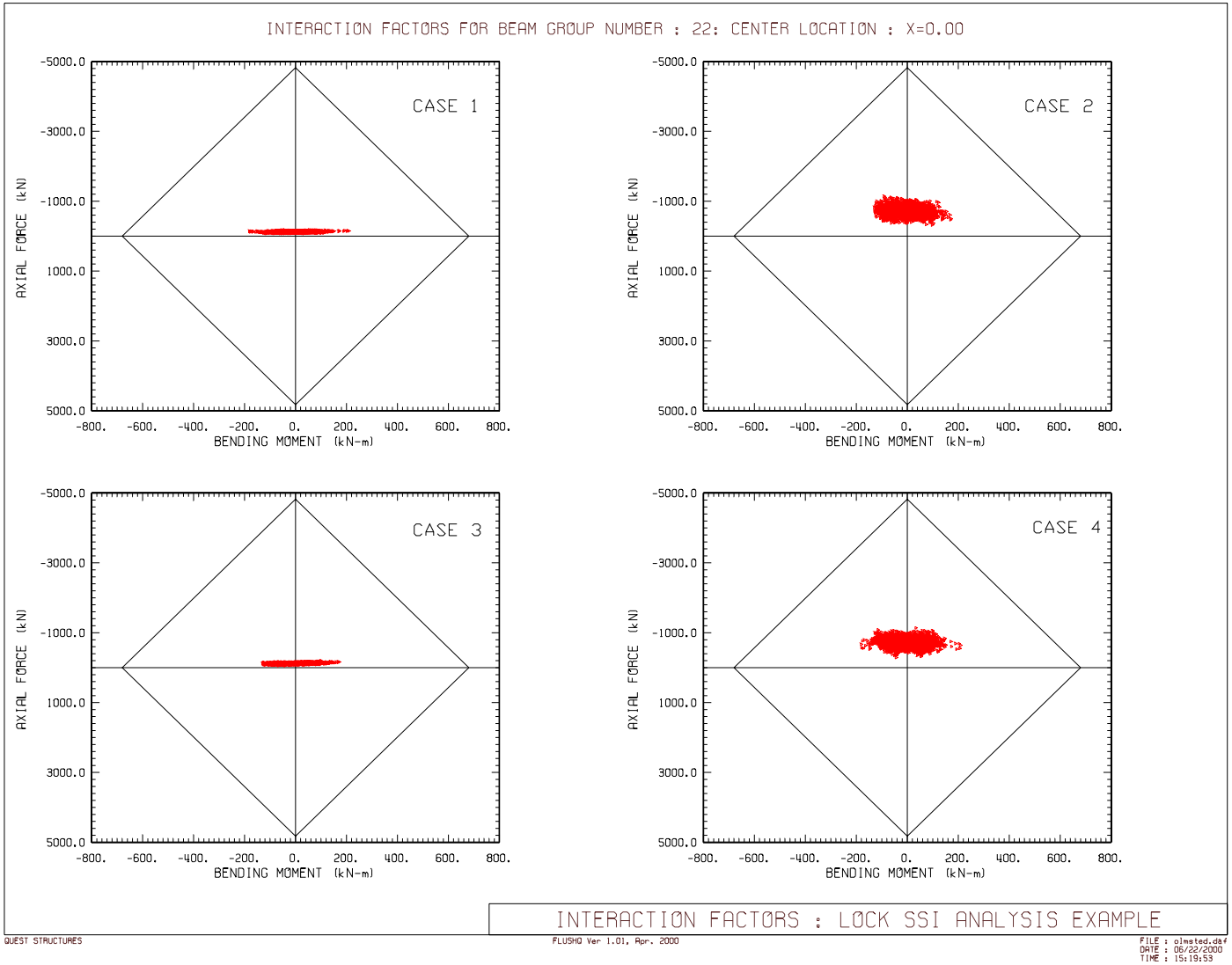

Figure 6.3-18. Comparison of Pile 22 (center) bending moment-axial force demands with bending moment-axial force capacities for load combination cases shown in Table 6.3-4.

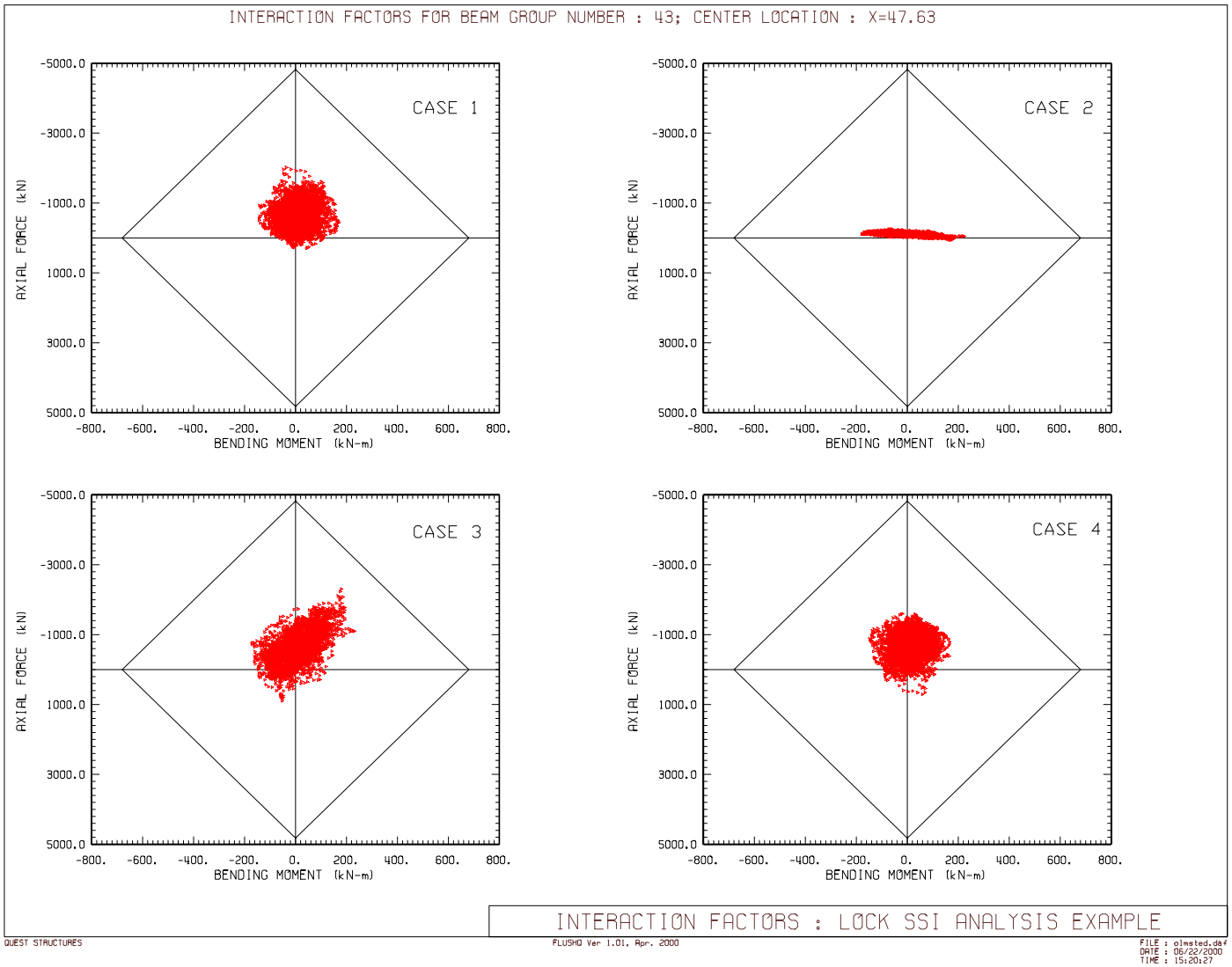

Figure 6.3-19. Comparison of Pile 43 (land side) bending moment-axial force demands with bending moment-axial force capacities for load combination cases shown in Table 6.3-4.

Table 6.3-6

Absolute and relative displacements at selected piles and lock walls locations of chamber monolith for MDE excitation

					(TH Horizontal) + (TH Vertical) + Static				(TH Horizontal) - (TH Vertical) + Static			
	Location				Horizontal Displacement cm (in)		Vertical Displacement cm (in)		Horizontal Displacement cm (in)		Vertical Displacement cm (in)	
		Node	X, m	Y, m	Absolute	Relative	Absolute	Relative	Absolute	Relative	Absolute	Relative
Pile Displacement	Left	347	-47.63	74.37	8.65 (3.40)	2.59 (1.02)	5.74 (2.26)	0.66 (0.26)	8.47 (3.34)	2.21 (0.87)	5.39 (2.12)	0.48 (0.19)
		377	-47.63	54.56	6.06 (2.39)		5.09 (2.00)		6.26 (2.46)		4.91 (1.93)	
	Middle	2163	0.00	74.37	8.82 (3.47)	2.77 (1.09)	5.26 (2.07)	0.38 (0.15)	8.67 (3.41)	2.86 (1.13)	5.41 (2.13)	0.36 (0.14)
		2193	0.00	54.56	6.05 (2.38)		4.88 (1.92)		5.81 (2.29)		5.05 (1.99)	
	Right	3965	47.63	74.37	8.83 (3.48)	2.62 (1.03)	5.84 (2.30)	0.67 (0.26)	8.70 (3.42)	2.64 (1.04)	6.13 (2.41)	0.70 (0.27)
		3995	47.63	54.56	6.21 (2.45)		5.17 (2.04)		6.05 (2.38)		5.43 (2.14)	
Lock Displacement	Left Wall	194	-49.71	85.34	9.34 (3.68)	0.70 (0.28)	6.01 (2.37)	0.07 (0.03)	9.22 (3.63)	0.75 (0.30)	5.52 (2.17)	0.05 (0.02)
		212	-49.71	74.37	8.64 (3.40)		5.94 (2.34)		8.47 (3.34)		5.46 (2.15)	
		739	-41.48	94.53	9.94 (3.91)	1.25 (0.49)	5.54 (2.18)	0.06 (0.02)	9.90 (3.90)	1.39 (0.55)	5.48 (2.16)	0.05 (0.02)
		765	-41.48	74.37	8.69 (3.42)		5.48 (2.16)		8.51 (3.35)		5.43 (2.14)	
	Middle Wall	1681	-7.93	94.53	9.43 (3.71)	0.63 (0.25)	5.29 (2.08)	0.04 (0.01)	9.28 (3.65)	0.62 (0.24)	5.24 (2.06)	0.02 (0.01)
		1703	-7.93	74.37	8.80 (3.47)		5.25 (2.07)		8.66 (3.41)		5.22 (2.06)	
		2628	7.93	94.53	9.43 (3.71)	0.55 (0.21)	5.32 (2.10)	0.06 (0.02)	9.28 (3.65)	0.55 (0.22)	5.66 (2.23)	0.07 (0.03)
		2650	7.93	74.37	8.89 (3.50)		5.26 (2.07)		8.73 (3.44)		5.59 (2.20)	
	Right Wall	3566	41.48	94.53	12.01 (4.73)	3.13 (1.23)	5.20 (2.05)	-0.07 (-0.03)	11.98 (4.72)	3.23 (1.27)	5.33 (2.10)	-0.10 (-0.04)
		3592	41.48	74.37	8.88 (3.50)		5.27 (2.07)		8.76 (3.45)		5.43 (2.14)	
		4112	49.71	85.34	10.51 (4.14)	1.67 (0.66)	6.15 (2.42)	0.09 (0.04)	10.47 (4.12)	1.77 (0.70)	6.50 (2.56)	0.10 (0.04)
		4130	49.71	74.37	8.84 (3.48)		6.06 (2.39)		8.70 (3.43)		6.40 (2.52)	

Table 6.3-6
Continued

					- (TH Horizontal) + (TH Vertical) + Static				- (TH Horizontal) - (TH Vertical) + Static			
	Location				Horizontal Displacement cm (in)		Vertical Displacement cm (in)		Horizontal Displacement cm (in)		Vertical Displacement cm (in)	
		Node	X, m	Y, m	Absolute	Relative	Absolute	Relative	Absolute	Relative	Absolute	Relative
Pile Displacement	Left	347	-47.63	74.37	9.04 (3.56)	2.40 (0.95)	8.95 (3.52)	3.72 (1.46)	9.21 (3.63)	2.30 (0.90)	6.22 (2.45)	0.61 (0.24)
		377	-47.63	54.56	6.63 (2.61)		5.23 (2.06)		6.92 (2.72)		5.61 (2.21)	
	Middle	2163	0.00	74.37	9.07 (3.57)	2.86 (1.12)	5.22 (2.05)	0.38 (0.15)	9.22 (3.63)	2.76 (1.09)	5.33 (2.10)	0.37 (0.15)
		2193	0.00	54.56	6.21 (2.44)		4.84 (1.91)		6.46 (2.54)		4.96 (1.95)	
	Right	3965	47.63	74.37	8.96 (3.53)	2.92 (1.15)	4.60 (1.81)	-0.29 (-0.12)	9.09 (3.58)	2.90 (1.14)	5.49 (2.16)	0.59 (0.23)
		3995	47.63	54.56	6.04 (2.38)		4.89 (1.93)		6.20 (2.44)		4.90 (1.93)	
Lock Displacement	Left Wall	194	-49.71	85.34	10.54 (4.15)	1.49 (0.59)	6.02 (2.37)	0.06 (0.03)	10.65 (4.19)	1.44 (0.56)	6.50 (2.56)	0.06 (0.02)
		212	-49.71	74.37	9.05 (3.56)		5.96 (2.35)		9.22 (3.63)		6.44 (2.54)	
		739	-41.48	94.53	11.90 (4.69)	2.82 (1.11)	5.52 (2.17)	0.02 (0.01)	11.95 (4.70)	2.69 (1.06)	5.54 (2.18)	-0.06 (-0.02)
		765	-41.48	74.37	9.08 (3.58)		5.51 (2.17)		9.26 (3.65)		5.59 (2.20)	
	Middle Wall	1681	-7.93	94.53	9.75 (3.84)	0.63 (0.25)	5.41 (2.13)	0.06 (0.02)	9.90 (3.90)	0.64 (0.25)	5.59 (2.20)	0.06 (0.02)
		1703	-7.93	74.37	9.12 (3.59)		5.35 (2.11)		9.27 (3.65)		5.52 (2.17)	
		2628	7.93	94.53	9.75 (3.84)	0.69 (0.27)	5.14 (2.02)	0.06 (0.02)	9.91 (3.90)	0.69 (0.27)	5.13 (2.02)	0.01 (0.00)
		2650	7.93	74.37	9.06 (3.56)		5.08 (2.00)		9.21 (3.63)		5.12 (2.02)	
	Right Wall	3566	41.48	94.53	9.99 (3.93)	0.99 (0.39)	5.36 (2.11)	0.01 (0.01)	10.02 (3.94)	0.90 (0.36)	5.39 (2.12)	0.03 (0.01)
		3592	41.48	74.37	8.99 (3.54)		5.35 (2.10)		9.12 (3.59)		5.36 (2.11)	
		4112	49.71	85.34	9.53 (3.75)	0.57 (0.23)	5.62 (2.21)	0.06 (0.02)	9.57 (3.77)	0.49 (0.19)	5.65 (2.22)	0.06 (0.02)
		4130	49.71	74.37	8.95 (3.52)		5.56 (2.19)		9.09 (3.58)		5.59 (2.20)	

Table 6.3-7
Combined Static and Dynamic Concrete Section Forces and Moments for Load Combinaiton Case 3

LOAD COMBINATION: -1.0(Horizontal) + 1.0(Vertical) + 1.0(Static)

Section	Time History Peak values			At Peak Moment		At Peak Axial		At Peak Shear	
	Moment kN-m (k-ft)	Axial Force kN (kips)	Shear Force kN (kips)	Axial Force kN (kips)	Shear Force kN (kips)	Moment kN-m (k-ft)	Shear Force kN (kips)	Moment kN-m (k-ft)	Axial Force kN (kips)
H 1	-2,191.31 (-492.60)	-911.73 (-62.47)	-1,878.33 (-128.70)	-661.58 (-45.33)	339.33 (23.25)	-989.78 (-222.50)	-165.80 (-11.36)	2,048.07 (460.40)	-668.00 (-45.77)
H 2	-665.04 (-149.50)	-1,311.91 (-89.89)	-268.54 (-18.40)	-1,307.54 (-89.59)	-268.54 (-18.40)	-657.48 (-147.80)	-267.67 (-18.34)	-665.04 (-149.50)	-1,307.54 (-89.59)
H 3	-754.46 (-169.60)	-2,710.23 (-185.70)	-741.41 (-50.80)	-410.40 (-28.12)	128.45 (8.80)	587.20 (132.00)	-691.20 (-47.36)	721.54 (162.20)	-2,705.85 (-185.40)
H 4	-433.06 (-97.35)	-2,107.47 (-144.40)	-367.64 (-25.19)	-89.98 (-6.17)	-331.44 (-22.71)	407.75 (91.66)	-11.32 (-0.78)	-333.63 (-75.00)	-379.32 (-25.99)
H 5	3,381.27 (760.10)	-2,294.28 (-157.20)	-1,465.30 (-100.40)	88.15 (6.04)	1,255.58 (86.03)	-1,881.25 (-422.90)	-1,243.17 (-85.18)	-2,148.16 (-482.90)	-2,193.58 (-150.30)
H 6	-1,616.57 (-363.40)	-2,295.74 (-157.30)	-584.81 (-40.07)	-1,954.23 (-133.90)	-584.81 (-40.07)	-1,437.30 (-323.10)	-569.63 (-39.03)	-1,616.57 (-363.40)	-1,954.23 (-133.90)
H 7	-1,481.78 (-333.10)	-2,241.74 (-153.60)	-430.98 (-29.53)	-1,590.82 (-109.00)	-373.77 (-25.61)	729.55 (164.00)	-430.98 (-29.53)	729.55 (164.00)	-2,241.74 (-153.60)
H 8	-1,874.13 (-421.30)	-2,533.63 (-173.60)	-662.01 (-45.36)	560.73 (38.42)	315.97 (21.65)	650.36 (146.20)	-550.07 (-37.69)	984.89 (221.40)	-2,497.15 (-171.10)
H 9	-2,772.72 (-623.30)	-2,669.37 (-182.90)	-1,748.44 (-119.80)	-260.51 (-17.85)	721.27 (49.42)	1,647.71 (370.40)	-1,344.17 (-92.10)	1,352.33 (304.00)	-2,419.80 (-165.80)
H 10	1,482.67 (333.30)	-1,936.71 (-132.70)	-708.13 (-48.52)	-1,137.95 (-77.97)	-226.51 (-15.52)	-562.73 (-126.50)	-390.85 (-26.78)	17.29 (3.89)	-1,308.41 (-89.65)
H 11	2,723.79 (612.30)	-2,786.12 (-190.90)	-1,520.76 (-104.20)	419.45 (28.74)	677.63 (46.43)	-1,852.78 (-416.50)	-1,117.08 (-76.54)	-2,336.77 (-525.30)	-2,720.45 (-186.40)
H 12	-1,868.35 (-420.00)	-932.31 (-63.88)	-1,974.66 (-135.30)	-447.03 (-30.63)	-1,590.82 (-109.00)	-1,165.50 (-262.00)	-1,555.79 (-106.60)	-1,456.87 (-327.50)	-594.29 (-40.72)
H 13	1,932.41 (434.40)	-2,707.31 (-185.50)	-1,161.44 (-79.58)	99.58 (6.82)	593.13 (40.64)	-1,217.99 (-273.80)	-1,154.73 (-79.12)	-1,136.14 (-255.40)	-2,634.34 (-180.50)
H 14	-1,003.13 (-225.50)	-2,241.74 (-153.60)	-328.09 (-22.48)	736.59 (50.47)	-131.85 (-9.03)	812.29 (182.60)	-139.99 (-9.59)	-351.38 (-78.99)	-608.45 (-41.69)
H 15	-4,684.22 (-1,053.00)	-2,508.82 (-171.90)	-2,324.93 (-159.30)	325.75 (22.32)	1,901.69 (130.30)	4,417.76 (993.10)	-2,270.93 (-155.60)	4,492.94 (1,010.00)	-2,412.50 (-165.30)
H 16	-875.90 (-196.90)	-2,726.28 (-186.80)	-675.59 (-46.29)	-2,726.28 (-186.80)	594.73 (40.75)	-875.90 (-196.90)	594.73 (40.75)	804.73 (180.90)	756.30 (51.82)
V 1	8,696.73 (1,955.00)	1,728.01 (118.40)	1,620.01 (111.00)	1,108.47 (75.95)	1,620.01 (111.00)	4,056.55 (911.90)	659.39 (45.18)	8,696.73 (1,955.00)	1,108.47 (75.95)
V 2	-1,896.38 (-426.30)	-2,482.55 (-170.10)	-909.83 (-62.34)	1,065.70 (73.02)	-650.92 (-44.60)	-347.65 (-78.15)	-674.42 (-46.21)	-1,221.10 (-274.50)	-199.80 (-13.69)
V 3	-5,960.93 (-1,340.00)	3,574.23 (244.90)	-2,275.31 (-155.90)	-1,771.79 (-121.40)	-2,043.25 (-140.00)	4,016.07 (902.80)	382.53 (26.21)	-5,871.96 (-1,320.00)	-920.92 (-63.10)
V 4	-5,404.87 (-1,215.00)	-3,095.53 (-212.10)	-2,964.18 (-203.10)	-2,012.60 (-137.90)	-2,956.88 (-202.60)	-3,085.45 (-693.60)	-2,244.66 (-153.80)	-5,289.21 (-1,189.00)	-2,304.50 (-157.90)
V 5	-2,306.97 (-518.60)	3,885.10 (266.20)	-986.16 (-67.57)	-2,700.01 (-185.00)	-675.59 (-46.29)	-1,648.60 (-370.60)	-515.19 (-35.30)	-186.79 (-41.99)	1,000.61 (68.56)
V 6	10,876.47 (2,445.00)	4,925.70 (337.50)	-2,886.83 (-197.80)	4,919.86 (337.10)	2,034.50 (139.40)	10,823.09 (2,433.00)	1,993.63 (136.60)	-7,851.52 (-1,765.00)	-3,836.94 (-262.90)
V 7	425.49 (95.65)	-299.92 (-20.55)	748.12 (51.26)	62.64 (4.29)	690.47 (47.31)	-118.28 (-26.59)	-686.68 (-47.05)	370.42 (83.27)	105.96 (7.26)
V 8	-850.10 (-191.10)	-1,186.98 (-81.33)	-992.73 (-68.02)	738.93 (50.63)	-992.73 (-68.02)	67.66 (15.21)	113.74 (7.79)	-850.10 (-191.10)	738.93 (50.63)

H = Horizontal Section, V = Vertical Section
Note: Metric-unit forces and moments are for 1-m thick slice and those of English units are for 1-ft thick slice

Table 6.3-8
Static Concrtee Section Forces and Moments

LOAD COMBINATION: Static

Section	X-Coordinate m (ft)		Y-Coordinate m (ft)		Static Values					
					Moment kN-m (k-ft)		Axial Force kN (kips)		Shear Force kN (kips)	
H 1	-43.61	(-143.08)	86.91	(285.14)	-318.69	(-71.64)	-649.75	(-44.52)	-579.85	(-39.73)
H 2	-48.95	(-160.60)	82.91	(272.01)	82.25	(18.49)	13.23	(0.91)	-41.05	(-2.81)
H 3	-42.70	(-140.09)	82.91	(272.01)	80.52	(18.10)	-1,668.17	(-114.30)	-356.11	(-24.40)
H 4	-48.95	(-160.60)	78.64	(258.01)	-74.42	(-16.73)	-977.55	(-66.98)	-170.90	(-11.71)
H 5	-42.70	(-140.09)	78.64	(258.01)	186.88	(42.01)	-1,206.25	(-82.65)	-204.33	(-14.00)
H 6	-6.71	(-22.00)	82.91	(272.01)	-253.52	(-56.99)	-905.31	(-62.03)	-161.13	(-11.04)
H 7	0.00	(0.00)	82.91	(272.01)	37.26	(8.38)	-1,557.25	(-106.70)	-349.10	(-23.92)
H 8	6.71	(22.00)	82.91	(272.01)	-298.27	(-67.05)	-1,266.67	(-86.79)	-232.64	(-15.94)
H 9	-6.71	(-22.00)	78.64	(258.01)	-543.60	(-122.20)	-1,239.09	(-84.90)	-509.50	(-34.91)
H 10	0.00	(0.00)	78.64	(258.01)	37.05	(8.33)	-1,197.93	(-82.08)	-326.04	(-22.34)
H 11	6.71	(22.00)	78.64	(258.01)	-145.42	(-32.69)	-1,471.14	(-100.80)	-516.94	(-35.42)
H 12	43.61	(143.08)	86.91	(285.14)	-13.57	(-3.05)	-576.34	(-39.49)	-494.61	(-33.89)
H 13	42.70	(140.09)	82.91	(272.01)	157.88	(35.49)	-1,306.22	(-89.50)	-355.67	(-24.37)
H 14	48.95	(160.60)	82.91	(272.01)	-176.16	(-39.60)	-702.30	(-48.12)	-130.96	(-8.97)
H 15	42.70	(140.09)	78.64	(258.01)	346.53	(77.90)	-1,096.06	(-75.10)	-338.30	(-23.18)
H 16	48.95	(160.60)	78.64	(258.01)	63.84	(14.35)	-799.20	(-54.76)	-111.40	(-7.63)
V 1	-40.74	(-133.66)	76.20	(250.00)	1,139.69	(256.20)	57.39	(3.93)	-92.91	(-6.37)
V 2	-24.76	(-81.23)	76.20	(250.00)	-130.65	(-29.37)	178.93	(12.26)	-674.27	(-46.20)
V 3	-8.73	(-28.63)	76.20	(250.00)	-560.06	(-125.90)	-11.54	(-0.79)	-885.60	(-60.68)
V 4	8.73	(28.63)	76.20	(250.00)	-1,128.13	(-253.60)	31.15	(2.13)	-1,605.41	(-110.00)
V 5	24.76	(81.23)	76.20	(250.00)	-109.39	(-24.59)	106.51	(7.30)	-682.74	(-46.78)
V 6	40.74	(133.66)	76.20	(250.00)	685.51	(154.10)	148.72	(10.19)	-610.06	(-41.80)
V 7	-47.57	(-156.07)	84.72	(277.95)	138.70	(31.18)	-49.51	(-3.39)	150.18	(10.29)
V 8	47.57	(156.07)	84.72	(277.95)	-237.06	(-53.29)	-138.36	(-9.48)	-159.08	(-10.90)

Note: Metric-unit forces and moments are for 1-m thick slice and those of English units are for 1-ft
H = Horizontal Section, V = Vertical Section

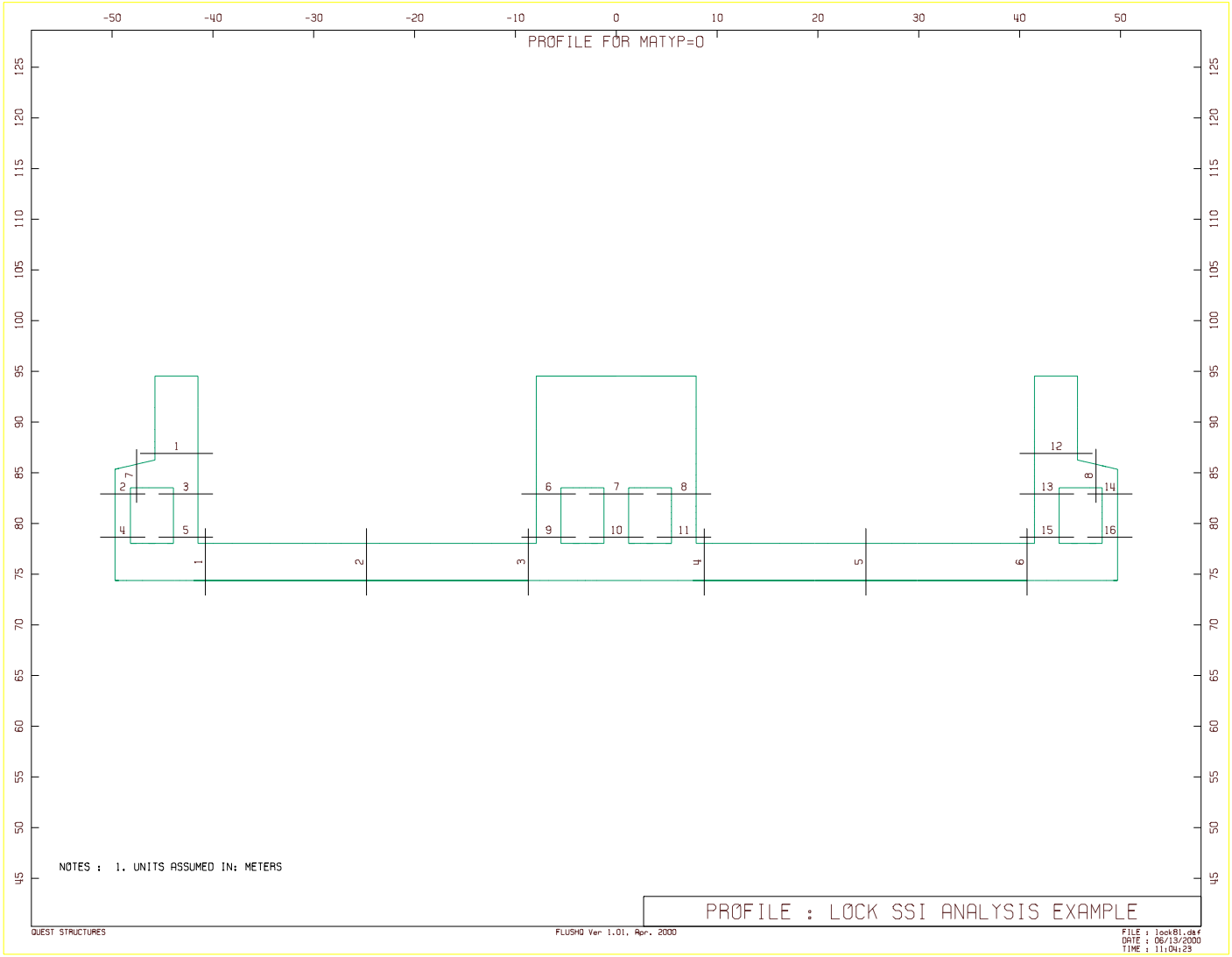

Figure 6.3-20. Critical sections for reinforced concrete forces and moments

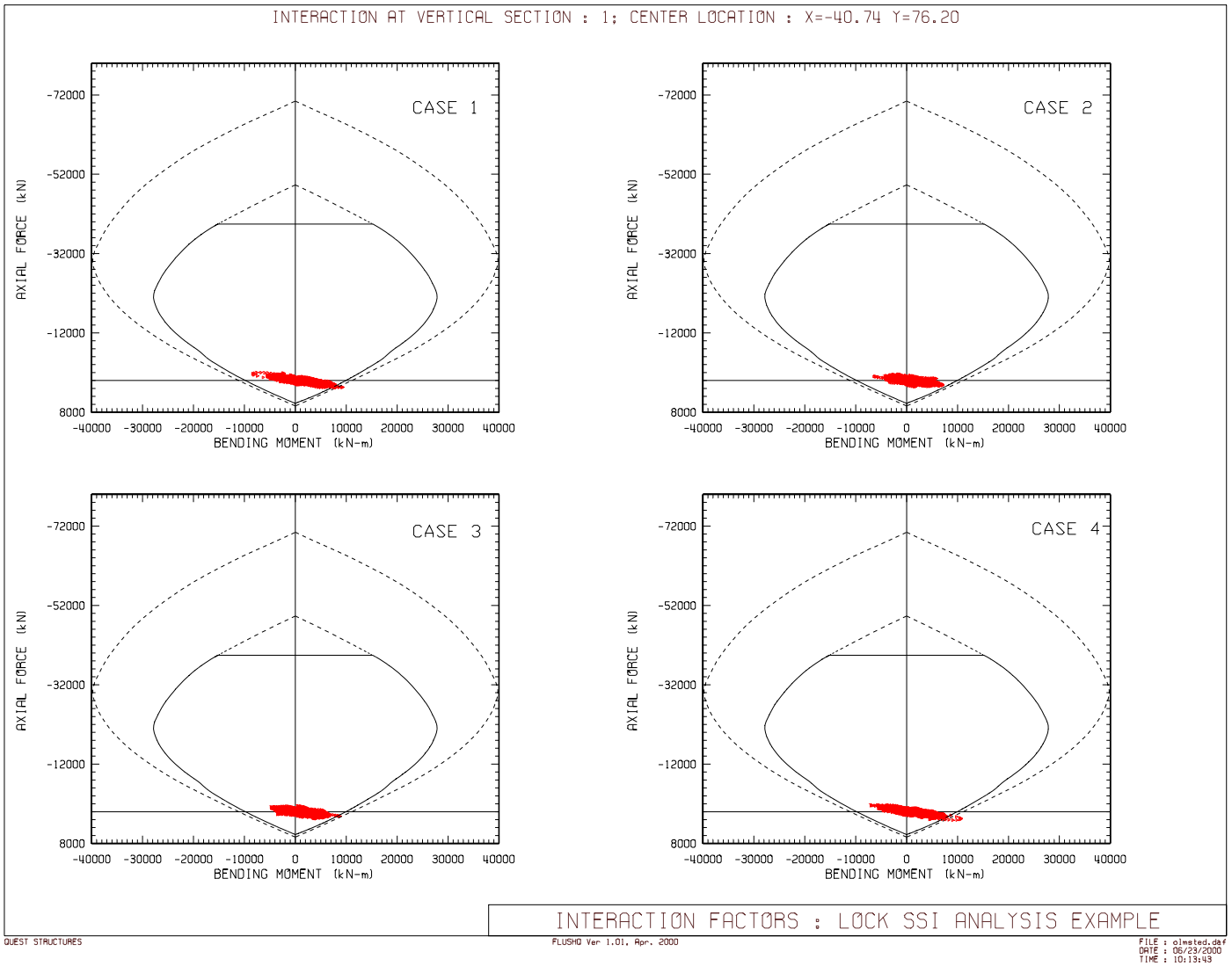

Figure 6.3-21. Combined static and seismic axial force vs. bending moment for concrete vertical section 1 shown in Figure 6.3-20)

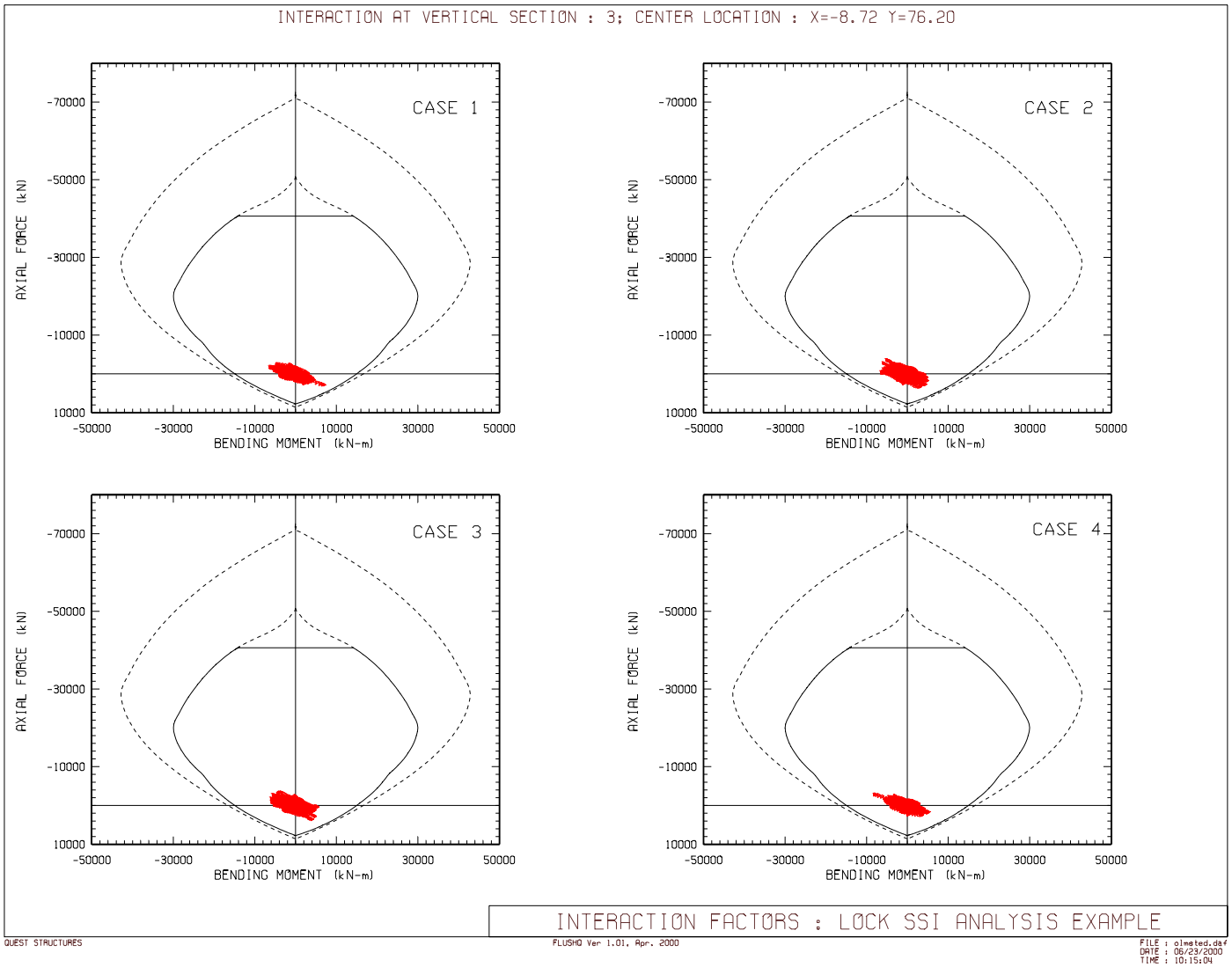

Figure 6.3-22. Combined static and seismic axial force vs. bending moment for concrete vertical section 3 (see Figure 6.3-20)

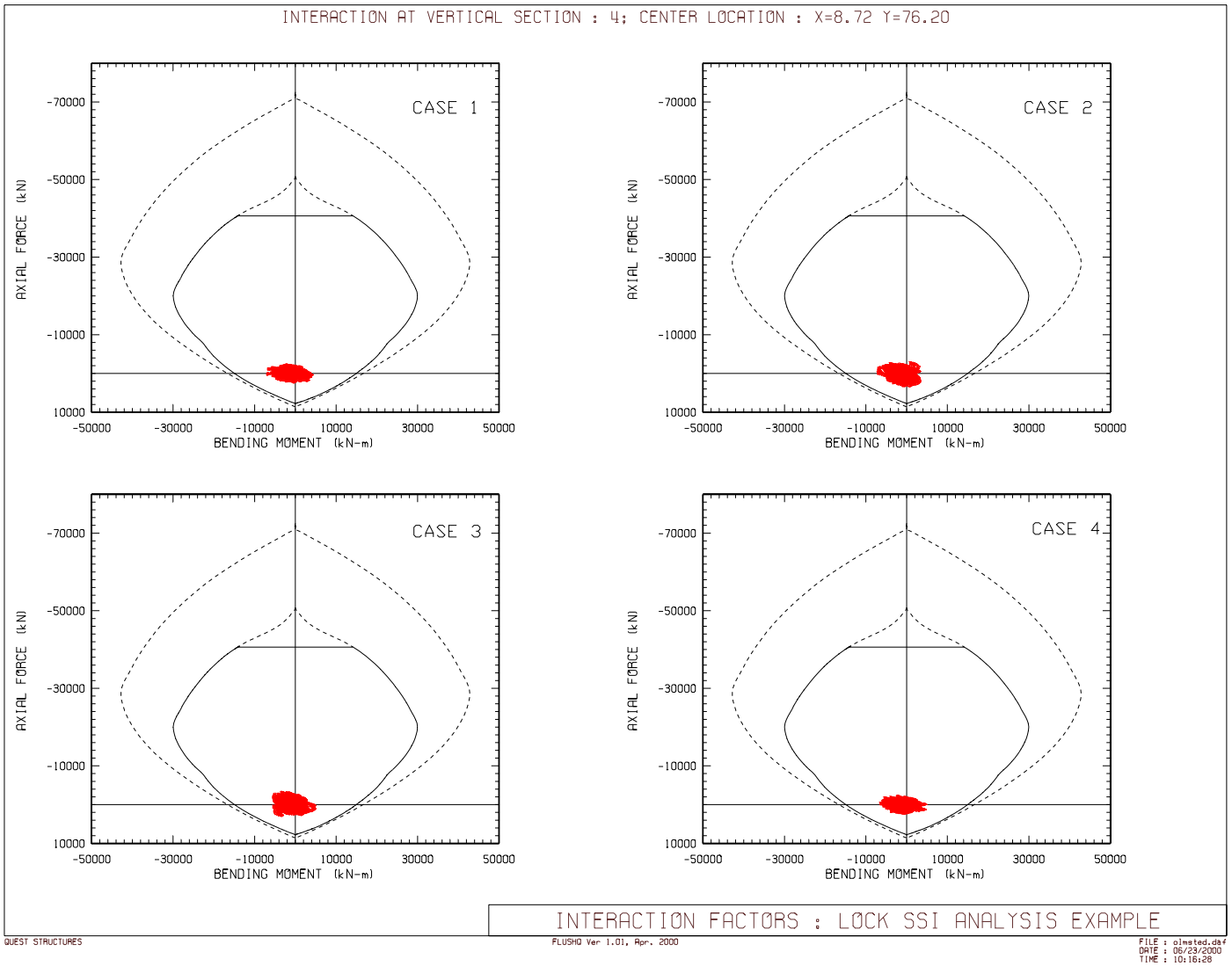

Figure 6.3-23. Combined static and seismic axial force vs. bending moment for concrete vertical section 4 (see Figure 6.3-20)

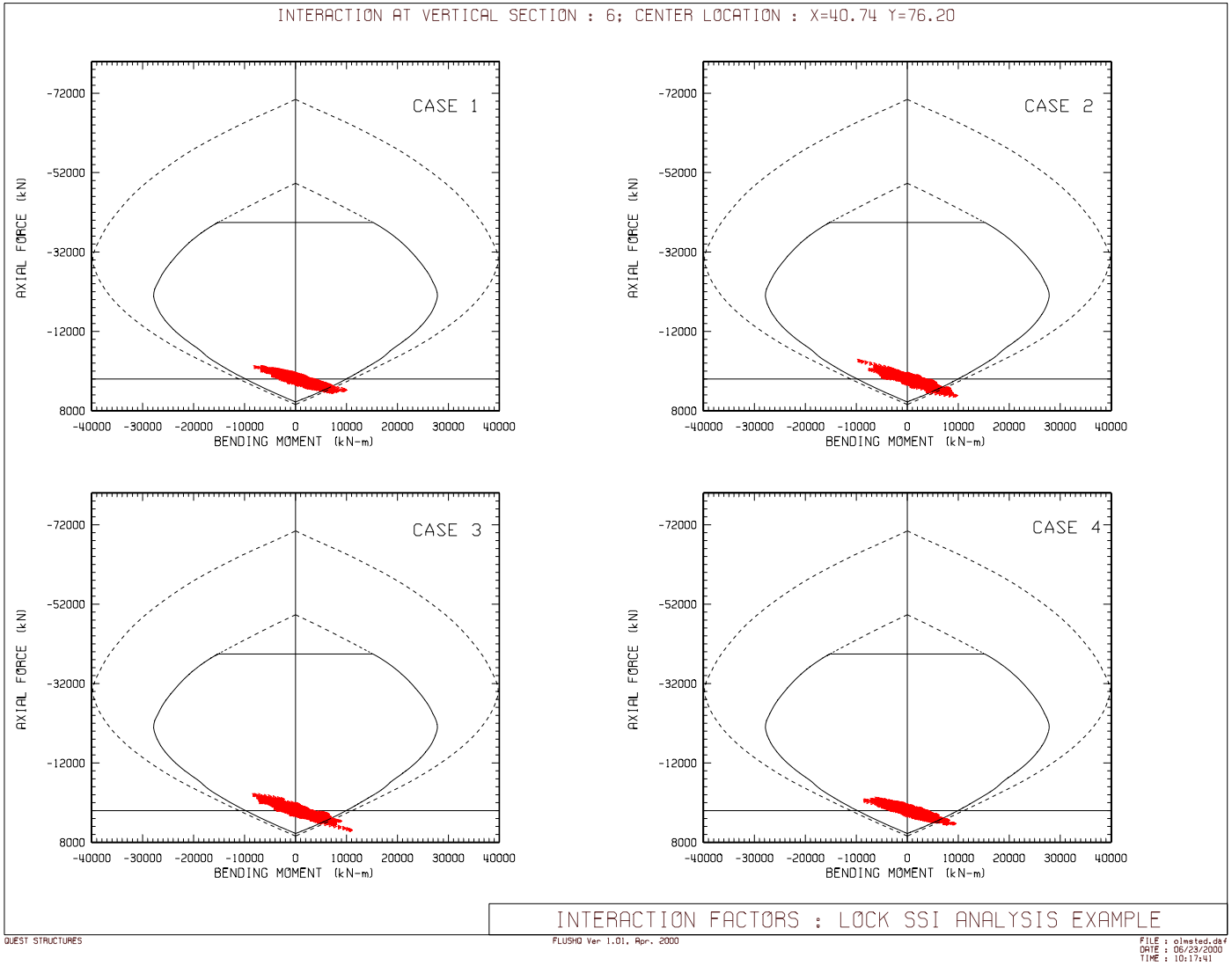

Figure 6.3-24. Combined static and seismic axial force vs. bending moment for concrete vertical section 6 (see Figure 6.3-20)

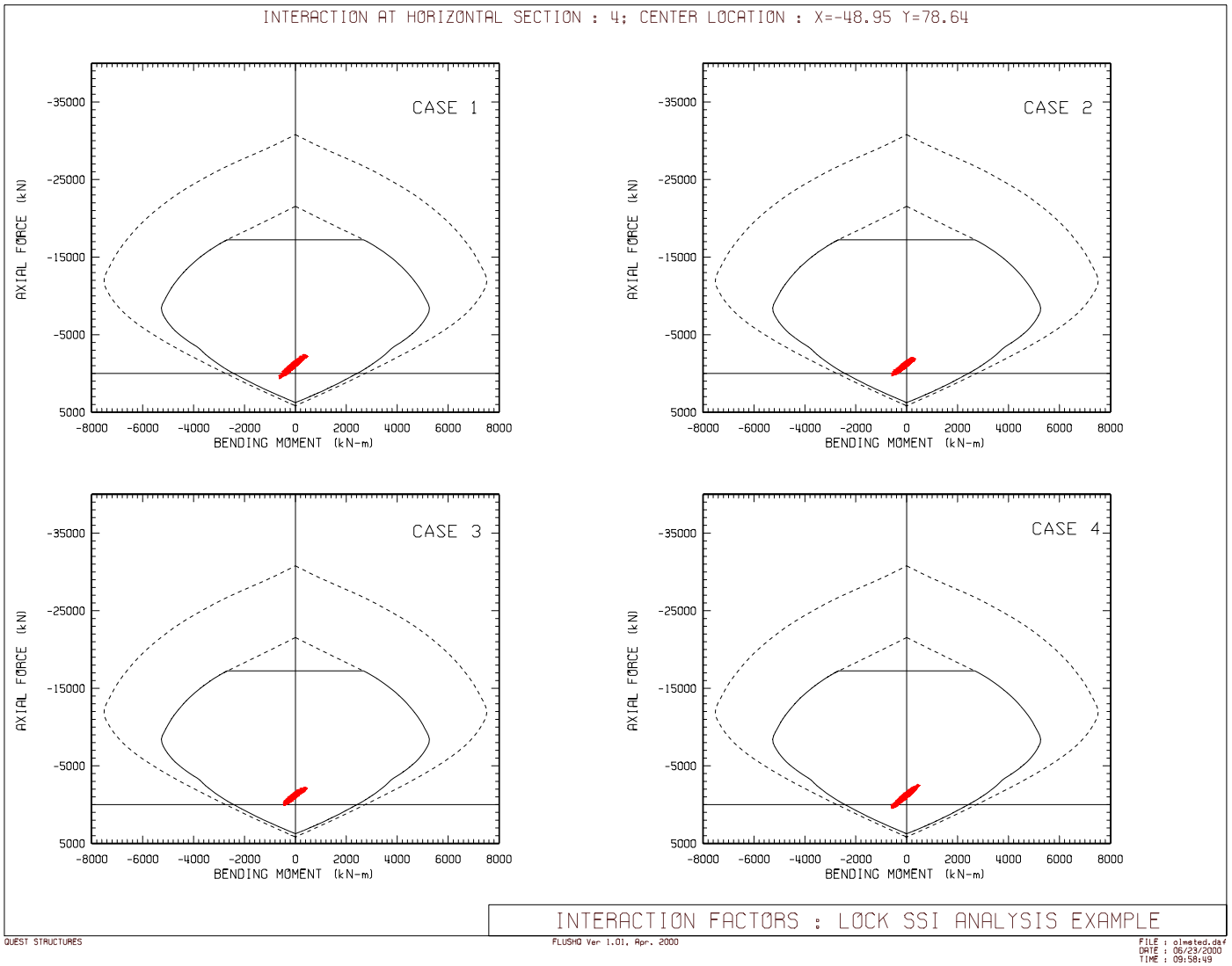

Figure 6.3-25. Combined static and seismic axial force vs. bending moment for concrete horizontal section 4 (see Figure 6.3-20)

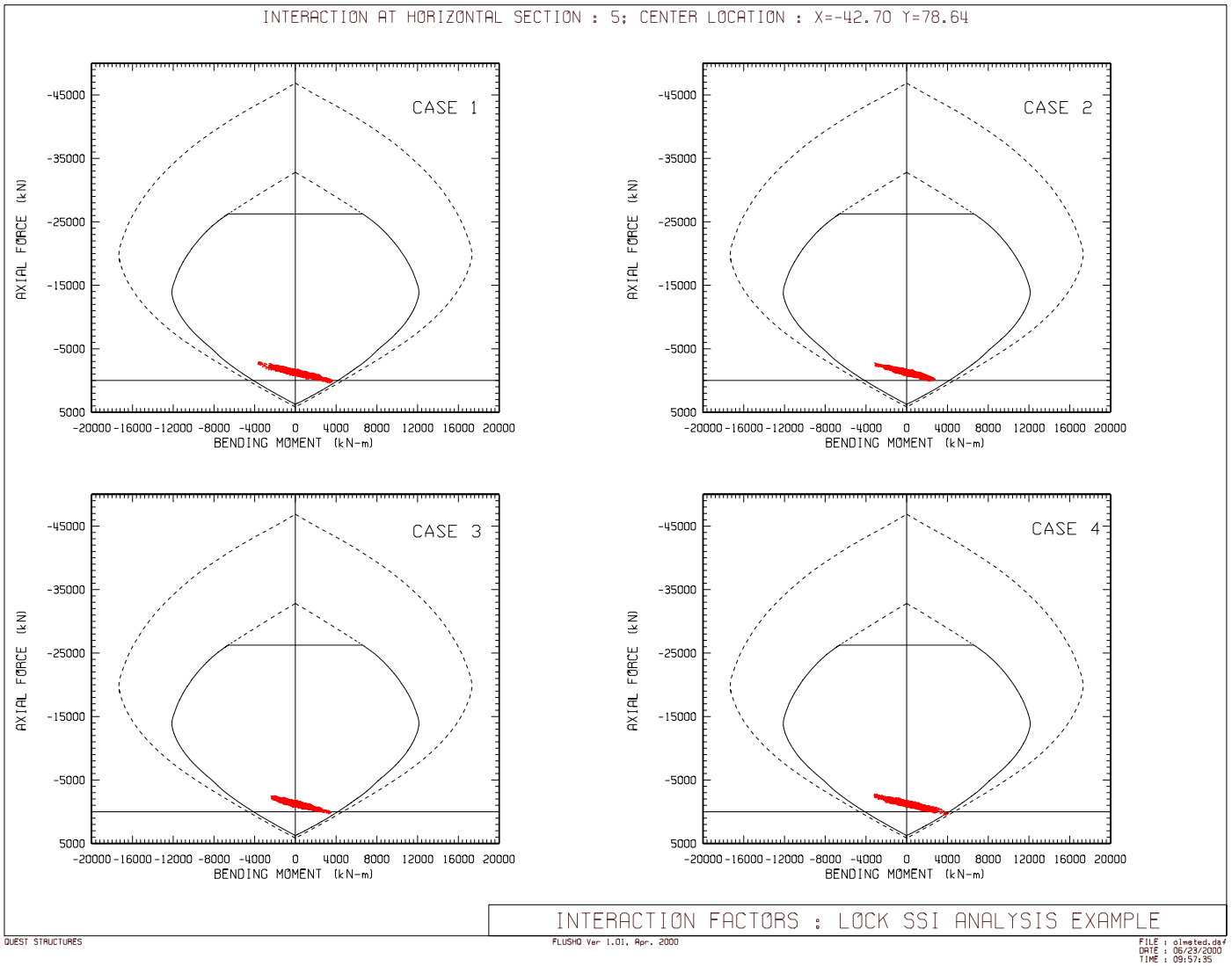

Figure 6.3-26. Combined static and seismic axial force vs. bending moment for concrete horizontal section 5 (see Figure 6.3-20)

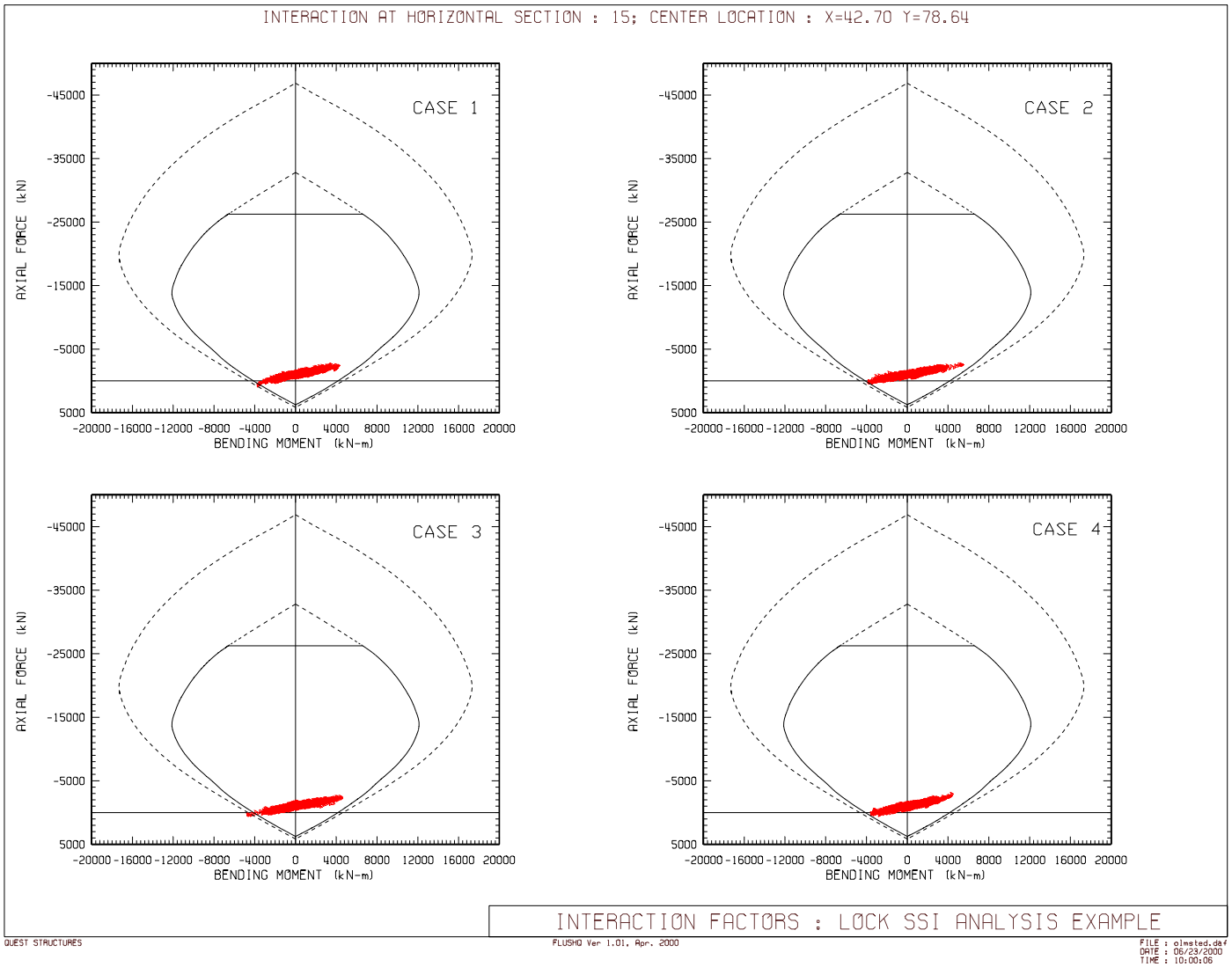

Figure 6.3-27. Combined static and seismic axial force vs. bending moment for concrete horizontal section 15 (see Figure 6.3-20)

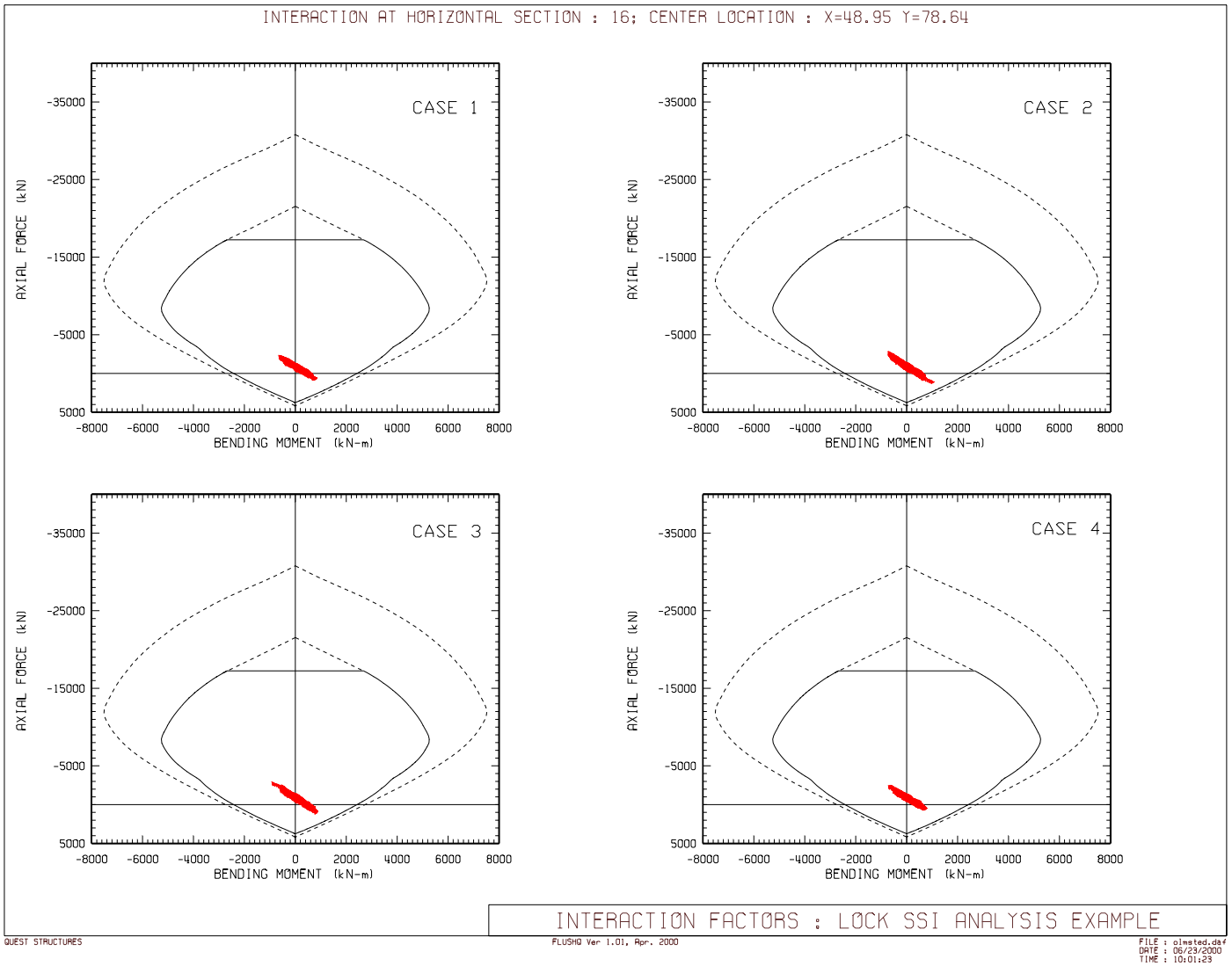

Figure 6.3-28. Combined static and seismic axial force vs. bending moment for concrete horizontal section 16 (see Figure 6.3-20)

Figure 6.3-29. Time history of axial force-bending moment interaction factors for vertical Section 6

6.3-10 Unit Conversion Table

Table 6.3-9
Unit Conversion Table

1	in	=	0.0254	m	1	m	=	39.3701	in
1	ft	=	0.3048	m	1	m	=	3.2808	ft
1	lb	=	0.4536	kg	1	kg	=	2.2046	lb
1	lbf	=	4.4485	N	1	N	=	0.2248	lbf
1	psi	=	6,895.12	Pa	1	Pa	=	1.45E-04	psi
1	k-ft	=	1.3559	kN-m	1	kN-m	=	0.7375	k-ft
1	ksi	=	6,895.12	kPa	1	kPa	=	1.45E-04	ksi
1	ksi	=	6.8951	mPa	1	mPa	=	0.1450	ksi
1	ksf	=	47.8828	kPa	1	kPa	=	0.0209	ksf
1	$k\text{-}s^2/ft$	=	14.5947	$kN\text{-}s^2/m$	1	$kN\text{-}s^2/m$	=	0.0685	$k\text{-}s^2/ft$
1	kcf	=	157.0957	kN/m^3	1	kN/m^3	=	0.0064	kcf

6.4 Seven Oaks Inclined Intake Tower

6.4-1 Background

This section provides an example time-history analysis for intake towers requiring three-dimensional finite-element evaluation. The example tower is the Seven Oaks Dam Intake Tower located in Santa Ana River Basin, San Bernardino County, California. The main feature of the tower is that it is inclined against the abutment and partially embedded into the foundation rock. The 68.6-m (225-foot) high tower was anchored to the inclined rock slope and designed to withstand the earthquake forces generated by a maximum probable earthquake (OBE) and the maximum credible earthquake (MCE) events. The structure is located 1.92 km (1.2 miles) from a branch of San Andreas Fault, capable of producing a magnitude M8+ earthquake. This tower was chosen for this analysis because of its unique 3D features and that a 3D model of the tower was available from previous analyses by Waterways Experiment Station. The structural response of the tower is primarily rotation about its most vertical centroidal axis (torsion), and resulting forces are transferred to the rock abutment by tension in steel rods anchored in the rock and extending into the tower. Because of the torsional response and the fact that the tower has no plane of symmetry, 3-D analyses were required. The accelerations used in the following five analyses are not the design accelerations for the tower, but results from a previous analysis using the Seven Oaks design acceleration records are also presented for reference.

6.4-2 Purpose and Scope

a. The main purpose of this example is illustration of the time-history analysis in evaluation of the global behavior of an inclined intake tower and its abutment anchorage system to seismic loading. Additional objectives include demonstration of the dominant torsional response, the importance of higher modes of vibration, and the effects of multiple ground motions that are essential in dynamic response analysis of inclined towers but may not be necessary for free-standing towers. The example, however, does not consider the local behavior and section capacities needed for the reinforcing steel design.

b. he time-history analysis is applied to earthquake response computation of the Seven Oaks Intake Tower. The analyses are carried out for five sets of acceleration time histories to investigate sensitivity of the dynamic response to characteristics of the earthquake ground motion. Design earthquakes and the selected acceleration time-histories are described; the structural modeling details, including three-dimensional finite-element representation of the tower, surrounding water, and the foundation-abutment are presented; the dynamic characteristics of the tower dominated by torsion and contribution from higher modes are determined; the tower responses to five sets of three-component earthquake acceleration time-histories are computed; and results in the form of stress contours, section force and moment demands, and anchor force demands are presented and discussed. The results for the five acceleration time-histories selected in this example are compared with the results from the design analyses.

6.4-3 Description of Intake tower

a. The U.S. Army Engineer District, Los Angeles, designed the intake structure for the Seven Oaks Dam, shown in Figure 6.4-1. The structure is a reinforced concrete intake tower inclined against and anchored to the rock abutment, as shown in Figure 6.4-2. The tower is partially embedded in the rock formation at the bottom. The maximum vertical height of the structure is 68.7m (225.5 ft), extending from elevation (El.) 2,080 ft at the foundation to El. 2305.5 ft at the top of the parapet. The high-level intake height is 50.3 m (165 ft) based on an expected sediment deposition over the project life from El. 2,100 ft to El. 2,265 ft. Structure configuration, starting from the foundation, includes a 6.1-meter-thick (20-foot-thick) concrete footing embedded into rock, a 50.3-meter-high (165-foot-high) semicircular structure with an 11-meter-diameter (36-foot-diameter) wet well inclined at a 4V on 1H slope against the abutment, and an 11.3-meter-high (37-foot-high) vertical circular high-

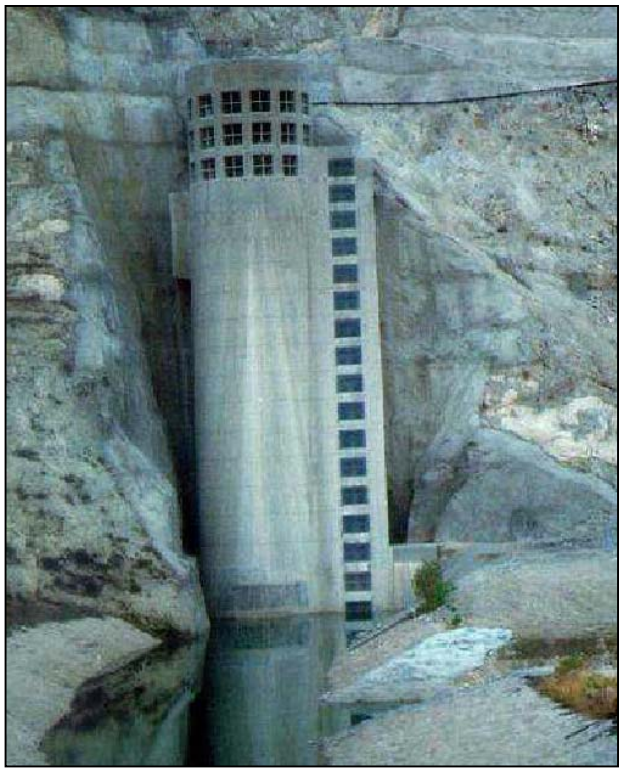

Figure 6.4-1 Seven Oaks Dam Intake Tower (Courtesy of Rayw Dewey, Portland District)

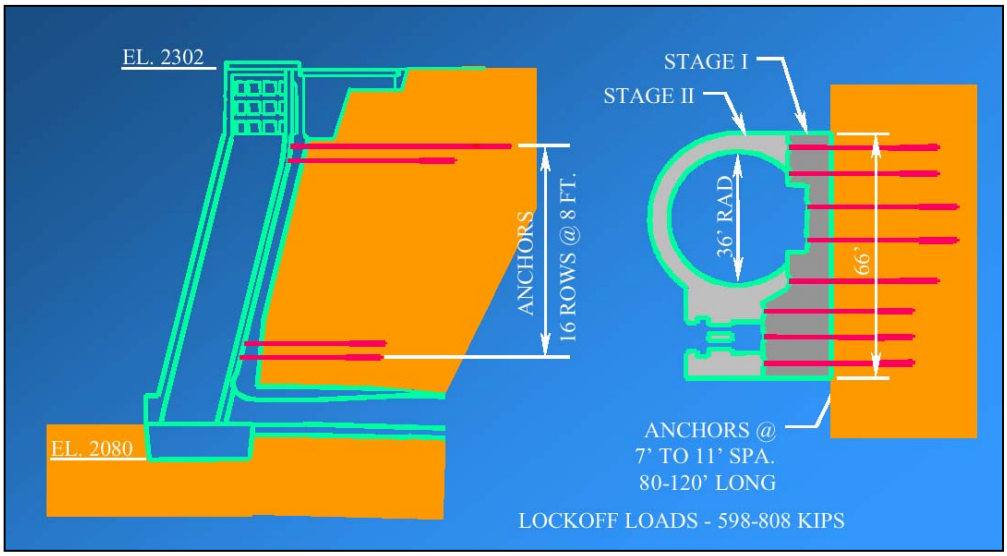

Figure 6.4-2 Seven Oaks Intake Tower Anchorage System (Courtesy of Ray Dewey, Portland Distrcit)

level intake covered with a maintenance deck. A trash structure surrounds the high-level intake and a 15.2-meter-long (50-foot-long) bridge connects the maintenance deck to an access road from the embankment dam.

b. A total of 128 anchors were used to fasten tower to the abutment. They were arranged in 16 rows of 8 post-tensioned anchors, as shown in Figure 6.4-2. Each post-tensioned anchor included seven low relaxation 0.6-in diameter tendons rated at 1,862 MPa (270 ksi). The intake structure was constructed in two stages. First the back-face concrete was placed against the sloping rock face followed by installation and pre-stressing of the anchors. Then the front-face concrete was placed to complete the construction.

6.4-4 Earthquake Ground Motions

Seven Oaks Intake Tower was designed for the Maximum Credible Earthquake (MCE) and Operational Earthquake (OBE). The MCE was a magnitude M8+ earthquake on a branch of San Andreas Fault located 1.92 km (1. miles) from the site. The peak ground acceleration for the MCE was estimated at 0.7g. The seismic performance for the MCE included inelastic response with cracking and yielding, but maintaining the ability to lower the pool in controlled manner. The OBE was chosen as the maximum probable earthquake (MPE) with 1% chance of occurrence per year (63% in 100 years). The MPE was postulated as an M7.5 to 8 earthquake on a fault located 19 km (12 miles) from the site, capable of producing a peak ground acceleration of 0.5g. The seismic performance for the OBE included a nearly elastic response, where the tower remains fully operational with minor damage not requiring extensive repair. The OBE performance requirements turned out to be more stringent and thus the OBE controlled the design.

a. No attempt was made to use the design ground motions described above in this example. Instead a generic target response spectrum representative of the southern California seismic environment was developed and used to select five sets of acceleration time histories for this example. Two methods were used to develop acceleration records for the analyses:

- Four of the records were scaled from existing earthquake records to a best fit of the target response spectrum.
- One set of spectrum-compatible was developed to closely match the target spectra.

Table 6.4-1 lists all five earthquake records and corresponding scaling factors. All acceleration records with the exception of SMPAC include two horizontal and one vertical component. Vertical component of SMPAC was not computed and is not included in this example. The smooth target spectrum and the spectra for the scaled motions in the primary (x) direction are compared in Figure 6.4-3. The scale factor for both horizontal components of direction in each of the four scaled record sets was based on a fit of x acceleration data to the target spectrum shown in Figure 6.4-3. Spectrum fits for the y-direction for the four-scaled sets are shown in Figure 6.4-4. Acceleration time-histories for the five records are shown in Figures 6.4-5 to 6.4-9. While maximum accelerations are similar in the x-direction for all records and have been scaled to 0.5g, significant differences exist in the y-direction due to the use of the x-direction scaling factor for both horizontal records.

b. The "design" accelerations used in the original analysis of the tower are shown in Figure 6.4-10 for comparison and reference only. They are in no way related to the target spectra of Figures 6.4-3 and 6.4-4. The design acceleration time histories included records in the x-, y-, and z-directions. These accelerations and results from this analysis are included only for reference.

Table 6.4-1
Earthquake Records for Example Analyses

Record Name	Component deg	Scale Factor	Analysis Designation
1966 Parkfield Earthquake, Cholame #8 (CHO)	320 50 up	1.7962	CHO
1989 Loma Prieta Earthquake, Gavilan College (GGC)	337 67 up	1.3596	GGC
1987 Whittier Narrows Earthquake, Garvey Reservoir (GRV)	330 60 up	0.8987	GRV
1971 San Fernando Earthquake, Pacoima Dam (PAC)	254 164 up	0.4915	PAC
Spectrum-matched Pacoima Dam (SMPAC)	Both	None	SMPACX

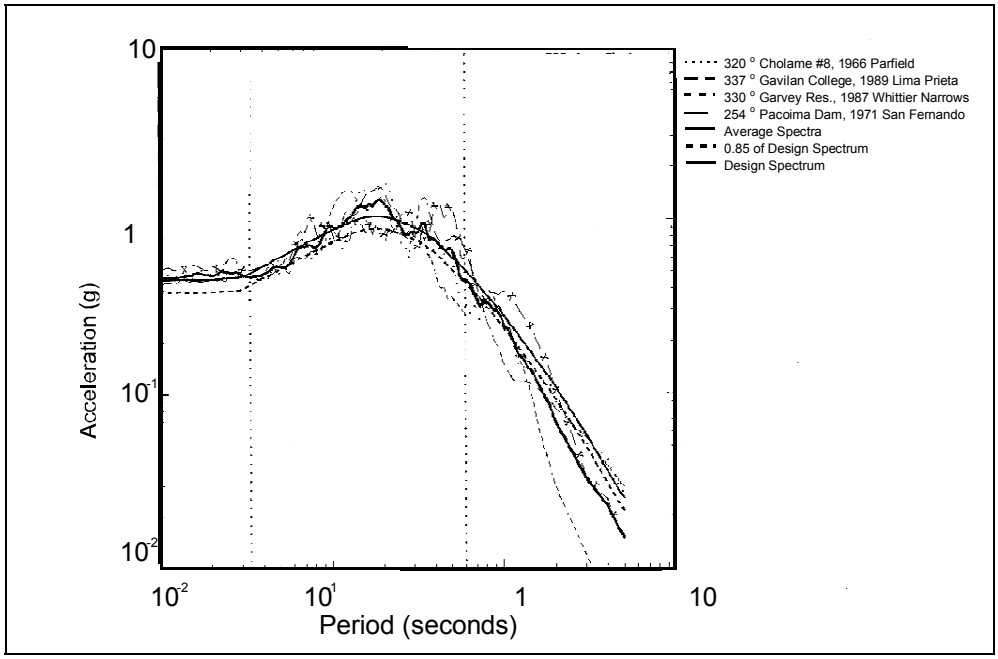

Figure 6.4-3. Target and scaled spectra, x-direction

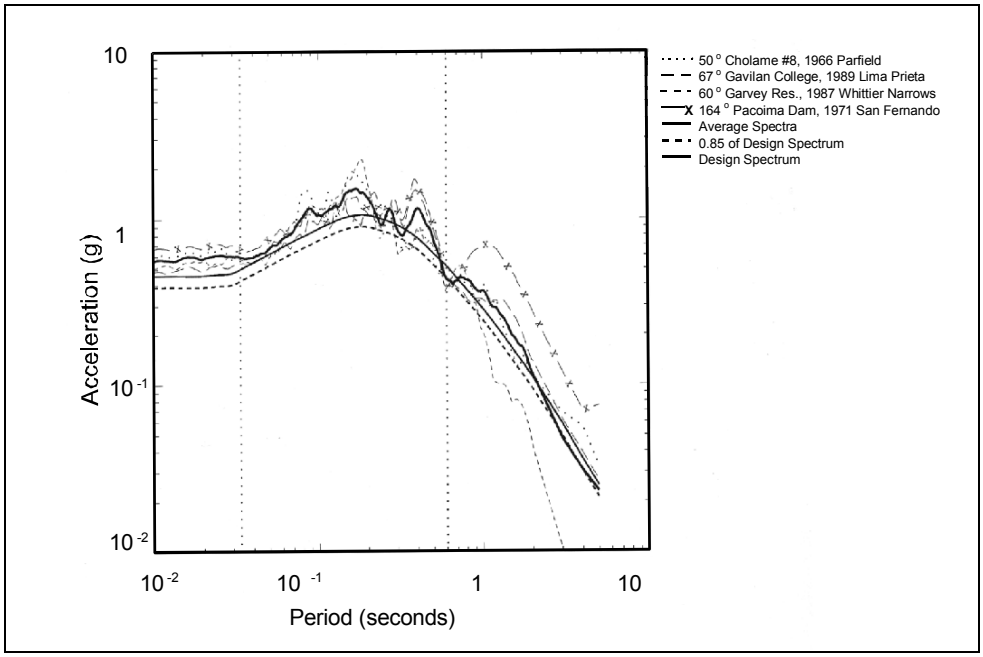

Figure 6.4-4. Target and scaled spectra, y-direction

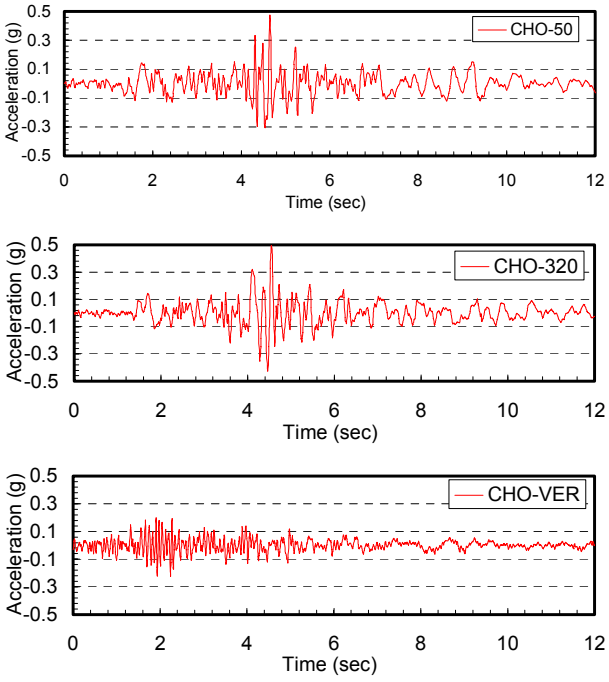

Figure 6.4-5. 1966 Parkfield earthquake, Cholame #8 (CHO)

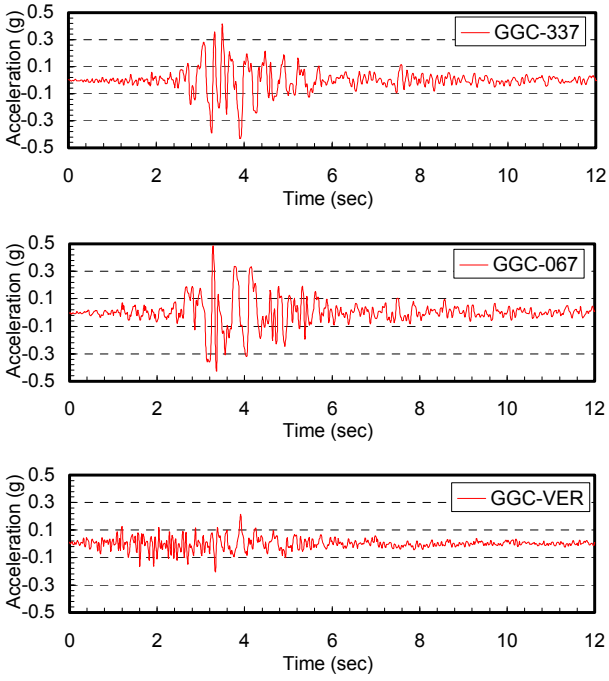

Figure 6.4-6. 1989 Loma Prieta earthquake, Gavilan College (GGC)

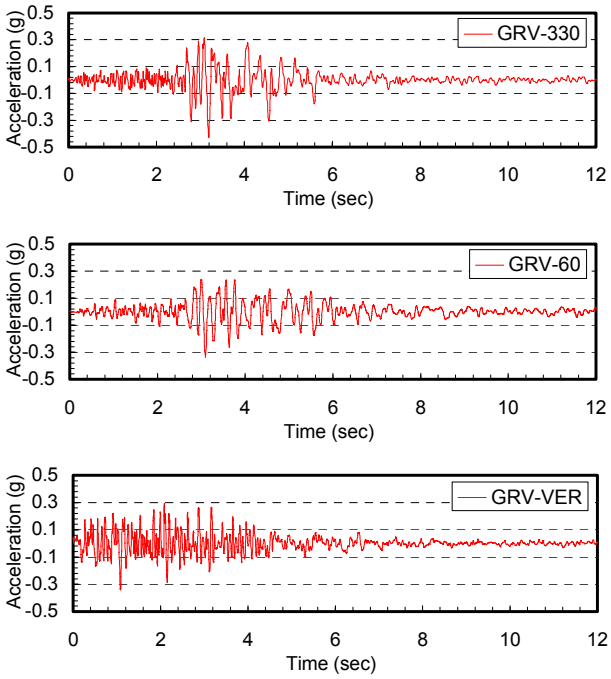

Figure 6.4-7. 1987 Whittier Narrows earthquake, Garvey Reservoir (GRV)

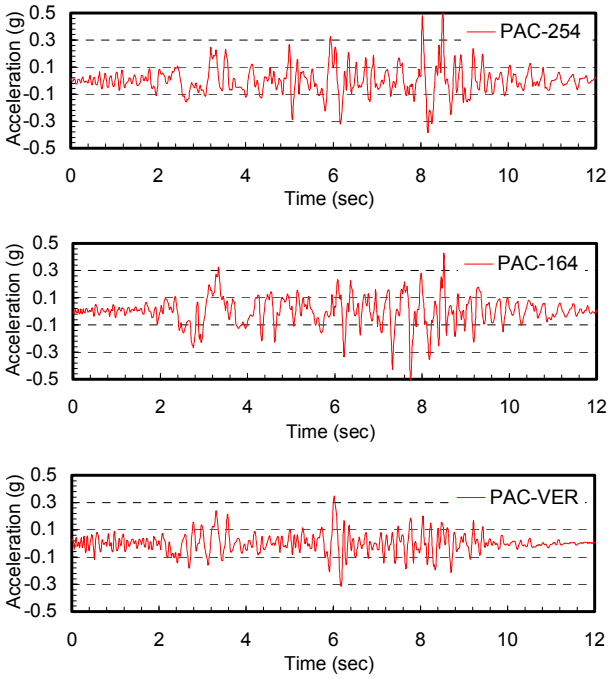

Figure 6.4-8. 1971 San Fernando earthquake, Pacoima Dam (PAC)

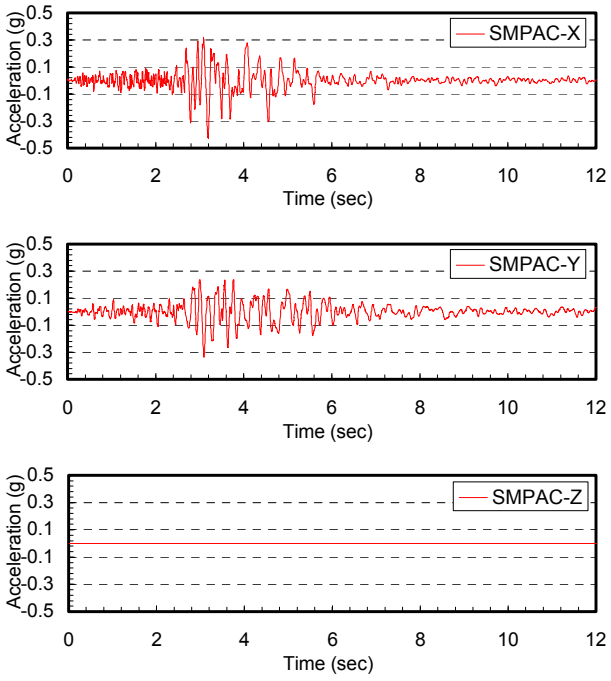

Figure 6.4-9. Spectrum matched PAC (SMPAC)

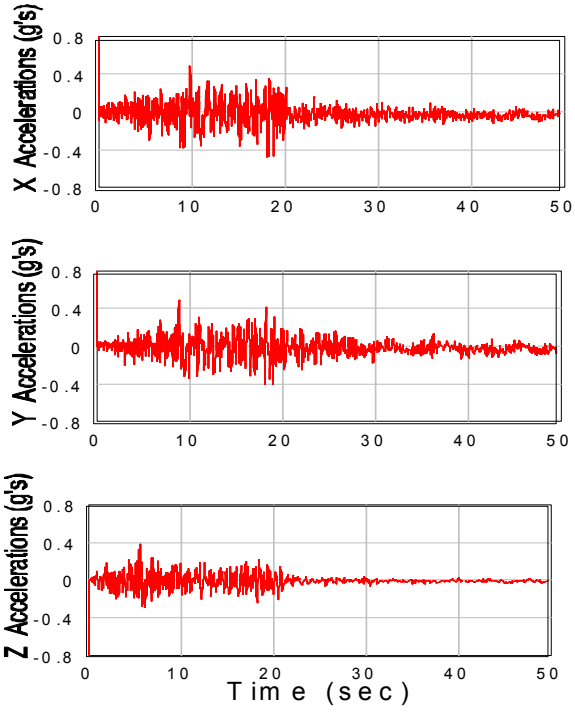

Figure 6.4-10. Seven Oaks design accelerations

6.4-5 Structural Model

The three-dimensional geometry of the tower, severe seismic demand, and the substantial hydrodynamic forces acting on the tower requires a 3D finite-element (FE) model which includes the tower- water and the tower-foundation-abutment interaction effects.

a. The concrete intake tower (see Figure 6.4-11and Figure 6.4-13) was modeled using 2,084 eight-node solid elements and 169 beam elements. Solid elements were used in the body of the tower and beam elements were used to model the trash-rack. Moments in the trash-rack were transmitted to the solid elements by extending beams into the solid elements. The eight-node solids are linear isoparametric elements using linear geometry and displacement interpolation functions.

b. The foundation rock was modeled using 2,642 eight-node solid elements. The minimum width of the foundation model was three times the base width of the tower. Foundation rock was included in the model from the rock/concrete interface to a distance approximately equal to the height of the tower, and from the base of the tower downward to a distance of approximately half of the height of the tower. All outer nodes of the foundation model (i.e. nodes at the bottom, sides and back of the model) were fixed in space. Accelerations in the global x, y, and z directions were applied to the outer rock boundaries (see Figure 6.4-12). Foundation elements were assigned zero mass to eliminate erroneous wave reflections at the fixed boundaries due to finite size of the foundation model.

c. The tower-rock interface consisted of 240 nodes shared by the abutting concrete and rock elements. Normal and tangential forces at these nodes were used to check the adequacy of steel anchors between the tower and the abutment rock.

d. The inertia forces of the impounded water were represented by the equivalent hydrodynamic added-mass lumped to the submerged exterior and interior nodes of the tower. The added-mass coefficients of the surrounding water were those computed for design of the tower using boundary element method described in Section 2-20.*c*. The added-mass coefficients for the water inside the wet well were approximately obtained from the weight of water.

e. Static loads consisted of the gravity due to self-weight and hydrostatic pressures of the inside and outside water. Note that due to unsymmetrical cross-section of the tower, hydrostatic pressures generally do not cancel out and should be considered in the analysis. The water loads were applied as hydrostatically varying pressures on surfaces of the submerged elements.

f. Earthquake loads were applied as ground acceleration time-histories in x, y, and z directions along the outer foundation boundaries. Structural damping was assumed to be 5% of critical.

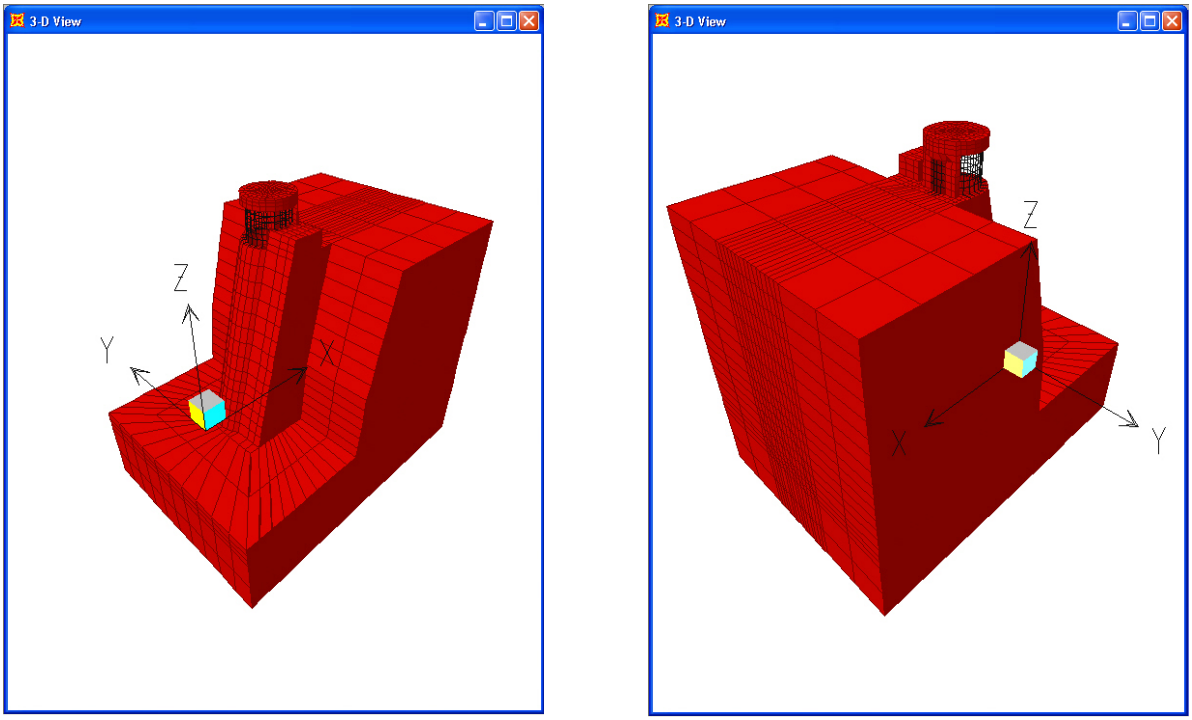

Figure 6.4-11. 3-D views of tower-foundation-abutment finite-element model

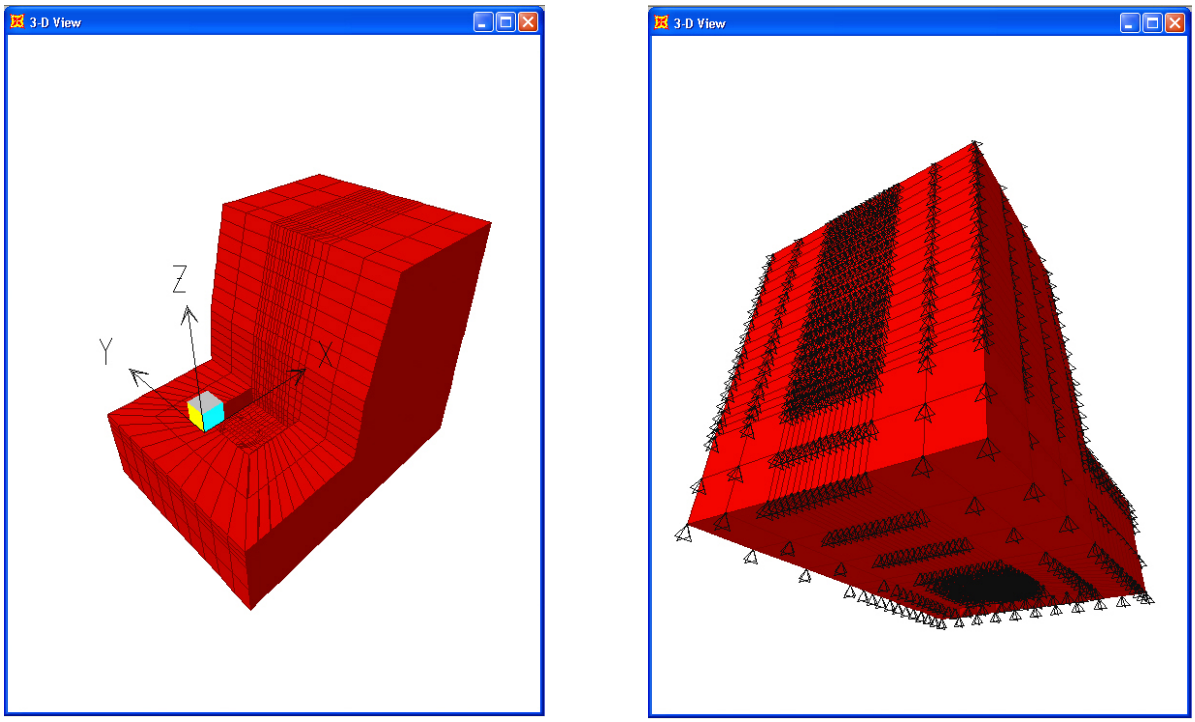

Figure 6.4-12. 3-D views of foundation-abutment finite-element model

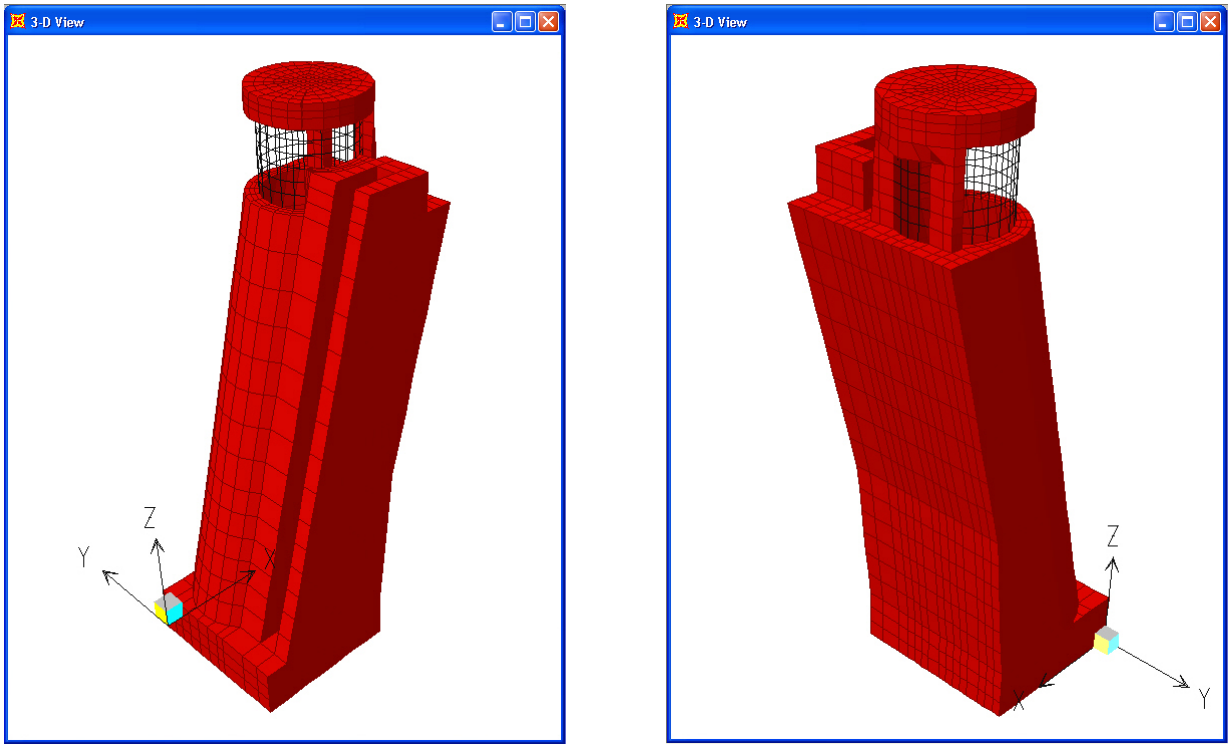

Figure 6.4-13. 3-D views of tower finite-element model

6.4-6 Computation of Earthquake Response

a. Dynamic characteristics of tower. The natural periods and mode shapes of the tower were obtained using the finite-element model described above. The Ritz-Vector feature of SAP2000 was employed to obtain 100 mode shapes and periods for the full reservoir. The resulting vibration periods and the associated modal participation factors are given in Table 6.4-2. The results show that 100 percent modal participation was achieved in all three orthogonal x, y, and z directions. Figures 6.4-14 and 6.4-15 show deflected shapes for the 8 lowest modes of vibration. Modes 1 and 2 involve bending of the high-level intake in directions perpendicular (x-direction) and parallel to the abutment (y-direction), respectively. Modes 3 to 8 and higher (not shown) indicate dominant torsion response. That the vibration response involves torsion is a result of the restraint along the height of the tower. The results show that an important characteristic of the dynamic response of the Seven Oaks Tower is that 65 modes were necessary to achieve a 90% mass participation in all three global directions (see Table 6.4-2), as opposed to dynamic characteristics of freestanding towers that is dominated by the two lowest modes of vibration.

b. Earthquake response of tower. Earthquake response of Seven Oaks intake tower was computed for the five ground motions discussed in 6.4.4. A 5 percent modal damping ratio was used. The tower response for structural evaluation included maximum and minimum stresses within the tower and at the tower-abutment interface for identification of overstressed regions, section forces and moments along the height for comparison with section capacities, and anchor forces to assess adequacy of the anchorage system. Each of these response quantities are discussed below.

c. *Stress contours.* Maximum and minimum stress values are presented in the form of contour plots for determining locations and magnitudes of high stresses. These plots generally provide a cursory assessment of overstressed regions, their damage potential, and effects on stability of the tower. Better estimate of damage

requires careful study of other parameters discussed in Chapter 4. In this example only normal stresses at the tower-abutment interface and vertical stresses within the tower are presented. However, shear stresses should always be examined to assure that shear failure would not occur.

(1) Tower-abutment interface stresses. Figure 6.4-15 shows node numbers at the tower-abutment interface used to compute anchor forces. Figure 6.4-16 through Figure 6.4-20 display contour plots of maximum and minimum normal stresses at the tower-abutment interface for the five seismic input employed in this example. Results show that peak maximum (tension) and minimum (compression) stresses occur at the edges of the back face and then dropping toward the centerline of the semicircular wet well. This type of stress distribution clearly indicates a torsion response behavior. The peak tensile stress reaches 2 MPa (300 psi) and peak compressive stress -1.4 MPa (-200 psi) at about mid-height of the back face.

(2) Stresses within the tower. Figures 6.4-21 through 6.4-28 show maximum and minimum vertical stresses within the tower for the Pacoima Dam (PAC) record of the 1971 San Fernando earthquake. Stress contours are presented for the back face (downstream), right face, front face (upstream), and the left face of the tower and high-level intake. Localized high vertical stresses develop at the edges of the back face of the tower and near the bottom of the high-level intake main supports (Figures 6.4-21 and 6.4-22). The high vertical stresses for the wet well occur at the bottom and 1/3 height of the right and front faces of the tower (Figure 6.4-24 and 6.4-26). For the multi-level intake structure, high vertical stresses are confined to the base of the structure (Figure 6.4-26 and 6.4-28). However, for the tower peak stresses are well below tensile and compressive strengths of concrete. Peak tensile stresses as high as 7 MPa (1,000 psi) develop at the base of the high-level intake supports, but reinforcing steels built into the design of tower can easily resist them.

c. *Tower section forces and moments.* For design and evaluation of the tower, section forces and moments should be computed and examined along the height of the tower. Section forces may be computed from stresses of the elements forming the section using a spreadsheet program. Alternatively, the section forces and moments can be computed directly by the structural analysis program should the program have such capability. In this example SAP2000 capability to compute group joint forces was used to determine section forces and moments. Figure 6.4-29 through 6.4-34 show the maximum and minimum section forces and moments along the height of the tower for each of the ground motions. The computed section forces and moments are usually compared with the ultimate section capacities to estimate reinforcing steels for new designs or assess adequacy of existing structures. The results in Figures 6.4-29 to 6.4-31 show that horizontal shear forces (F_x and F_y) for various input ground motions vary much less than the normal section forces (F_z). This is because horizontal section forces arise mainly from the horizontal components of ground motions that were scaled to remain at the approximate level of the horizontal smooth response spectra. The resulting scale was then applied to the corresponding vertical components of the ground motions without any further adjustment. Consequently variations of vertical components of ground motions are by far greater than those of the horizontal components. Such greater variation in vertical ground motion is expected to affect the axial or normal section forces, as illustrated in Figure 6.4-31. This figure also shows that the embedded portion of the tower remains in compression and that magnitudes of maximum compressions along the height of the tower are greater than magnitudes of maximum tensions. The peak section shear forces occur near the bottom of the tower and they are twice larger in the direction normal to the abutment (x-dir.) than they are in the direction parallel to the abutment (y-dir.). Figures 6.4-32 to 6.4-34 show peak section moments also occur near the bottom and that torsion response produces the largest moment or torque (M_z). The positive bending moments with respect to x-axis (M_x) are substantially greater than positive bending moments with respect to y-axis (M_y). This indicates that the tower primarily bends toward the multi-level intake than into the abutment.

d. *Anchor Forces.* To avoid separation and pounding between the tower and abutment during earthquake ground shaking, the tower was securely attached to the abutment rock. The attachment was accomplished by 128 post-tensioned steel anchors, each penetrating into the rock a length required to mobilize a rock mass

equal to the dynamic tensile design force of the anchor (Figure 6.4-2). The anchor design forces were estimated as summation of the direct tensile force demands and the normal forces required resisting shear force demands computed for the tower-abutment interface nodal points. To assess adequacy of existing steel anchors, the earthquake force demands at the tower-abutment interface nodal points should be computed and compared with the anchor capacities. This evaluation is conducted in two steps. First envelopes of maximum interface forces are obtained and compared with the total strength capacity of all steel anchors. Second time-history force demands are compared with the individual capacity of the anchors.

(1) Envelope Forces. Envelopes of maximum and minimum normal and shear forces at the tower-abutment interface are computed from the interface normal and shear stresses. In this example SAP2000 capability of group joint forces was used to compute these forces for the entire tower-abutment interface. Figure 6.4-35 to 6.4-37 show computed group forces per unit tributary length. In Figure 6.4-35 interface normal forces are compared with the normalized anchor capacities along the height of the tower. The comparison shows that tensile normal force demands are well the capacity of the anchors.

(2) Time-history of anchor forces.

(3) Figure 6.4-38 displays maximum normal force time-histories for all five input ground motions at the location of Node 1733 (see Figure 6.4-15). These forces are to be resisted by the anchors and can be compared with capacity of the anchor closest to this location. The design force for the anchor closest to Node 1733 is 4,825 kN (1,085 kips), which well above the maximum normal force of 2,000 kN (450 kips) at this location. Time histories of normal forces for all interface nodal points were also computed and are compared with the total capacity of all 128 anchors in Figure 6.4-39. This figure shows that total interface normal force demand remains adequately below the anchor design load of 497,044 kN (111,740 kips), except for a momentary instance of less than one-hundredth of a second for the Pacoima Dam record (PAC). Note that this negligible exceedance of extremely short duration has no structural significance.

Table 6.4-2
Vibration periods and moal participation factors

Mode	Period (sec)	Individual Mode			Cummulative		
		UX	UY	UZ	UX	UY	UZ
1	0.1206	0.55	0.18	0.01	0.55	0.18	0.01
2	0.1070	0.00	1.91	0.00	0.55	2.10	0.02
3	0.0985	1.31	3.08	0.00	1.86	5.17	0.02
4	0.0799	12.32	0.84	0.01	14.18	6.02	0.03
5	0.0745	11.33	0.39	0.28	25.52	6.40	0.30
6	0.0663	0.08	0.22	0.24	25.60	6.63	0.55
7	0.0644	0.58	0.05	0.81	26.18	6.68	1.36
8	0.0617	2.58	0.25	5.11	28.76	6.92	6.47
9	0.0558	1.44	0.24	20.01	30.20	7.17	26.48
10	0.0550	16.77	0.85	10.18	46.97	8.02	36.66
11	0.0519	0.06	0.16	4.60	47.02	8.18	41.26
12	0.0499	2.82	0.25	4.49	49.84	8.43	45.75
13	0.0496	1.44	0.76	0.03	51.28	9.18	45.78
14	0.0468	1.58	0.04	8.53	52.86	9.22	54.30
15	0.0446	0.00	0.01	0.23	52.86	9.23	54.54
16	0.0435	0.09	0.78	1.74	52.95	10.01	56.28
17	0.0428	0.17	4.35	0.56	53.12	14.35	56.83
18	0.0423	0.15	18.50	1.49	53.27	32.85	58.33
19	0.0408	0.07	1.77	0.03	53.34	34.62	58.36
20	0.0396	0.02	8.44	1.48	53.35	43.07	59.84
21	0.0392	1.46	0.11	0.00	54.82	43.18	59.84
22	0.0379	0.02	0.23	0.07	54.84	43.41	59.91
23	0.0377	2.65	0.47	3.07	57.49	43.87	62.98
24	0.0368	2.89	5.10	0.34	60.38	48.97	63.32
25	0.0367	0.32	0.01	0.38	60.69	48.98	63.70
26	0.0358	0.11	0.00	0.14	60.80	48.98	63.84
27	0.0352	0.15	4.89	0.05	60.95	53.88	63.89
28	0.0348	4.96	2.89	0.13	65.91	56.77	64.02
29	0.0343	2.57	0.47	0.51	68.48	57.23	64.53
30	0.0340	0.03	2.04	0.54	68.51	59.27	65.06
31	0.0336	0.25	1.97	0.40	68.76	61.24	65.46
32	0.0330	4.75	5.11	0.34	73.51	66.36	65.80
33	0.0321	0.99	0.26	0.54	74.50	66.62	66.34
34	0.0318	0.05	0.29	0.02	74.55	66.91	66.36
35	0.0315	1.30	1.60	0.11	75.85	68.51	66.46
36	0.0313	0.21	0.20	2.69	76.06	68.71	69.15
37	0.0310	1.95	1.35	0.59	78.01	70.06	69.75
38	0.0306	0.48	3.80	4.56	78.49	73.86	74.30
39	0.0304	2.32	0.04	1.88	80.81	73.90	76.19
40	0.0302	0.06	0.01	0.21	80.87	73.91	76.40
41	0.0302	0.07	2.42	0.56	80.93	76.34	76.96
42	0.0295	0.31	3.56	0.81	81.25	79.90	77.77
43	0.0293	0.60	0.61	0.53	81.85	80.51	78.30
44	0.0288	0.05	0.16	0.19	81.90	80.67	78.49
45	0.0284	0.37	0.58	0.35	82.27	81.25	78.83
46	0.0282	0.15	0.13	0.00	82.42	81.38	78.84
47	0.0279	0.01	0.02	0.10	82.43	81.40	78.94
48	0.0277	0.00	0.62	0.00	82.43	82.02	78.94
49	0.0272	0.10	0.79	0.02	82.53	82.80	78.96
50	0.0268	0.00	0.47	1.04	82.53	83.27	80.00

Table 6.4-2 Continued
Vibration periods and modal participation factors

Mode	Period (sec)	Individual Mode			Cummulative		
		UX	UY	UZ	UX	UY	UZ
51	0.0266	0.00	1.02	0.85	82.54	84.28	80.84
52	0.0262	0.33	0.49	0.30	82.87	84.77	81.14
53	0.0260	0.95	0.07	0.70	83.82	84.84	81.84
54	0.0256	0.15	1.14	0.62	83.98	85.97	82.46
55	0.0254	1.76	0.37	0.45	85.74	86.35	82.90
56	0.0247	0.96	0.70	0.46	86.70	87.05	83.36
57	0.0242	0.04	0.43	0.73	86.73	87.49	84.08
58	0.0240	1.61	0.14	0.17	88.35	87.63	84.25
59	0.0236	0.01	1.37	0.05	88.36	89.00	84.31
60	0.0235	0.09	0.05	4.33	88.45	89.05	88.64
61	0.0230	2.02	0.04	0.15	90.47	89.09	88.79
62	0.0222	0.25	0.23	3.01	90.73	89.32	91.79
63	0.0219	0.70	0.19	0.84	91.42	89.51	92.64
64	0.0218	0.73	0.31	0.34	92.16	89.82	92.98
65	0.0212	0.11	0.33	0.85	92.27	90.15	93.83
66	0.0208	0.13	0.46	0.49	92.40	90.61	94.32
67	0.0204	2.74	0.05	0.00	95.14	90.66	94.32
68	0.0195	0.57	0.39	0.50	95.71	91.05	94.82
69	0.0193	1.50	0.00	0.46	97.20	91.06	95.28
70	0.0191	0.23	0.81	0.33	97.44	91.86	95.61
71	0.0183	0.04	0.54	0.54	97.48	92.41	96.15
72	0.0180	0.06	0.64	0.27	97.54	93.04	96.42
73	0.0178	0.86	0.17	0.01	98.40	93.21	96.43
74	0.0167	0.10	0.40	0.14	98.50	93.60	96.57
75	0.0164	0.28	0.02	0.21	98.78	93.63	96.77
76	0.0163	0.18	0.43	0.06	98.95	94.06	96.83
77	0.0149	0.22	0.79	0.02	99.17	94.85	96.85
78	0.0148	0.11	0.62	0.47	99.28	95.47	97.32
79	0.0146	0.03	1.65	0.39	99.31	97.12	97.72
80	0.0140	0.01	2.50	0.05	99.32	99.62	97.77
81	0.0135	0.10	0.04	0.94	99.42	99.66	98.71
82	0.0134	0.36	0.06	0.03	99.78	99.72	98.74
83	0.0126	0.01	0.18	0.11	99.79	99.90	98.86
84	0.0121	0.01	0.00	0.85	99.80	99.90	99.71
85	0.0119	0.09	0.01	0.08	99.89	99.91	99.79
86	0.0107	0.00	0.00	0.14	99.89	99.91	99.93
87	0.0104	0.05	0.01	0.01	99.94	99.92	99.94
88	0.0103	0.03	0.02	0.00	99.97	99.94	99.94
89	0.0090	0.00	0.00	0.04	99.97	99.94	99.98
90	0.0087	0.02	0.01	0.00	99.99	99.95	99.98
91	0.0085	0.00	0.04	0.00	99.99	99.98	99.98
92	0.0072	0.00	0.00	0.01	99.99	99.99	99.99
93	0.0070	0.00	0.01	0.00	99.99	100.00	99.99
94	0.0067	0.01	0.00	0.00	100.00	100.00	99.99
95	0.0053	0.00	0.00	0.00	100.00	100.00	100.00
96	0.0051	0.00	0.00	0.00	100.00	100.00	100.00
97	0.0048	0.00	0.00	0.00	100.00	100.00	100.00
98	0.0040	0.00	0.00	0.00	100.00	100.00	100.00
99	0.0037	0.00	0.00	0.00	100.00	100.00	100.00
100	0.0036	0.00	0.00	0.00	100.00	100.00	100.00

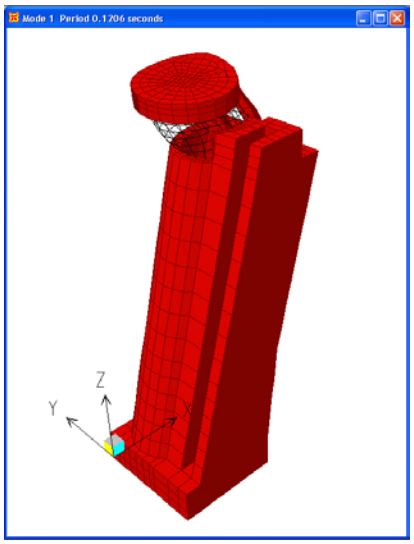

Mode 1. T = 0.1206 sec.

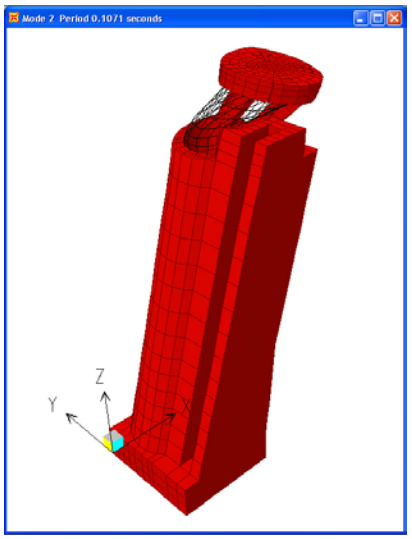

Mode 2. T = 0.1071 sec.

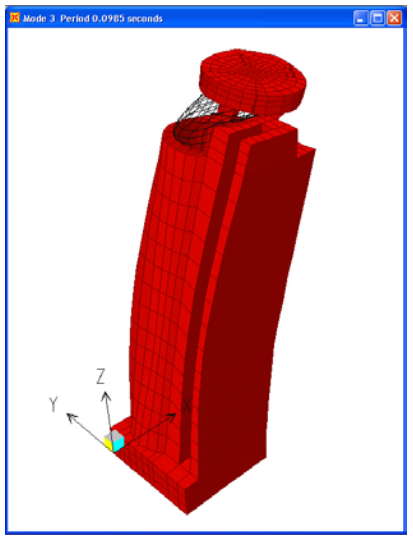

Mode 3. T = 0.0985 sec.

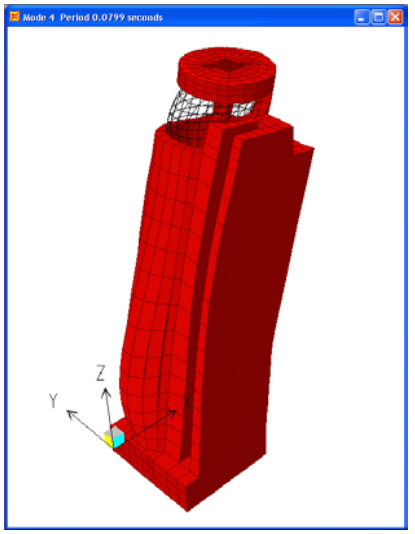

Mode 4. T = 0.0799 sec.

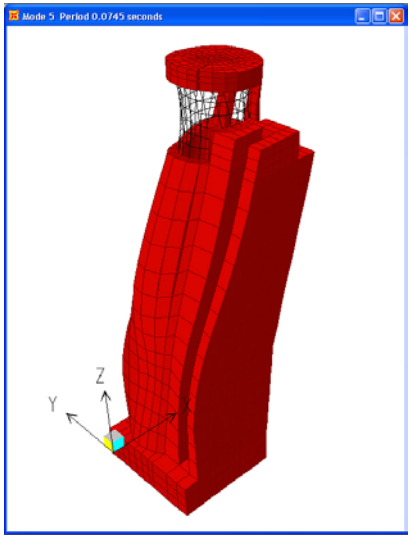

Mode 5. T = 0.0745 sec.

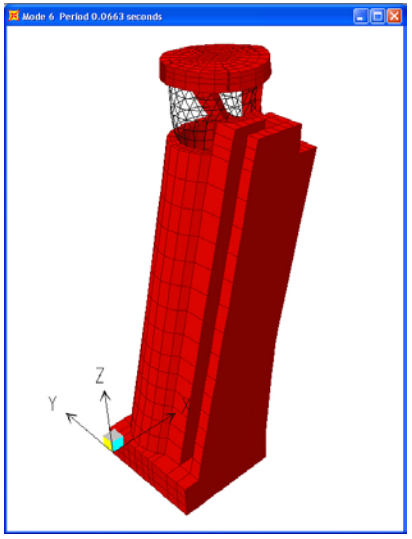

Mode 6. T = 0.0663 sec.

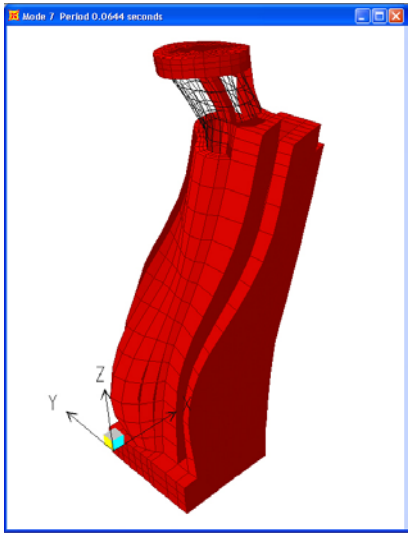

Mode 7. T = 0.0644 sec.

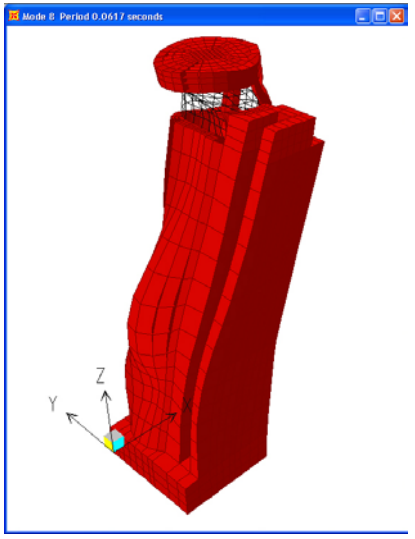

Mode 8. T = 0.0617 sec.

Figure 6.4-14 Vibration mode shapes

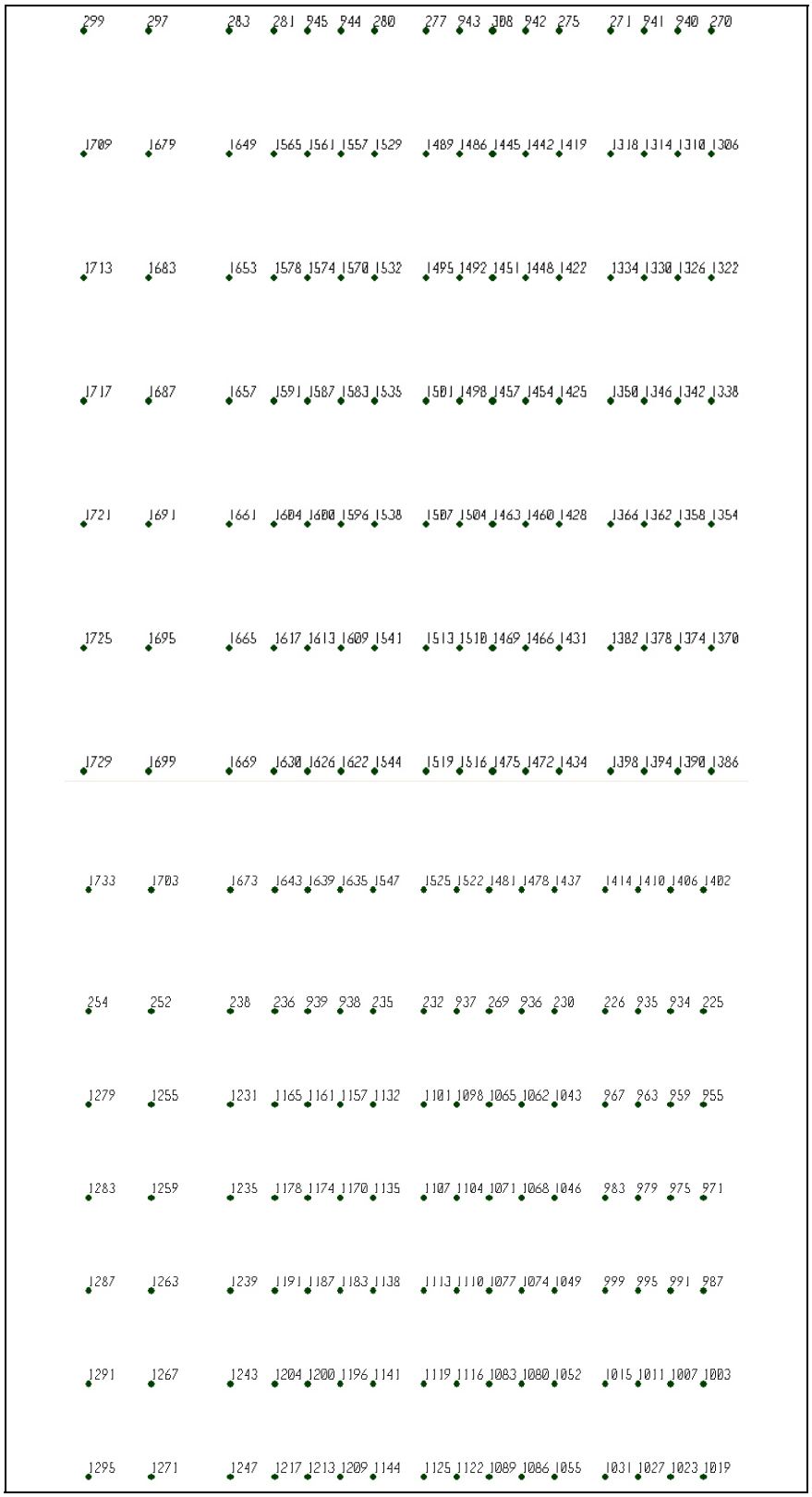

Figure 6.4-15. Node numbering at tower-rock interface

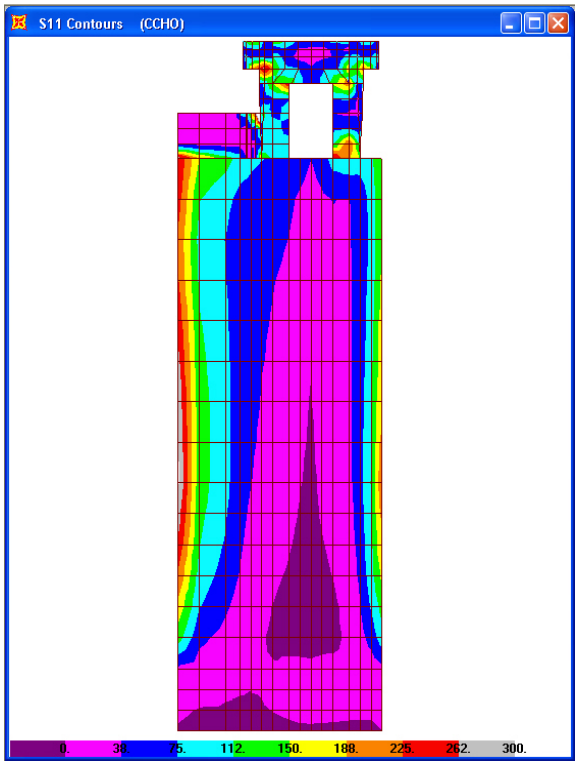

CHO Maximum Stresses (psi)

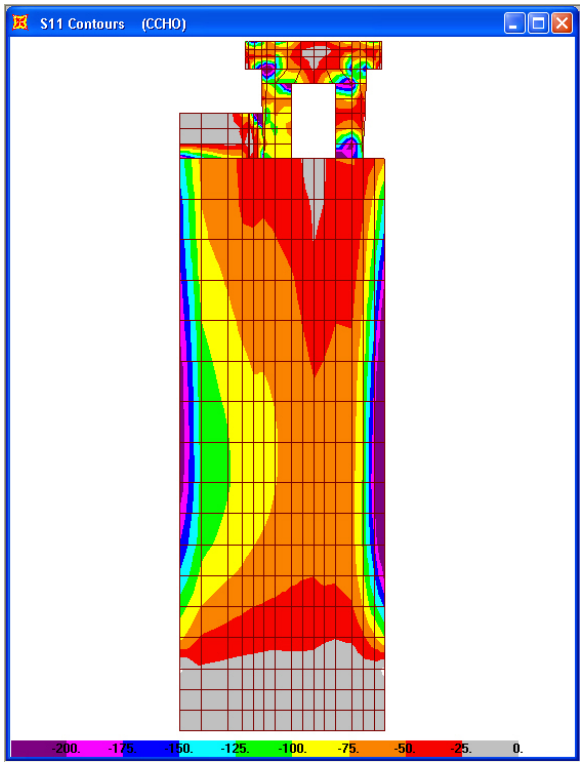

CHO Minimum Stresses (psi)

Figure 6.4-16. Normal stress contours at tower-abutment interface for CHO

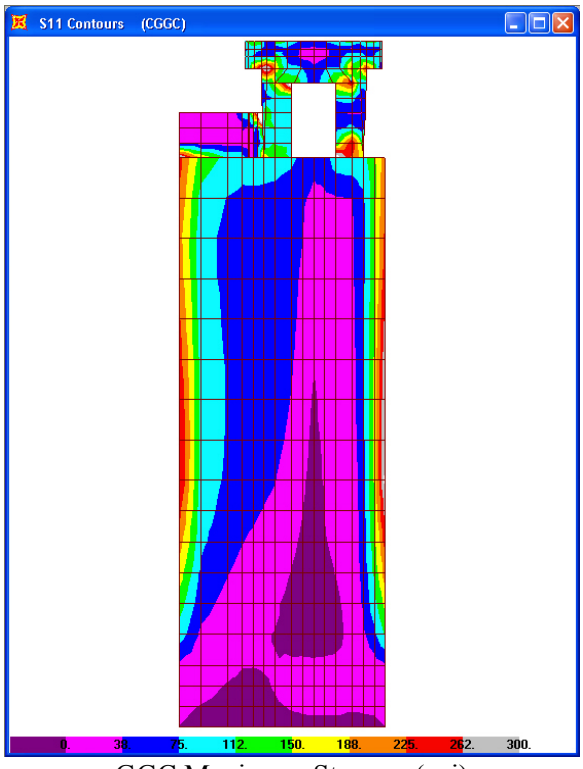

GGC Maximum Stresses (psi)

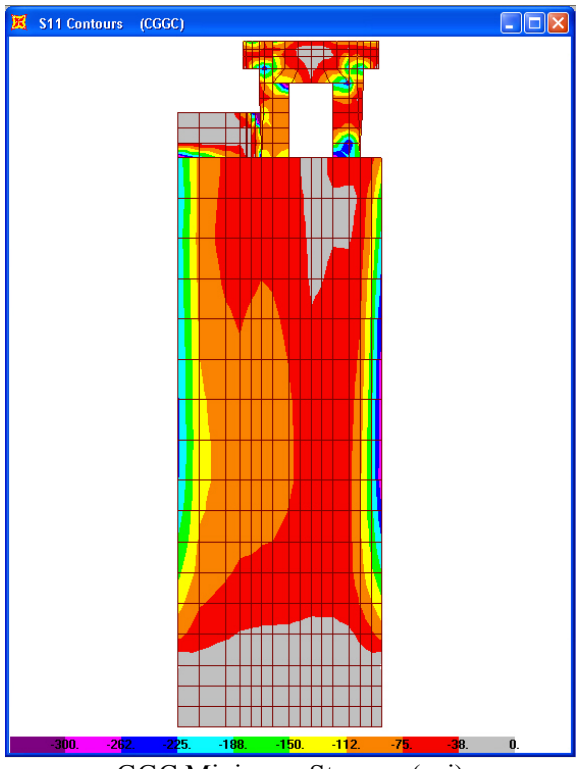

GGC Minimum Stresses (psi)

Figure 6.4-17. Normal stress contours at tower-abutment interface for GGC

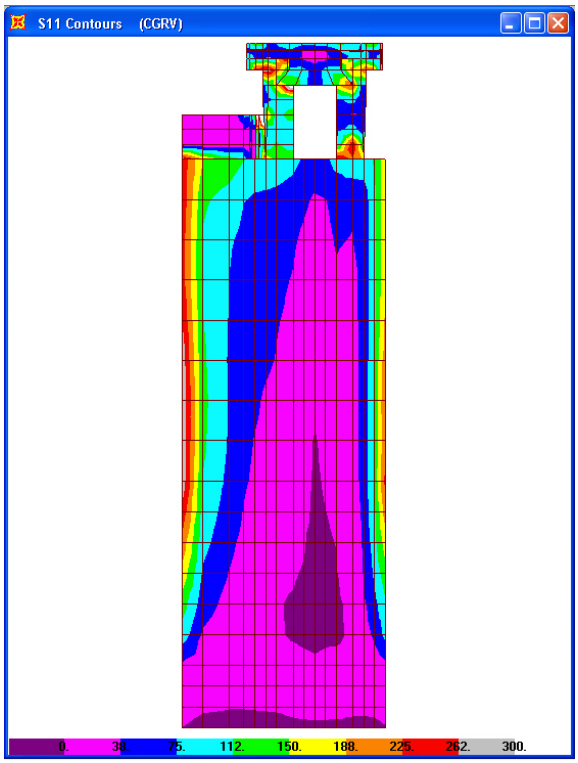

GRV Maximum Stresses (psi)

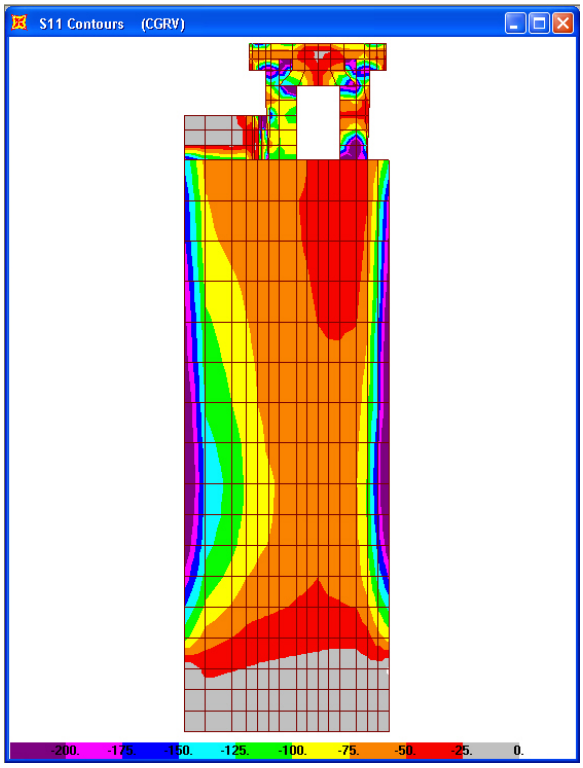

GRV Minimum Stresses (psi)

Figure 6.4-18. Normal stress contours at tower-abutment interface for GRV

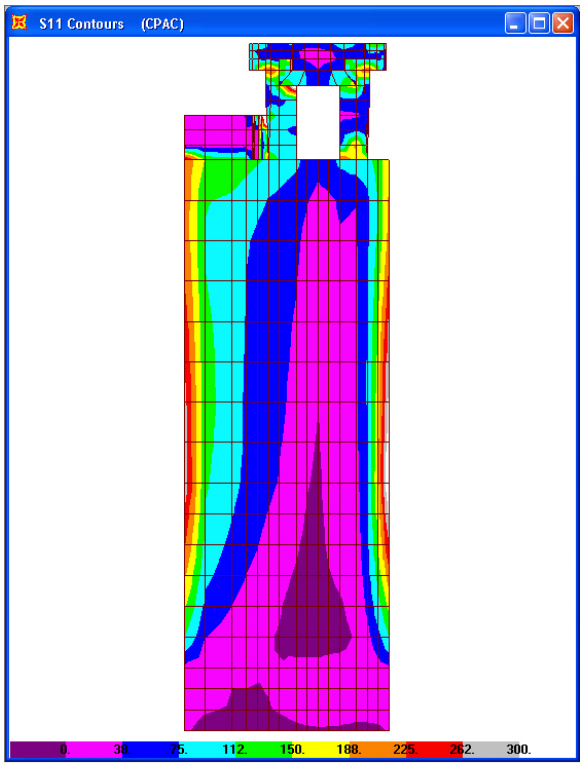

PAC Maximum Stresses (psi)

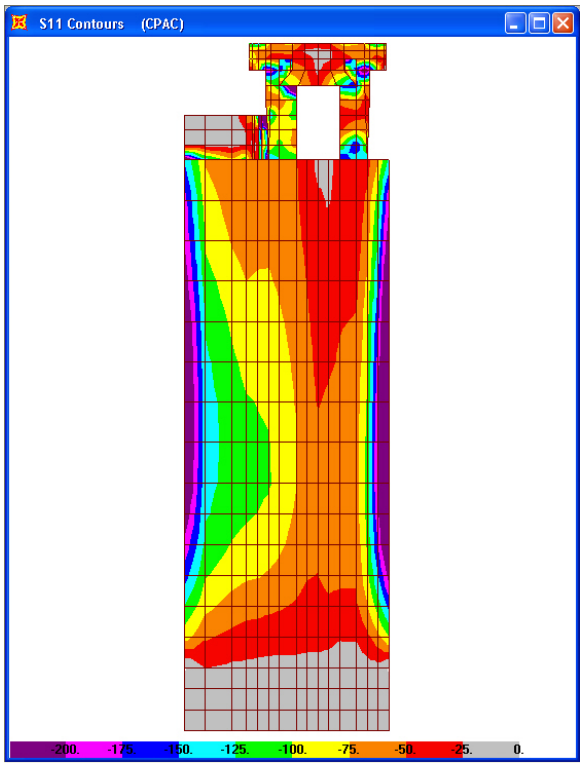

PAC Minimum Stresses (psi)

Figure 6.4-19. Normal stress contours at tower-abutment interface for PAC

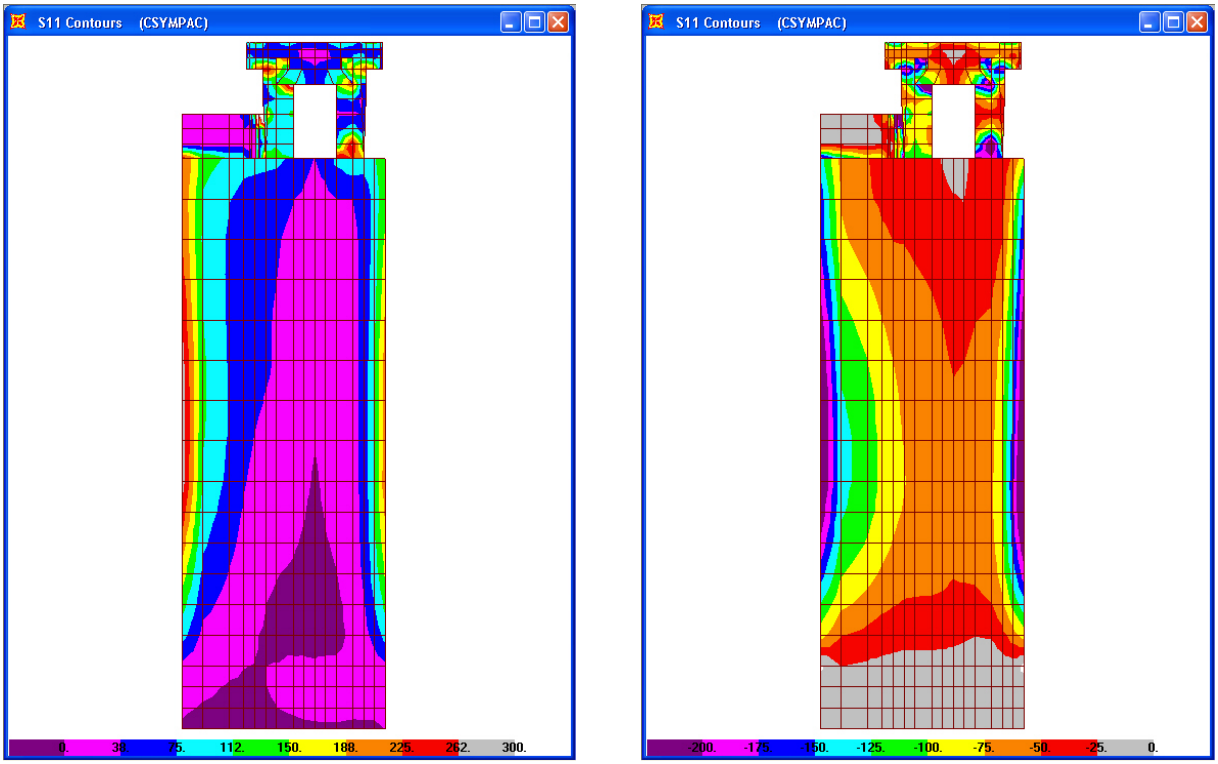

SMPAC Maximum Stresses (psi) SMPAC Minimum Stresses (psi)

Figure 6.4-20. Normal stress contours at tower-abutment interface for SMPAC

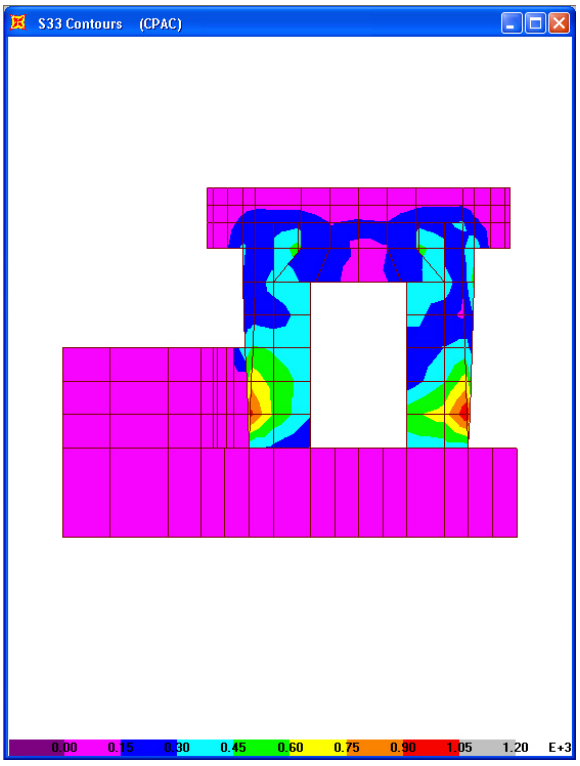

PAC Maximum Stresses (psi)

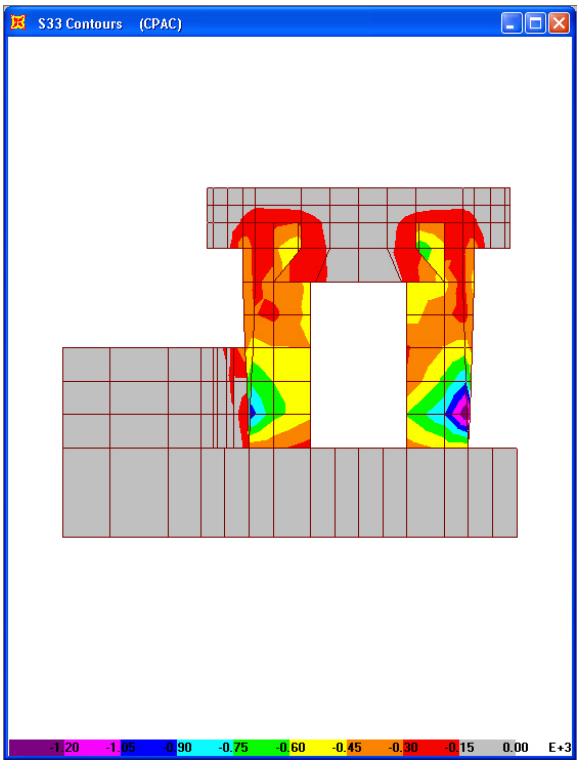

PAC Minimum Stresses (psi)

Figure 6.4-21. Vertical stresses in back face (downstream) of high-level intake for PAC

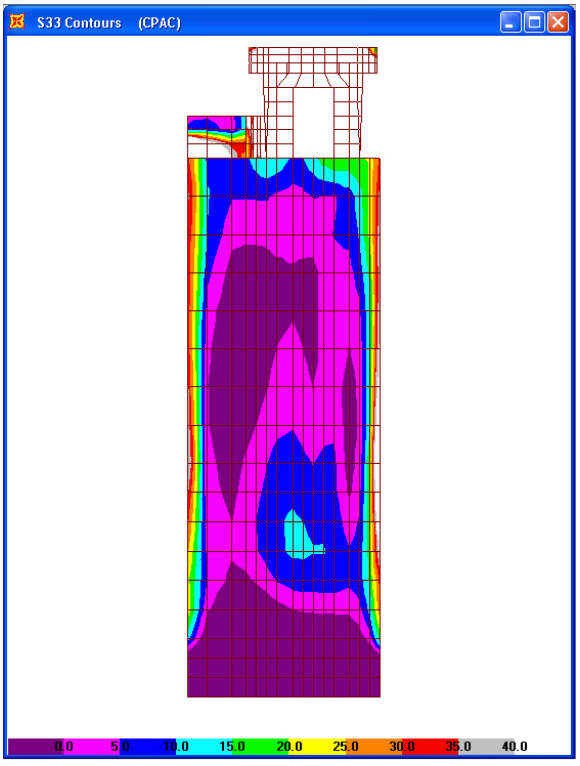

PAC Maximum Stresses (psi)

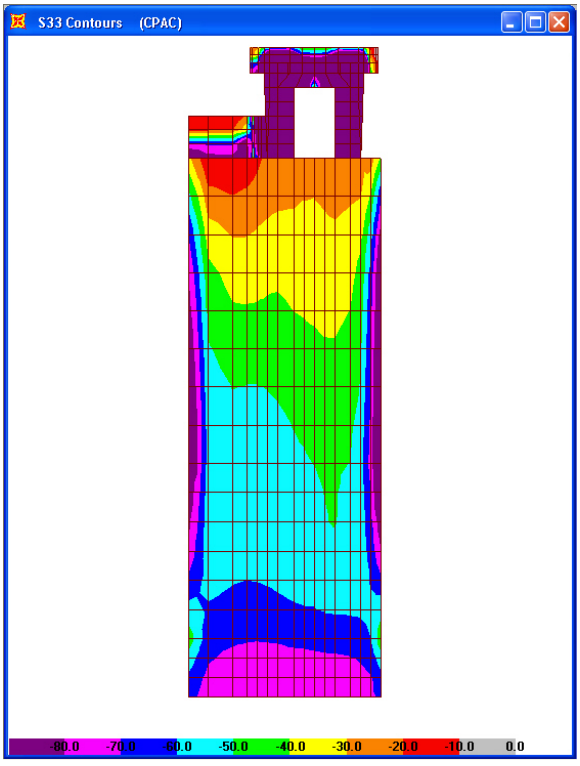

PAC Minimum Stresses (psi)

Figure 6.4-22. Vertical stresses in back face (downstream) of tower for PAC

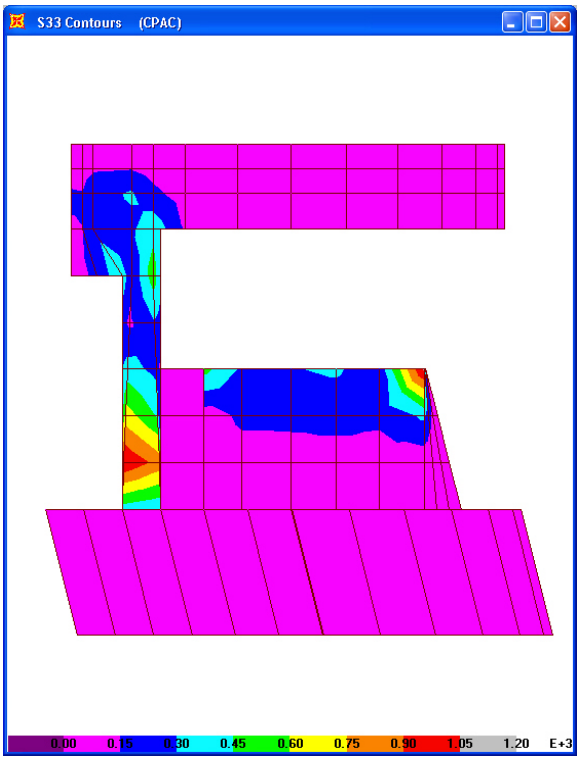

PAC Maximum Stresses (psi)

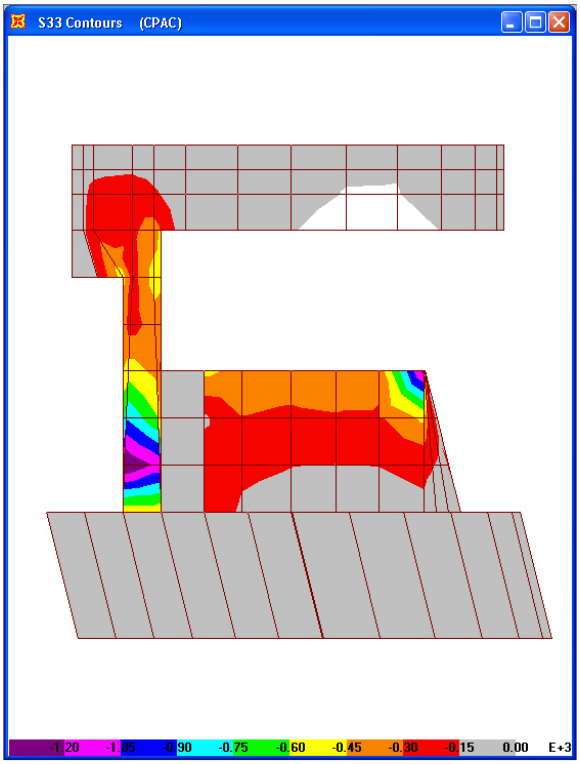

PAC Minimum Stresses (psi)

Figure 6.4-23. Vertical stresses in right face of high-level intake for PAC

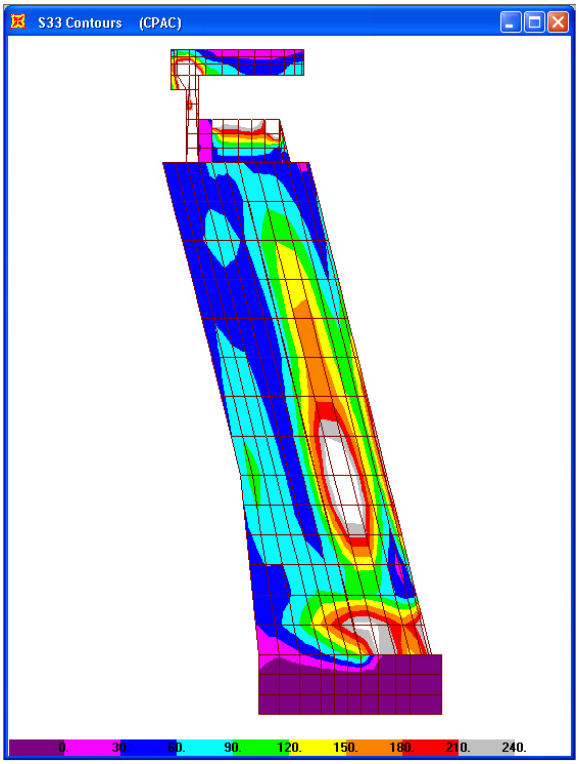

PAC Maximum Stresses (psi)

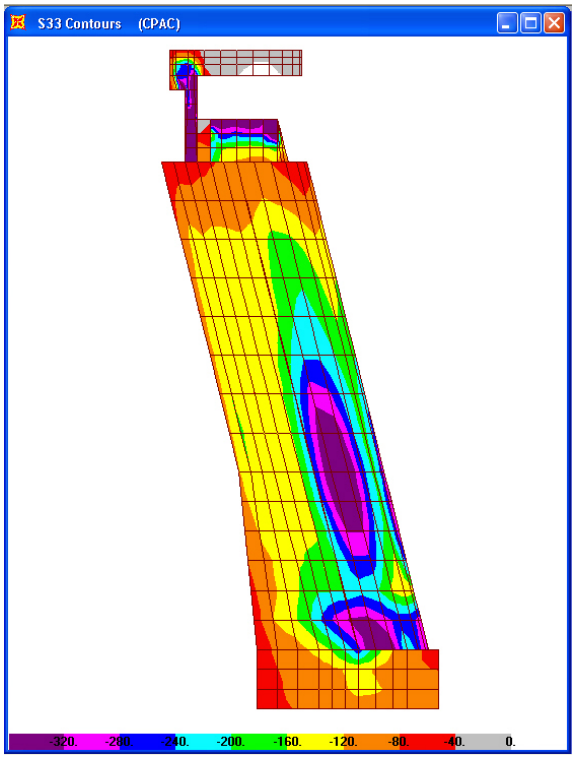

PAC Minimum Stresses (psi)

Figure 6.4-24. Vertical stresses in right face of tower for PAC

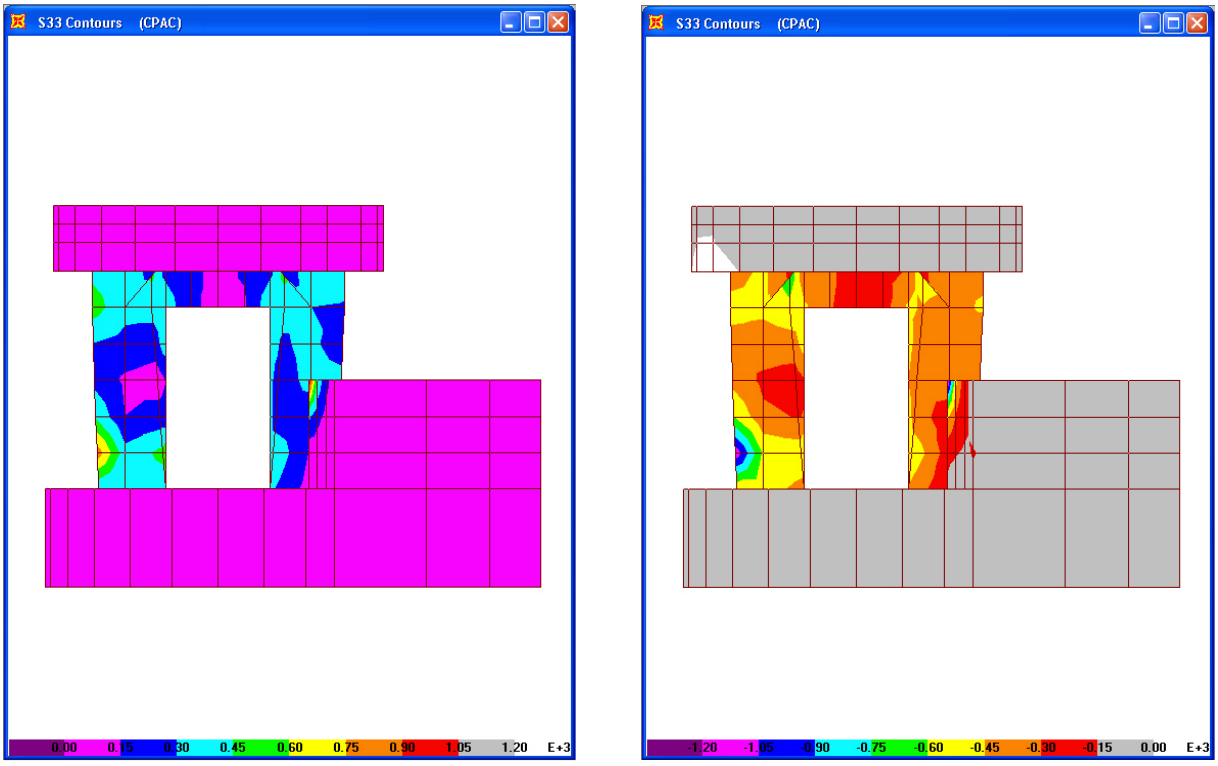

PAC Maximum Stresses (psi) PAC Minimum Stresses (psi)

Figure 6.4-25. Vertical stresses in front face (upstream) of high-level intake for PAC

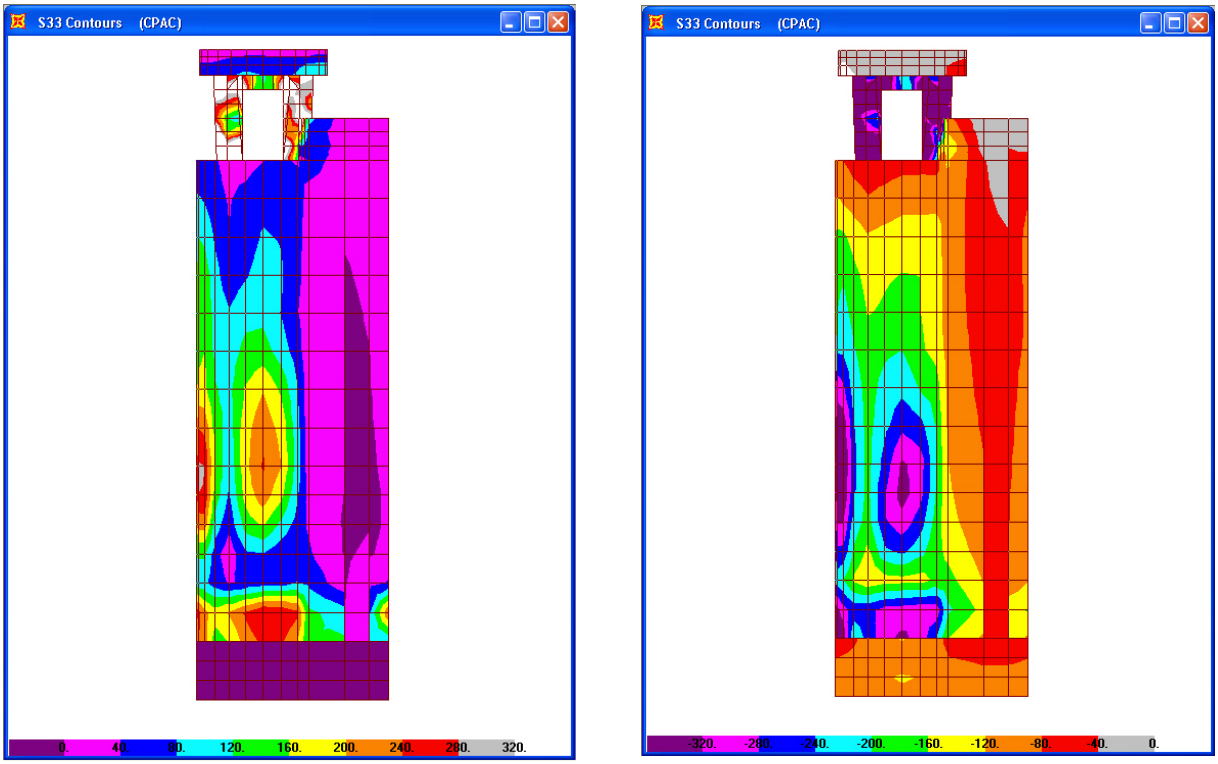

PAC Maximum Stresses (psi) PAC Minimum Stresses (psi)

Figure 6.4-26. Vertical stresses in front face (upstream) of tower for PAC

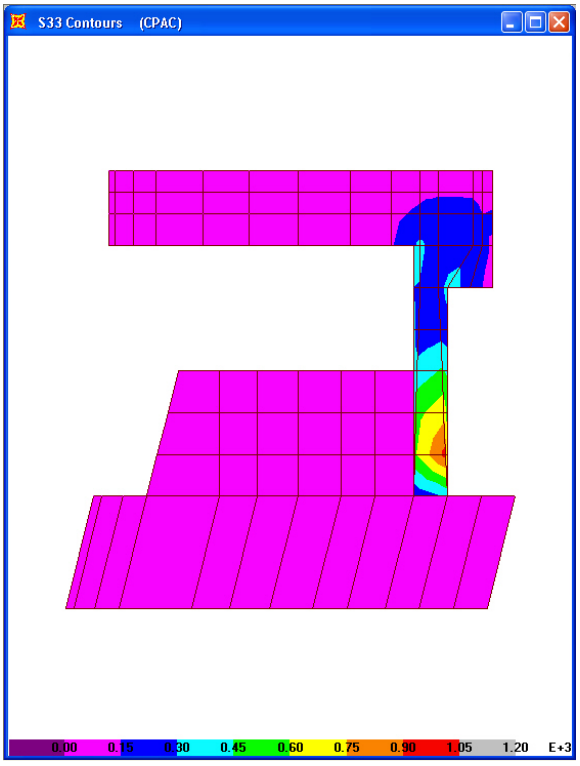

PAC Maximum Stresses (psi)

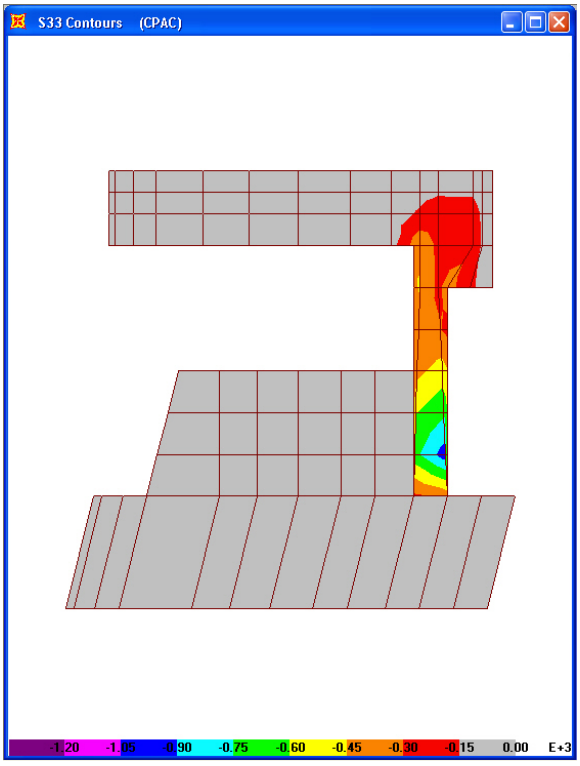

PAC Minimum Stresses (psi)

Figure 6.4-27. Vertical stresses in left face of high-level intake for PAC

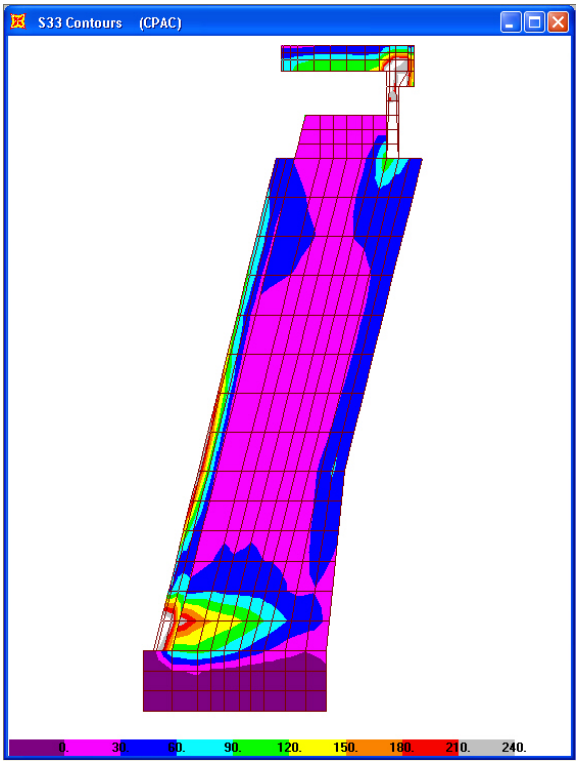

PAC Maximum Stresses (psi)

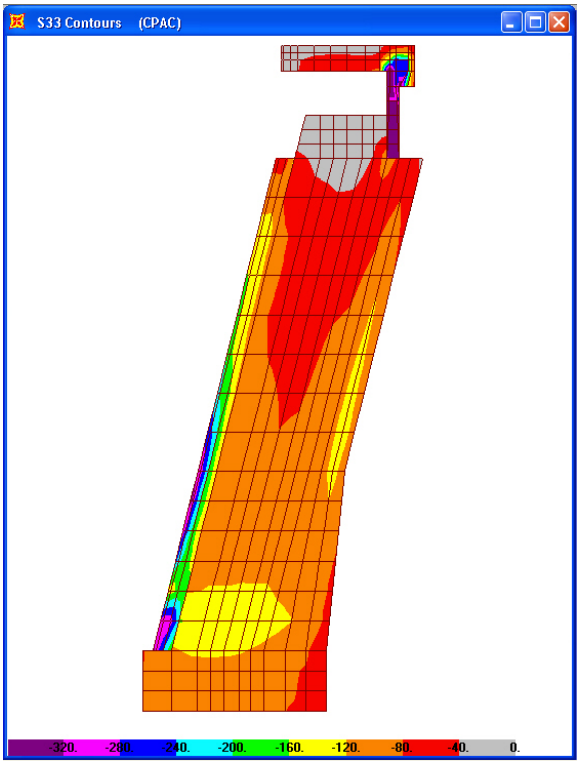

PAC Minimum Stresses (psi)

Figure 6.4-28. Vertical stresses in left face of tower for PAC

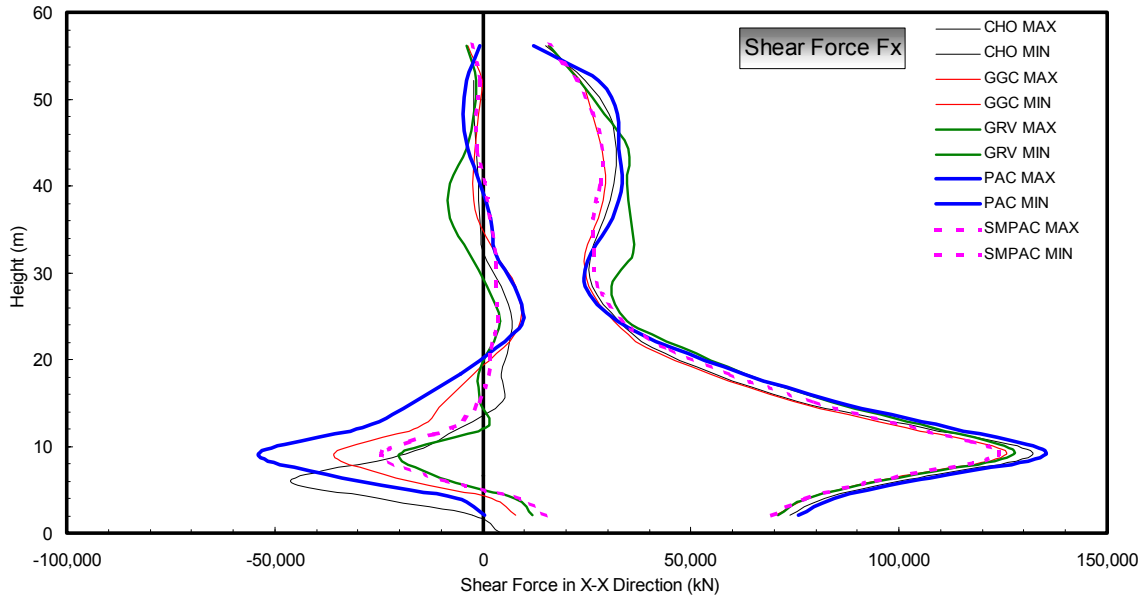

Figure 6.4-29. F_x shear force diagram (normal to abutment)

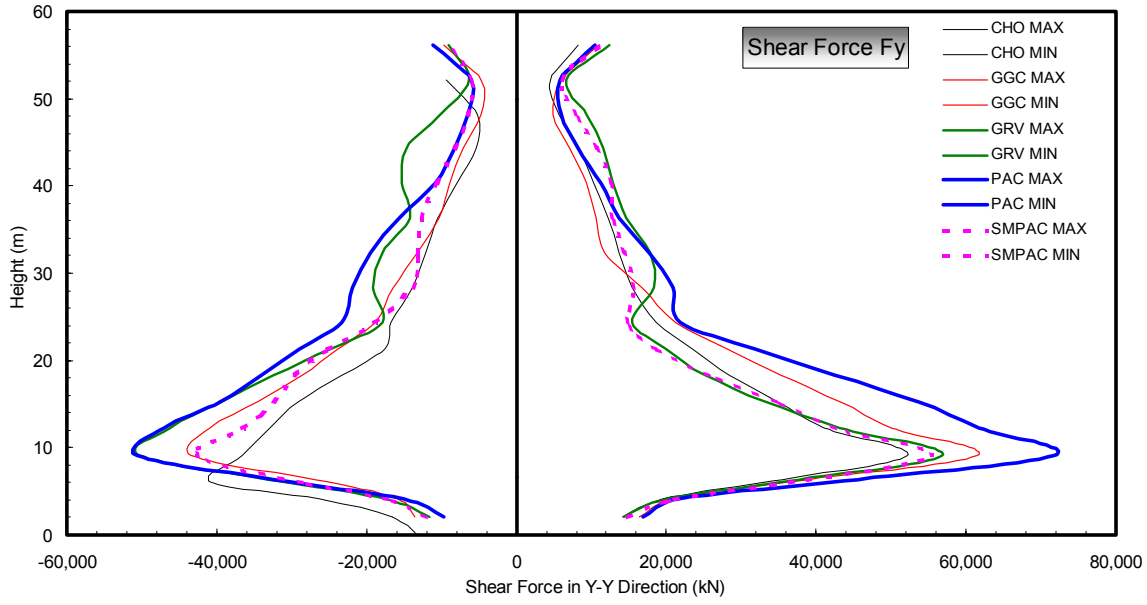

Figure 6.4-30. F_y shear force diagram (parallel to abutment)

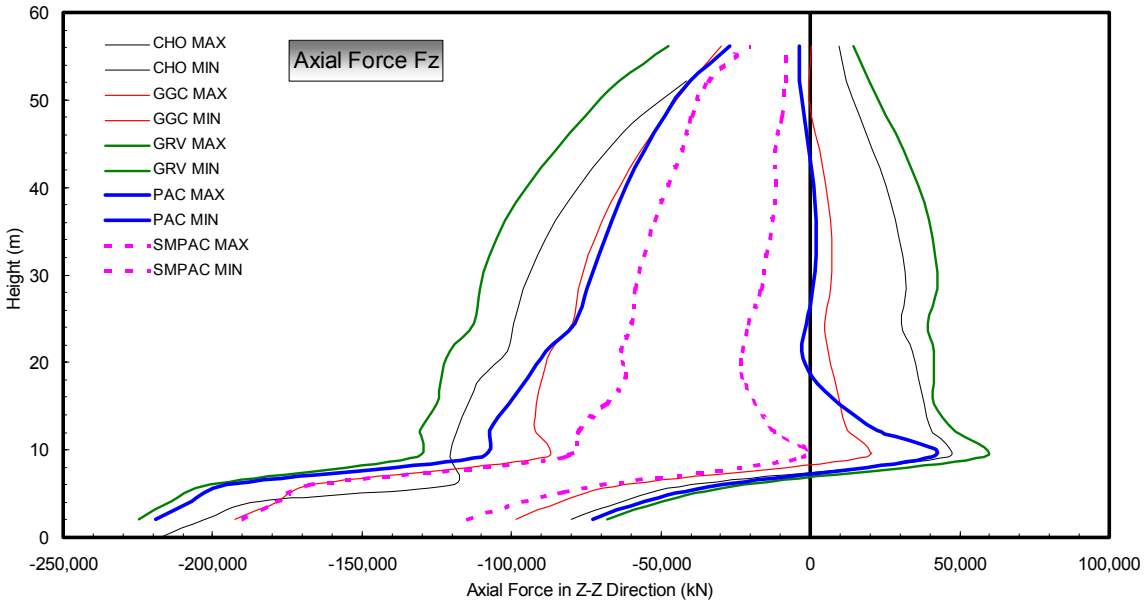

Figure 6.4-31. F_z (vertical) axial force diagram (+ = tension, - = compression)

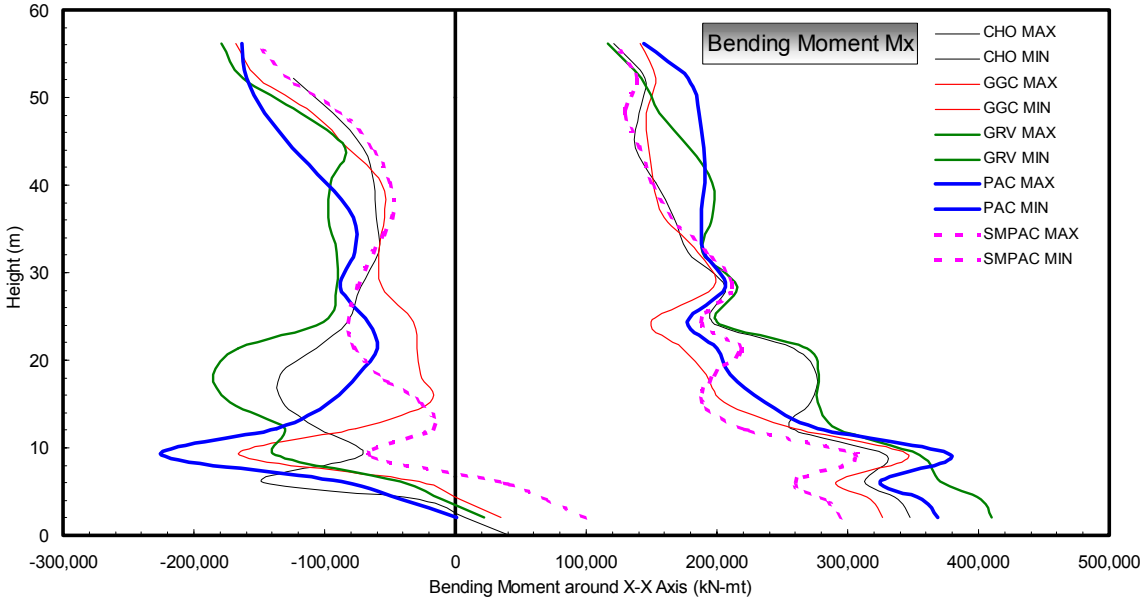

Figure 6.4-32. M_x bending moment diagram

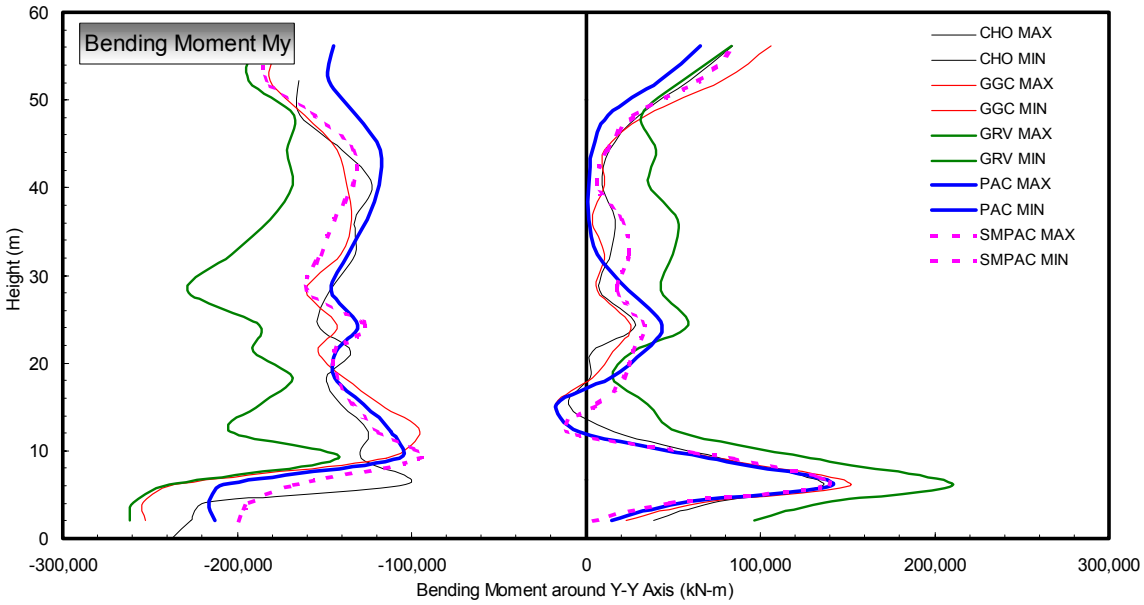

Figure 6.4-33. M_y bending moment diagram

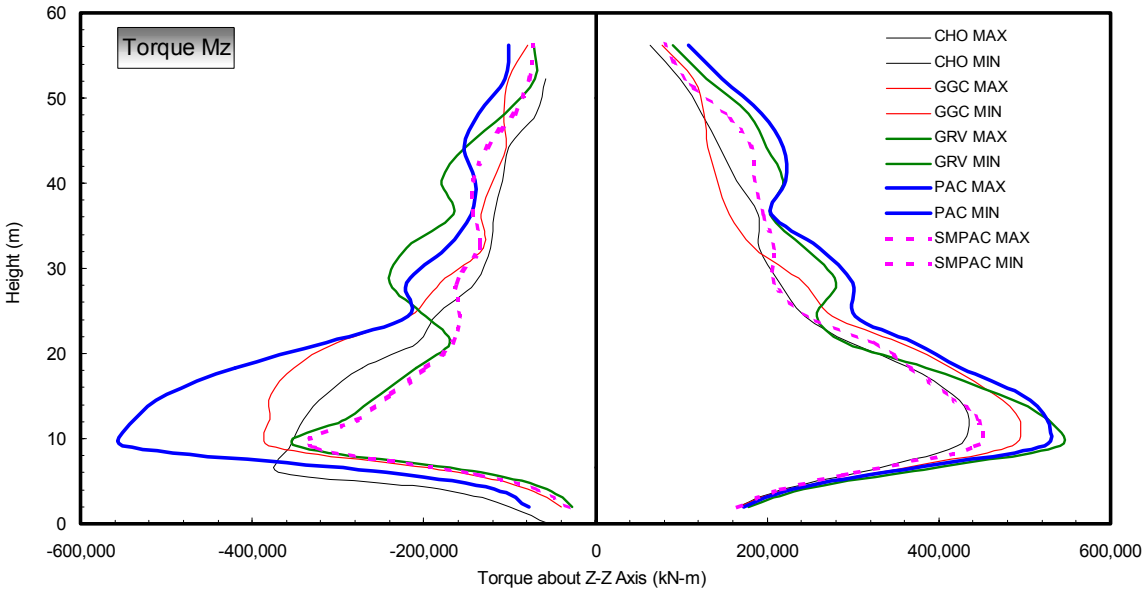

Figure 6.4-34. M_z torque moment diagram

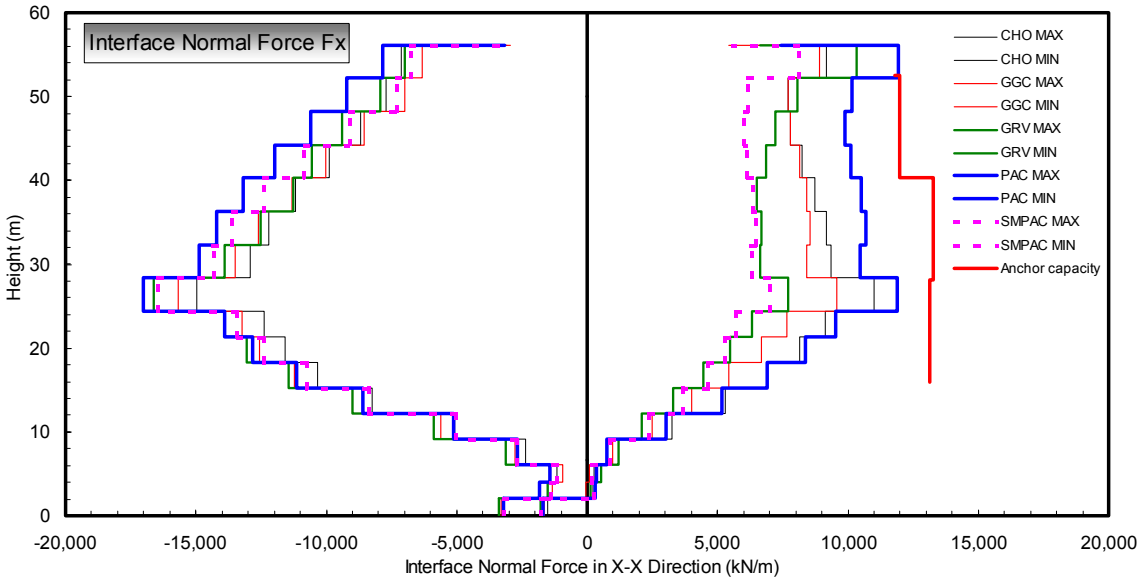

Figure 6.4-35. Tower-abutment interface normal forces

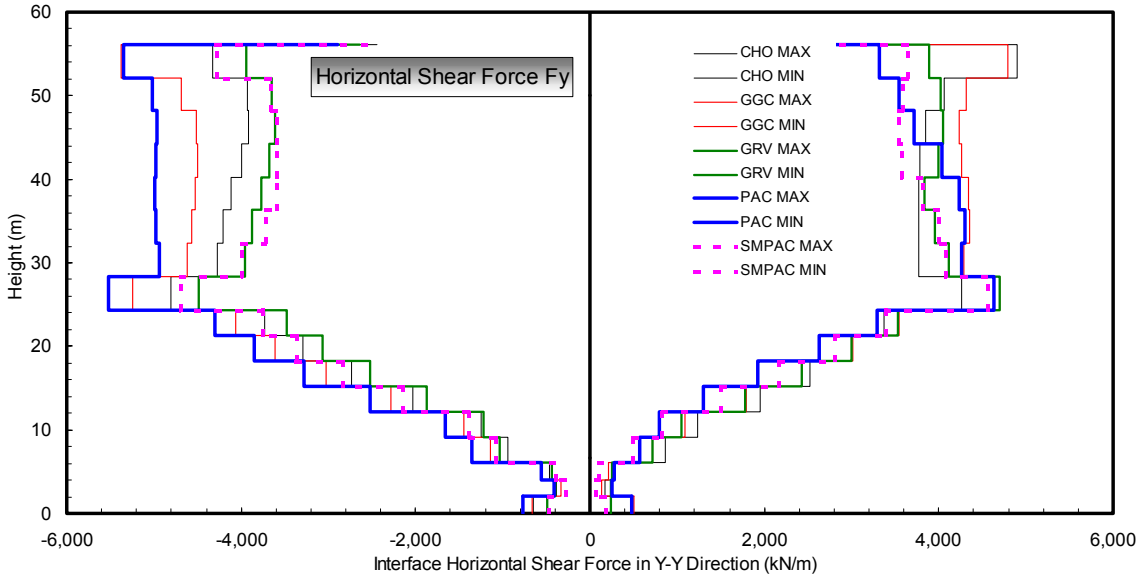

Figure 6.4-36. Tower-abutment interface horizontal shear forces

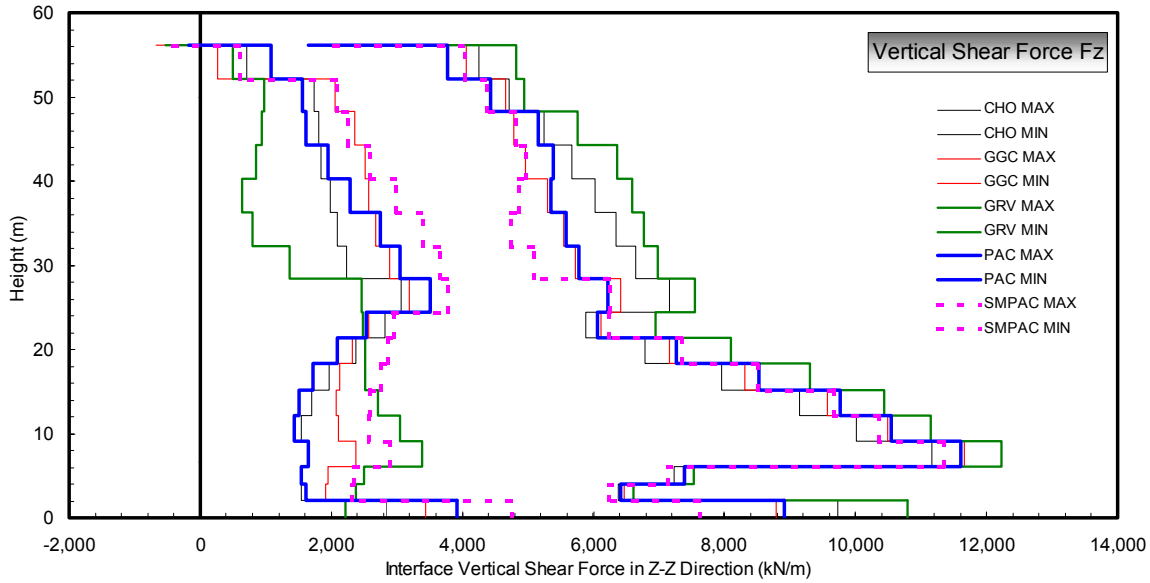

Figure 6.4-37. Tower-abutment interface vertical shear forces

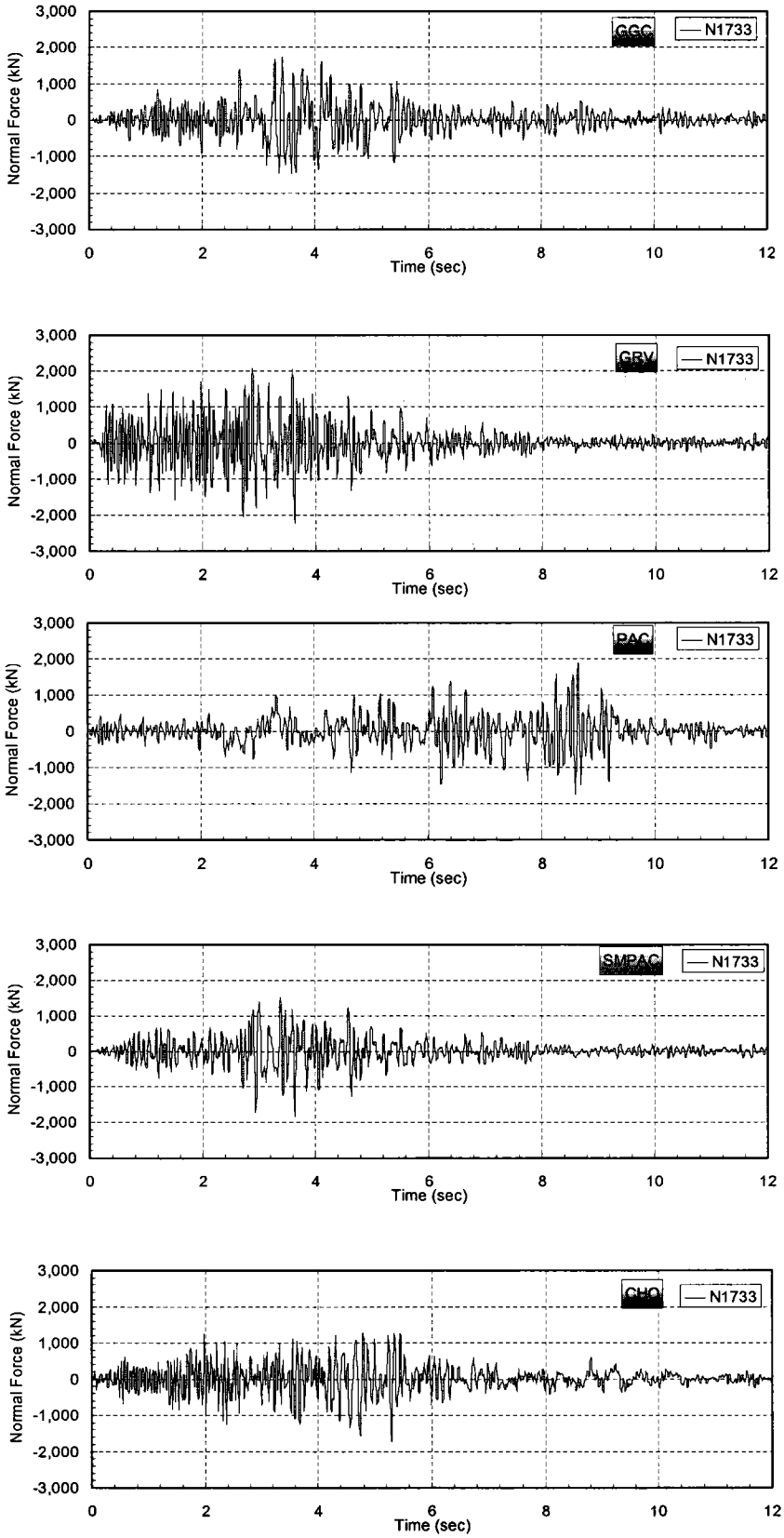

Figure 6.4-38. Time-history of anchor forces at Node N1733

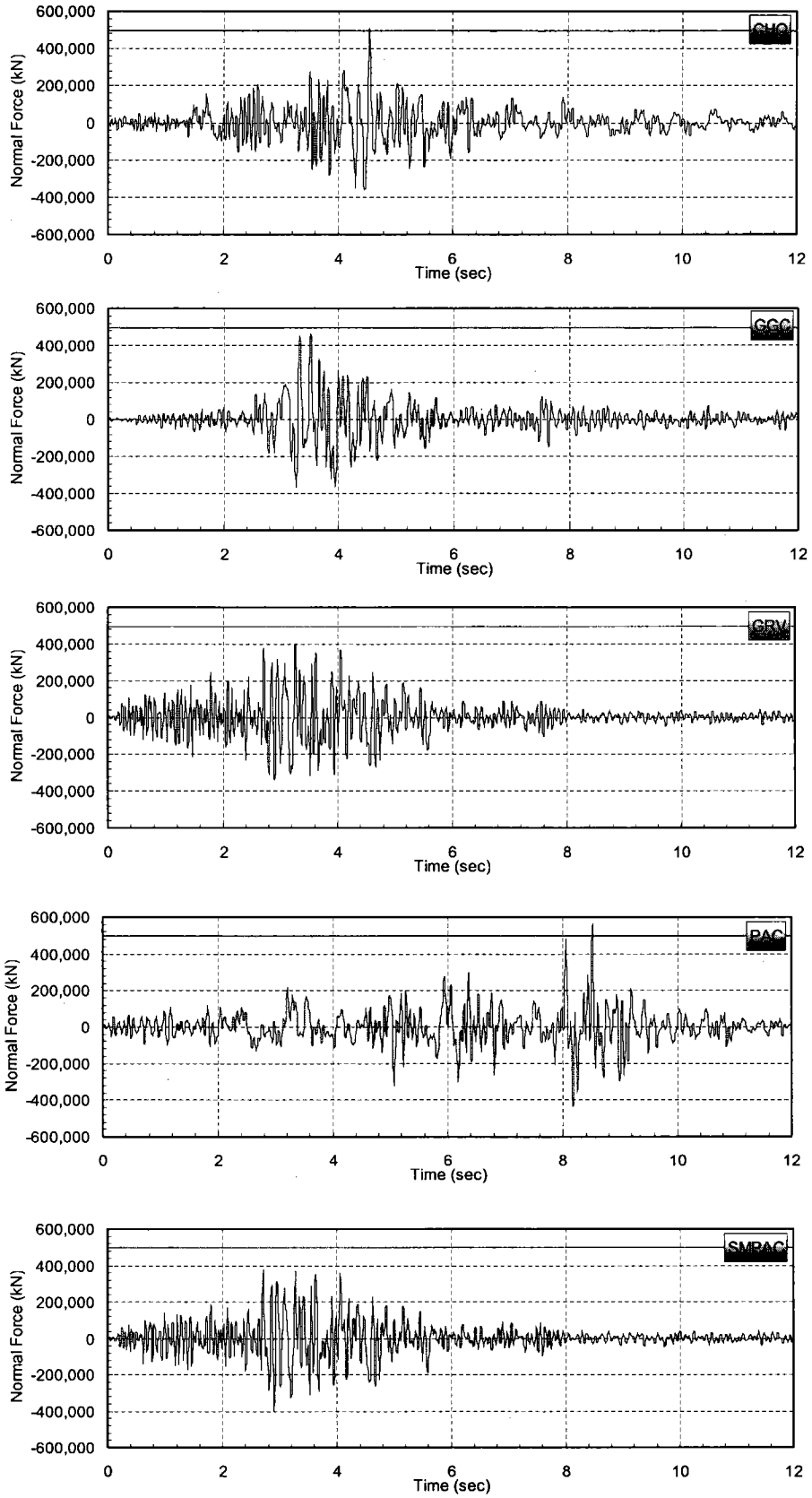

Figure 6.4-39. Comparison of time-history of total interface normal force with anchor design force